Physiology of small contractile arteries

Ca^{2+}-sensitization in myogenic tone and glucose transport in endothelial cells.

by

Nathalie Gaudreault

B.Sc., Laval University, 1996
M.Sc., Laval University, 1999

A thesis submitted in partial fulfilment of
The requirements for the degree of
Doctor of Philosophy

In

The Faculty of Graduate Studies

Department of Physiology

The University of British Columbia

December 2004

Abstract

Recent evidence suggests the involvement of Ca^{2+} sensitization in the development of myogenic tone, possibly mediated by PKC and Rho-kinase. To investigate this, rat cerebral arteries were mounted on a pressure myograph, and pressure-induced constrictions and changes in intracellular $[Ca^{2+}]_i$ were recorded. The ratio of the change in diameter to change in $[Ca^{2+}]_i$ was greater for pressure-induced constriction compared with constriction produced by depolarization with 60 mM KPSS. Pressure-induced constriction in depolarised arteries was not associated with further increases in $[Ca^{2+}]_i$ but was abolished by selective inhibitors of PKC, and Rho kinase. These data suggest that in addition to increases in $[Ca^{2+}]_i$, enhanced myofilament Ca^{2+} sensitivity, mediated by PKC and Rho kinase activation, occurs during myogenic tone development.

Although it is well established that elevated intracellular glucose concentration leads to endothelial dysfunction, how and why glucose tends to accumulate in ECs remains poorly understood. The effects of hyperglycaemia on the expression and subcellular distribution of GLUT-1 to 5 and SGLT-1 in ECs of rat microvasculature were examined. We found, through immunohistochemistry and fluorescence microscopy that all transporters except SGLT-1 were expressed preferentially at the cell-to-cell junction and on the abluminal side of these cells. Hyperglycaemia, significantly downregulated GLUT-1, 3, 4 and 5 and dramatically upregulated GLUT-2; leaving SGLT-1 unchanged.

To determine the functionality of these glucose transporters in ECs, glucose uptake was monitored with a fluorescent glucose analog in live coronary

arteries. The arteries were mounted in an arteriograph chamber on the stage of a confocal microscope. Results show a dense accumulation of glucose at the ECs periphery, as predicted by the subcellular distribution of the transporters. In addition, an increase in glucose uptake was observed in the presence of insulin.

We conclude that the high susceptibility to glucose toxicity of ECs may be the result of the subcellular organization of their GLUTs, and the increased expression of GLUT-2. The asymmetric subcellular organisation of GLUTs may facilitate transcellular glucose exchange between the blood and the cells of the vascular wall. Finally, it was demonstrated that the endothelium of coronary arteries is insulin sensitive.

Contents

List of Tables

List of Figures

Chapter 1

Chapter 2

Chapter 3

Appendices

List of Abbreviations

AA	Arachidonic acid
ANOVA	analysis of variance
ADP	adenosine diphsphate
AGE	advanced glycation end-product
ATP	adenosine triphosphate
BBB	blood brain barrier
BAEC	bovine aortic endothelial cells
CaM	calmodulin
CCD	charge-coupled device
CH^{3+}	carbonium ions
CPI-17	PKC targeted protein phosphatase-1 inhibitor of 17KDa
DABCO	1,4-diazabicyclo[2.2.2] octane (triethylenediamine)
DAG	Diacylglycerol
DAPI	4′,6-diamidino-2-phenylindole dihydrochloride
DCCT	Diabetes Control and Complications Trial
2DG	2-deoxy-D-glucose
DMSO	dimethyl sulfoxide
EC(s)	endothelial cell(s)
EDTA	ethylenediaminetetraacetic acid
EGM-2	endothelial growth medium-2
EGF	endothelial growth factor
EGTA	ethylene glycol-bis(2-aminoethylether)-N,N,N′,N′-tetraacetic acid
eNOS	endothelial nitric oxide synthase
EPR	exhaustive proton reassignment
FFA	free fatty acid
FITC	fluorescein isothiocyanate
FRET	fluorescence resonance energy transfer
GAPDH	glyceraldehydes-3-phosphate dehydrogenase

GDP	guanosine diphosphate
GLUT	facilitative glucose transporter
GTPγS	non-hydrolysable GTP analogue
HCAEC(s)	human coronary artery endothelial cell(s)
HDL	high density lipoprotein
hEGF	epidermal growth factor, recombinant
HETE	hydroxyeicosatetraenoic acid
hFGF	fibroblastic growth factor, recombinant
HMIT	H^+-myo-inositol cotransporter
Hoechst	trihydrochloride, trihydrate
HUVEC	human umbilical vein-derived ECs
IGEPAL	Ethoxylate octylphenol
IGF	Insulin-like growth factor
ILK	Integrin-linked kinase
IP_3	Ionositol-1,4-5-triphosphate
$_iPA_2$	Phospholipase A_2 isoform
K_{ca}	Ca^{2+}-activated potassium channel
kDa	kilo Dalton
Km	Michaelis constant=[substrate] at which the velocity(V) is $½V_{max}$
LDL	low density lipoprotein
LGCC	ligand-gated Ca^{2+} channel
Lyso PC	lysophospholipids choline
MAP-kinase	mitogen-activated protein-kinase
MBS	myosin binding site
MDG	α-methyl-D-glucose
MLC	myosin light chain
MLCK	myosin light chain kinase
MLCP	myosin light chain phosphatase
Mono	monoclonal
MYPT1	myosin phosphatase target 1
NADPH	nicotinamide adenine dinucleotide phosphate
2-NBDG	2-[N-(7-nitrobenz-2-oxa-1,3-diazol-4-yl) amino]-2-deoxyglucose

6-NBDG	6-[N-(7-nitrobenz-2-oxa-1,3-diazol-4-yl) amino]-2-deoxyglucose
n.d.	not determined
*N*F-κB	nuclear factor-κB
NIH	National Institute for Health
NO	nitric oxide
3OMG	3-O-methyl-D-glucose
PA	phosphatidic acid
PARP	poly ADP-ribose polymerase
PAI	plasminogen activator inhibitor
PBS	phosphate buffered saline
PC-PLC	phosphatidylcholine-specific phospholipase C
PC-PLD	phosphatidylcholine-specific phospholipase D
PDGF	platelet-derived growth factor
PI-PLC	phosphatidylinositol 4,5,-diphosphate
PI3-kinase	phosohatidylinositol-3 kinase
PKM	protein kinase M
PLA	phospholipase A
PMCA	Ca^{2+}-ATPase pump
poly	polyclonal
PSF	point-spread-function
PSS	physiological salt solution
RAGE	receptor for AGE
RhoA-GEF	RhoA-guanine nucleotide exchanger factor
RhoA-GTP	RhoA-guanosine triphosphate
Rho-GDI	Rho-guanine nucleotide dissociation inhibitor
R3-IGF	insulin-like growth factor-1
RyR	ryanodine receptor
SAC	stretch-activated cation channel
SERCA	sarcoplasmic reticulum Ca^{2+}-ATPase pump
SMC(s)	smooth muscle cell(s)
SM22	smooth muscle specific protein 22KDa
SGLT	sodium-dependent glucose transporter

SE	standard error
SOC	store operated Ca^{2+}-entry mechanisms
SPC	sphingosyl phosphorylcholine
SR	sarcoplasmic reticulum
STOC	spontaneous transient outward current
STZ	streptozotocin
TBS-T	tris-buffered saline-tween
TGF	United Kingdom Prospective Diabetes Study
TLC	Thin layer chromatography
TNF-α	Tumour necrosis factor-α
Trp	Transient receptor potential channel
Tween	Polyoxyethylene sorbitan monolaurate
UKPDS	transforming growth factor
VE	vascular Endothelial
VEGF	vascular endothelial growth factor
VGCC	voltage-gated Ca^{2+} channel
VLDL	very low density lipoprotein
Vmax	maximal transport velocity
ZIP	Zipper-interacting protein

Acknowledgements

Many people have contributed, throughout the past 6 years, to this Ph.D. Some have provided intellectual guidance and technical help but others, even from a considerable distance, have provided me with unfailing moral support. It is therefore with great pleasure that I take this opportunity to express my gratitude to each of them.

I would like to express my sincere gratitude to my supervisor Dr. Ed Moore, for giving me the opportunity to do my Ph.D. in his laboratory, for his patience and understanding, and most of all for giving me the freedom and latitude to pursue my own goals and ideas. I must also thank Ed for his many revisions of my manuscripts including this thesis, for correcting my English style and grammar, and offering suggestions for improvement. I am also indebted to Dr. David Scriven for his detailed and constructive comments on my manuscripts, and for his broad computer knowledge, which he so generously shared.

I am deeply grateful to Dr. Ismail Laher for the many opportunities he provided to learn new techniques, meet people from the scientific community, and participate in various activities with members of his laboratory. Special thanks to Dr. Guy Lagaud for sharing his expertise in pressure myography with me, and for the opportunity to participate to his project.

I would like to thank Dr. Raymond Pederson and Jennifer Martin for providing the streptozotocin and help with the animal injections, and Dr.

Kenneth Baimbridge for the primary neuron cultures. I am also grateful to Dr. Christopher McIntosh for his critical reading of the manuscript presented in chapter 2 and valuable discussions. I would also like to thank all members of my Ph.D. committee, Dr. Pederson, Dr. Laher and Dr. McNeill, for guiding my work and providing me with valuable comments on my thesis. For their financial support, I thank the Heart and Stroke Foundation of British Columbia and the Yukon.

I would like to thank Tim Blanche from the Department of Ophthalmology, who provided technical and intellectual support in the development of techniques used to measure fluorescent glucose uptake in cells of the vascular wall. I would also like to thank Pauline Dan and Jodene Eldstrom for sharing with me their expertise and knowledge, for their help and friendship.

This thesis represents a significant scientific accomplishment in my life and has been made a lot easier by all the people who supported me and believed in me. I would like to thank my parents, Normand and Mariette for their unconditional love, encouragement and constant involvement in my life in spite of our geographical separation.

Finally, I thank Tim for sharing this adventure with me, for his inspiration, love and support, and for helping me be a better scientist and a better person.

Preamble

The prevalence of cardiovascular diseases, associated with coronary atherosclerosis, is eminent in diabetics, such that this population is more at risk for cardiovascular diseases than non-diabetics. This increased susceptibility to cardiovascular diseases in diabetic patients has been associated, amongst other risk factors, with early and poorly controlled elevated blood sugar levels. The endothelium, the first line of protection of the vascular wall, has been shown to be dysfunctional in persons with diabetes, an impairment attributed to glucose toxicity.

Despite a strong association between glucose toxicity and endothelial dysfunction, very little is known about glucose transport regulation in endothelial cells (ECs). A critical question remains; how and why does glucose accumulate in ECs?

The ultimate goal was to study the regulation of glucose transport in ECs of a whole vessel preparation because ECs and smooth muscle cells (SMCs) function as a unit and modulate each other's actions. The development of an experimental design and protocol that preserves this close structural relationship was therefore the objective of this study.

Over the course of this Ph.D. I have been given the opportunity to work in the laboratory of Dr. Ismael Laher in the Department of Pharmaceuticals and Therapeutics. In close collaboration with Dr. Guy Lagaud, a post-doctoral fellow, I learned different techniques for studying, *in vitro*, the physiology of small

contractile arteries. My work with Dr. Lagaud concerned the involvement of Ca^{2+}-sensitization mechanisms in the myogenic response of the rat cerebral arteries. This work was published in the American Journal of Physiology in 2002 (Lagaud *et al.*, 2002). Chapter 1 presents the parts of this published material, which I was involved with; the data collection, analyses and part of the redaction. Complementary data further to this work are also included in Chapter 1, and will be submitted for publication in the near future.

In the second part of this Ph.D., having acquired techniques for microdissection and isolation of blood vessels in Dr. Laher's laboratory, I undertook a study of glucose transport regulation in ECs of intact arteries of the rat. I succeeded in exposing the cells of interest by opening freshly dissected vessel longitudinally without damage to the endothelium. With this new approach, I investigated the expression and subcellular distribution of the different glucose transporter isoforms of the ECs using immunohistochemistry and fluorescence microscopy in Dr. Edwin Moore's laboratory in the Department of Physiology. This work is presented in Chapter 2 and was recently accepted for publication in Diabetologia.

In the third part of my Ph.D. I combined the *in vitro* techniques of pressure myography from Dr. Laher's laboratory with confocal fluorescence microscopy to measure, in real time, glucose uptake in individual ECs of the intact vascular wall. The use of a fluorescent glucose analog provided the ideal tool for studying glucose kinetics of individual cells in their native environment. Chapter 3 is a logical extension of chapter 2 in that it presents a preliminary assessment of the functionality of the transporter isoforms identified in intact coronary arteries. It also includes the initial experiments performed in cultured ECs as groundwork

for the ultimate experiments in whole vessels. This work will also shortly be submitted for publication.

Bonne lecture!

Chapter 1
Ca^{2+}-sensitization mechanisms in myogenic tone

1.1 Introduction

1.1.1 The contractile apparatus

A link between smooth muscle contraction and increased cytoplasmic calcium concentration was first established in 1965 (Filo *et al.*, 1965). The "sliding filament theory" originally exclusively attributed to skeletal muscle (Hill, 1970), was then found applicable to smooth muscle cells (SMCs). Skeletal muscle cells have cytoskeletal anchoring proteins composed of thick myosin-containing and thin actin / tropomyosin - containing filaments. These proteins are organized into repeating contractile units called sarcomeres and their alignment gives cardiac and skeletal muscle cells their characteristic striated appearances. SMCs lack this organized striation even though they also contain myofibrils comprising thick and thin filaments. These filaments are mostly, but not exclusively, aligned along the long axis of the cell, and allow shortening of the SMCs in more than one direction. The functional unit of the thick filament is a hexamer composed of two 205kDa myosin heavy chains, each of which has two myosin light chains (MLC), one of 20kDa (MLC_{20kDa}) and one of 17kDa (MLC_{17kDa}). Each heavy chain contains an amino-terminal 'head group' and a carboxyl-terminal 'tail'. Both 17 and 20kDa light chains bind to the heavy chains at the junction between the head and tail domains. The sites of adenosine triphosphate (ATP) hydrolysis and actin binding sites are located at the N-terminus of the heavy chain on the myosin head, and ATP hydrolysis is actin dependent. The N-terminus is also referred to

as the actin-activated Mg^{2+}-ATPase activity site (Allen and Walsh, 1994; Somlyo and Somlyo, 1994; Walsh *et al.*, 1995). For both skeletal and smooth muscle, contraction occurs by the formation and breakdown of cross-bridges between the myosin head and actin filaments. The affinity of myosin for actin increases upon hydrolysis of ATP to adenosine diphosphate (ADP). When ADP dissociates from the myosin head, it induces a conformational change leading to the sliding of the filaments. Subsequent binding of ATP to the myosin head reduces its affinity for actin, allowing it to detach in preparation for the formation of a new cross-bridge.

Dissimilarities in contractile regulatory mechanisms distinguish contraction in striated versus smooth muscles. Whereas in skeletal muscle Ca^{2+} binds to troponin to activate cross-bridge cycling, troponin is absent from smooth muscle. Indeed, in SMCs, Ca^{2+} binds to calmodulin (CaM), which activates myosin light chain kinase (MLCK), an enzyme responsible for myosin phosphorylation, and consequently activates cross-bridge cycling. The level of MLC_{20kDa} phosphorylation regulates the number of cross-bridges cycling and therefore the shortening velocity of smooth muscle (Murphy, 1976; Somlyo and Somlyo, 1976; Dillon *et al.*, 1981; Wingard *et al.*, 2001). Calcium is the main regulator of force development in skeletal muscle. A rise in intracellular calcium concentration ($[Ca^{2+}]_i$) induces a contraction, which is maintained until $[Ca^{2+}]_i$ is decreased. The excitation-contraction coupling process is comparatively simple in skeletal muscle. It involves a neuronal action potential inducing membrane depolarization, triggering Ca^{2+} release from the sarcoplasmic reticulum (SR). In SMCs, increased $[Ca^{2+}]_i$ is achieved through Ca^{2+} release from the SR and Ca^{2+} entry from the extracellular fluid, although sustained $[Ca^{2+}]_i$ is dependent on a

supply of extracellular Ca^{2+} (Dillon *et al.*, 1981). While skeletal muscle contraction is induced uniquely through electromechanical coupling, smooth muscle contraction also occurs independently of changes in membrane potential, also referred to as pharmacomechanical coupling.

1.1.2 Ca^{2+} regulation

Measurements of $[Ca^{2+}]_i$ following pharmacomechanical stimulus-induced contraction in smooth muscle revealed an intriguing discrepancy between $[Ca^{2+}]_i$ and tone maintenance (Morgan and Morgan, 1982). It soon became apparent that smooth muscle contraction occurred at surprisingly low levels of $[Ca^{2+}]_i$. During smooth muscle contraction, three types of Ca^{2+} profiles can be recorded. The most common, for example due to α-adrenergic receptor activation, involves peak Ca^{2+} increases during force development followed by a decline in $[Ca^{2+}]_i$ to near basal levels during force maintenance. A second profile is observed with KCl depolarization that produces parallel changes in $[Ca^{2+}]_i$ and force development. Finally, a third category of $[Ca^{2+}]_i$ changes is observed with agents such as prostaglandins which produce sustained levels of tone with small or undetectable changes in $[Ca^{2+}]_i$ (Morgan *et al.*, 1992).

From these observations, it has been concluded that smooth muscles have two phases of contraction. The first is associated with force development and involves a high rate of energy consumption while the second component occurs during tone maintenance and involves a slow rate of energy consumption. Murphy and coworkers in 1981 proposed the "Latch bridge hypothesis" in one of the first attempts to explain the mechanism of prolonged smooth muscle tone

(Murphy, 1976; Dillon *et al.*, 1981; Guth and Junge, 1982). The "latch bridge" refers to an attached, non-cycling or lower rate cycling cross-bridge maintaining force developed during contraction. This static cross-bridge is associated with low phosphorylation levels of MLC_{20kDa} concomitant with high force generation and a reduced contraction rate and ATP consumption. This capacity of smooth muscle to sustain contraction with low energy utilization is well served in the functioning of the airways of the lungs, coordinated contraction of the different layers of smooth muscle in the uritogenital system, the peristaltic movements of the gastrointestinal tract and the regulation of blood pressure by the vasculature where constant tone is required for prolonged periods.

At first glance, smooth muscle contraction is preceded by an increase in $[Ca^{2+}]_i$. Smooth muscle depolarization is the main stimulus for Ca^{2+} entry which occurs through voltage-gated Ca^{2+} channels (VGCC, L- and T-type), mechanical stretch that activates Ca^{2+}-permeable ion channels and stretch-activated cation channels (SAC). Other important pathways of Ca^{2+} entry involve ligand-gated Ca^{2+} channels (LGCC) and store operated Ca^{2+} entry mechanisms (SOC). LGCC encompass both P2X receptors (an ATP operated cation channel) and G-protein-coupled receptors. SOC involve indirect interaction between the SR and the plasma membrane. They are believed to be responsible, upon depletion of the internal store, for the activation of a Ca^{2+}-permeable cation conductance at the plasma membrane. Ca^{2+} induced Ca^{2+} release from the SR, mediated by inositol-1,4,5-triphosphate (IP_3) and ryanodine receptors (RyR), also contributes to the rise in $[Ca^{2+}]_i$, although to a lesser extent. RyR mediated Ca^{2+} release may also act as a negative feedback process leading to relaxation. Localized Ca^{2+} release by RyR, termed "Ca^{2+} sparks" activates Ca^{2+}-activated potassium (BK or K_{Ca})

channels in the vicinity of RyR. The efflux of K^+ mediated by K_{Ca} channel opening hyperpolarizes the cell membrane and thus closes VGCC (Patterson *et al.*, 2002) and reduces Ca^{2+} entry. A decrease in $[Ca^{2+}]_i$ leads to relaxation. Ca^{2+} extrusion mechanisms include the plasma membrane Ca^{2+}-ATPase pumps (PMCA) and the Na^+/Ca^{2+} exchanger using respectively ATP and Na^+ entry to move Ca^{2+} against the electrochemical gradient. Ca^{2+} store repletion by the sarcoplasmic reticulum Ca^{2+}-ATPase pump (SERCA) and mitochondrial Ca^{2+} uptake contribute to the decrease in $[Ca^{2+}]_i$ (Sanders, 2001).

Thus, mechanical stretch, autonomic nervous system stimuli, hormones, and various transmitters can trigger contraction. At high $[Ca^{2+}]_i$ (500-700nM), 4 molecules of Ca^{2+} bind to CaM and are believed to increase its affinity for the enzyme MLCK (Allen and Walsh, 1994; Walsh *et al.*, 1995; Horowitz *et al.*, 1996b). The activated Ca^{2+}(4)-CaM-MLCK complex catalyses the phosphorylation of the MLC_{20kDa} on residue Ser-19. Phosphorylated myosin binds to actin filaments with high affinity, permitting actin-dependent ATP hydrolysis. The resulting hydrolysis of ATP drives the sliding of myosin along the actin filaments and, hence, the contraction of the muscle. Following a decrease in $[Ca^{2+}]_i$, Ca^{2+} dissociates from CaM, inactivating MLCK and preventing further phosphorylation of MLC_{20kDa}. Myosin light chain phosphatase (MLCP) activity then dominates, dephosphorylating MLC_{20kDa}, reducing cross-bridge cycling and resulting in muscle relaxation (Allen and Walsh, 1994; Walsh *et al.*, 1995; Horowitz *et al.*, 1996b). Figure 1.1 summarizes the basic molecular aspects of contraction and relaxation in smooth muscle. A different model, wherein CaM remains associated with MLCK, has been proposed by Wilson et al. in 2002 (Wilson *et al.*, 2002) and was based on the earlier proposals by Kretsinger et al

(Persechini and Kretsinger, 1988; Kretsinger, 1992; Kawasaki *et al.*, 1998). In this model, CaM is bound to the contractile apparatus in the absence of Ca^{2+}. In response to a rise in $[Ca^{2+}]_i$, Ca^{2+} binds to CaM inducing a conformational change that activates MLCK (Van Lierop *et al.*, 2002; Wilson *et al.*, 2002). The basis of this proposal stemmed from experiments wherein purified CaM was add to a CaM-depleted permeabilized rat-tail arterial preparation in the absence of Ca^{2+}. Following a rapid washout of the unbound CaM, a Ca^{2+}-dependent contraction was observed, confirming that a pool of tightly bound CaM to the Triton-X-100 insoluble fraction supported the Ca^{2+}-dependent mediated contraction (Wilson *et al.*, 2002). Wilson et al. also suggested that MLCK was the myofilament component to which CaM bound. This proposed mechanism gives CaM a similar function as that assumed by troponin in skeletal muscle. More recently, Geguchadze et al., using a fluorescent biosensor and fluorescence resonance energy transfer (FRET) detection, found no evidence of CaM binding without activating MLCK at minimal $[Ca^{2+}]_i$ (Geguchadze *et al.*, 2004). As the FRET experiments were performed in transfected HEK-293 cell lines, these results may indicate that the Ca^{2+}-independent anchorage of CaM to MLCK is specific to contractile SMCs. On the other hand, it is possible that the CaM is permanently bound to a component of the myofilament in close proximity but not directly associated with MLCK. Further investigations will be required to determine the exact site of attachment of CaM (Wilson *et al.*, 2002).

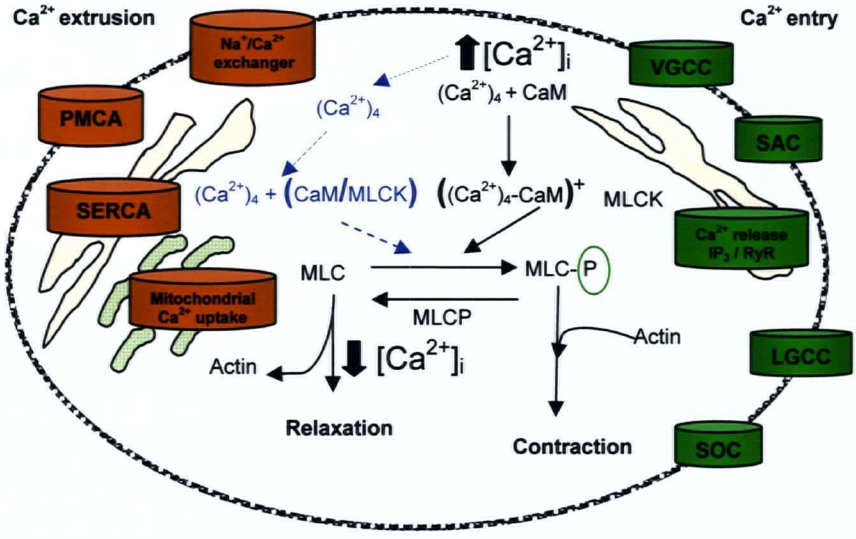

Figure 1.1 **Ca^{2+} regulation and Ca^{2+}-dependent contraction in SMCs.**
Increased cytoplasmic [Ca^{2+}] occurs mainly through Ca^{2+} release from the sarcoplasmic reticulum (SR) mediated by Inositol-1,4,5-triphosphate (IP_3) and ryanodine receptor (RyR) stimulation. Extracellular Ca^{2+} entering the cell also contributes to the increased $[Ca^{2+}]_i$. Ca^{2+} entry occurs through the activation of L-type and T-type voltage-gated Ca^{2+} channels(VGCC), ligand-gated Ca^{2+} channels (LGCC), stretch-activated cation channels (SAC) and also through store operated Ca^{2+} entry mechanisms (SOC). Following a rise in $[Ca^{2+}]_i$, 4 molecules of Ca^{2+} bind to CaM. The $(Ca^{2+})4$-CaM complex translocates to the contractile elements, binds and activates MLCK. In blue, new proposed models show CaM is already associated with the contractile elements. Ca^{2+} binds to CaM inducing a conformational change that activates MLCK. The activated $(Ca^{2+})4$-CaM-MLCK complex phosphorylates myosin light chain (MLC_{20kDa}) and initiates cross-bridge cycling. Ca^{2+} extrusion from the cell occurs through the Na^+/Ca^{2+} exchanger and plasma membrane Ca^{2+}-ATPase pump (PMCA). The sarcoplasmic reticulum Ca^{2+}-ATPase pump (SERCA) and mitochondrial Ca^{2+} uptake contributes to the extrusion of Ca^{2+} from the cytoplasm. A lower $[Ca^{2+}]_i$ deactivates the $(Ca^{2+})4$-CaM-Kinase complex and reduces the rate of MLC_{20kDa} phosphorylation. Dephosphorylation of MLC_{20kDa} by myosin light chain phosphatase (MLCP) induces relaxation.

1.1.3 Ca^{2+} sensitization

Typically, force generation by SMC involves a rapid rise in $[Ca^{2+}]_i$. During sustained contraction, this fast elevation in $[Ca^{2+}]_i$ gradually fades so that levels remain only slightly above resting values in order to maintain the force

developed. Ligands binding to α1-adrenergic and muscarinic G-protein coupled receptors can, under some conditions, induce contraction without any apparent changes in $[Ca^{2+}]_i$ (Morgan and Morgan, 1982; Somlyo and Somlyo, 1994), also suggesting the existence of modulatory mechanisms increasing Ca^{2+} sensitivity of the contractile apparatus.

The increased Ca^{2+} sensitivity occurring during sustained contraction is associated with MLCP inhibition (Kitazawa *et al.*, 1991; Somlyo and Somlyo, 2000). MLCP is composed of three subunits, a catalytic subunit (37kDa, PP-1C), a regulatory subunit or myosin binding site (MBS) or myosin phosphatase target 1 (MYPT1) subunit (110-130kDa) and a subunit of unknown function (20kDa) (Allen and Walsh, 1994; Fukata *et al.*, 2001). When the MBS subunit is phosphorylated on residue Thr-695, MLCP is prevented from binding to and dephosphorylating MLC_{20kDa}, so that contraction is prolonged. Potential modulators of MLCP activity have been identified. Signalling molecules including RhoA/Rho-associated kinase (Uehata *et al.*, 1997; Fukata *et al.*, 2001), protein kinase C (PKC) and arachidonic acid (AA) inactivate MLCP and cause sustained contraction at lower $[Ca^{2+}]_i$ (Fu *et al.*, 1998; Solaro, 2000; Somlyo and Somlyo, 2000). The phosphorylation of MYPT subunit is associated with its translocation to the plasma membrane. As shown by Shin et al., MLCP translocates to the plasma membrane upon agonist stimulation, where catalytic and targeting MYPT subunits dissociate when phosphorylated by Rho-kinase (Shin *et al.*, 2002). Thus, Ca^{2+}-sensitization is a result of MLCP inhibition and the consequent increase in MLC phosphorylation.

1.1.4 PKC

PKC was first discovered by Nishizuka in 1977 (Inoue *et al.*, 1977; Takai *et al.*, 1977). PKC with its 10 isoforms constitute the largest family of serine/threonine specific kinases (Webb *et al.*, 2000). Ligands stimulating Gαq activate three main phospholipid groups. Phosphoinositide-specific phospholipase C (PI-PLC) catalyses the formation of the second messengers IP_3 and 1,2, -diacylglycerol (DAG) through the hydrolysis of phosphatidylinositol 4,5,- diphosphate (PIP_2). IP_3 promotes Ca^{2+} release from the sarcoplasmic SR while DAG is a potent activator of PKC (Andrea and Walsh, 1992). Phosphatidylcholine-specific phospholipases C (PC-PLC) and D (PC-PLD) are also activated upon ligand binding to G-protein coupled receptors. PC-PLC and PC-PLD generate only DAG upon hydrolysis and are therefore more likely to be involved in Ca^{2+}-independent mechanisms. DAG promotes the translocation of inactive PKC from the cytosol to the plasma membrane where it becomes activated, as shown in Figure 1.2. PKC can also be activated by arachidonic, linoleic, and oleic acids (Webb *et al.*, 2000). Since activated PKC is thought to be a membrane-associated protein, its access to contractile proteins would be limited. One suggested mechanism by which activated PKC could physically interact with the contractile apparatus is through calpain hydrolysis. PKC is proteolytically cleaved by calpain to release its catalytic subunit, protein kinase M (PKM) that can phosphorylate proteins in the cytosol (Tapley and Murray, 1984; Pontremoli *et al.*, 1990).

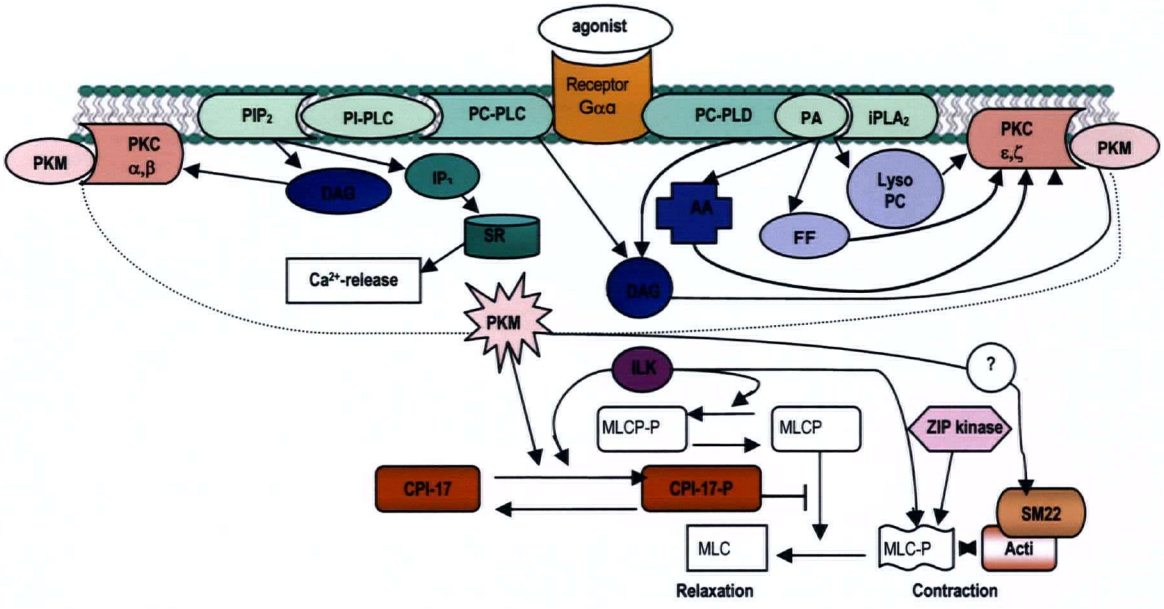

Figure 1.2 **Ca^{2+}-dependent and Ca^{2+}-independent activation of PKC.**
Activation of phosphoinositide-specific-phospholipase C (PI-PLC) and not phosphatidylcholine-specific-phospholipase C (PC-PLC) and phosphatidylcholine-specific-phospholipase D (PC-PLD) lead to Ca^{2+} release. Therefore Ca^{2+}-independent isoforms of PKC are more likely to be activated through the PC-PLC and PC-PLD pathways. Both phosphatidic acid (PA) and phosphatidylinositol-4,5-biphosphate (PIP_2) produce 1,2-diacylglycerol (DAG), which in turn activates PKC. PIP_2 also generates IP_3 leading to Ca^{2+} release from the SR. Other known activators of PKC are AA and $iPLA_2$ through free fatty acid (FFA) and the lysophospholipid choline (Lyso PC). PKC activation induces the release of its catalytic subunit, protein kinase M (PKM). PKM phosphorylates CPI-17 leading to inhibition of MLCP. PKM is also believed to phosphorylate a smooth muscle specific protein of 22kDa (SM22) but its functional role is still undetermined. Integrin-linked-kinase (ILK) induces Ca^{2+}-independent contraction through CPI-17, inhibition of MLCP and direct phosphorylation of MLC. MLC is also phosphorylated by Zip-kinase in a Ca^{2+}-independent manner.

Comparable force generation is correlated with the levels of MLC_{20KDa} phosphorylation in both intact and skinned smooth muscle preparations. Changes in Ca^{2+}-sensitivity induced by PKC activators occur in both intact and α-toxin permeabilised smooth muscle preparations (Weber *et al.*, 1999). However, force produced by α-adrenergic agonists is lower in skinned preparations, possibly due to the disruption of a PKC-dependent signal pathway that usually

leads to MLCP inhibition. Evidence for this comes from biochemical analysis of Triton-X100-treated rat-tail arterial smooth muscles. In these preparations, the content of PKC α, β, ζ and CPI-17 (see below) is significantly decreased, while other proteins such as calponin, caldesmon, MLCK and PP1m seem to be retained (Kitazawa *et al.*, 1999; Weber *et al.*, 2000).

Recent studies implicate an important regulatory role for caveolin in PKCα and RhoA translocation from the cytosol to the plasma membrane. Using a peptide capable of interacting with the caveolin-1 scaffolding domain (the site of interaction with signalling molecules), Taggart et al. were able to inhibit carbachol-induced translocation of PKCα and RhoA in rat uterine smooth muscle (Taggart *et al.*, 2000). Moreover, caveolin-1 knockout mice have decreased responses to angiotensin II, endothelin-1, and phorbol ester (Drab *et al.*, 2001).

Force generation in smooth muscle can occur at very low levels of $[Ca^{2+}]_i$ (Katsuyama and Morgan, 1993; Weber *et al.*, 1999). MLCK seems to be the kinase responsible for MLC phosphorylation; however, because of its considerably reduced activity at low $[Ca^{2+}]_i$, its singular activity cannot entirely explain the force generated and the amount of MLCK phosphorylated during sustained contraction maintained at low $[Ca^{2+}]_i$ (Somlyo and Somlyo, 2003). Ligand binding to G-protein coupled receptors activates PC-PLC or PC-PLD, generating DAG, which in turn activates Ca^{2+}-independent isoforms of PKC. Both PKCε and PKCζ have been identified in vascular smooth muscles (Horowitz *et al.*, 1996a; Throckmorton *et al.*, 1998). In saponin-permeabilized single ferret aortic SMCs, the application of a constitutively active form of PKCε (and not PKCζ) stimulates contraction independently of MLC_{20KDa} phosphorylation and extracellular $[Ca^{2+}]_i$

(Horowitz *et al.*, 1996a). Moreover, phorbol esters activate PKCε but not PKCζ while phenylephrine induces PKCε translocation from the cytosol to the plasma membrane and PKCζ translocation from perinuclear localization to the interior of the nucleus. Thus, PKCε has been suggested as the isoform responsible for Ca^{2+}-independent regulation of vascular tone.

Both MLC_{20KDa} and MLCK are potential targets for PKC. PKC catalyses the phosphorylation of serine 1, 2 and threonine 9 of MLC_{20KDa}, however phosphorylation at these residues results in either no effect or a 50% reduction of the actomyosin ATPase activity (Nishikawa *et al.*, 1983; Ikebe *et al.*, 1985). Furthermore, phosphorylation of MLCK by PKC decreases its affinity for Ca^{2+}-CaM, thus indirectly reducing MLC_{20KDa} phosphorylation at serine 19 (Ikebe *et al.*, 1985; Nishikawa *et al.*, 1985). Therefore, the role of PKC in Ca^{2+}-sensitization cannot be attributed to a direct interaction with MLC_{20KDa} or MLCK since phosphorylation of the targeted sites by PKC is more likely to result in relaxation rather than a sustained contraction (Umemoto *et al.*, 1989; Andrea and Walsh, 1992; Webb *et al.*, 2000).

PKC can enhance contraction by indirectly inhibiting MLCP activity. CPI-17 is a novel, 17kDa, smooth muscle specific inhibitor of protein phosphatase-1 that has been identified as a PKC substrate. In its phosphorylated form, CPI-17 inhibits the catalytic subunit of MLCP (Somlyo and Somlyo, 2000; Fukata *et al.*, 2001). In the presence of both PKCα and CPI-17, MLC_{20KDa} phosphorylation is increased and contraction maintained at constant $[Ca^{2+}]_i$ (Kitazawa *et al.*, 1999). CPI-17 phosphorylation is increased in response to receptor-mediated stimulation (histamine and phenylephrine) but not following K^+ depolarization.

Levels of CPI-17 phosphorylation are reduced when arteries are incubated with inhibitors of Rho-kinase and PKC (Kitazawa *et al.*, 2000; Fukata *et al.*, 2001). Muscarinic receptor (m3) activating signalling pathways through Rho-kinase and PKC may act cooperatively in order to inhibit MLCP activity and induce a sustained contraction (Murthy *et al.*, 2003). Recent reports have identified SM22 as a potential substrate of PKC. SM22 is an abundant smooth muscle specific protein of 22KDa, which may bind to actin, however, at this time its physiological function is not known (Morgan and Gangopadhyay, 2001).

Other possible substrates of PKCε are the smooth muscle specific thin filament associated proteins calponin and caldesmon (Horowitz *et al.*, 1996a). Caldesmon phosphorylation as well as myristoylated, alanine-rich C-kinase substrate (MARCKS) phosphorylation have been observed following phorbol 12,13-dibutyrate (PDBu) stimulation of bovine carotid arterial smooth muscles (Throckmorton *et al.*, 1998). Unphosphorylated caldesmon and calponin are both associated with actin and act as inhibitors of cross-bridges cycling activity. Upon phosphorylation, their affinity for actin is decreased and cross-bridge cycling activity restored. Their phosphorylation may contribute to the development of force induce by Ca^{2+}-independent PKC isoform.

1.1.5 Rho-associated kinase

Agonists binding to both Gα12/13 (Gohla *et al.*, 2000) and Gαq (Chikumi *et al.*, 2002) protein-coupled receptors induce the dissociation of heterotrimeric G protein complexes, allowing the activation of the small monomeric G protein, RhoA. Endogenous activators of RhoA include growth factors, cytokines,

integrins, and hormones such as bradykinin and lysophosphatidic acid (Van Aelst and D'Souza-Schorey, 1997; Hall, 1998). The activation of RhoA is believed to induce its translocation to the plasma membrane. The translocation of a GFP-tagged RhoA from the cytosol to the plasma membrane, upon agonist stimulation, has been demonstrated in porcine tracheal smooth muscles by Miyazaki et al. (Miyazaki *et al.*, 2002). This translocation of the GFP-tagged RhoA coincides with increased myosin phosphorylation and sustained contraction (Miyazaki *et al.*, 2002). In the cytosol, RhoA is present in a complex with a guanosine diphosphate (GDP) and a Rho-guanine nucleotide dissociation inhibitor (Rho-GDI). Activation of a RhoA-guanine nucleotide exchanger factor (RhoA-GEF) by the Gα-subunit leads to the dissociation of GDP and subsequent formation of a RhoA-guanosine triphosphate (RhoA-GTP) complex. RhoA-GTP translocates to the plasma membrane and activates a serine/threonine kinase termed Rho-kinase (Somlyo and Somlyo, 2000). Activated Rho-kinase phosphorylates and inactivates the regulatory subunit of MLCP independently of changes in the Ca^{2+}-CaM-MLCK pathway (Kureishi *et al.*, 1997; Uehata *et al.*, 1997; Iizuka *et al.*, 1999; Solaro, 2000; Somlyo and Somlyo, 2000; Sward *et al.*, 2000; Fukata *et al.*, 2001).

Two indirect mechanisms linking Rho-kinase to the inhibition of MLCP have been proposed. In the first instance, CPI-17, when phosphorylated by Rho-kinase on residue Thr-38, blocks the activity of MLCP (Koyama *et al.*, 2000). A second and more recently proposed player, a MYPT1-associated kinase (M110 kinase), referred to as zipper-interacting protein (ZIP)-like kinase, phosphorylates MLCP at its inhibitory site (MacDonald *et al.*, 2001). MacDonald et al. suggest that ZIP-like kinase may play a role of intermediate in the

inhibition of MCLP by Rho-kinase. Despite the lack of a direct phosphorylation of ZIP-like kinase by Rho-kinase, the authors suggest that a link between the two kinases is present since the activation of ZIP-like kinase is inhibited by Y-27632 (Rho-kinase inhibitor) in vivo. Thus, ZIP-like kinase is a putative candidate linking the plasma membrane Rho-kinase and MLCP associated with the contractile apparatus (MacDonald *et al.*, 2001) see Figure 1.3.

Rho-kinase is also modulated by several intracellular molecules and pathways. AA, produced by PLC activation subsequent to receptor binding to $G\alpha q$, also induces Ca^{2+} sensitization in vitro. Formation of AA by phospholipase A_2 ($_iPLA_2$) is Ca^{2+}-independent in smooth muscles (Guo *et al.*, 2003). AA inhibits MLCP either by directly activating Rho-kinase or by causing the dissociation of MBS from the catalytic subunit of MLCP, so reducing its activity (Somlyo and Somlyo, 2000; Fukata *et al.*, 2001). The activation of Rho-kinase by AA is produced by the binding of AA to its c-terminus that acts as an inhibitory site. The release of the autoinhibitory site from the catalytic unit containing the RhoA binding site, leads to activation of Rho-kinase (Araki *et al.*, 2001).

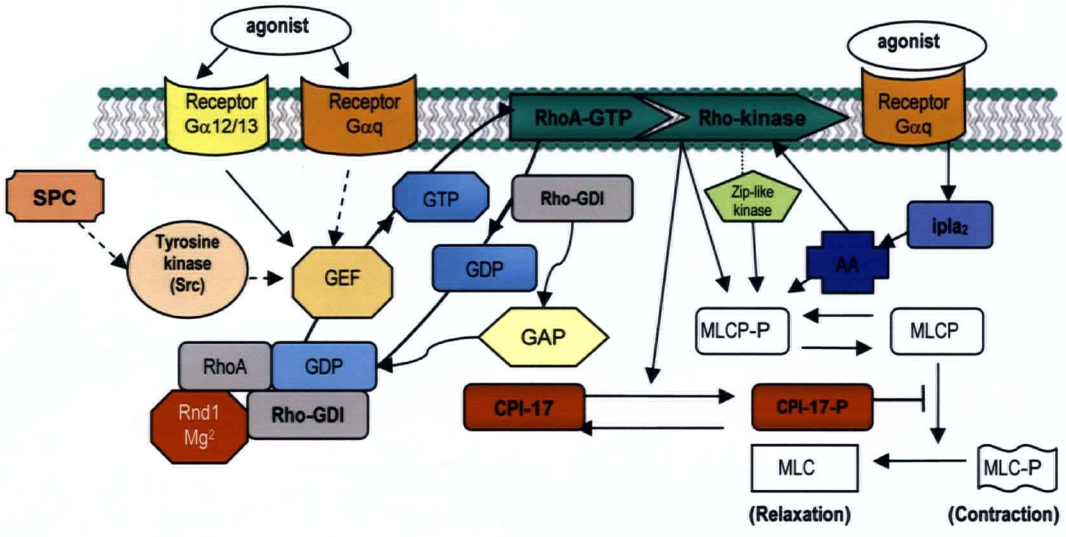

Figure 1.3 **Ca^{2+}-sensitization mechanisms in smooth muscle contraction.**
RhoA is located in the cytosol and is associated with guanosine diphosphate (GDP) and guanine nucleotide dissociation inhibitor (GDI) molecules. The RhoA/Rho-kinase pathway is activated by ligand binding to G-protein coupled receptors (Gα12/13 and Gαq)). RhoA dissociation from GDP is activated by Rho guanine nucleotide exchanger factors (GEF). Sphingosylphosphorylcholine (SPC) acting through the Src family of tyrosine kinase also stimulates GEF. The reverse reaction is catalyzed by a GTPase-activating protein (GAP). Rho-guanosine triphosphate (Rho-GTP) is translocated to the plasma membrane and activates Rho-kinase. Rho-kinase inhibits MLCP through direct phosphorylation and by activating a novel zipper-interacting protein (zip)-like kinase. PKC targeted protein phosphatase-1 inhibitor of 17kDa (CPI-17) is phosphorylated by both PKC and Rho-kinase and in turn inhibits MLCP activity. Arachidonic acid (AA),a product of the Ca^{2+}-independent phospholipase A_2 isoform ($_iPLA_2$), also inhibits MLCP directly and indirectly by activating Rho-kinase. Rnd1 and Mg^{2+} prevent the translocation of RhoA to the plasma membrane and therefore play an important role in vascular relaxation and associated pathologies.

A newly identified member of the Rho family, Rnd1, which is constitutively bound to GTP, regulates the RhoA/Rho kinase pathway (Loirand *et al.*, 1999). Rnd1 is able to prevent Ca^{2+} sensitization induced by carbachol or GTPγS (a non-hydrolysable GTP analogue). It is thought that Rnd1 is able to

interact directly with RhoA without targeting MLCK or MLCP (Loirand *et al.*, 1999). Rnd1 expression in smooth muscles is increased by sex hormones such as estrogen and progesterone (Loirand *et al.*, 1999). These steroid hormones also decrease vascular contractile activity by stimulating the production of NO (Mendelsohn and Karas, 1999; Mendelsohn, 2000; Varbiro *et al.*, 2000). Accordingly, Rnd1 as part of the RhoA-Rho-kinase pathway may also play an important role in the protective cardiovascular effects induced by steroid hormones. Mg^{2+} can also regulate RhoA activation. At normal concentrations, Mg^{2+} reinforces the GDP-RhoA binding interaction, decreasing the dissociation rate, and therefore reducing the activation of RhoA. Moreover, a low $[Mg^{2+}]_i$ increases the activity of GEF allowing an increased formation of Rho-GTP and activation of Rho-kinase (Maesaki *et al.*, 1999; Shimizu *et al.*, 2000; Zhang *et al.*, 2000). Some studies have linked hypomagnesaemia with hypertension (Kawano *et al.*, 1998), leading to a possible role for Mg^{2+} related RhoA/Rho-kinase activity in the pathogenesis of hypertension.

An additional activator of Rho-kinase is sphingosylphosphorylcholine (SPC), a product of deacylation of spingomyelin, which is the most abundant lipid in the cell membrane. Sphingosylphosphorylcholine is able to increase the Ca^{2+} sensitivity of the contractile apparatus, an effect that is blunted by Y-27632 (Todoroki-Ikeda *et al.*, 2000; Shirao *et al.*, 2002). Shirao et al. have also demonstrated in primary cultures of SMCs that SPC induces translocation of cytosolic Rho-kinase to the plasma membrane (Shirao *et al.*, 2002). Thus, it would appear that SPC is an endogenous activator of Rho-kinase during Ca^{2+}-independent smooth muscle contraction, although its production and temporal relationship to Ca^{2+} sensitization has yet to be confirmed.

More recently, Sakurada et al. have shown a novel pathway of activation for RhoA and Rho-kinase in vascular smooth muscle. They demonstrate that both high KCl and receptor agonist stimulation induce Ca^{2+}-dependent RhoA-Rho-kinase mediated contraction (Sakurada *et al.*, 2003). Noradrenaline and KCl induced a contraction that was accompanied with a 4 to 5 fold increase in the GTP-bound form of RhoA. The removal of extracellular Ca^{2+} abolished both the contraction and RhoA stimulation. The use of Rho-kinase inhibitors also implicated Rho-kinase in this process. Both Y-27632 and HA1077 suppressed (by 60 to 70%) noradrenaline and KCl induced contraction and inhibited MLC phosphorylation. Similar observations with the thromboxane A_2 mimetic U46619, a receptor agonist which like noradrenaline activates PLC to mobilise Ca^{2+} from the SR, suggest that $G\alpha q$ mediates the Ca^{2+}-dependent RhoA/Rho-kinase activation (Sakurada *et al.*, 2003). Thus, Ca^{2+} is likely playing an active role in Ca^{2+}-sensitization in concert with other Ca^{2+}-independent mechanisms. Further investigation will be needed to determine which Ca^{2+}-dependent signalling molecules are involved in the activation of the RhoA/Rho-kinase pathway.

1.1.6 Myogenic tone

In the absence of neuronal, chemical, and hormonal stimulation, the small arteries of the circulation exist in a state of partial constriction. The intrinsic tone is produced in response to transmural pressure, a phenomenon first described in 1902 by Bayliss and referred to as myogenic tone (Bayliss, 1902). A myogenic response has been observed in a wide variety of small arteries and arterioles from different vascular beds and its strength has been shown to be dependent on the diameter of the vessel. The strongest myogenic response has been recorded

from vessels of intermediate diameter (Davis, 1993). Differences in the strength of the myogenic response are also found between vascular beds. For example, cerebral (Lagaud *et al.*, 1999) and skeletal muscle arteries (Watanabe *et al.*, 1993) have a stronger myogenic response than mesenteric arteries of a similar diameter. The main purpose of such inherent contractile ability of the vascular smooth muscle is attributed to the maintenance of a basal level of vascular tone but it also contributes to the autoregulation of blood flow. In order to meet metabolic requirements, regional vasoactive factors (nitric oxide, metabolite accumulation, pH changes, constrictor and dilator mechanisms) modulate the underlying basal constriction of resistance arteries and thus reduce or enhance the perfusion of organs, muscles and tissues, independently of each other (Davis and Hill, 1999). The basal tone of resistance arteries contributes substantially to the total peripheral resistance encountered by the heart and is therefore one of the factors that determines the systemic blood pressure. It is only since the development of the pressure myograph in 1984 that the properties and characteristics of the myogenic tone have been systematically studied (Halpern *et al.*, 1984). It is therefore not surprising that a great deal of effort is still underway aimed at understanding the mechanisms of myogenic tone.

1.1.7 Signalling mechanisms in myogenic tone

The initiation of the myogenic response is triggered by an increase in the intraluminal pressure. It has been suggested that the increase in pressure stretches the vascular smooth muscles, altering the vessel wall tension. The wall tension (T) can be calculated from the Laplace relation ($T = P \times r$), where P is the intraluminal pressure and r the vessel radius. Experiments with bat wing and cat

mesenteric arteries have demonstrated that as P increases, the radius of the vessel is adjusted in order to keep T constant (Johnson, 1989). Subsequent observations established a correlation between the vascular wall tension and the level of both $[Ca^{2+}]_i$ and MLC phosphorylation (Zou *et al.*, 1995), providing strong evidence that the wall tension acts as the mechanostimulus in the myogenic response.

The theory of mechanotransduction implies that a sensor element is responsible for transducing changes in wall tension to constriction of the vessel via intracellular signalling pathways. The site and nature of this sensor element remains to be identified. Growing evidence suggests that a group of adhesion molecules, the integrins, play a central role in this mechanotransduction mechanism. The emergent interest in the integrins comes from the mechanical link they form between the extracellular matrix and the cytoskeleton. External stress on the integrins directly affects the cytoskeleton of the cell, activating intracellular signalling and more importantly induces the phosphorylation of proteins associated with the cytoskeleton (Davis *et al.*, 2001; Martinez-Lemus *et al.*, 2003). Despite that, integrins, through their molecular function, represent the ideal sensor element; there is still little direct evidence of their participation in the myogenic response.

Previous work has shown that synthetic peptides containing amino acid sequences specific to the $\alpha v\beta_3$-integrins induce a vasodilation in myogenically active rat cremaster arterioles (Mogford *et al.*, 1996). This vasodilation was inhibited by antibodies targeting the β_3 subunit of the integrins (Pierschbacher and Ruoslahti, 1987; Mogford *et al.*, 1996). Conversely, the activation of $\alpha_5\beta_1$

(Mogford *et al.*, 1997) and $\alpha_4\beta_1$ (Waitkus-Edwards *et al.*, 2002) integrins enhance the myogenic response. Although these findings support a role for the integrins in the myogenic response, they also indicate that multiple integrins and downstream intracellular pathways may be involved. The integrins have also been associated with the regulation of $[Ca^{2+}]_i$ (D'Angelo *et al.*, 1997b). The binding of appropriate ligands to the integrins can initiate Ca^{2+} entry into SMCs (Xie *et al.*, 1998), an essential event in the generation of a myogenic response. Recently proposed mechanisms implicate the modulation of L-type VGCC by the integrin ligands (Martinez-Lemus *et al.*, 2003).

The integrins may also modulate the myogenic tone through collaboration with the cytoskeleton (Davis *et al.*, 2001). The integrins are located at a site of assemblage for several components of the cytoskeleton. The compressible and elastic structural components of the cytoskeleton are a potential mechanical stress sensor itself. Thus, mechanical strain has been shown to induce a reorganisation of the cytoskeleton elements (Smith *et al.*, 1997), providing evidence for the active participation of the cytoskeleton in response to external mechanical stress. Moreover, depolymerization of the microtubules has been shown to enhance contractility in response to agonist stimulation (Leite and Webb, 1998; Paul *et al.*, 2000).

Downstream targets of the interaction between the extracellular matrix and the integrins are also potential modulators of myogenic tone. Several non-receptor protein kinases; focal adhesion kinase (FAK), MAPK and other signalling proteins such as members of the Rho family of small GTPases are recruited to the plasma membrane and produce Ca^{2+}-dependent and Ca^{2+}-

sensitization signalling mechanisms in response to mechanical stress. The integrins link these cytoskeleton anchored cascades of kinases with the extracellular matrix (Hall, 1998; Karandikar and Cobb, 1999), again adding to the evidence that integrins are potentially the site of initiation of mechanical stressed induced myogenic tone. Further investigations are needed to clarify the mechanism of action of the integrins but to this day, they remain the most plausible candidates to fulfill the role of a sensor element in the signal transduction pathway in the myogenic response.

As in conventional SMC contraction, the myogenic response is largely dependent on Ca^{2+}-entry to induce MLC phosphorylation and the eventual vasoconstriction. The removal of extracellular Ca^{2+} abolishes the development of myogenic tone (Uchida and Bohr, 1969, Osol, 1985 #622; McCarron *et al.*, 1989; Kuo *et al.*, 1990). Furthermore, the loss of myogenic tone observed with the use of inhibitors of VGCC (Knot and Nelson, 1995; Setoguchi *et al.*, 1997), major contributors of Ca^{2+}-entry in SMC, re-enforces the general agreement that extracellular Ca^{2+} is critical to the maintenance of myogenic tone.

Numerous studies have also established that an increase in transmural pressure induces a vascular SMC depolarization (Harder, 1984; Harder *et al.*, 1985; Harder *et al.*, 1987; Knot and Nelson, 1995; Wesselman *et al.*, 1997; Knot and Nelson, 1998). The proposed signalling events leading to SMC membrane depolarization include the activation of the SAC, Cl^- channel, K_{Ca} channel intracellular Ca^{2+} store and AA pathway.

A hypothetical pathway, involving SAC channel, suggest that the activation of inward current of Na^+, K^+, and Ca^{2+} is induced by a stretch deformation of the SMCs (Kirber *et al.*, 1988; Davis *et al.*, 1992; Setoguchi *et al.*, 1997; Wu and Davis, 2001). While the Ca^{2+} entry could itself generate the contraction, the influx of cations is more likely to produce a membrane depolarization and the subsequent activation of the L-type VGCC, increasing the influx of Ca^{2+}. In agreement with this sequence of events, the inhibition of L-type VGCC prevents the myogenic response without affecting the stress-induced depolarization (Knot and Nelson, 1995). The importance of SAC in the development of myogenic tone is however questionable. First, VGCC and K_{Ca} channels are also activated by increased intraluminal pressure. Secondly, the demonstration of SAC activation was performed only in single isolated SMC using a variant of the patch clamping technique to induce a stretch or pressure stimulus, neither of which is likely to mimic the wall tension changes produced in the myogenic response. A specific blocker for the SAC would provide direct evidence of such mechanisms in a whole vessel preparation (Schubert and Mulvany, 1999), but unfortunately, one does not exist. Nevertheless, recent evidence implicates the activation of transient receptor potential 6 (Trp6) channel in response to mechanotransduction mechanism in resistance arteries. It was demonstrated that pressure induced depolarization and myogenic constriction were both reduced by the use of antisense RNA for the Trp channel 6 (Welsh *et al.*, 2002). These Trp channels 6, which exhibit biophysical properties similar to that of the cation current found in vascular SMCs, may therefore represent an important modulator of the myogenic tone.

In addition, Cl^- channel activation has also been suggested to participate in the membrane depolarization following pressure-induced myogenic tone (Nelson *et al.*, 1997). The opening of Cl^- channels and consequent efflux of Cl^- could potentially cause the membrane depolarization induced by an increase in transmural pressure. Despite the presence of volume-regulated Cl^- channel in the vascular SMCs, the lack of a specific inhibitor for this channel and controversy existing, for the moment, regarding the occurrence of a concomitant cation current, prevents a clear understanding of the role of the Cl^- channel in the regulation of the myogenic tone (Welsh *et al.*, 2000).

The increase in $[Ca^{2+}]_i$, due to the activation of VGCC is theorized to enhance the frequency of Ca^{2+} released events mediated by RyR (Ca^{2+} sparks), and activates in turn the K_{Ca} channels. The efflux of K^+ mediated by the opening of K_{Ca} channels, hyperpolarizes the cell membrane and thus closes the VGCC (Patterson *et al.*, 2002) and reduces Ca^{2+} influx. This activation of K_{Ca} channels is thought to be a negative feedback mechanism regulating SMC membrane depolarization and myogenic tone (Brayden and Nelson, 1992; Knot and Nelson, 1995). Ca^{2+} sparks have also been closely associated with the synchronised opening of groups of K_{Ca} channel producing spontaneous transient outward currents (STOCs). In coronary artery, these STOCs have been shown to occur following stretch-activated membrane depolarization (Wu and Davis, 2001). This feedback mechanism is thought to protect the cells from excess Ca^{2+}-entry and limit the degree of contraction. More recently, a decrease in the sensitivity of the K_{Ca}, induced by the deletion of its β_1-subunit, has been shown to impair the coupling between Ca^{2+} sparks and the activation of K_{Ca} channel, consequently increasing arterial tone and blood pressure (Brenner *et al.*, 2000). Therefore, the

regulation of K_{Ca} channel sensitivity to STOCs is likely to play a key role in the development of hypertension.

In SMCs, one of the functions of the SR is to the regulate Ca^{2+}-entry. This is based on the observation that when the SR is empty, Ca^{2+} influx is mobilised primarily to replenish the SR store and only subsequently becomes available to the contractile machinery. After restoration, the SR emits sequential vectorial release of Ca^{2+} regulating the membrane depolarization and thus the opening of the VGCC and level of Ca^{2+}-entry. This regulating pathway has been described by Van Breemen and referred to as the superficial buffer-barrier theory (van Breemen *et al.*, 1995). Its implication in the myogenic response has yet to be directly demonstrated. Further evidence implicating Ca^{2+}-induced Ca^{2+}-release in myogenic tone comes from studies showing that the depletion of intracellular Ca^{2+}-store with ryanodine and the inhibition of SR Ca^{2+}-ATPase pump, both enhanced the myogenic response (Watanabe *et al.*, 1993). Ca^{2+}-entry is closely associated with the degree of emptying of the SR, and is thought to rely on a physical coupling between the SR and plasma membrane Ca^{2+} channel or the release of messengers enhancing Ca^{2+} influx. The influx in Ca^{2+} induced by the depleted store of the SR are referred to as capacitative Ca^{2+}- entry or store-mediated Ca^{2+} entry mechanisms. Evidence, of such opening of non-selective cation channels following Ca^{2+}-store depletion have been found in resistance arteries (Trepakova *et al.*, 2000; Trepakova *et al.*, 2001). The activation of such non-selective cation channel produces a membrane depolarization responsible for the stimulation of VGCC and subsequent Ca^{2+}-entry. The channel responsible for the capacitative Ca^{2+}-entry current has yet to be identified but is thought to be derived from the Trp channel gene family.

Growing evidence indicates the participation of several intracellular second messengers in the myogenic response. Inhibitors of tyrosine kinase, tyrosine phosphatase (Masumoto *et al.*, 1997), G protein (Osol *et al.*, 1993), $_{i}PLA_2$ (Kauser *et al.*, 1991), PLC (Osol *et al.*, 1993) and cytochrome P-450 (Kauser *et al.*, 1991), have all been shown to modulate, to some extent, the myogenic response.

The activation of PLA and PLC liberates AA. The latter can be metabolized by the enzyme P-450 4A to form 20-hydroxyeicosatetraenoic acid (20-HETE) (Imig *et al.*, 1996). 20-HETE induces vasoconstriction accompanied with depolarization. Moreover, 20-HETE is a potent inhibitor of K_{Ca}, and may therefore induce membrane depolarization by inhibiting the K^+ outward current in SMCs (Ma *et al.*, 1993). The inhibition of K_{Ca} by 20-HETE has been suggested to be mediated by PKC activation (Lange *et al.*, 1997). More recently, 20-HETE induced contraction has also been associated with the increased activation of Rho-kinase (Randriamboavonjy *et al.*, 2003).

Inhibitors of PLC such as U-73122 abolish myogenic tone. In accordance with the involvement of PLC activation in myogenic response, increased levels of IP_3 and DAG have been measured in response to step increases in transmural pressure (Narayanan *et al.*, 1994). A role for IP_3 in myogenic tone has yet to be demonstrated, however, DAG is a potent activator of PKC, which may be associated with Ca^{2+}-sensitization mechanisms.

1.1.8 Ca^{2+}-sensitization in myogenic tone

In addition to depolarization induced Ca^{2+}-entry via L-type VGCC, previous studies have indicated the participation of other regulatory mechanisms in the myogenic response. As pressure-induced constriction produces greater change in the arterial diameter to $[Ca^{2+}]_i$ ratio than does KCl-induced depolarization, the involvement of Ca^{2+}-sensitization pathways in the mechanism of myogenic tone has been suggested (Laporte *et al.*, 1994; D'Angelo *et al.*, 1997a; VanBavel *et al.*, 1998; Dessy *et al.*, 2000; Lagaud *et al.*, 2002; Yeon *et al.*, 2002). PKC as well as Rho-kinase are potential regulators of sustained myogenic tone (Lagaud *et al.*, 2002; Yeon *et al.*, 2002). Specific activators (phorbol-ester, indolactam) of PKC enhance the myogenic response while inhibitors (staurosporine, calphostin C) reduce it (Hill *et al.*, 1990; Osol *et al.*, 1991; Laporte *et al.*, 1994; Miller *et al.*, 1997). In addition, pressure-induced activation of PKC induces a vasoconstriction without any further increase in Ca^{2+}-entry or MLC phosphorylation (Hill *et al.*, 1990; Laporte *et al.*, 1994). The Rho-kinase inhibitor Y-27632 also reduces myogenic tone in a concentration-dependent manner (VanBavel *et al.*, 2001; Schubert *et al.*, 2002). Evidence of PKC and Rho-kinase participation has been reinforced by observations of their translocation to the plasma membrane during development of vascular myogenic tone (Dessy *et al.*, 2000; Yeon *et al.*, 2002). More recently, Bolz et al. demonstrated that sphingosine kinase also modulates myogenic tone via the RhoA/Rho-kinase pathway (Bolz *et al.*, 2003). While it is well accepted that both PKC and Rho-kinase participate in the myogenic response, their contribution to the Ca^{2+}-sensitization pathway requires further understanding.

1.1.9 Hypothesis

In the present study, we tested the hypothesis that PKC and Rho-kinase regulation of pressure-activated myogenic tone occur independently of changes in membrane potential. A steep relationship between the level of extracellular K^+ and the membrane potential regulates the pressure-induced vasoconstriction in cerebral arteries. This is explained by the feedback mechanism involving the K_{ca} channels, whereby the initial pressure-induced depolarization activates the L-type VGCC leading to an increase in $[Ca^{2+}]_i$. The loaded SR spontaneously releases Ca^{2+} (sparks) which in turn activates the K_{ca} channels producing a membrane hyperpolarisation which in turn prevents further Ca^{2+} influx (Knot and Nelson, 1998). Ca^{2+}-sensitization, as a regulator of pressure-induced constriction, was investigated under conditions in which changes in the activity of K_{ca} channels were prevented by pre-treating cerebral arteries with a solution of 60 mM K^+. At this concentration of external K^+, the membrane potential of smooth muscles in rat cerebral arteries is clamped at approximately -21 mV, and further activation of the VGCC is unlikely to occur (Knot and Nelson, 1998).

1.1.10 Pressure myography

The pressure myograph system has been used for the in vitro study of vessels of 75 to 250 μm diameter under pressure (Halpern *et al.*, 1984). This approach reflects conditions that approximate the in vivo milieu of the vessel more closely than other methods such as ring segments or strips of arteries suspended in a tissue bath between two wires connected to a force transducer (Furchgott and Zawadzki, 1980). Furthermore, this technique exposes the arterial wall to a real transmural pressure. The system allows both static and dynamic

experiments. In addition, the incorporation of a video analyser permits the simultaneous recording of wall thicknesses and the inside diameter, both of which are necessary for the calculation of wall tension. The pressure myograph consists of two microcannulae, axially oriented in a tissue bath. The microcannulae face each other, and their tips of approximately 60 μm in diameter, approach the bottom glass coverslip at a 45º angle. The isolated arterial segments are mounted between the cannulae and secured with fine surgical suture. The distal cannula is clamped while the other is connected to a pressure transducer and a peristaltic pump from which a pressure servo unit controls the intraluminal pressure. The tissue bath is placed on the stage of an inverted microscope, allowing the pressurized vessel to be transilluminated through the glass bottom coverslip. An in-line video camera captures the image of the arterial diameter, which is projected and measured on a video monitor.

1.1.11 Ca^{2+} measurements

The use of a Ca^{2+} sensitive fluorescent indicator (Fura-2) and a ratio fluorescence spectrometer coupled to an inverted microscope, a vessel chamber and a dimension analysis system allow the simultaneous recording of changes in vascular tone and in cytosolic free Ca^{2+}. When Ca^{2+} binds to Fura-2 the excitation spectrum is shifted from 340-350nm to 380-390 nm wavelengths. Thus, the concentration of Ca^{2+} is measured from the ratio of amplitudes of a pair of excitation wavelengths (Tsien, 1988). This prevents variations induced by inconsistency in dye loading, cell thickness, local optical path length, and changes in illumination from influencing the calculation. The use of fluorescent indicators offers the possibility of visualisation by imaging, and produces a much

faster response than Ca^{2+} sensitive microelectrodes. It is possible to record signals from smaller cells than it was with previous absorbance indicators and chemiluminescent proteins. These fluorescent indicators can be calibrated and are less sensitive to bleaching. Moreover, the biggest advantage is that cells can be loaded with these fluorescent dyes without any disruption of the plasma membrane (Cobbold and Rink, 1987; Tsien, 1988). Fura-2 AM is membrane permeant, and therefore diffuses easily into the cytosol of the cells. Intracellular Fura-2 AM is quickly de-esterified by cytosolic esterase, and converted to an anionic membrane impermeant Fura-2, trapped in the cell. A photomultiplier is positioned behind an adjustable aperture and used as a photodetector.

1.2 Methods

All chemicals were purchased from Sigma-Aldrich Ltd. (Oakville, ON, Canada) unless otherwise stated. Animal handling was done in accordance with the guidelines of the Canadian Council on Animal Care and the Principles of laboratory animal care (NIH publication no. 85-23, revised 1985).

1.2.1 Arterial diameter measurements

Male Sprague-Dawley rats (200 - 300g) were anaesthetized with intraperitoneal injections of a mixture of sodium pentobarbital (Somnotol, 30 mg/kg) and heparin (Hepalean, 500 U/kg), and then killed by decapitation. The brain was excised and transferred to a dissection dish filled with ice-cold physiological salt solution (PSS). A small branch (0.6-1.0 mm long) of distal second-order middle cerebral arteries (inner diameter of 100-200μm) was dissected from surrounding connective tissues, and transferred to the myograph

chamber (Living Systems Instrumentation, Burlington, VT). The chamber was filled with oxygenated PSS heated to 37°C.

The proximal end of the artery was fed onto the tip (diameter of ~60 μm) of a glass microcannula and tied with single strands (20 μm) of 4-0 braided nylon suture; the perfusion pressure was then gently raised to clear the vessel of blood. The distal end of the artery was then similarly mounted to the outflow microcannula. After several minutes of perfusion, the distal outflow cannula was closed, and the transmural pressure was slowly increased to 60 mmHg by using an electronic pressure servo system (Living Systems Instrumentation). Thus, pressure-induced constrictions were recorded under conditions of no flow.

The PSS in the vessel chamber was continuously re-circulated by superfusion (MasterFlex, Cole-Parmer Instrumentation Co., Vernon Hills, IL) around the pressurized artery at a flow of 20-25 ml/min passing through an external reservoir that was bubbled with a gas mixture of 95% O_2, 5% CO_2. A pH micro-probe was positioned in the bath and used to adjust the reservoir gassing rate such to maintain the pH at 7.4 ± 0.04. A heating pump (NESLAB Instruments, inc., Portsmouth, NH) connected to a glass heat exchanger warmed the PSS to 37°C.

The arteriograph containing a cannulated pressurized artery was placed on the stage of an inverted microscope (Olympus IX70, UAPO/340 20X objective, Melville, NY) with a CCD (monochrome black and white) video camera (XC-73/73CE, Sony) attached to a viewing tube. The arterial preparation was allowed to equilibrate for 60 min. Arterial dimensions were viewed on a ULTRAK KM-

12A monitor (Carrolton, TX) and measured using a video dimension analyser system V94 (Living Systems Instrumentation) that provides automatic continuous readout measurements of luminal diameter and wall thickness. The information is up-dated every 17 ms, and the precision of the diameter measurement is within 1%. Cerebral myogenic tone developed spontaneously and consistently during equilibration, resulting in significantly reduced luminal diameter. Once attained, it remains stable for hours unless perturbed by changes in transmural pressure or the addition of vasoactive compounds (Skarsgard *et al.*, 1997).

1.2.2 Measurements of $[Ca^{2+}]_i$

Arteries were loaded with Fura-2, a Ca^{2+}-sensitive fluorescent dye. Fura-2AM (10μl of 1 mM stock solution, Molecular Probes, Eugene, OR) was premixed with an equal volume of a 0.01% solution of pluronic acid (Pluronic F-127, Molecular Probes) and 0.05% anhydrous dimethylsulfoxide (DMSO) diluted in PSS to yield a final concentration of 5 μM. The cannulated middle cerebral artery mounted in the myograph chamber, was incubated in the Fura-2AM/PSS loading solution for 1 hour at ~30ºC, followed by a washout period of 30 min at 37ºC and 10 mm Hg of intraluminal pressure.

Excitation was achieved by fluorescence microscopy using a 75-W xenon light source and a filter wheel rotating at ~50 Hz and containing 340- and 380-nm filters (High-speed Multi-Wavelength Illuminator, Photon Technology International, Monmouth Junction, NJ). Fluorescence emission was detected with a photomultiplier detection system 810/814 (Photon Technology International).

The 340/380 ratios were obtained at a rate of 20 points/sec of the 510 nm emission using Felix quantitative ratio fluorescence software (Photon Technology International). Motion artefacts were typically limited to <10% in the individual fluorescence signals and were not detectable in the 340/380 ratio.

1.2.3 Experimental procedures

After the development of myogenic tone during the equilibration period (60 min), the relation between pressure and vessel diameter was studied. Intravascular pressure was decreased to 10 mm Hg and then raised in 20 mm Hg steps from 20 to 100 mm Hg, while corresponding changes in vessel diameter and 340/380 ratio were measured. At each step, diameter was monitored for 5-10 min until steady state was achieved. The protocol was repeated and the results averaged. After the study of the relation between pressure and vessel diameter in the absence of any compounds, transmural pressure was lowered to 20 mmHg, a manoeuvre that places the vessel below the lower limit of the pressure range for myogenic tone. Luminal diameter was allowed to stabilize for 15-20 min before pharmacologic agents were added into the bath to study their effects on pressure-induced myogenic tone.

The effects of calphostin C (1 μM) and a Rho kinase inhibitor, Y27632 (1 μM) on the pressure-diameter responses were examined under conditions where further changes in membrane potential were prevented with 60 mM KPSS (Knot and Nelson, 1998). The activators and inhibitors were used at concentrations previously described by others, and us, as selective for their intracellular targets in isolated arterial preparations (Henrion and Laher, 1993; Osol *et al.*, 1993;

Gokina and Osol, 1998; Bakker *et al.*, 1999; Kandabashi *et al.*, 2000; Matrougui *et al.*, 2001). Inhibitors were added to superfusing buffer and allowed to circulate for 20 min until a new steady state diameter was reached. This was followed by reassessment of the constriction and 340/380 ratio due to the change in transmural pressure. At the conclusion of each experiment, the superfusion solution was changed to a calcium-free PSS that contained 2 mM Ethylene glycol-bis(2-aminoethylether)-N,N,N',N'-tetraacetic acid (EGTA) and no $CaCl_2$. Vessels were incubated for 20 min and then the pressure steps were repeated to obtain the "passive" diameter of each vessel at each pressure value in order to calculate the percentage of myogenic constriction.

1.2.4 Expression of the results and statistical analysis

Myogenic tone at each pressure was expressed as a percent decrease in diameter from the "passive" diameter (% constriction) or as a percent decrease in myogenic response (% inhibition) using the equations below.

$$\% \text{ constriction} = 100 \times [(D_{Ca\text{-free}} - D_{PSS}) / D_{Ca\text{-free}}]$$

$$\% \text{ inhibition} = 100 \times [1 - (D_{Ca\text{-free}} - D_{PSS}) / (D_{Ca\text{-free}} - D_{PSS} + \text{inhibitor}]$$

Where D is the arterial diameter in the indicated solution. The K^+-induced increase in 340/380 ratio was measured in each tissue. Therefore, in the present study the changes in 340/380 ratio were normalized to the change in the ratio produced by 60 mM KPSS in the same vessel. All results are expressed as mean ± SE of n experiments. One vessel was taken from each animal. Statistical

evaluation was done by ANOVA followed by Newman-Keuls tests. Means were considered significantly different when $P < 0.05$.

1.2.5 Drugs and solutions

The ionic composition of the PSS was (in mM): NaCl 119, KCl 4.7, KH_2PO_4 1.18, $NaHCO_3$ 24, $MgSO_4$-$7H_2O$ 1.17, $CaCl_2$ 1.6, glucose 5.5 and EDTA 0.026. The solution of depolarizing high K^+ solution was made by equimolar substitution for NaCl. Calphostin C was purchased from Biomol Research Laboratories, Inc. (Plymouth Meeting, PA) and vasopressin from Sigma (Ontario, Canada). Y-27632 was a gift from Welfide Corporation (Osaka, Japan). Y-27632 was dissolved in deionised water (NANOpure). Calphostin C was dissolved in DMSO (total of 0.0001% of DMSO in Krebs buffer solution). The effects of DMSO had been previously tested in our laboratory and did not alter the pressure-diameter relation or the vascular responses to norepinephrine and acetylcholine. Comparative constrictor responses were obtained from control arteries and arteries loaded with Fura-2-AM. Interactions between Fura-2 and calphostin C or Y-27632 were absent (Appendix 1).

1.3 Results

1.3.1 Myogenic tone in rat cerebral resistance arteries

Cerebral arteries developed graded myogenic constrictions over the physiologic intraluminal pressure range of 40-100 mmHg. Figure 1.4A shows a representative trace of the steady state response of middle cerebral arteries (mean of diameter at rest 169.5 ± 7.7 μm; n = 15) to increases in intraluminal

pressure. Figure 1.4B shows that myogenic tone of middle cerebral arteries is associated with a small change in the 340-to-380nm (340/380) fluorescence ratio of Fura 2 from 1.60 ± 0.31 at 20 mmHg to 2.57 ± 1.79 at 60 mmHg. However, no significant change in the 340/380 ratio was obtained when the pressure was further increased (from 60 mm Hg to 100 mm Hg). Data summarized in Figure 1.4C are normalized to 60 mM KPSS and show a significant changes at each transmural pressure in 340/380 ratio with greatest changes recorded at 60 (34.6 ± 4.1%; n = 24) and 100 mmHg (43.5 ± 5.8 %; n = 24). Removal of the endothelium or pre-treatment of vessels with L-NAME (200 μM) and indomethacin (10 μM) have been tested previously in this laboratory and did not change pressure-induced constriction (Lagaud *et al.*, 1999).

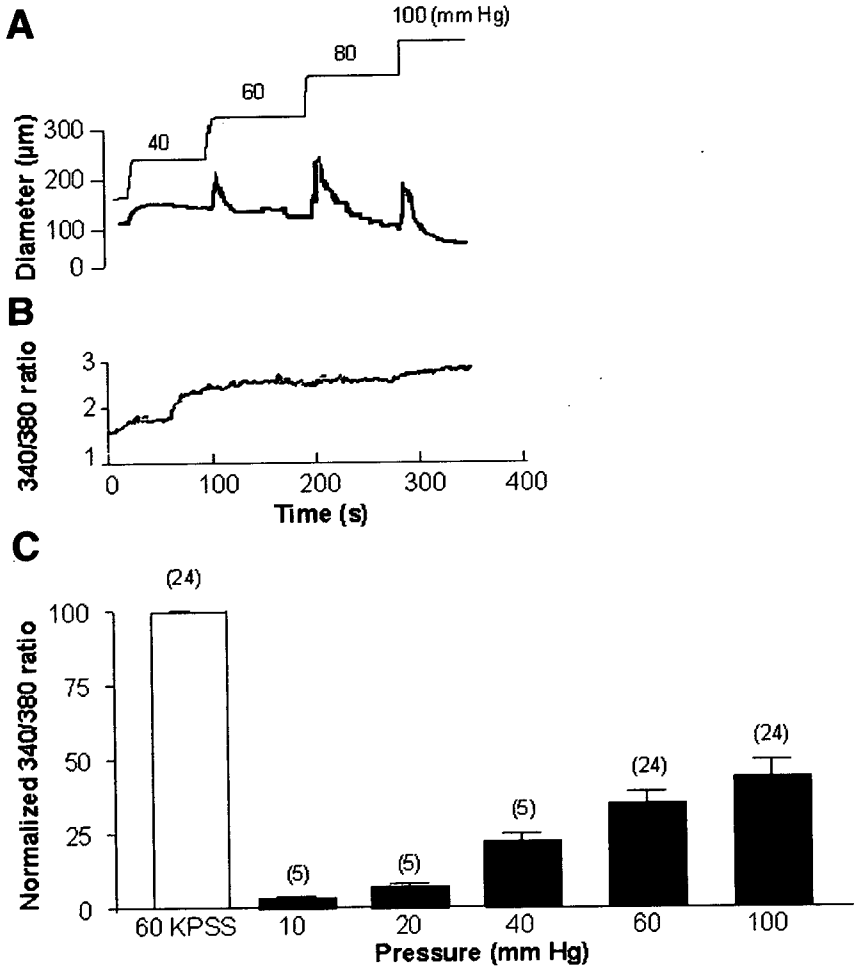

Figure 1.4 Effects of intraluminal pressure on rat cerebral arteries diameter and 340/380 fluorescence ratio.

Original traces showing myogenic tone development (A) and accompanying changes in 340/380 fluorescence ratio (B) in response to elevation of intraluminal pressure from 10 to 100 mmHg. (C): Histograms showing the normalised change in 340/380 fluorescence ratio in response to elevation of intraluminal pressure from 10 to 100 mmHg. Values are means ± S.E, (n=). Each bar is significantly different from the others, $P < 0.001$.

1.3.2 Effect of 60 mM KPSS on myogenic tone

A series of experiments were designed to examine primary events independent of depolarization in pressure-induced myogenic tone of cerebral arteries. Thus, the role of raised K^+ concentrations on pressure-induced

contraction (Figure 1.5A, B and C) was investigated. Step-wise increases of transmural pressure (20 to 100 mm Hg) in the presence of 60 mM KPSS, which clamps the arteries at -21mV (depolarized cerebral arteries) (Knot and Nelson, 1998), produced myogenic responses (Figure 1.5A). Thus, simultaneous recordings of diameter and $[Ca^{2+}]_i$ in Figure 1.5A and B show that pre-treatment of cerebral arteries with 60 mM KPSS induced a contraction. The diameter was reduced to 48.80 ± 4.2% (n = 7 at 20 mmHg) of its original value which was associated with a transient increase in 340/380 fluorescence ratio followed by a plateau phase. Step-wise increases of transmural pressure above 20 mmHg in the presence of 60 mM KPSS produced a myogenic response without any significant changes in 340/380 fluorescence ratio (Figure 1.5B). These results suggest that additional mechanisms, independent of the increase in $[Ca^{2+}]_i$, may be important components of myogenic contraction.

Data summarized in Figure 1.5C are normalized to 60 mM KPSS and show that 60 mM KPSS caused a significant increase in $[Ca^{2+}]_i$ at 20 mmHg (88.3 ± 3.2%, n = 6) compared with responses to pressure of 60 mm Hg (54.4 ± 7.3%, n = 6) and 100 mm Hg (48.6 ± 8.1%, n = 6). The pressure-induced constriction caused by 60 and 100 mmHg was accompanied by a transient increase in 340/380 fluorescence ratio (Figure 1.5C). At higher K^+ concentrations such as 100 mM, the arteries were maximally contracted so that increases in transmural pressure did not produce additional myogenic tone and the arterial diameter was maintained.

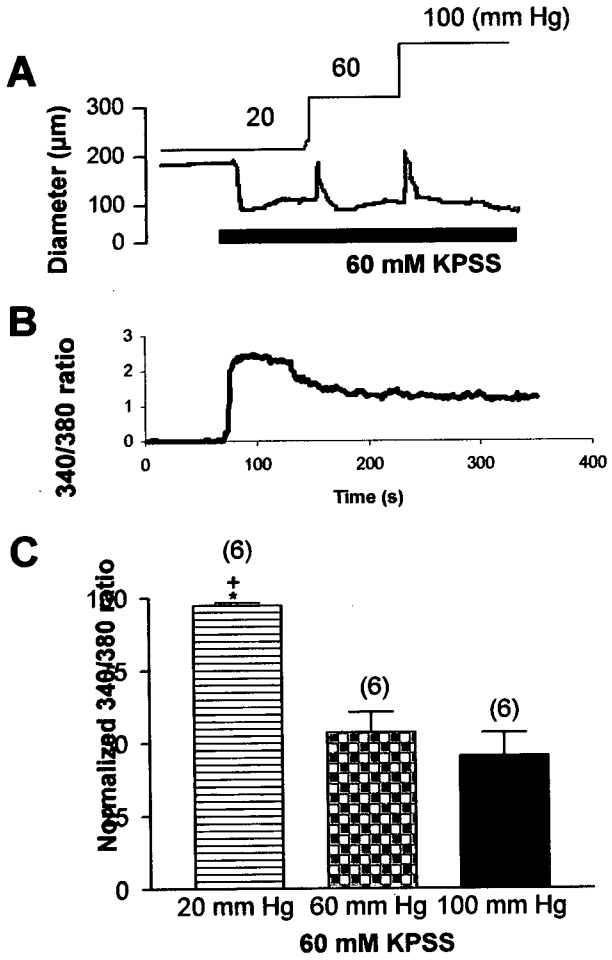

Figure 1.5 Effects of intraluminal pressure on depolarised cerebral arteries. Original traces show that changes in intraluminal pressure from 20 to 100 mm Hg caused transient myogenic tone (A), and accompanying changes in 340/380 fluorescence ratio (B). Normalized 340/380 fluorescence ratio in response to elevation of intraluminal pressure from 20 to 100 mmHg on depolarized arteries (60 mM KPSS) in the same vessel (C). Values are means ± S.E. **P < 0.01, significantly different from response obtained at 60 mmHg. +P < 0.001, significantly different from response obtained at 100 mmHg; (n=).

1.3.3 Calphostin C inhibits vascular tone

The effect of the PKC inhibitor, calphostin C, on the activity of cerebral arteries was tested. Calphostin C inhibits myogenic tone induced by 60 mmHg intraluminal pressure (Figure 1.6A). The arteries subjected to 60 mmHg were

allowed to equilibrate for an hour after which they gradually contracted. The sustained contraction was reversed by the addition of calphostin C, resulting in dilation of greater amplitude than that induced by the initial increase of pressure to 60 mmHg. The vasodilation induced by calphostin C occurred independently of any changes in $[Ca^{2+}]_i$, while the dilation induced by the removal of Ca^{2+} from the solution (0 Ca^{2+}) was accompanied with a decrease in 340/380 ratio (Figure 1.6B). Calphostin C also inhibited the tone developed in arteries pre-treated with indolactam (1μM; a PKC activator), while it did not alter the constriction induced by a 60 mM KPSS depolarising solution (Figure 1.7).

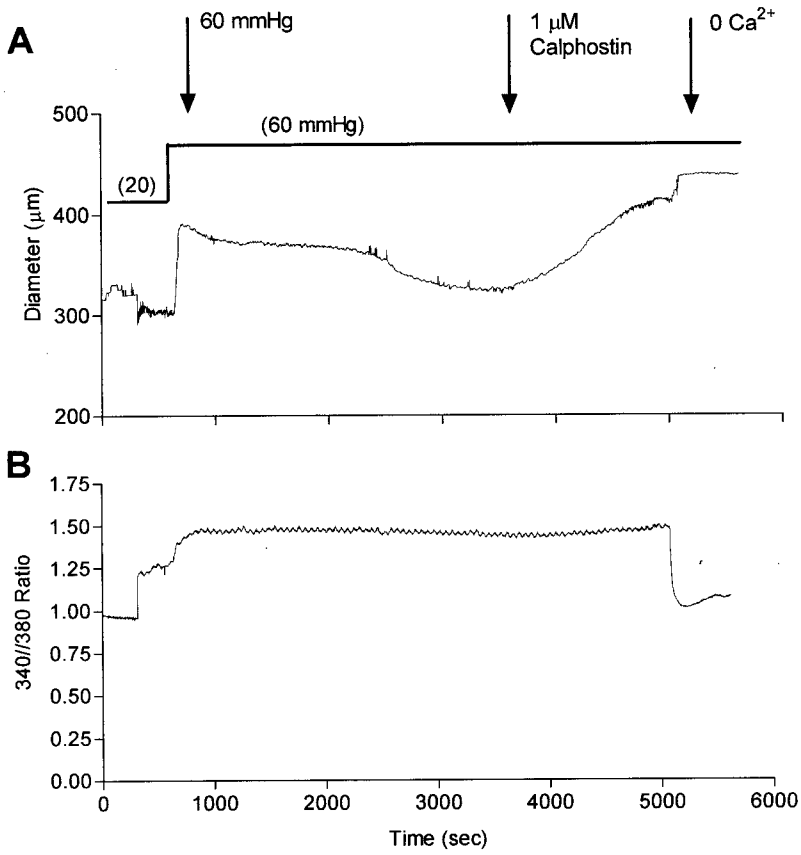

Figure 1.6 Effect of calphostin C on myogenic tone and 340/380 ratio.
Representative traces showing the inhibition of myogenic tone by calphostin C in rat cerebral arteries. Increases in intraluminal pressure to 60 mmHg induced a vasodilation followed by a transient vasoconstriction. The addition of calphostin C induced a vasodilation followed by a plateau phase. Further removal of Ca^{2+} in the bath dilated the artery to its maximum (A). The increase in intraluminal pressure was accompanied with an increase in the 340/380 fluorescence ratio which remain unchanged with the addition of calphostin C until it decreased following the removal of extracellular Ca^{2+} (B).

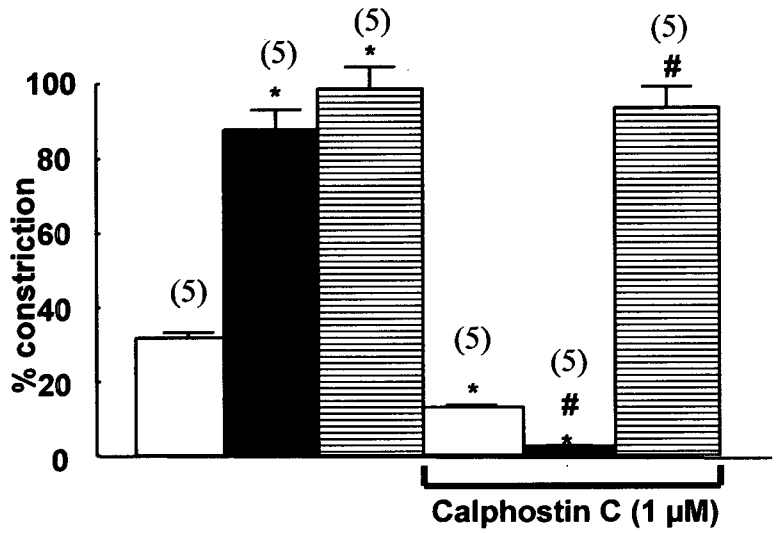

Figure 1.7 Effect of calphostin C on pre-contracted arteries.
Histograms showing the effects of 60 mmHg increase in pressure (▭), indolactam (1 μM; ■) and 60 mM KPSS (▤) in the absence and in the presence of calphostin C (1 μM). *P < 0.001, significantly different from pressure-induced contraction at 60 mmHg. #P < 0.001, significantly different from the relative control response induced by indolactam (1 μM); (n=).

1.3.4 Effect of calphostin C and Y-27632 in depolarized arteries.

Pharmacological inhibitors were used on depolarized cerebral arteries to determine whether the ability of arteries to maintain their diameters in the absence of pressure-induced depolarization is mediated by PKC or Rho-kinase Ca^{2+}-sensitization pathways. Figure 1.8A and B show representative traces of the effects of a PKC inhibitor, calphostin C on cerebral arteries placed in a depolarizing solution. In the presence of calphostin C (1 μM), application of 60 mM KPSS resulted in a significant contraction of the cerebral artery. Step-wise increases of transmural pressure in the presence of 60 mM KPSS and calphostin C resulted in a loss of myogenic tone development (Figure 1.8A). This was

accompanied by a transient elevation of 340/380 fluorescence ratio followed by a plateau phase (Figure 1.8B). Data in Figure 1.8C are normalized to 60 mM KPSS and summarize the effects of 60 mM KPSS on the 340/380 fluorescence ratio, in the presence of calphostin C (1 μM).

A commonly used inhibitor of Rho-kinase, Y-27632, was also examined in rat cerebral resistance arteries as shown in Figure 1.9. In the presence of Y-27632 (1 μM), application of 60 mM KPSS resulted in cerebral artery contraction (Figure 1.9A). Step-wise increases of transmural pressure failed to induce myogenic tone development in the presence of 60 mM KPSS and Y-27632 (Figure 1.9A). This was accompanied by an elevation of 340/380 fluorescence ratio in response to 60 mM KPSS, followed by a plateau phase, in which there was no change in response to 1μM of Y-27632 (Figure 1.9B). Data in Figure 1.9C are normalized to 60 mM KPSS and summarize the effects of 60 mM KPSS, in the presence of Y-27632 (1 μM).

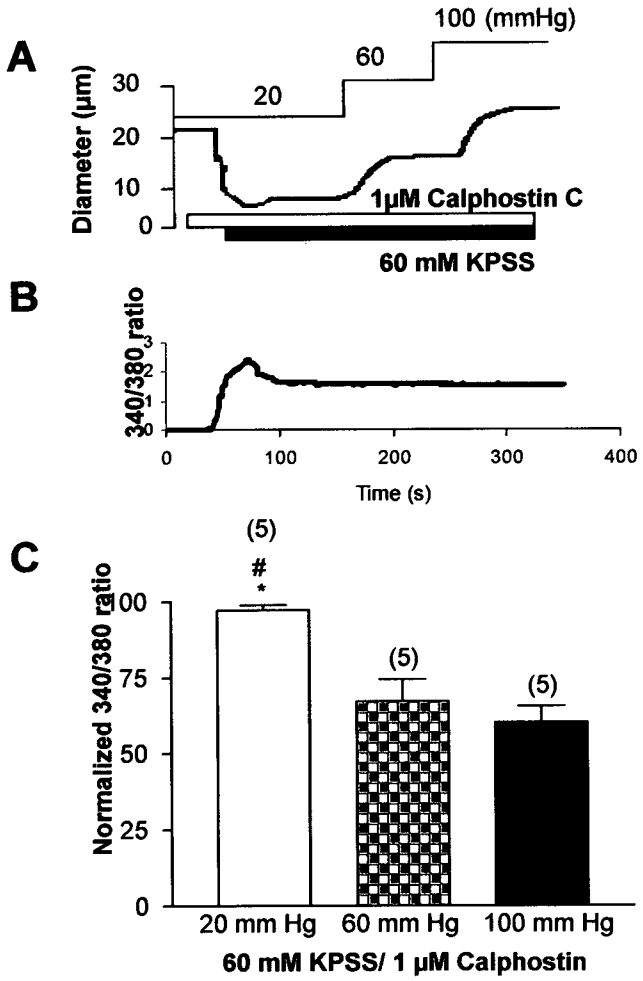

Figure 1.8 Effects of calphostin C on depolarized and pressurized arteries. Original traces show that in the presence of calphostin C (1 µM), 60 mM KPSS caused a vasoconstriction (A) accompanied with an increase in 340/380 fluorescence ratio (B). Changes in intraluminal pressure from 20 to 100 mm Hg increased the vessel diameter (A) without changes in 340/380 fluorescence ratio (B). Data in C show the 340/380 fluorescence ratio normalized to the change in the ratio produced by 60 mM KPSS in the same vessel; values are means ± S.E. *P < 0.01, significantly different from response obtained at 60 mmHg. #P < 0.001, significantly different from response obtained at 100 mmHg; (n=).

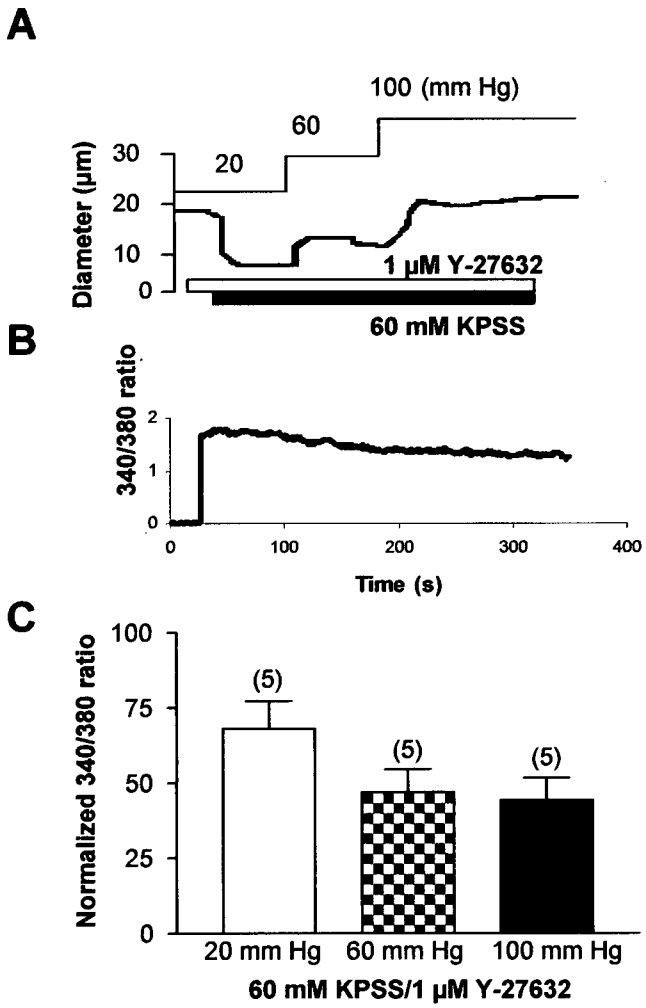

Figure 1.9 Effects of Y-27632 on depolarised and pressurized arteries.
Original traces show that in the presence of Y-27632 (1 μM), 60 mM KPSS caused a vasoconstriction (A) accompanied with an increase in 340/380 fluorescence ratio (B). Subsequent changes in intraluminal pressure from 20 to 100 mm Hg increased the vessel diameter (A) without changes in 340/380 fluorescence ratio. Data in C show the 340/380 fluorescence ratio normalized to the change in the ratio produced by 60 mM KPSS in the same vessel; values are means ± S.E; (n=).

Unlike, calphostin C, Y-27632 significantly inhibited the transient rise in 340/380 fluorescence ratio caused by the application of 60 mM KPSS (Figure 1.8B and Figure 1.9B). This was also reflected in the normalised 340/380 ratio at 20

mmHg which in the case of calphostin C (Figure 1.8) is comparable to the effect of 60 mM KPSS by itself (Figure 1.5) while in contrast, the addition of Y-27632 produced a reduced normalised ratio (Figure 1.9). The specificity of the Rho-kinase inhibitor Y-27632 was therefore further examined.

1.3.5 Y-27632 inhibits vascular tone

In order to determine to what extent Rho-kinase plays a role in contraction induced by 60 mM KPSS, we compared the effects of Y-27632 on cerebral arteries pre-contracted with three different stimuli; pressure induced myogenic tone, 60 mM KPSS induced contraction and G-protein mediated constriction by vasopressin. In pre-contracted arteries, the addition of Y-27632 (0.1-3.0 μM) induced a concentration dependent vasodilation in cerebral arteries (Figure 1.10). Myogenic tone was inhibited at all concentrations of Y-27632 used, with 22±3% inhibition occurring with 0.1μM Y-27632 and 83±6 % with 3.0μM Y-27632 (n=4; Figure 1.10). The vasoconstriction due to vasopressin (0.1μM; n=4) and 60 mM KPSS (n=8) were both studied at a pressure of 20 mmHg, a pressure at which myogenic tone is absent (Meininger *et al.*, 1991; Laporte *et al.*, 1994). Vasoconstrictor responses to both vasopressin and 60 mM KPSS were blunted by Y-27631 with the highest concentration of Y-27632 (3.0μM) reducing the response to vasopressin by 60±5% and that to 60 mM KPSS by 33±4% (Figure 1.10). Although the vasoconstriction to 60 mM KPSS was also reduced by Y-27632 in a concentration dependent manner, the extent of inhibition was significantly lower ($p<0.05$) than that occurring with either myogenic or vasopressin induced tone at each concentration (0.1-3.0μM) of the Rho-kinase inhibitor (Figure 1.10).

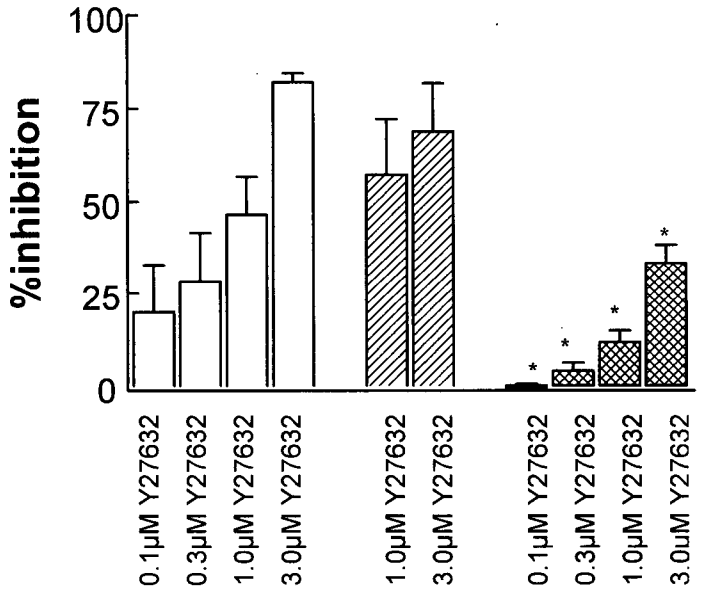

Figure 1.10 **Extent of Y-27632 inhibition of vascular tone.**
Myogenic tone was induced at an intraluminal pressure of 60 mmHg (▭). Vasoconstriction in response to both vasopressin (0.1 μM; ▨) and KPSS (60 mM; ▩) were determined in the absence of myogenic tone (intraluminal pressure=20 mmHg). Significant differences in the inhibitory responses induced by the same concentration of Y-27632 were observed between pre-contracted arteries with 60 mM KPSS and those pre-contracted with both intraluminal pressure of 60 mmHg and vasopressin (*, $p<0.05$, ANOVA; n=4-8).

1.3.6 Y-27632 inhibits Ca^{2+} entry

Since constriction to high K^+ occurs via the activation of VGCC, changes in intracellular Ca^{2+} in response to 60 mM KPSS before and after Y-27632 (60 min, 1μM) were measured in the absence of myogenic response (intraluminal pressure of 20 mmHg). A typical recording is shown in Figure 1.11. Exposure to 60 mM KPSS induced a rapid constriction followed by a moderate but constant vasoconstriction accompanied by a rapid and sustained rise in 340/380 fluorescence ratio, reflecting an increase in free intracellular Ca^{2+}. In the presence

of Y-27632, 60 mM KPSS induced a rapid transient constriction followed by a reduced vasoconstriction. The rapid rise in intracellular Ca^{2+} was also reduced by Y-27632.

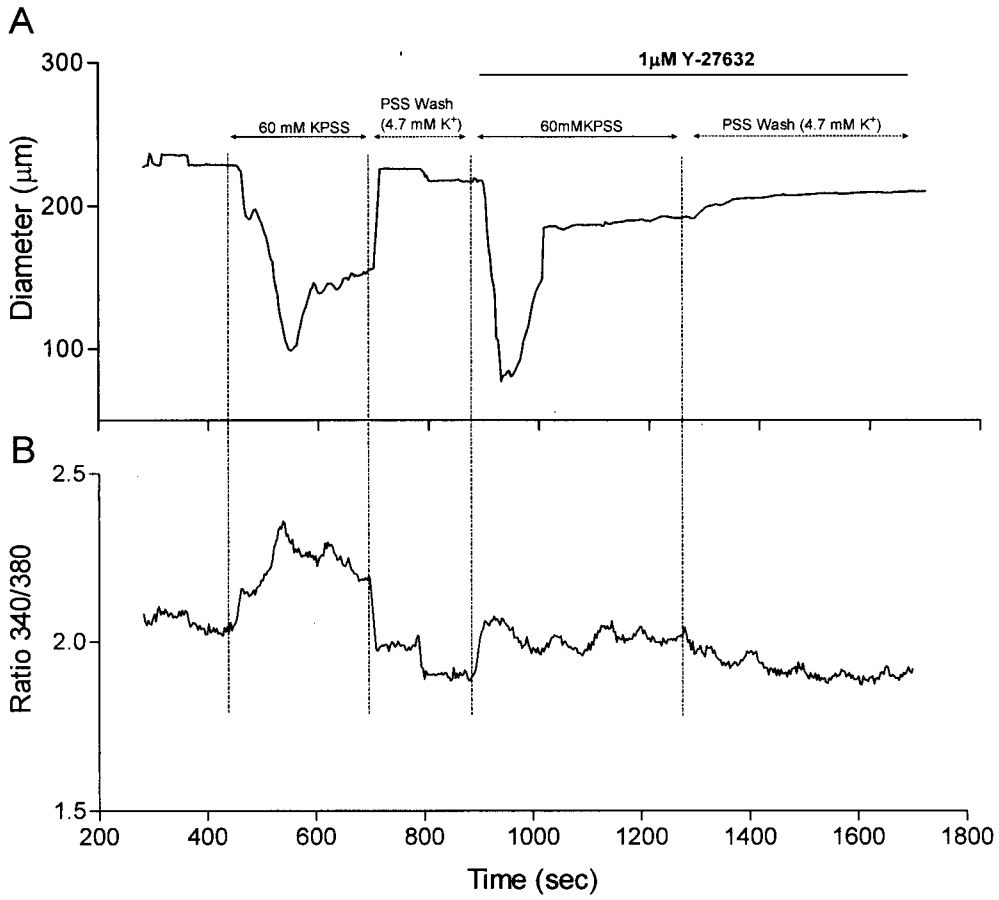

Figure 1.11 Effect of Y-27632 on depolarised arteries.
Representative trace of the changes in diameter (A) and in 340/380 fluorescence ratio (B) in cerebral arteries submitted to 60 mM KPSS and 1 µM Y-27632 in the absence of myogenic tone (intraluminal pressure=20 mmHg).

Receptor-independent Ca^{2+}-entry induced with 60 mM KPSS under control conditions (n=7) raised the 340/380 fluorescence ratio to 1.8±0.06 (Figure 1.12). In the presence of Y-27631 (1μM) and 60 mM KPSS, the 340/380 fluorescence ratio was significantly decreased to 1.4±0.09 ($p<0.05$; Figure 1.10). However, the 340/380 fluorescence ratio induced by 60 mM KPSS was unaltered by pre-treatment with an inhibitor of protein kinase C (calphostin C, 1μM; 340/380 ratio=1.8±0.1; Figure 1.12).

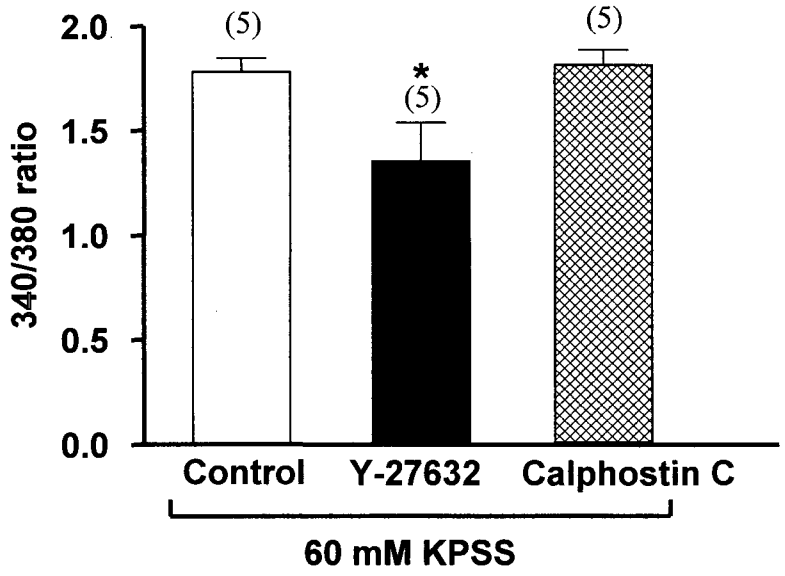

Figure 1.12 Effect of different pharmacologic inhibitors of Ca^{2+} sensitization.

Pre-contracted cerebral arteries with 60 mM KPSS induced increase in the 340/380 fluorescence ratio before (control) and after incubation with inhibitors of Rho-kinase (1 μM, Y-27632), and protein kinase C (1 μM, calphostin C). * $p<0.05$, ANOVA; (n=).

1.4 Discussion

Growing interest in the mechanism of myogenic constriction has increased our understanding of its cellular basis and added to our knowledge of the various signalling pathways involved. To this day, it is generally accepted that the principal mechanism of pressure-induced myogenic constriction involves a depolarization followed by the entry of extracellular Ca^{2+}. Then again, pressure-induced constriction has been associated with significantly lower increases in $[Ca^{2+}]_i$ when compared to high K^+-induced constriction (VanBavel *et al.*, 1998). Thus, a second underlying mechanism of the myogenic tone implies that in addition to an elevation of $[Ca^{2+}]_i$, an increase in myofilament Ca^{2+}-sensitivity may also occur. This study explored the interaction of these two pathways in the response of arterial diameter to increases in transmural pressure. Observations that pressure-induced constriction is maintained in cerebral arteries incubated in a depolarising solution (60 mM KPSS) are reported. In addition, the activation of PKC and Rho-kinase leading to Ca^{2+}-sensitization is shown to participate in the pressure-induced constriction in depolarised cerebral arteries.

1.4.1 Ca^{2+}-sensitization contribution to myogenic response

Several studies report that myogenic tone is only dependent on Ca^{2+}-entry via the L-type VGCC, and does not require any contribution by mechanisms that change the Ca^{2+}-sensitivity (Brayden and Nelson, 1992; Nelson *et al.*, 1995; McCarron *et al.*, 1997; Knot and Nelson, 1998). To determine the primary events in pressure-induced myogenic tone in cerebral arteries, a series of experiments were performed in which the arteries were incubated in a depolarizing solution (60 mM KPSS) and changes in diameter and 340/380 fluorescence ratio produced

by increased transmural pressure were measured. Under such conditions, cerebral arteries were still able to produce a myogenic response i.e. arteries maintained a relatively constant diameter with increases in transmural pressure (Figure 1.5). The fact that myogenic contraction still occurred in a 60 mM KPSS solution when presumably, the membrane potential is close to the theoretical K^+ equilibrium potential (Casteels *et al.*, 1977; Droogmans *et al.*, 1977; Knot and Nelson, 1998) suggests that K^+ channel activity alone cannot account for change in membrane potential that occurs during myogenic tone. Others have proposed that activation of Cl^- channels may be involved in pressure-induced depolarization of vascular SMCs of rat cerebral artery (Nelson *et al.*, 1997). However, it has been reported that the effects induced by Cl^- channel inhibitors may be due to inhibition of L-type VGCC (Doughty *et al.*, 1998). Step-wise increases of transmural pressure in depolarized arteries induced a transient contraction without a significant change in $[Ca^{2+}]_i$. At this external $[K^+]$, the membrane potential of SMCs of the rat cerebral arterial wall is approximately –21 mV, and further changes in membrane potential are unlikely to occur (Knot and Nelson, 1998). Therefore, the observed myogenic contraction is most likely due to an increase in Ca^{2+}-sensitivity of the myofilaments. The possible involvement of the PKC and/or Rho-kinase pathways in pressure-induced constriction of depolarised arteries was then investigated.

1.4.2 Ca^{2+}-sensitization is mediated by PKC and Rho-kinase

Despite an elevated $[Ca^{2+}]_i$ generated by membrane depolarization with 60 mM KPSS, cerebral arteries subjected to increased transmural pressure dilated in the presence of inhibitors of both PKC and Rho-kinase. Under conditions where

no additional Ca^{2+}-entry through VGCC is possible, Ca^{2+}-sensitization mechanisms are likely responsible for the constriction. If Ca^{2+}-sensitization mechanisms are prevented by the use of PKC and Rho-kinase inhibitors, the ability of the artery to actively respond to an increase in intraluminal pressure is consequently compromised. This could explain the passive response of the cerebral arteries dilating to increased intraluminal pressure in the presence of both 60 mM KPSS and inhibitors of PKC or Rho-kinase.

These results provide further evidence that PKC plays an active role in myogenic tone of small contractile arteries by modulating intracellular Ca^{2+}-sensitivity (Laher and Bevan, 1989; Hill *et al.*, 1990; Osol *et al.*, 1991; Osol *et al.*, 1993; Narayanan *et al.*, 1994; Lange *et al.*, 1997; Gokina and Osol, 1998). In addition, they implicate Rho-kinase as a mediator of Ca^{2+} sensitization in myogenic contraction. These findings are consistent with previous studies, which associate stretch-induced redistribution of PKC and RhoA to the plasma membrane with Ca^{2+} sensitization (Gong *et al.*, 1997; Dessy *et al.*, 2000; Yeon *et al.*, 2002). Furthermore, stretch-activated PKC and Rho-kinase are correlated with an increased phosphorylation of MLC_{20KDa} (Yeon *et al.*, 2002), confirming their involvement in force generation.

1.4.3 Activation of Rho-kinase by membrane depolarization

The inhibition of the myogenic response by PKC and Rho-kinase inhibitors in depolarised arteries provides indirect evidence that intracellular signalling leading to vasoconstriction of pressurised arteries involves a series of phosphorylation reactions, which ultimately decreases the activity of MLCP. The

activation of such pathways is often associated with ligands binding to G-protein coupled receptors (Somlyo and Somlyo, 2000). In accordance with these observations, Y-27632 significantly reduced the contraction induced by both intraluminal pressure and vasopressin (Figure 1.10). However, higher concentration of Y-27632 (3 μM) reduced, to a lesser extent but significantly, the vasoconstriction induced by 60 mM KPSS. What seemed to be a non-specific interaction of Y-27632 at an unrelated site, may in fact demonstrate that depolarization in SMC leads to both an increase in $[Ca^{2+}]_i$ and Ca^{2+}-sensitization. Recently, similar observations have been reported in isolated SMCs where sustained contraction induced by 60 mM KCl depolarization are practically abolished by both Rho-kinase inhibitor, Y-27632 and HA-1077 (Mita *et al.*, 2002; Sakurada *et al.*, 2003). The consequent reduction in force has been associated with the decrease in MLC_{20KDa} phosphorylation and the loss in Ca^{2+}-sensitization (Mita *et al.*, 2002). Both agonist (noradrenaline) and KCl depolarization increase the GTP-bound active form of RhoA (Sakurada *et al.*, 2003). KCl activation of RhoA is however Ca^{2+}-dependent and has been further associated with MLCP phosphorylation at Thr695, a well-known inhibitory site of the phosphatase (Sakurada *et al.*, 2003). Taken together, these latter observations suggest that a similar Ca^{2+}-sensitization pathway as the one described for agonist-induced contraction (Kitazawa *et al.*, 1991) is involved in KCl depolarization-induced contraction. While agonists activate RhoA through binding of G-protein coupled receptor, CaM and CaMKII have been implicated in the KCl depolarization induced RhoA activation (Sakurada *et al.*, 2003). Bolz et al. have demonstrated that sphingosine kinase also modulates myogenic tone via the RhoA/Rho-kinase pathway (Bolz *et al.*, 2003). Since the activity of sphingosine kinase increases with depolarization and the activation of VGCC (Alemany *et al.*, 2001), sphingosine

kinase could also be potentially responsible for Rho-kinase activation in KPSS depolarised arteries. Taken together, these results indicate that Ca^{2+}-sensitization mediated by Rho-kinase can be induced by membrane depolarization in addition to the classical activation through ligand binding to G-protein coupled receptor and the newly proposed stretch-induced mechanisms.

In the present study, Y-27632 simultaneously decreased the 340/380 fluorescence ratio recorded from the 60 mM KPSS depolarised arteries (Figure 1.11). While these observations, although obtained in whole arterial preparation, go against previous reports in SMC strips of rat tail artery (Mita *et al.*, 2002), they imply that Y-27632 interacts with unrelated sites and may indirectly be capable of blocking Ca^{2+}-entry. This latter observation seems to detract from the uncontrolled use of Y-27632 as a specific inhibitor of Rho-kinase. Y-27632 is a selective inhibitor of the Rho kinase and acts as a competitive inhibitor of ATP binding. It is ~200 times more selective for inhibiting Rho-kinase than PKC, cyclic AMP-dependent protein kinase and myosin light chain kinase (Uehata *et al.*, 1997). While Y-27632 reduced the 340/380 fluorescence ratio in depolarised arteries, inhibitors of PKC (calphostin C) did not, which indicates that the suggested inhibition of Ca^{2+}-entry is unique to Rho-kinase or its inhibitor. The possibility of an undesirable interaction between Y-27632 and Fura-2 has also been ruled out (Appendix 1). This suggests two possibilities: a potential lack of selectivity of Y-27632 or a novel role for Rho-kinase in Ca^{2+}-entry mechanisms. Further investigations will be required in order to elucidate the downstream mechanisms following the activation of Rho-kinase in depolarised arteries.

1.4.4 Summary

In summary, it was demonstrated that pressure induced myogenic tone in cerebral arteries involves Ca^{2+}-sensitization mechanisms. This increase in intracellular Ca^{2+}-sensitivity is hypothesised to be mediated by PKC and/or Rho-kinase. As the arteries were depolarised with 60 mM KPSS, additional pressure-induced changes in Ca^{2+} and K^+ channel activity were minimised. Therefore, the inhibition of myogenic tone in depolarised arteries by both PKC and Rho-kinase inhibitors is attributed to the inhibition of Ca^{2+}-sensitization pathways of the myogenic responses. Whereas Ca^{2+} entry via VGCC is an essential component of pressure-induced constriction of small arteries, these results provide evidence that other intracellular events are able to maintain active constriction in response to pressure changes under conditions where additional Ca^{2+}-entry into the cell is minimal. These results also support the participation of both PKC and Rho-kinase in Ca^{2+}-sensitization of myogenic responses. In addition, the activation of Rho-kinase by membrane depolarization has been demonstrated. Downstream effectors of Rho-kinase depolarization-induced activation remain to be identified, but they may be involved in indirect control of Ca^{2+}-entry mechanisms.

Chapter 2
Characterization of glucose transporters in endothelial cells of small contractile arteries

2.1 Introduction

2.1.1 The glucose paradox

In 1921-22, the discovery of insulin by Banting and Best changed the course of one of today's most prominent metabolic disorders (Banting and Best, 1990). Diabetes Mellitus, first described by the sweetness of the urine, is characterised by elevated plasma glucose levels resulting from defects in insulin secretion, insulin action or both (Kernohan *et al.*, 2003). Increased life expectancy acquired with insulin supplements, and the development of new diagnostic methods, have allowed diabetes to reach today epidemic proportions. Worldwide, the diabetic population is estimated to increase each year by 5.5 million and is expected to attain 300 million by the year 2025 (King *et al.*, 1998). Since fatal ketosis is no longer the predetermined fate of diabetic patients, new complications have emerged from long-term diabetes, regardless of its aetiology. Chronic hyperglycaemia can lead to renal failure, blindness, defective nerve conduction and impaired wound healing but, by far, the major cause of morbidity and mortality is attributed to cardiovascular diseases associated with atherosclerosis (Haffner *et al.*, 1990; Anonymous, 1995; Wolffenbuttel and van Haeften, 1995; Anonymous, 1999; Haffner *et al.*, 2000). In fact, myocardial infarction and stroke are more common among people with diabetes than in those without (Barrett-Connor *et al.*, 1991; Manson *et al.*, 1991; Koskinen *et al.*,

1992). Thus, diabetes mellitus has become an epidemic and a prime risk factor for cardiovascular diseases.

In the diabetic population, well known cardiovascular risk factors such as hypertension, dyslipidemia (increased level of very low density lipoprotein (VLDL) and low density lipoprotein (LDL) cholesterol and decreased level of high density lipoprotein (HDL)), obesity, hyperinsulinaemia and insulin resistance seem to be exacerbated (Howard, 1996a). Hyperglycaemia, a metabolic abnormality of diabetes, could potentially precipitate the onset of macrovascular disease by itself. Hyperglycaemia has been shown to inhibit the production of NO in arterial ECs (Williams *et al.*, 1998) and to stimulate the production of plasminogen activator inhibitor-1 (PAI-1) (Du *et al.*, 2000). In addition, by reducing the expression of hepatic perlecan heparan sulphate proteoglycan, hyperglycaemia contributes to the elevation of atherogenic cholesterol-enriched apolipoprotein B-containing residual particles (Ebara *et al.*, 2000). More importantly, hyperglycaemia is known to be directly toxic for the ECs (Sank *et al.*, 1994; Haller, 1997; Cosentino and Luscher, 1998; Williams *et al.*, 1998; Aronson and Rayfield, 2002; Lee *et al.*, 2002), the first line of protection of the vascular wall. Dysfunction of the ECs has been identified as the first step in the pathogenesis of atherosclerosis in non-diabetics (Lusis, 2000). Both the Diabetes Control and Complications Trial (DCCT) (Anonymous, 1995) and the United Kingdom Prospective Diabetes Study (UKPDS) (Anonymous, 1998), have previously attributed the high prevalence of microvascular complications (degeneration of the retina, renal glomerulus and vasa nervorum of peripheral nerves) to hyperglycaemia. However, the same studies failed to reach statistical significance in the case of macrovascular disease (atherosclerosis associated with

larger blood vessels), despite a trend showing its reduction with tight control of the glycaemia (Anonymous, 1998). Adding to this fact is that more effects on the reduction of the risks associated with macrovascular diseases were observed with treatments targeting dyslipidaemia or hypertension. How can such a discrepancy be explained? If hyperglycaemia is the triggering event in the development of macrovascular diseases, then why is the effect of glucose lowering drugs so minimal? A few plausible explanations have been put forward. Firstly, it is possible that the approaches used to lower the level of lipid cholesterol and reduce elevated blood pressure are simply more efficient than the one used to lower blood glucose. Secondly, the available glucose lowering therapies may not produce enough impact on the macrovascular state or thirdly, their administration may come too late into the process and/or be of too short duration to reverse the undesirable effect of long-term hyperglycaemia (Libby and Plutzky, 2002). Despite all the progress made towards a cure for diabetes, important aspects in the early stage of the disease remain unidentified. Earlier interventions may represent the only key solution to prevent the end-point of a long degenerative process induced by the toxic effects of hyperglycaemia.

On one hand, patients with insulin-dependent diabetes mellitus (Type 1), experience elevated blood glucose levels for decades before any signs of macrovascular diseases are manifested (Jacobs *et al.*, 1991). On the other hand, diagnoses of non-insulin dependent diabetes mellitus (Type 2) are often pronounced at a time where vascular diseases are already present (Medalie *et al.*, 1975; McPhillips *et al.*, 1990). Abundant evidence also indicates that macrovascular diseases are initiated in the pre-diabetic state. Random episodes of hyperglycaemia, in fasting or post-glucose-challenge, are also associated with

increased cardiovascular risk factors in non-diabetic subjects (Temelkova-Kurktschiev *et al.*, 2000). In addition, elevated blood glucose, after a glucose challenge, is highly correlated with atherosclerosis in people at high risk for diabetes Type 2 (Yamasaki *et al.*, 1995; Hanefeld *et al.*, 2000). Post-prandial changes are likely to occur before any changes in fasting plasma glucose can be detected and are responsible for the pre-diabetic onset of macrovascular diseases (Haller, 1997; Hanefeld and Temelkova-Kurktschiev, 2002; Lee *et al.*, 2002). Thus, the pathogenesis of macrovascular disease in diabetes is insidious, takes time to develop and is triggered by early events in the progression of the diseases. In the face of hyperglycaemia-induced macrovascular diseases, we proposed to take a step back and investigate the events leading to the high predisposition of the endothelium to glucose toxicity.

2.1.2 The endothelium

The endothelium is the first line of protection for the vascular wall since it occupies a strategic position between the blood and underlying tissue. The role and function of ECs varies between vascular beds; in capillaries ECs regulate gas and nutrient exchange or prevent the passage of harmful substances, while in larger vessels they also control vascular tone by releasing vasoconstrictors and vasodilators (Davis and Hill, 1999). In small contractile vessels deprived of the vasa vasorum (small blood vessels irrigating the walls of large blood vessels), such as coronary arteries, the ECs must allow transport between the blood and cells of the vascular wall, but they must also protect the vessel's integrity, through selective permeability. Elucidating the processes whereby ECs mediate the exchange of plasma molecules with the vascular wall, while at the same time

safeguarding its functional integrity, is important for understanding how EC dysfunction relates to systemic diseases such as diabetes, in which the main causes of morbidity and mortality are vascular diseases (Grundy *et al.*, 1999).

A healthy endothelium contributes to the homeostasis of the vascular wall. This can be achieved through the release of antithrombotic factors, preventing thrombocyte, leukocyte and erythrocyte adhesion, vasodilating substances such as NO and prostaglandins and contracting factors such as endothelin and thromboxane (Badimon *et al.*, 1992; Haller, 1997). In isolated vessels, any injury to the endothelium is reflected by an altered endothelial vasoreactivity (Badimon *et al.*, 1992). It is therefore not surprising that endothelial injury or dysfunction leads to increased vessel permeability, disturbed coagulation and fibrinolysis (Schror, 1997), impaired vascular reactivity (French, 1966; Ross and Glomset, 1976; Goldstein and Brown, 1977), and precede any atherogenic process (Badimon *et al.*, 1992; Lusis, 2000).

Impaired endothelial function is also observed in coronary and peripheral circulation of diabetics (Williams *et al.*, 1998). In animal models, diabetes has been associated with an increased frequency of ECs death and transendothelial transport of macromolecules (Lin *et al.*, 1993). Endothelial dysfunction identified in both diabetic patients and animals has also been linked with a reduced bioavailability of NO (Cosentino and Luscher, 1998; Mompeo *et al.*, 1998). A decreased production of NO, results in an unbalanced vascular tone with increased contractility, and consequent amplification of the shear stress on the endothelium. In both diabetic patient and animals, endothelial dysfunction has

been attributed to the toxic effect of hyperglycaemia (Sank *et al.*, 1994; Cosentino and Luscher, 1998; Lee *et al.*, 2002).

2.1.3 Hyperglycaemia

The growing evidence that hyperglycaemia represents on its own a major risk factor for the development of both micro- and macrovascular disease has stimulated a great interest in the molecular mechanisms by which an elevated concentration of glucose can lead to endothelial dysfunction. From a large body of evidence, four main hypotheses have been put forward. As high plasma glucose saturates the ability ofECsto metabolize glucose, the excess is catabolised or reduced by other, potentially toxic, pathways. First, the polyol pathway converts glucose to sorbitol via the enzyme aldose reductase (Greene *et al.*, 1987; Brolin and Naeser, 1988; Burg and Kador, 1988; Simmons and Winegrad, 1989). At first, the accumulation of sorbitol was thought to produce osmotic damage to the cell, since sorbitol does not diffuse easily across cell membrane. However, the relative accumulation of sorbitol in the cell is far less than other glucose derivatives, and therefore, cannot account for the increased osmotic pressure (Van den Enden *et al.*, 1995). Sorbitol production is also accompanied by a decrease in nicotinamide adenine dinucleotide phosphate (NADPH), which interferes with antioxidation reactions (Kashiwagi *et al.*, 1994), ultimately reducing the availability of NO, a potent vasodilator (Harlan *et al.*, 1984; Rosen and Freeman, 1984; Hunt *et al.*, 1990; Tesfamariam and Cohen, 1992; Kashiwagi *et al.*, 1994). Sorbitol is itself converted to fructose via sorbitol dehydrogenase and cofactor NAD^+. An increased ratio of NADH/NAD^+ inhibit glyceraldehyde-3-phosphate dehydrogenase (GAPDH) and raises the concentration of triose

phosphate, both contributing to the exacerbation of the flux and reflux of glucose through the polyol pathway and the formation of advanced glycation end-products (AGEs).

Second, intracellular hyperglycaemia induces the formation of AGEs (Degenhardt *et al.*, 1998). At first, this was believed to occur through non-enzymatic reactions between glucose and extracellular macromolecules (Brownlee *et al.*, 1988; Hogan *et al.*, 1992), a process found later on to be much slower than the actual formation of intracellular AGE from glucose-derived dicarbonyl precursors. In EC, the intracellular formation of AGEs occurs within a week of hyperglycaemia (Giardino *et al.*, 1994). Three main AGE precursors: glyoxal, 3-deoxyglucosone and methylglyoxal are obtained respectively form glucose auto-oxidation, decomposition of the Amadori products, and fragmentation of glyceraldehyde-3-phosphate and dihydroxyacetone phosphate (Thornalley, 1990; Wells-Knecht *et al.*, 1995). The AGE precursors react with amino groups of intracellular and extracellular proteins to form AGEs. These AGEs impair cell replication, increase formation of lipoprotein and immune reaction adhesion complexes (Brownlee *et al.*, 1985; Cerami *et al.*, 1988), disturb the coagulation process, increase endothelin (a potent vasoconstrictor) release, (Brownlee, 1992), and alter the elasticity of large vessels by enhancing intermolecular cross-linking of type 1 collagen (Huijberts *et al.*, 1993). In addition, the AGEs can bind to AGE receptors such as the receptor for AGE (RAGE), which induces, through a cascade of cellular signalling events, the production of reactive oxygen species (Yamagishi *et al.*, 1998). In ECs, binding of ligands to AGE receptors has been shown to induce the expression of pro-coagulatory and

pro-inflammatory molecules and increase the permeability of the capillary walls (Doi *et al.*, 1992; Schmidt *et al.*, 1995; Abordo *et al.*, 1996; Lu *et al.*, 1998).

Third, excess glucose increases the production of diacylglycerol (DAG), which in turn activates PKC (Lee *et al.*, 1989; Inoguchi *et al.*, 1994; King *et al.*, 1996). PKC activation can also be enhanced through AGE receptors and through the polyol pathway (Keogh *et al.*, 1997; Portilla *et al.*, 2000). Increased levels of DAG and PKC have been found in diabetic animal models. Exposure of cultured vascular cells to hyperglycaemia and the isolation of vascular tissue from diabetic animals has revealed the predominance of the activation of PKC β isoform in these cells (Ishii *et al.*, 1998). PKC is believed to exert an inhibitory function on endothelial nitric oxide synthase (eNOS) production or on its enzymatic activity (Hirata *et al.*, 1995; Ohara *et al.*, 1995), with the end result being impaired vascular relaxation. PKC also increases endothelin-1-stimulated MAP-kinase activity (Tomlinson, 1999). In ECs and SMCs, PKC enhanced the activity of vascular endothelial growth factor (VEGF) which increases the vascular wall permeability, and induces the overexpression of fibrinolytic inhibitor PAI-1 and the activation of nuclear factor (*NF*)-κB.

Fourth and last, is the increased flux through the hexosamine pathway, which affects both gene expression and protein function. In this pathway, an intermediate of glycolysis, fructose-6-phosphate, is converted to glucosamine-6-phosphate by the enzyme glutamine: fructose-6-phosphate amidotransferase. Glucosamine-6-phosphate participates in the synthesis of proteoglycan and the formation of O-linked glycoproteins. An increased flux through the hexosamine

pathway produces changes in gene expression such as transforming growth factor-α (TGF-α), TGF-β1 and PAI-1 (Kolm-Litty *et al.*, 1998; Du *et al.*, 2000).

Specific inhibitors for each of these pathways have been shown to improve the deleterious effect caused by intracellular hyperglycaemia in cultured cells and diabetic animal models. Many attempts have been made to unify all four hypotheses into one single interlinked process. Despite the growing evidence that each of these pathways affects the other, a consensus has yet to be reached. Among the proposed unified theories stands the overproduction of superoxide by the mitochondrial electron-transport chain, the MAPKs serving as glucose transducers, the redox imbalance (increased tissue/ratio of free cytosolic NADH/NAD^+), and the increased production of VEGF. The ultimate goal of each unified theory is to develop an effective inhibition of a single pathway that reduces all glucotoxic effects induced by hyperglycaemia.

Hyperglycaemia has long been associated with impaired endothelial functions (Aronson and Rayfield, 2002). As most studies have focused on the mechanism by which elevated intracellular glucose induces endothelial dysfunction (Brownlee, 2001; Sheetz and King, 2002), very few have raised the questions of how and why ECs accumulate toxic levels of glucose. It is only recently that the regulation of glucose transport in ECs has been examined (Mann *et al.*, 2003), and most of this work has been in the blood-brain and blood-retina barriers (Olson and Pessin, 1996; Barrett *et al.*, 1999; Joost and Thorens, 2001). The integrity of ECs of small contractile vessels is also affected by hyperglycaemia, and the coronary arteries are among the most susceptible to

atheroma, but few studies have directly examined glucose transporters in these vessels (Mann *et al.*, 2003). Despite having the same embryonic origin, there is a strong heterogeneity between ECs of different vascular beds, and even those within the same vascular bed are known to have morphological, physiological and biochemical differences (Garlanda and Dejana, 1997; Ghitescu and Robert, 2002). Data derived from one vascular bed may not be applicable to the rest of the vasculature.

2.1.4 Glucose transporters

Since glucose is a hydrophilic polar molecule, which cannot freely penetrate the double lipid layer of the plasma membrane, a system of carriers, composed of transmembrane proteins, is used to carry glucose in and out of the cells. Over the last 15 years or so, several laboratories have been investigating the molecular structure and mechanisms of the regulation of these proteins involved in the transport of glucose. Two distinct systems of glucose transport have been identified. Glucose can cross the plasma membrane through facilitated diffusion, or be carried through by a secondary active transport system involving the co-transport of Na^+.

The passive transport of glucose is mediated by the facilitative glucose transporters (GLUTs) family. The mechanism of facilitated diffusion involves a 12-transmembrane spanning regions protein forming a pore through the plasma membrane. This pore allows the free movement of glucose in both inward and outward directions, with a net movement of glucose down a concentration gradient. The first GLUT was isolated in 1977 from ghost erythrocytes by

Kasahara and Hinkle (Kasahara and Hinkle, 1977). Nearly ten years later, Mueckler et al. sequenced the first isoform of the large family of GLUTs (Mueckler *et al.*, 1985). The protein structure analysis has revealed five regions that possess both hydrophobic surface, linked to the plasma membrane, and hydrophilic surface, allowing the pore formation. The proposed mechanism of diffusion involves the binding of glucose to the pore complex by means of weak hydrogen bonds (Mueckler *et al.*, 1985). The transport of glucose inside the cell is believed to occur in four steps. The first step corresponds to the binding of glucose to the extracellular site of the transporter. The attachment of glucose would then induce a change in the conformation of the transporter, allowing glucose to occupy the intracellular binding site on the transporter. The release of glucose into the cytosol causes the transporter to take back its original conformation (Appleman and Lienhard, 1989).

Following the cloning of GLUT-1, four more isoforms were discovered (GLUT-2 to GLUT-5) and extensively studied (Mueckler, 1994). A sixth isoform was identified, but later revealed to be a pseudogene not expressed as a protein (Kayano *et al.*, 1990), and a putative seventh isoform was a cloning artefact (Waddell *et al.*, 1992; Burchell, 1998). With the completion of the Human Genome Project, new members of the GLUT family, sharing between 28 and 65 % identity in terms of amino acid sequence and all carrying the sugar transporter signature (consisting of highly conserved glycine and tryptophan residues) were found. In total, 13 members of the gene family of the solute carrier 2A (gene symbol SLC2A) have been identified (Joost and Thorens, 2001). Each GLUT has now been renamed according to its gene symbol approved by the Human Genome Organization Gene Nomenclature Committee (Joost *et al.*, 2002). Under this new

nomenclature system, the GLUTs family has been divided in three distinct classes based on sequence similarity. Class I is characterised by a glutamine in helix 5 and an STSIF-motif in the extracellular loop 7, and comprises GLUT-1 to 4. These isoforms have been well characterised and are often, with GLUT-5, referred to as the classical GLUTs. They differ from each other by their tissue distribution, affinity for glucose and hormonal regulation. Class II lacks a tryptophan following a conserved region (GPXXXP) in helix 10, which corresponds to the binding site for cytochalasin B and forskolin in GLUT-1. Class II includes GLUT-5 and three other related isoforms, GLUT-7, GLUT-9 and GLUT-11. Both GLUT-5 and GLUT-11 have been shown to transport fructose with greater affinity than glucose. Class III unlike the two previous classes, has a shorter extracellular loop 1, and the glycosylation site is in the larger loop 9. Class III includes the last five isoforms, GLUT-6, GLUT-8, GLUT-10, GLUT-12, and the H^+-coupled myo-inositol cotransporter (HMIT1). In addition, four pseudogenes have been identified, of which three of them, including the previously named GLUT-6, share between 80 and 95% similarity with GLUT-3 (Joost and Thorens, 2001; Joost *et al.*, 2002). Each transporter has unique kinetics, and different rates for the transport of sugar into and out of cells.

Glucose can also be carried by a secondary active transporter, the sodium-dependent glucose transporter (SGLT). The active cotransport of glucose was first described by Crane in 1960 (Crane, 1960). The SGLT protein forms a pore across the plasma membrane from which both glucose and water can be transported. The pore, which contains the glucose-binding site, is formed of four transmembrane helices in close proximity to the C-terminus of the protein. The N-terminal domain has been proposed to act as a Na^+ binding or translocation

site. The interaction between the N- and C-terminal domains is thought to result in the cotransport of Na^+ and glucose (Wright *et al.*, 1998). Glucose can be transported against its concentration gradient using the energy generated by the Na^+-electrochemical gradient provided by the activity of the Na^+/K^+ ATPase. The high-affinity SGLT-1 was cloned in 1987 from rabbit intestine (Hediger *et al.*, 1987). SGLT-1 active transport of glucose has been well characterised in the epithelial cells of the brush border of the small intestine and proximal tubules of the kidneys (Wright *et al.*, 1998; Wright, 2001). A low affinity SGLT-2 has been cloned from the pig kidney epithelial cells. It has 76% identity to its homologue SGLT-1. While most of the kinetic properties are similar between SGLT-1 and SGLT-2, a reduced Na^+/glucose coupling (from 2:1 to 1:1) has been found in the case of SGLT-2 (Mackenzie *et al.*, 1996). SGLT-2 is predominantly located on the apical membrane of convoluted proximal tubule epithelial cells of the kidney (Wallner *et al.*, 2001). A low affinity SGLT-3 has also been identified in both small intestine and renal epithelial cells (Kong *et al.*, 1993; Mackenzie *et al.*, 1994). The stoichiometry of this third SGLT protein is similar to that of SGLT-1 with a coupling of 2 Na^+ for 1 glucose (Diez-Sampedro *et al.*, 2001). SGLT-3 shares 76 to 89% similarity with SGLT-1. Three more SGLT-like transporters are part of the same gene family (gene symbol SLC5A), identified from the Human Genome Project, and remain to be completely characterised (Kong *et al.*, 1993; Wood and Trayhurn, 2003). Table 2.1 summarise the principal characteristics of each isoform of the GLUT and SGLT families.

Table 2.1 Summary of the principal characteristics of the sugar transporters.

Isoform	M.W. (~kDa)	Glucose affinity (~K_m)	Other affinity (~K_m)	Tissue expression	Functional characteristics	Asymmetric distribution
GLUT-1	45 55-65	20mM 3OMG 5-7mM 2DG	17mM galactose >5M fructose mannose	Most tissue, erythrocytes, EC of blood barrier, brain	basal transport	basolateral membrane
GLUT-2	56	42mM 3OMG 7-16mM 2DG	66mM fructose 36-86mM galactose	liver, intestine, pancreatic β-cell	trans-epithelial transport glucose sensor	basolateral membrane
GLUT-3	48	10mM 3OMG 1-2mM 2DG	6-8mM galactose	Brain, adipocyte	neuronal transporter	
GLUT-4	50	2-4mM 3OMG 5mM 2DG		muscle, adipocyte, heart	insulin-sensitive transporter	
GLUT-5	50-55		6-14mM fructose	intestine, testis, kidney, adipocyte, muscle	fructose transporter	apical membrane
GLUT-6	46	Low affinity, high k_m		spleen, leukocyte, brain, adipocyte	not responsive to insulin	
GLUT-7	n.d.	n.d.	n.d.	n.d.	n.d.	n.d.
GLUT-8	37-50	2mM 2DG	maybe fructose	testis, brain, blastocyst, adipocyte, muscle	not responsive to insulin	
GLUT-9	59	n.d.	n.d.	liver, kidney	n.d.	
GLUT-10	57	0.3mM 2DG		liver, pancreas, muscle, heart		
GLUT-11	45	n.d.	maybe fructose	heart, muscle	may be a fructose transporter	
GLUT-12	50	n.d.	n.d.	heart, prostate, muscle, adipocyte, small intestine	Insulin-sensitive transporter	
HMIT	67-83	No hexose transport	0.1mM myo-, scillo-, muco-, chiro-inositol	Brain, adipocyte	Transport of H^+/ myo-inositol	
SGLT-1	71-77	0.4mM MDG	Galactose	kidney proximal tubule (straight part), intestine	Na^+-dependent transport	apical membrane
SGLT-2	73	2mM MDG	Transport only glucose	Kidney proximal convoluted tubule	Kidney Na^+-dependent transporter	apical membrane
SGLT-3	73	6mM MDG	Transport only glucose	kidney, intestine, liver, spleen	Na^+-dependent transport	
SGLT-4	n.d.	n.d.	n.d.	n.d.	n.d.	
SGLT-5	n.d.	n.d.	n.d.	n.d.	n.d.	
SGLT-6	n.d.	n.d.	n.d.	n.d.	n.d.	

Class I, Class II, Class III, 3-O-methyl-D-glucose (3OMG), 2-deoxy-D-glucose (2DG), α-methyl-D-glucose (MDG), not determined (n.d.). (Thorens *et al.*, 1988; James *et al.*, 1989; Gould *et al.*, 1992; Bell *et al.*, 1993; Mueckler, 1994; Thorens, 1996; Walmsley *et al.*, 1998; Hirsch and Rosen, 1999; Carayannopoulos *et al.*, 2000; Phay *et al.*, 2000; Dawson *et al.*, 2001; Doege *et al.*, 2001; Joost and Thorens, 2001; Wright, 2001; Rogers *et al.*, 2002; Mann *et al.*, 2003; Wood and Trayhurn, 2003).

The tissue and subcellular distribution, as well as the kinetic properties of the isoforms, are critical for determining the net glucose transport rate, and play a central role in the regulation of intracellular glucose concentration. What then is known of the tissue and subcellular distribution of the GLUTs and SGLTs in the vasculature system? Despite the evidence implicating glucose toxicity in the prevalence of both micro- and macro-vascular disease in diabetes, it is only recently that an interest in the regulation of glucose transport in EC and SMC has been shown (Mann *et al.*, 2003).

GLUT-1 was thought for the longest time to be the only glucose transporter present in the ECs (Pardridge *et al.*, 1990). In both ECs and SMCs, it regulates the basal transport of glucose (Charron *et al.*, 1989; Pardridge *et al.*, 1990; Pekala *et al.*, 1990; Farrell and Pardridge, 1991; Hemmila and Drewes, 1993; Lutz and Pardridge, 1993; Maher *et al.*, 1993; Sank *et al.*, 1994; Cornford *et al.*, 1995; Bolz *et al.*, 1996; Gaposchkin and Garcia-Diaz, 1996; Urabe *et al.*, 1996; Leino *et al.*, 1997; Shi *et al.*, 1997; Vannucci *et al.*, 1997; Cornford *et al.*, 1998b; Takagi *et al.*, 1998; Dobrogowska and Vorbrodt, 1999; Nualart *et al.*, 1999; Simpson *et al.*, 1999). Of all vascular tissue, the BBB has been by far the EC source in which glucose transport regulation has been the most studied and characterised. This is not surprising given the importance of glucose as a primary source of energy for the brain and the tight junctions of the BBB, regulating the passage of substances to the brain (Garlanda and Dejana, 1997). Asymmetric distribution of GLUT-1 has been reported in the BBB (Farrell and Pardridge, 1991; Cornford *et al.*, 1998b) and in cerebral microvasculature (Bolz *et al.*, 1996; Dobrogowska and Vorbrodt, 1999; Hirsch and Rosen, 1999). In each case, GLUT-1 was found in greater abundance on the abluminal membrane (Farrell and Pardridge, 1991; Bolz *et al.*,

1996; Cornford *et al.*, 1998a; Dobrogowska and Vorbrodt, 1999; Hirsch and Rosen, 1999). The presence of GLUT-3 has been reported on human intraplacental microvessel ECs (Hauguel-de Mouzon *et al.*, 1997). GLUT-3 mRNA has also been found through in situ hybridization in ECs of brain microvessels following a long period of reperfusion after ischemia (Urabe *et al.*, 1996) and in ECs of human brain tumour vessels (Nishioka *et al.*, 1992). GLUT-3 protein expression was detected only in the tumour vessels while it was not in the post-ischemic cortical ECs (Nishioka *et al.*, 1992; Urabe *et al.*, 1996). GLUT-3, if expressed in the endothelium, is likely to play a role in the cells in critical need for glucose. Insulin-sensitivity as well as the presence of GLUT-4 has also been reported in ECs of calf retinal (King *et al.*, 1983) and brain microvessels (Frank and Pardridge, 1981), in forebrain of bovine BBB (McCall *et al.*, 1997), and in fat and muscle capillary ECs of the rat (Vilaro *et al.*, 1989). However, in cultured cardiac ECs (Thomas *et al.*, 1995), cultured aortic ECs (McCall *et al.*, 1997), and human muscle capillary ECs (Friedman *et al.*, 1991) studies have reported the absence of GLUT-4. The role of GLUT-4 in the vascular system is still controversial and may be specific to EC of only certain vascular beds. GLUT-5 has been detected in cerebral microvasculature ECs (Mantych *et al.*, 1993a; Mantych *et al.*, 1993b), but its functionality and role in these cells remain to be determined. An SGLT-1-like glucose transporter has been identified on the luminal membrane of brain capillaries and, was shown to be mostly functional during period of hypoglycaemia (Matsuoka *et al.*, 1998; Nishizaki and Matsuoka, 1998). To our knowledge, the presence of GLUT-2 and the novel GLUT isoforms in ECs has not yet been assessed (Mann *et al.*, 2003).

GLUT expression can be altered in diabetes. In diabetic animal models, down-regulation (Asada *et al.*, 1998; Hajduch *et al.*, 1998; Hirsch and Rosen, 1999), as well as up-regulation (Vannucci *et al.*, 1997; Vannucci *et al.*, 1998; Reagan *et al.*, 1999) of GLUT expression has been reported in a variety of tissues. Yet again, in ECsof the vasculature very little is known regarding the regulation of glucose transporters (Mann *et al.*, 2003). The expression of GLUT-1 is reduced in brain capillary ECs of STZ-induced diabetic rats but not in post-prandial hyperglycaemia (Pouliot and Beliveau, 1995). Similar observations in bovine retinal and aortic ECs support the lack of effect of acute hyperglycaemia on GLUT-1 expression (Kaiser *et al.*, 1993; Mandarino *et al.*, 1994; Vinals *et al.*, 1999). Accordingly, it has been shown that ECs are unable to decrease their rate of glucose transport in ambient elevated glucose concentration (Kaiser *et al.*, 1993; Giardino *et al.*, 1994; Howard, 1996b). Since ECs are highly specialized cells and play a major role in the transport of glucose from the blood through the vascular walls, especially in small vessels deprived of vasa vasorum this inability to down-regulate glucose uptake could be responsible for their high susceptibility to glucose toxicity.

While a short-term elevation of glucose concentration seems to have no effect on the expression of GLUT-1, hypoglycaemia has been show to up-regulate GLUT-1 expression in bovine brain microvascular ECs (Takakura *et al.*, 1991), rat heart (Hirsch and Rosen, 1999) and BBB ECs (Simpson *et al.*, 1999). The up-regulation of GLUT-1 following a period of hypoglycaemia is thought to compensate for the low ambient glucose concentration. The observations of an increased rate of glucose uptake in ECs exposed to glucose starvation support this idea (Takakura *et al.*, 1991; Gaposchkin and Garcia-Diaz, 1996). As only

limited studies have found other GLUT isoforms in ECs, an even smaller number have looked at the effect of diabetes and hyperglycaemia on their expression. In bovine BBB, diabetes was shown to have no effect on the expression of GLUT-4 (Mantych *et al.*, 1993b), while in rat placental vasculature, GLUT-3 expression has been up-regulated by both diabetes and elevated glucose concentration (Mantych *et al.*, 1993b).

2.1.5 Hypothesis

Given the EC's susceptibility to hyperglycaemia, we hypothesized that the expression and subcellular distribution of the transporters would favour intracellular glucose accumulation, and that there would be an inappropriate adaptation to the diabetic state.

2.1.6 Native endothelium preparation

In this study, we examined the expression and subcellular distribution of the classical GLUTs (1-5) and SGLT-1 in en face preparations of rat coronary, cerebral, renal and mesenteric artery endothelia. Because it has been demonstrated that the endothelial cells and SMCs are functioning as a unit, the structural relation between them should be preserved in any experimental design. The ECs, when cultured, tend to lose their specialized properties acquired during differentiation. The ECs of the BBB develop tight junctions and express selective transporters to protect the brain against toxic and harmful substances. These properties are found only in brain capillary ECs and are therefore specific to the brain. This organ-specificity is believed to be determined and maintained by their surrounding environment and interaction with

neighbouring cells. For example, the loss of expression of GLUT-4 and GLUT-1 after the third and tenth passage respectively of cultured brain ECs has been previously reported (McCall *et al.*, 1997). Specialization of the endothelium can be organ-specific or function-specific, expressing different phenotypes even in the same organ. Markers of these phenotypes are mainly enzymes and proteins produced and expressed by different types of ECs (Garlanda and Dejana, 1997). For these reasons, freshly dissected vessels from four different vascular beds were used in this investigation. The coronary, cerebral, renal and mesenteric arteries have been selected for their variable levels of susceptibility to damage induced by hyperglycaemia and prevalence of vascular disease (Taylor *et al.*, 1994; Mavrikakis *et al.*, 1998; Perler and Becker, 1998). Moreover examining the specific structure of ECs from different vascular beds will allow the identification of possible differences in their specialized properties.

2.1.7 Fluorescence microscopy and deconvolution

The utilisation of a 3D microscopy imaging system provides a precise evaluation of the location and disposition of the transporters, and with a greater resolution than is possible with a conventional fluorescent microscope. Other biochemical methods based on cell fractionation disrupt the architecture of the cell. On the other hand, immunohistochemistry coupled with electron microscopy can localise proteins with a greater resolution, however the uncertainty of the labelling once the tissue has been embedded for sectioning renders this technology problematic. Although confocal microscopy provides a more straightforward approach, it has been demonstrated that image restoration generates greater resolution for discretely organized objects from which the

emitted fluorescence intensity is low (Carrington *et al.*, 1989; Carrington *et al.*, 1995). Deconvolution is superior because out of focus light is not rejected, as is the case with a confocal microscope whose pinhole is closed so as to maximize resolution, but is instead collected and used to reconstruct the original image (Moore *et al.*, 1990). Moreover, our imaging system is equipped with a cooled charge-coupled device (CCD) camera (the image detector) with a quantum efficiency 5X higher than the image detector in a confocal. When this quantum efficiency is added to the loss of signal through the confocal pinhole, our imaging system becomes approximately 50X more sensitive than a confocal microscope. In addition, the high quantum efficiency of the cooled CCD camera means that total light exposure of the specimen can be reduced, which in turn minimizes photo bleaching and photo damage which are inherent problems in confocal microscopy. The use of this system in conjunction with immunohistochemistry, and on an intact fixed vessel preserved the molecular and structural organisation of the GLUTs and SGLTs examined.

2.1.8 STZ animal model

The effect of long-term hyperglycaemia on the expression and subcellular distribution of the GLUT in ECs was examined in the streptozotocin (STZ) diabetic rat. This is the predominant animal model chosen for the study of diabetes. Streptozotocin (2-deoxy-2-(3-methyl-3-nitrosurea) 1-d-glucopyranose) (α+β), was first isolated in 1959 from Streptomyces achromogenes (Herr *et al.*, 1959). This broad-spectrum antibiotic agent is an N-nitroso derivative of D-glucosamine, composed of a cytotoxic moiety, 1-methyl 1-nitrosurea, positioned on carbon-2 of 2-deoxy-D-glucose (Rerup, 1970). The administration of

streptozotocin has been shown to induce hyperglycaemia, polydipsia, polyuria, weight loss, albuminuria and glomerular ultra structural changes comparable to those seen in diabetes type I (Tomlinson *et al.*, 1992). Streptozotocin produces its diabetogenic actions through cytotoxic destruction of the β-cell of the islets of Langerhans of the pancreas (Junod *et al.*, 1969; Tomlinson *et al.*, 1992). Previous studies have shown that STZ toxicity is restricted to cells expressing GLUT-2 (Schnedl *et al.*, 1994). The transport of the toxin by GLUT-2 but not GLUT-1 has been recognized as a requirement for the destruction of the neuroendocrine cells. STZ achieves an efficient killing of the cells by initiating the fragmentation of the DNA. The cytotoxic portion of STZ generates free-alkylating radicals, carbonium ions (CH^{3+}) and nitric oxide (NO), all agents reducing the level of cellular nucleotides and related compounds (Yamamoto *et al.*, 1981; Uchigata *et al.*, 1982). Burkart et al. identified NAD^+ depletion caused by poly ADP-ribose polymerase (PARP) activation, as the metabolic event leading to cell death. This study demonstrated that knockout PARP-/- mice were completely resistant to the STZ toxin. The STZ-treated knockout mice were normoglycaemic, maintained a normal level of secreted insulin, and preserved their islet ultrastructure (Burkart *et al.*, 1999). It has been previously demonstrated that a stable hyperglycaemia for up to 3 months, can be induced with intravenous or intraperitoneal injection of STZ at doses exceeding 40mg/kg (50mg/kg to 70mg/kg) and can be restored within weeks with insulin treatment at the 50mg/kg STZ dose but not with higher doses of STZ (Ar'Rajab and Ahren, 1993). Moreover, with lower doses of STZ, a small but sufficient number of pancreatic β-cells still secrete insulin and prevent ketoacidosis thus allowing the animal to survive without insulin supplementation (Junod *et al.*, 1969).

2.2 Methods

All chemicals were purchased from Sigma-Aldrich Ltd. (Oakville, ON) unless otherwise stated. Animal handling was done in accordance with the guidelines of the Canadian Council on Animal Care and the Principles of laboratory animal care (National Institute of Health (NIH) publication no. 85-23, revised 1985).

2.2.1 Animals

Male Wistar rats (200-235 g; University of British Columbia Animal Care Centre, Vancouver, B.C.) were given STZ (50 mg/kg, dissolved in saline) or saline (1 ml/100 g) via injection through the tail-vein. Animals were sacrificed 8 weeks later with a peritoneal injection of pentobarbital (30 mg/kg). During this period, bi-weekly morning measurements of tail-vein blood glucose (One Touch II glucometer, Lifescan Canada LTD, Burnaby, B.C.) and body weight were recorded.

2.2.2 Tissue preparation

Segments of approximately 0.6 to 1.0 mm in length of septal coronary, middle cerebral, second order interlobar renal and mesenteric arteries, which are 100 μm to 250 μm in diameter, were carefully dissected. The tissue was immersed in ice-cold oxygenated (95% O_2/ 5% CO_2) Krebs buffer solution (in mmol/l: 119 NaCl, 4.7 KCl, 1.18 KH_2PO_4, 1.17 $MgSO_4$, 24.9 $NaCO_3$, 11.1 dextrose, 2.5 $CaCl_2$, pH 7.4) during the dissection.

The vessel was cut longitudinally to expose the luminal side of the vessel, avoiding damage to the endothelium, and then fixed in 2% paraformaldehyde dissolved in phosphate buffered saline, (PBS; in mmol/l: 137 NaCl, 8 NaH_2PO_4, 2.7 KCl, 1.5 KH_2PO_4; pH 7.4) for 10 min. Fixation was quenched with a 10-min rinse in 100 mmol/l glycine (pH 7.4) and the cells were permeabilized with 0.06% saponin in PBS for 10 min at room temperature followed by 3 x 10-min rinses with PBS.

2.2.3 Immunohistochemistry

Non-specific binding sites were blocked by incubating the fixed, permeabilized tissue in 10% donkey serum dissolved in PBS for two hours at room temperature. Vessels were then incubated overnight at 4°C with two antibodies raised in different species; one against a glucose transporter isoform (GLUT-1 to 5 or SGLT-1), and one against an EC or membrane marker (Vascular Endothelial (VE)-cadherin, von Willebrand factor, or caveolin-1). The optimal antibody concentrations were determined empirically. All antibodies were diluted in antibody buffer (in mmol/l: 75 NaCl, 18 Na3 citrate with 2% donkey serum, 1% bovine serum albumin, 0.06% saponin, and 0.02% NaN3). The antibody sources, concentrations, epitope, and suppliers are listed in Table 2.2.

Table 2.2 List of the primary antibodies.

1° ANTIBODY	IMMUNOHISTO-CHEMISTRY μg/ml	WESTERN BLOTTING μg/ml	EPITOPE	Supplier
Mouse human VonWillebrand Factor (mono IgG)	40	–		Serotec Inc., Raleigh, NC
Goat human VE-cadherin (C-19) (poly IgG)	6.6	0.2	Intracellular domain, Carboxy terminus	Santa Cruz Biotechnology, Santa Cruz, CA
Mouse caveolin-1 (mono IgM)	80	–		Transduction Laboratories, Lexington, KY
Mouse α-actin (mono IgG)	–	5.8		
Rabbit GLUT-1 (H-43) (poly IgG)	10	1	Intracellular domain, carboxy terminus, aa 218-260	Santa Cruz Biotechnology, Santa Cruz, CA
Rabbit GLUT-2 (Neat serum)	dilution 1:500[a]	Dilution 1:500[a]	Intracellular domain, carboxy terminus, 25 aa	East Acres Biologicals, Southbridge, MA
Goat GLUT-3 (M-20) (poly IgG)	10	0.8	Intracellular domain, Carboxy terminus	Santa Cruz Biotechnology, Santa Cruz, CA
Mouse GLUT-4 (mono IgG)	30	5	Intracellular domain	Biogenesis, inc. Kingston, NH
Rabbit GLUT-5 (poly IgG)	10	2	Intracellular domain, carboxy terminus, aa 490-502	Alpha Diagnostic, Int. San Antonio, TX
Rabbit SGLT-1 (poly IgG)	10	–	Extracellular domain, aa 402-420	Alpha Diagnostic, Int. San Antonio, TX

[a]The exact antibody concentration has not been determined.

Excess antibody was removed by 3 x 10 min rinses in antibody wash solution (in mmol/l: 75 NaCl, 18 Na3 citrate with 0.06% saponin). The tissue was then incubated for 2 hours with two donkey affinity-purified secondary antibodies that had been solid-phase adsorbed to minimize species cross-reactivity (Jackson ImmunoResearch Laboratories, West Grove, PA). The secondary antibodies were conjugated to either fluorescein isothiocyanate (FITC) or Texas Red and diluted in antibody buffer. Following incubation with the secondary antibodies, the tissue was rinsed 3 x 10 min in antibody wash solution. The cells' nuclei were then labelled with DAPI (4', 6-diamidino-2-phenylindole dihydrochloride; 0.3 μmol/l, Molecular Probes, Eugene, OR), for 5 min, followed by 3 x 10 min rinses in PBS. The labelled vessels were mounted on a coverslip in DABCO (1,4-diazabicyclo[2.2.2] octane (triethylenediamine) mounting medium (90% glycerol, 10% 10X PBS, 2.5% triethylenediamine, and 0.02% NaN3). To avoid compression of the vessel the edge of the coverslips were suspended on a thin layer of clear nail polish that had been applied to the slide. Small sub-resolution beads were added to the DABCO (TetraSpeck Fluorescent microsphere standards, 0.22μm diameter, Molecular Probes). These fluoresce at all the wavelengths used (DAPI, FITC and Texas Red) and enabled alignment of the data sets.

Two control experiments were conducted. In the first, vessels were labelled with a primary antibody and an inappropriately targeted secondary antibody. In the second, the primary antibody was omitted.

The adherens junctions, of which VE-cadherin is an integral part, separate the luminal from the abluminal sides of the cell (Leach *et al.*, 1993; Firth, 2002).

We used the position of this molecule to optically dissect the cells into luminal and abluminal sides. This was not possible for the GLUT-3 transporter, whose antibody was also raised in goats. In this case, we used mouse anti-von Willebrand factor to mark the endothelial cells, and used the contact points of neighbouring cells to demarcate the luminal-abluminal boundary (Farrell and Pardridge, 1991).

2.2.4 Acetylated LDL uptake

Arteries were dissected in Krebs solution as described above and cut longitudinally to expose the endothelial cells. The arteries were then incubated for 4 hours at 37°C in an incubator equilibrated with 5% C02, immersed in culture medium (GIBCO RPMI medium 1640, Invitrogen, Burlington, ON) to which 1% serum replacement and 10 μg/ml of acetylated low density lipoprotein labelled with 1,1'-dioctadecyl-3,3,3',3'-tetramethylindo-carbocyanine perchlorate (Dil-Ac-LDL; Biomedical Technologies Inc., MA) were added. After a 10-min wash in fresh media, without Dil-Ac-LDL, the artery was incubated for 5 min with a nucleic acid stain (Hoechst 33342, trihydrochloride, trihydrate, 200 μg/ml; Molecular Probes). The vessel was washed for 10 min in fresh media, and then mounted open on a coverslip in fresh media, sealed to the slide with clear nail polish, and imaged immediately.

2.2.5 Western blots

Tissue lysate and homogenate were obtained from rat septal coronary artery, human coronary artery endothelial cells (HCAECs, see chapter 3), epididymal adipose tissue, heart ventricle, jejunum, and brain cortex. After

dissection, the arteries were longitudinally opened as described above. This procedure exposes, primarily, the endothelium to the lysis buffer (0.025 mol/l Phosphate buffer pH 7.4, 150 mmol/l NaCl, 2.5 mmol/l ethylenediaminetetraacetic acid (EDTA), 0.5% ethoxylate octyl phenol (IGEPAL), 10% Glycerol) in which the tissue was incubated for 30 min on ice. With this procedure most of the endothelial proteins were present in the lysate with some contamination of SMC proteins which could not be avoided (Figure 2.3). HCAECs grown in a T-25 flask (see chapter 3), were rinsed with ice cold PBS. While kept on ice, 0.8 ml of lysis buffer was added to the flask and the cells scraped off with a scraper. The lysate was then vortexed and incubated on ice for 30 min All other tissues were dissected and homogenized, in the same ice-cold lysis buffer, using two 20-second pulses of a Polytron (type PT 10 OD) at medium to high speed and further incubated on ice for 30 min The homogenized tissues and lysed HCAECs were centrifuged at 4 ºC for 10 min at a 1000g to remove any cellular debris. Protein concentrations were determined using a modified Lowry reagent protein assay kit (Pierce, Rockford, IL). Two parts of tissue lysate or homogenate were combined with one part of sample buffer (3X concentrate, 0.175 mol/l Tris, 44% Glycerol, 15% β-2-mercapto-ethanol, 7% SDS, 0.01% Bromophenol Blue, pH 6.8) and boiled for 5 min (GLUT-2 gave better results with the omission of the boiling step). Tissue samples and the prestained protein ladder (unboiled; Fermentas, Burlington, ON) were loaded and resolved on a 5% stacking and 12.5% running SDS-PAGE and the proteins were transferred to nitrocellulose membrane. Antibody incubations with the membranes were performed at 37 ºC with gentle agitation. Non-specific binding sites were blocked with 10% non-fat dry milk in Tris-buffered saline Tween (TBS-T; 50 mmol/l Tris, 0.09% NaCl, and 0.01% Tween (Polyoxyethylene sorbitan

monolaurate); pH 7.6). The membranes were then incubated with primary antibodies diluted in 5% non-fat dry milk in TBS-T, rinsed with TBS-T and further incubated with the appropriate horseradish peroxidase conjugated secondary antibodies (1:20000, either anti-mouse, anti-rabbit or anti-goat; Jackson ImmunoResearch Laboratories) also diluted in 5% non-fat dry milk in TBS-T. After a final rinse in TBS-T, the membranes were treated with the Western Lightning chemiluminescence Reagent Plus detection system (Perkin Elmer Life Sciences, Boston, MA) and developed on Kodak BioMax film (Amersham Biosciences Inc. Baie D'Urfe, PQ). Control experiments were performed without the primary antibodies and demonstrate specificity of the labelled single band for each protein probed (Appendix 2).

A BLAST search (National Center for Biotechnology Information, Washington, DC) was conducted to ensure that the antibodies used in this study only targeted the proteins of interest.

2.2.6 Immunostaining controls

Antibody specificity was also tested by labelling tissues in which the glucose transporters had been previously characterized (Sato *et al.*, 1996; Thorens, 1996; Concha *et al.*, 1997). As positive and negative immunostaining controls, red blood cells, pancreatic islets, neuronal primary culture, epididymal adipose tissue and segments of the jejunum, were labelled with antibodies against GLUT-1, 2, 3, 4 and 5 and SGLT-1. Blood samples were collected from rat-tail vein, heparinized (10%) and centrifuged for 5 min at 17000g. The plasma was removed and the erythrocytes fixed and labelled as described above. Whole

pancreas, epididymal adipose tissue and segments of the jejunum were dissected from rats in Krebs solution, embedded in Tissue Tek (Sakura, Torrance, CA) and flash frozen in liquid nitrogen-cooled isopentane at -60°C. Cross-sections of these tissues were cut on a cryostat, thaw-mounted on Superfrost slides (VWR, Edmonton, AB), fixed, and labelled as described above. Primary cultures of rat neurons were obtained from Dr. Kenneth Baimbridge, Department of Physiology, UBC, Vancouver, B.C. (Abdel-Hamid and Baimbridge, 1997; Krebs *et al.*, 2003). The neurons were fixed, and labelled as described above.

2.2.7 3D Image acquisition, deconvolution and analysis

A series of two-dimensional fluorescent images was acquired through the depth of the cell with a standard Nikon Diaphot 200 inverted microscope equipped for epifluorescence (100W Hg illumination, 60X oil immersion objective, NA 1.4, 4X adaptor). The pixel size was 100 x 100 nm and the Z spacing was 250 nm. Images were recorded with a CCD camera with a SITe SI502AB chip, peak quantum efficiency of 80%, with a 16-bit dynamic range (Photometrics, Tucson, AZ). For each wavelength, a three-dimensional data set was acquired using narrow bandpass filters specific for Fluorescein, Texas Red, and DAPI (XF22, XF43, XF06; Omega Optical, Brattleboro, VT). Images were background and dark current subtracted and corrected for photobleaching as previously described (Moore *et al.*, 1993). A flat field was used to correct for non-uniform illumination and camera sensitivity across the field of view. Images were deconvolved using the algorithm developed by Carrington et al. (Carrington *et al.*, 1995) with an empirically determined point-spread-function (PSF) on an exhaustive proton reassignment (EPR) client-server (Scanalytics,

Billerica, MA). Small fluorescent microspheres (100 nm diameter, Molecular Probes), of the appropriate wavelength, were used to measure the microscope's PSF. After deconvolution, each image was thresholded by partitioning the image grey-scale histogram based on visual inspection of both the image and its histogram. The background was segmented from the image by assigning a zero value to all pixels with a grey level lower than the threshold. Deconvolved and thresholded images were aligned using the fiduciary markers. All images are 3D reconstruction of the indicated depth.

2.2.8 Data quantification and analysis

Each imaged cell was isolated from the en face endothelium of an intact vessel through digital dissection (using cell junction marker VE-Cadherin, Figure 2.2B). To quantify the distribution of the GLUTs and SGLT-1, the 3D images of a single cell were divided into a series of non-overlapping 5 μm thick segments along their long axis. Each segment was then divided into a luminal and abluminal section using VE-cadherin and neighbouring cells as guides. Then, the number of labelled voxels on both sides was counted for the whole volume of the segment. The total number of labelled voxels on each side was summed along the length of the entire cell and expressed as a ratio of the number of abluminal to luminal voxels. The data are presented as mean ± Standard Error (SE) and compared using analysis of variance (ANOVA) with multiple comparisons as required.

2.3 Results

2.3.1 Weight and blood glucose

The mean weights and morning blood glucose concentrations of the control Wistar rats at sacrifice were 493 ± 10 g and 3.90 ± 0.03 mmol/l respectively (n=5). STZ-diabetic rats (n=8) had a significantly lower mean weight at sacrifice than the control animals (367 ± 11 g, $p<0.05$) and significantly elevated morning blood glucose concentrations (18.90 ± 0.72 mmol/l, $p<0.05$). Daily morning weight and blood glucose measurements confirmed that the diabetic state of the STZ-injected rats was sustained throughout the experiment (Figure 2.1).

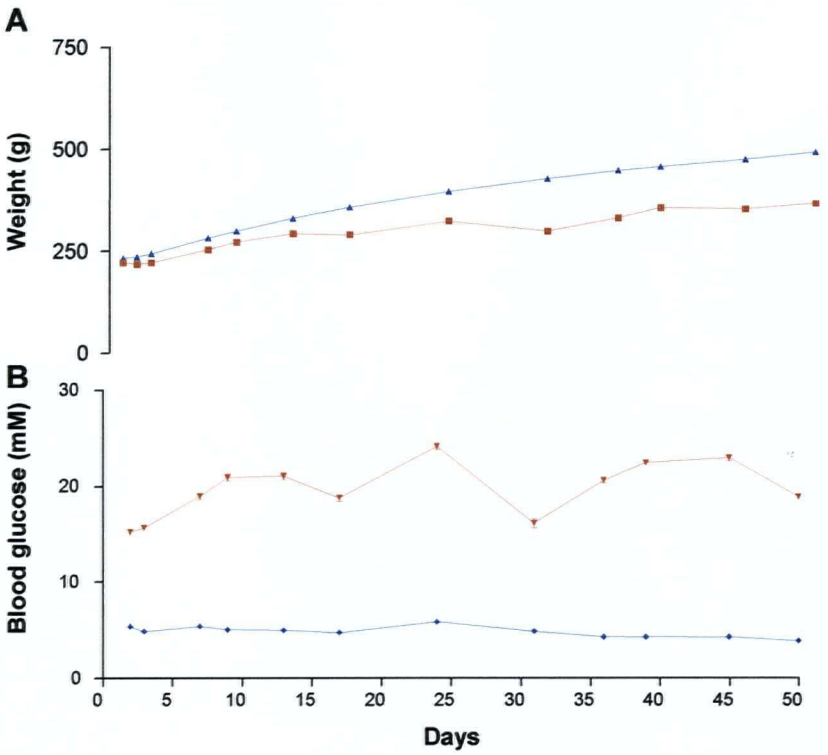

Figure 2.1 Daily morning weight and blood glucose measurements.
Morning weight (A) and blood glucose level (B) of Wistar rats following Streptozotocin (50mg/kg; STZ) or Saline (1ml/100g; Control) injection. The error bars are hidden by the symbols.

2.3.2 Identification of endothelial cells

ECs were distinguished from other cells of the vascular wall using morphological criteria and specific markers. The nuclei of ECs are oriented parallel to the lumen due to the shear stress produced by blood flow (Galbraith *et al.*, 1998), whereas SMC nuclei are oriented perpendicularly. This is reflected in the fusiform shape of the DAPI-labelled nuclei and in their orientation, parallel to the long axis of the vessel, as shown in Figure 2.2A.

In addition, ECs were identified by immunolabelling with two different EC markers: VE-cadherin (Figure 2.2B) and von Willebrand factor (used with GLUT-3 labelling; Figure 2.2D). Both antibodies react positively with the top monolayer of the vascular wall where labelled nuclei run parallel to the lumen.

To determine if the endothelium was well preserved during the dissection procedures, cell viability was tested by visualizing Ac-LDL uptake (Netland *et al.,* 1985). Fluorescence was observed in all cells of the top layer of freshly dissected vessels incubated with Ac-LDL for four hours. This demonstrates that the ECs were intact and viable immediately prior to being fixed (Figure 2.2C).

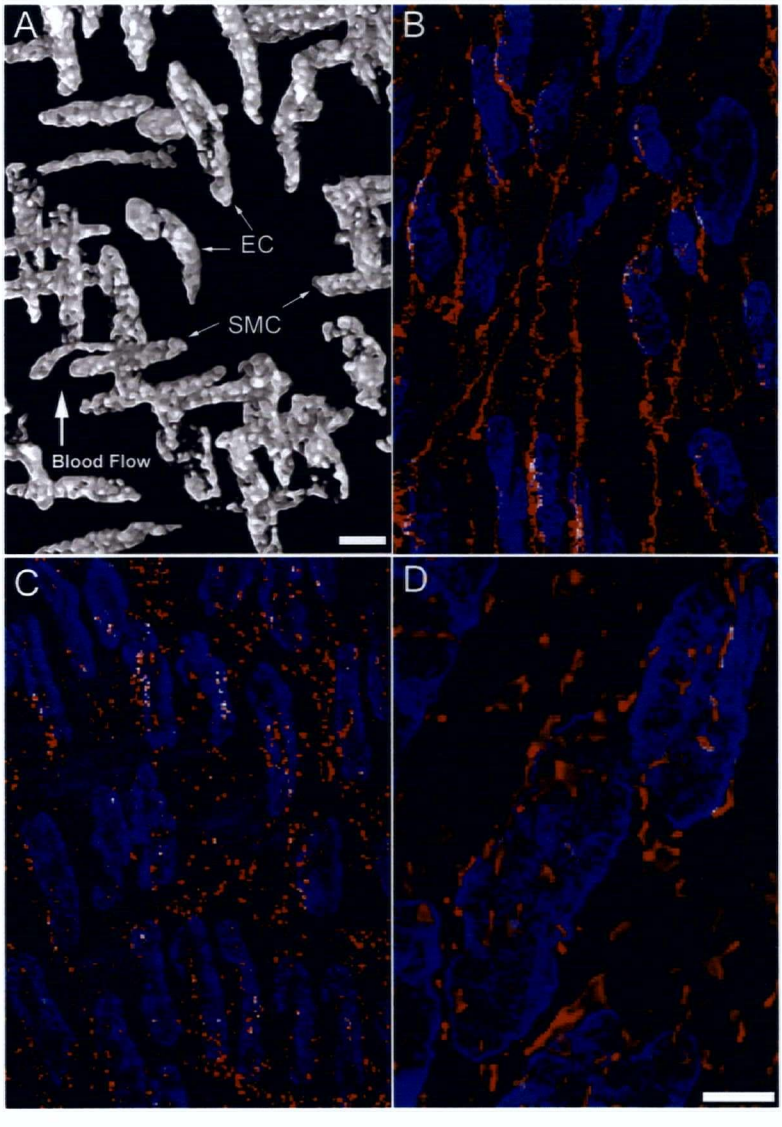

Figure 2.2 Identification of ECs

Deconvolved images of en face septal coronary artery ECs. A) Smooth muscle cell (SMC) and endothelial cell (EC) nuclei are indicated. The white arrow indicates the blood flow orientation. The image is 10 μm deep, scale bar 8 μm (A-C). B) VE-cadherin (red) and nuclei (blue). The image is 1.25 μm deep. C) Ac-LDL (red) and nuclei (blue). The image is 1.25 μm deep. D) von Willebrand factor (red) and nuclei (blue). The image is 3.25 μm deep. Scale bar 2 μm.

2.3.3 Antibody specificity

Antibody specificity was first tested using Western Blots. The presence of EC and SMC proteins in the lysate was determined with VE-cadherin and α–actin antibodies in both vessel preparation and the cultured HCAECs (Figure 2.3). Positive controls (HCAECs, fat, heart, brain and jejunum lysates) were used to establish the molecular weight band identified by the different antibodies. Single bands, for GLUT-1 (~62 kDa), GLUT-2 (~72 kDa), GLUT-3 (~47 kDa), GLUT-4 (~47kDa) and GLUT-5 (~55 kDa), were found from en face septal coronary artery lysate (Figure 2.4). The SGLT-1 antibody did not recognize denatured protein and we were unable to produce a Western Blot for this antibody.

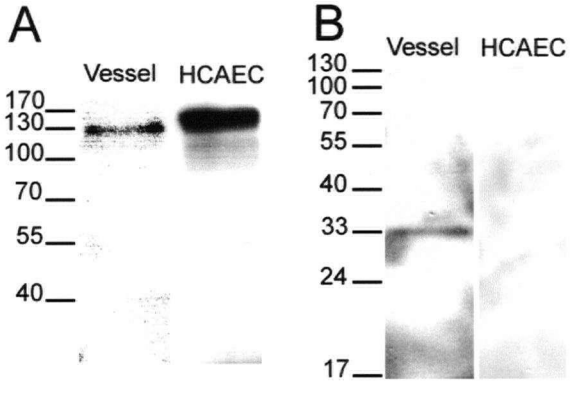

Figure 2.3 EC and SMC identification in coronary artery tissue lysate.
Rat tissue lysates from septal coronary artery blood vessel and cultured HCAECs 30 μg of protein, were separated by 12% SDS-PAGE. After transfer of the proteins to nitrocellulose, detection was performed using antibodies against A) VE-cadherin and B) SMC specific α-actin. The position of molecular weight markers is indicated on the left side in kDa.

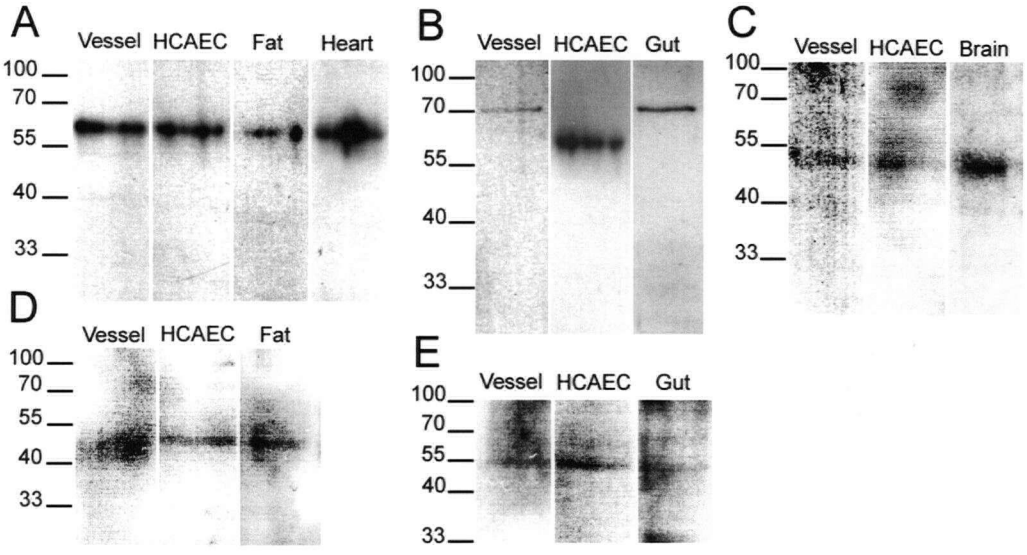

Figure 2.4 Determination of antibody specificity with Western blots.
Rat tissue lysates from septal coronary artery blood vessel, HCAECs, epididymal adipose tissue, heart, jejunum and brain cortex. 30 μg (A-C) or 45 μg (D and E) of protein, were separated by 12% SDS-PAGE. After transfer of the proteins to nitrocellulose, detection was performed using antibodies against A) GLUT-1, B) GLUT-2, C) GLUT-3, D) GLUT-4, and E) GLUT-5. The position of molecular weight markers is indicated on the left side in kDa.

Due to their similarity in molecular weight, the Western blot could not determine the isoform specificity of the antibodies utilized. We therefore used protocols established by others, and labelled cells and subcellular structures for which the glucose transporters had been well characterized; erythrocytes, pancreatic islets, neurons, adipose tissue and epithelial cells of the jejunum (Sato *et al.*, 1996; Thorens, 1996; Concha *et al.*, 1997). GLUT-1 (Figure 2.5A), GLUT-2 (Figure 2.5B) and GLUT-5 (Figure 2.5E) were found in erythrocytes. The side view of the images (see insets), demonstrates the characteristic biconcave shape of the cell, indicating that the label was predominantly on the membrane. GLUT-3 (Figure 2.5C), GLUT-4 (Figure 2.5D) and SGLT-1 (Figure 2.5F) were absent, in

agreement with previous studies (Concha *et al.*, 1997). Cross-sections of pancreatic islets showed the presence of GLUT-2 (Figure 2.5H) but not GLUT-1 (Figure 2.5G) in accordance with earlier data (Sato *et al.*, 1996). We also show positive controls for GLUT-3 (Figure 2.5I) labelling in neurons and GLUT-4 (Figure 2.5J) labelling in adipocytes (Figure 2.5I and J), as shown by other authors (Leino *et al.*, 1997). Lastly, we looked at the distribution of GLUT-2, GLUT-5 and SGLT-1 in epithelial cells of the jejunum, a tissue for which the glucose transporter organization is well established (Thorens, 1996). Our results show a mostly basolateral distribution for GLUT-2 (Figure 2.5K), GLUT-5 present on both the apical and basolateral membranes (Figure 2.5l) and an apical distribution for SGLT-1 (Figure 2.5M), confirming published results (Blakemore *et al.*, 1995).

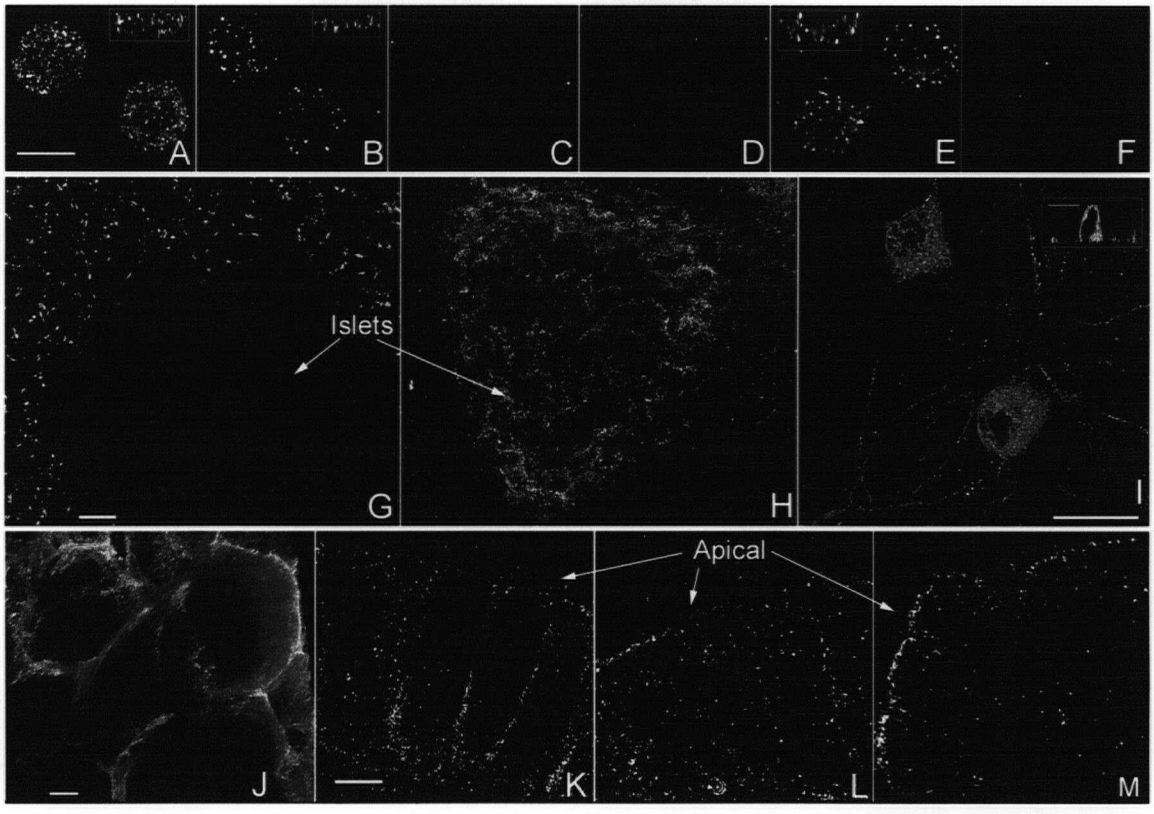

Figure 2.5 Immunohistochemistry demonstrating antibody specificity.
All images were deconvolved and represent a 3D reconstruction of whole cells or section of cells or tissues from rats. A-F) Erythrocytes (3.75 μm deep), scale bar 5 μm, stained for A) GLUT-1, B) GLUT-2, C) GLUT-3, D) GLUT-4, E) GLUT-5, and F) SGLT-1. The insets in A, B and E are cross-sections (average of 2.5 μm deep) of a side view of the erythrocytes. G and H) Cross-sections of pancreatic islet (0.75 μm deep), scale bar 20 μm, stained for G) GLUT-1 and H) GLUT-2. I) Neuronal primary culture labelled with GLUT-3. The image is 8 μm deep and the scale bar is 20 μm. The inset is a cross-section of a side view of the neuron body. J) Cross-section of epididymal adipose tissue (10 μm deep) labelled with GLUT-4, scale bar is 20 μm. K-M) Jejunum epithelial cell cross-sections (0.5 μm deep, apical surface facing up) stained for K) GLUT-2, L) GLUT-5 and M) SGLT-1, scale bar is 5 μm.

No immunostaining was observed when primary antibodies were applied in combination with a secondary antibody targeting an irrelevant species. Figure 2.6 shows ECs labelled with a single primary antibody and two secondary antibodies. The relevant secondary antibody produced labelling in ECs (Figure 2.6A&B for FITC, I for Texas Red). The irrelevant secondary antibodies, in each

case, did not produce any labelling in ECs (Figure 2.6G for FITC and C&F for Texas Red). The middle column in Figure 2.6B, E, and H, shows, as a landmark, the nucleus of each cell labelled with DAPI.

Figure 2.7 shows GLUT-3 (Figure 2.7A), GLUT-5 (Figure 2.7D) and SGLT-1 (Figure 2.7G) labelling. GLUT-3 antibody's immunoreactivity was partly abolished by equal volume of competitive blocking peptides (Figure 2.7B) and completely by 5X excess (Figure 2.7C). Similarly, GLUT-5 and SGLT-1 antibody's immunoreactivity was partly abolished by 5X excess (Figure 2.7E&H, respectively) and mostly by 10X excess of the blocking peptide (Figure 2.7F&I respectively).

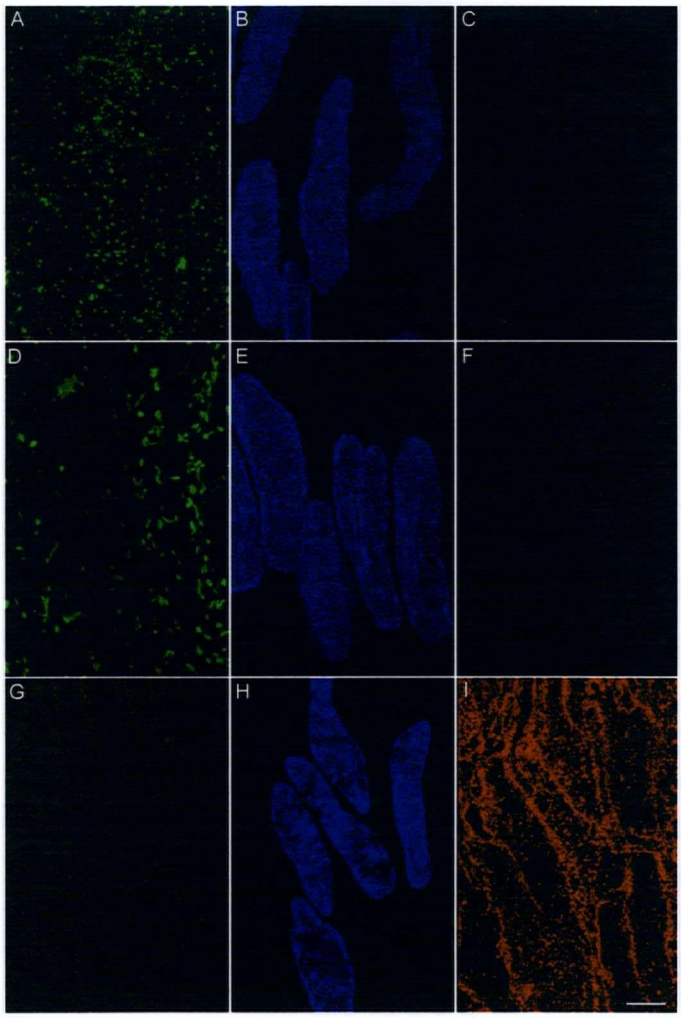

Figure 2.6 Secondary antibody cross-reactivity controls.
Images are 3D reconstruction of coronary artery ECs, view of the cells from the lumen. ECs are labelled with a single primary antibody, rabbit anti-GLUT-1 (A-C), mouse anti-von Willebrand Factor (D-F) and VE-cadherin (G-I) and dual secondary antibody, donkey anti-rabbit FITC and donkey anti-goat Texas Red (A-C).

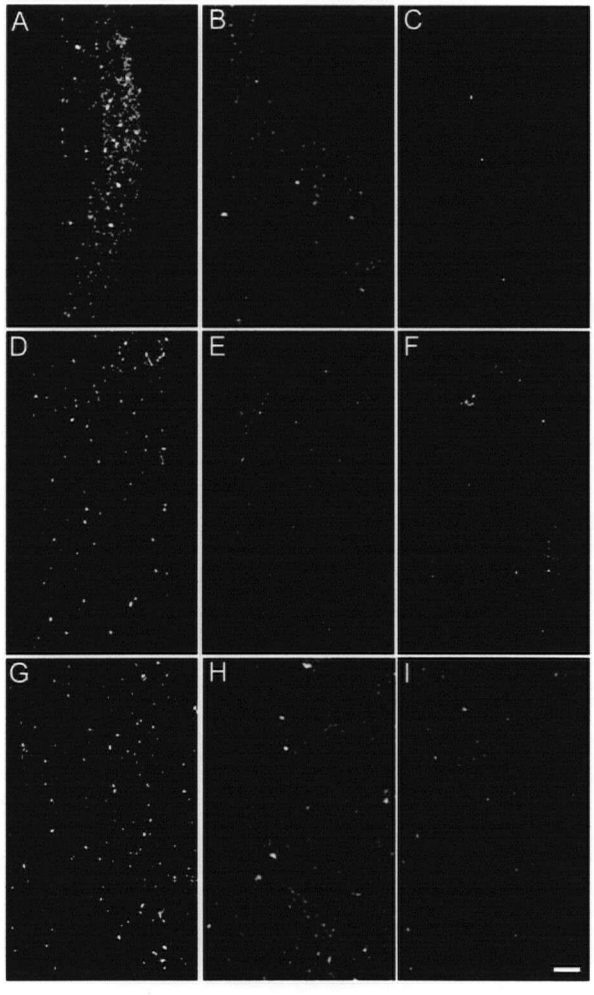

Figure 2.7 Competitive blocking peptide controls.
Images are 3D reconstruction of coronary artery EC, view of the cells from the lumen. ECs labelled with GLUT-3 (A), GLUT-5 (D) and SGLT-1 (G) antibodies. Each respective antibodies were also pre-incubated with equal volume (B) 5 X excess volume (C, E & H), and 10 X excess volume (F & I) of competitive blocking peptide prior to labelling. Scale bar is 5 μm.

2.3.4 Immunolocalization

The relative distribution of GLUT-1 (green), VE-cadherin (red), and the nucleus (blue) in a coronary artery EC is displayed in Figure 2.8. The adherens junctions, as labelled by VE-cadherin, are discontinuous, as expected for an endothelium experiencing shear stress (Noria *et al.*, 1999). The transporters were

distributed in discrete clusters, mostly around the periphery of the nucleus and close to the edge of the cell. From the side view (Figure 2.8B), it can be seen that the bulk of the nucleus was on the abluminal side of the cell, and that clusters of GLUT-1 were located on both the luminal and abluminal sides. Additional details were observed by rotating the image presented in Figure 2.8A 90 degrees about the X-axis and extracting three 0.5 μm thick cross-sections from the indicated locations (Figure 2.8C, D and E). These cross-sections demonstrated that GLUT-1 was located in the same region of the cell as was VE-cadherin, and that when split into luminal and abluminal segments using VE-cadherin as a guide (Figure 2.8F and G), the majority of the transporters appeared to be on the abluminal side.

En face 3D data set and cross-sections (comparable to Figure 2.8C, D and E) of EC from all four vascular beds labelled for GLUT-1 (Figure 2.9), GLUT-2 (Figure 2.10), GLUT-3 (Figure 2.11), GLUT-4 (Figure 2.12), GLUT-5 (Figure 2.13) and SGLT-1 (Figure 2.14) are shown. The distributions of GLUT-2, 3, 4, 5 and SGLT appeared similar to that of GLUT-1; the transporters were distributed in discrete clusters present on both sides of the cell, and had a high density in proximity to the cell-to-cell junctions. The arrangement was the same in each of the vascular beds.

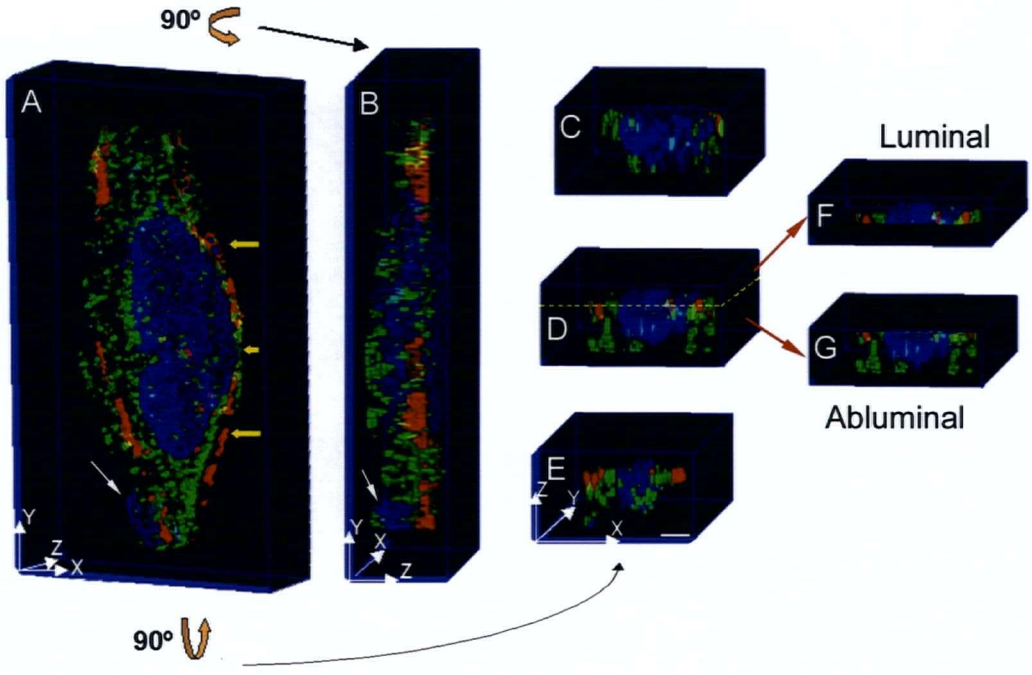

Figure 2.8 Digital manipulations schematic of the quantitative analysis.is. Coronary EC labelled with antibodies specific for GLUT-1 (green), VE-cadherin (red) and nuclei with DAPI (blue), scale bar is 2 μm in each direction. A) 3D reconstruction, view of the cells from the lumen. The white arrow indicates a small section of an adjacent cell. B) Side view obtained from a 90° rotation about the Y-axis, luminal surface on the right. C-E) Half micron thick cross-sections were obtained from (A) at the points indicated by the yellow arrows, and then rotated 90° about the X-axis, luminal surface on top. The yellow dashed line in D indicates where this cell segment was divided into luminal (F) and abluminal (G) sections. White pixels indicate colocalization between VE-cadherin and GLUT-1 (A, B), or between GLUT-1 and DAPI (C, D, G

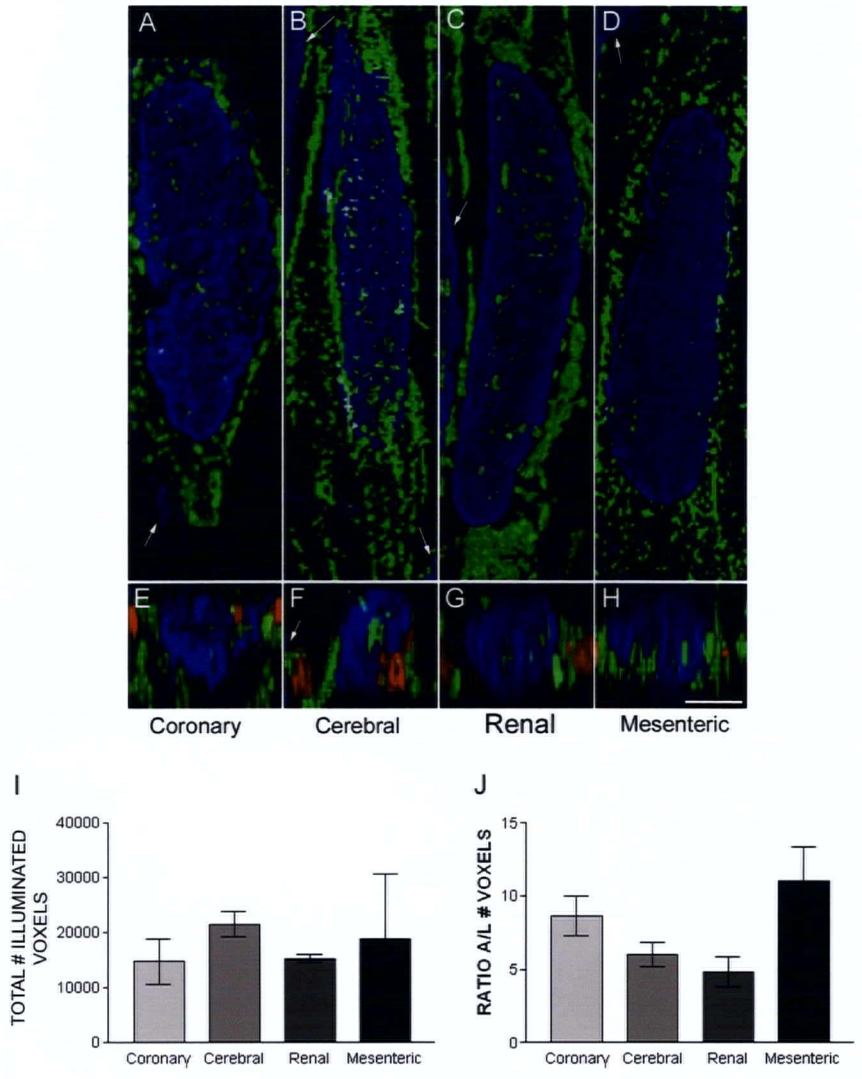

Figure 2.9 GLUT-1 subcellular distribution in ECs.Cs.
EC of coronary (A, E), cerebral (B, F), renal (C, G), and mesenteric (D, H) arteries labelled with antibodies specific for GLUT-1 (green), VE-cadherin (red) and nuclei with DAPI (blue). A-D) 3D reconstruction, view of the cells from the lumen. The white arrow indicates a small section of an adjacent cell. E-H) Half-micron thick cross-sections were obtained from (A-D), and then rotated 90° about the X-axis, luminal surface on top. White pixels indicate colocalization between GLUT-1 and DAPI (A-D) or between VE-cadherin and GLUT-1 (E-H). Scale bar is 2 μm in each direction. I) Plot of the total number of illuminated voxel per cell (mean ± S.E.), each bar is the average of 4 cells from 3 rats for each vascular bed. J) Plot of the ratio of the number of abluminal to luminal voxels per cell (mean ± S.E.).

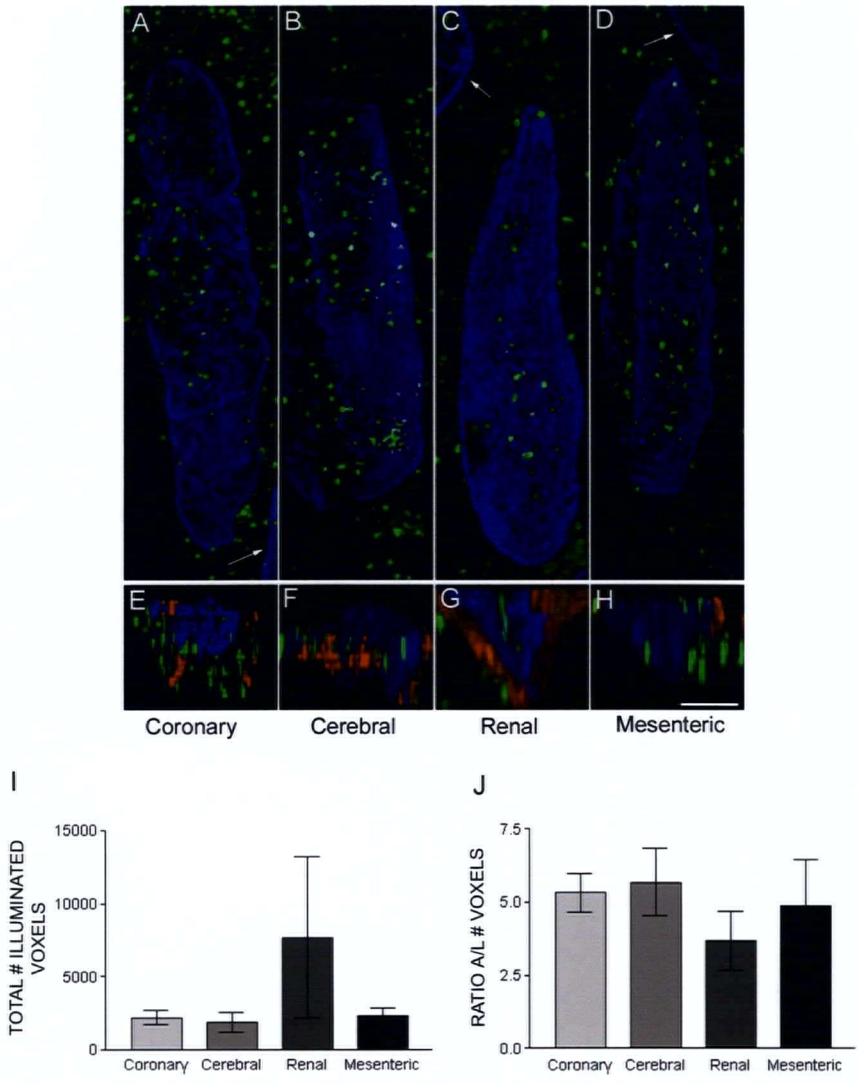

Figure 2.10 GLUT-2 subcellular distribution in ECs.

EC of coronary (A, E), cerebral (B, F), renal (C, G), and mesenteric (D, H) arteries labelled with antibodies specific for GLUT-2 (green), VE-cadherin (red; E) or caveolin (red; F-H) and nuclei DAPI (blue). A-D) 3D reconstruction, view of the cells from the lumen. The white arrow indicates a small section of an adjacent cell. E-H) Half-micron thick cross-sections were obtained from (A-D), and then rotated 90° about the X-axis, luminal surface on top. White pixels indicate colocalization between GLUT-2 and DAPI (A-D) or between VE-cadherin or caveolin and GLUT-2 (E-H). Scale bar is 2 μm in each direction. I) Plot of the total number of illuminated voxel per cell (mean ± S.E.), each bar is the average of 4 cells from 3 rats for each vascular bed. J) Plot of the ratio of the number of abluminal to luminal voxels per cell (mean ± S.E.).

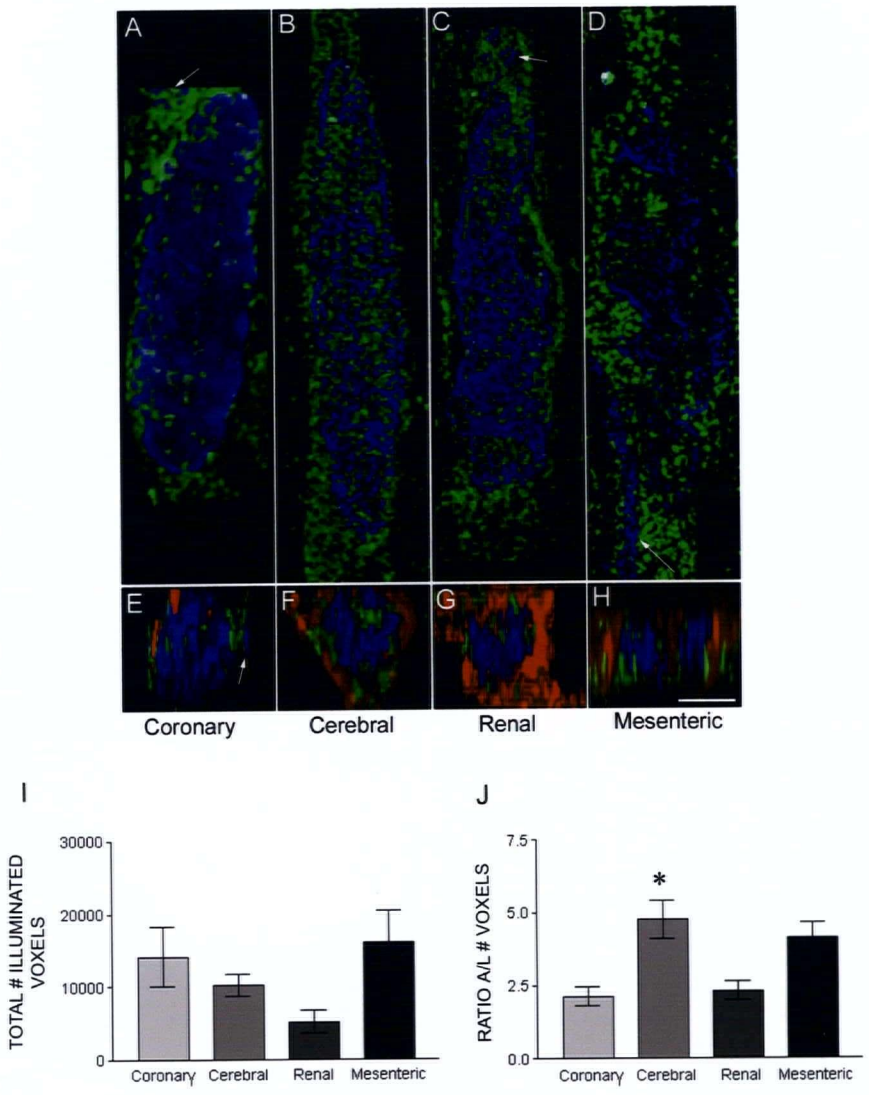

Figure 2.11 GLUT-3 subcellular distribution in ECs.
EC of coronary (A, E), cerebral (B, F), renal (C, G), and mesenteric (D, H) arteries labelled with antibodies specific for GLUT-3 (green), caveolin (red) and nuclei with DAPI (blue). A-D) 3D reconstruction, view of the cells from the lumen. The white arrow indicates a small section of an adjacent cell. E-H) Half-micron thick cross-sections were obtained from (A-D), and then rotated 90° about the X-axis, luminal surface on top. White pixels indicate colocalization between GLUT-3 and DAPI (A-D) or between caveolin and GLUT-3 (E-H). Scale bar is 2 μm in each direction. I) Plot of the total number of illuminated voxel per cell (mean ± S.E.), each bar is the average of 6 cells from 3 rats for each vascular bed. J) Plot of the ratio of the number of abluminal to luminal voxels per cell (mean ± S.E.). The ratio of cerebral artery was significantly higher than the ratio of coronary and renal arteries * ($p<0.01$).

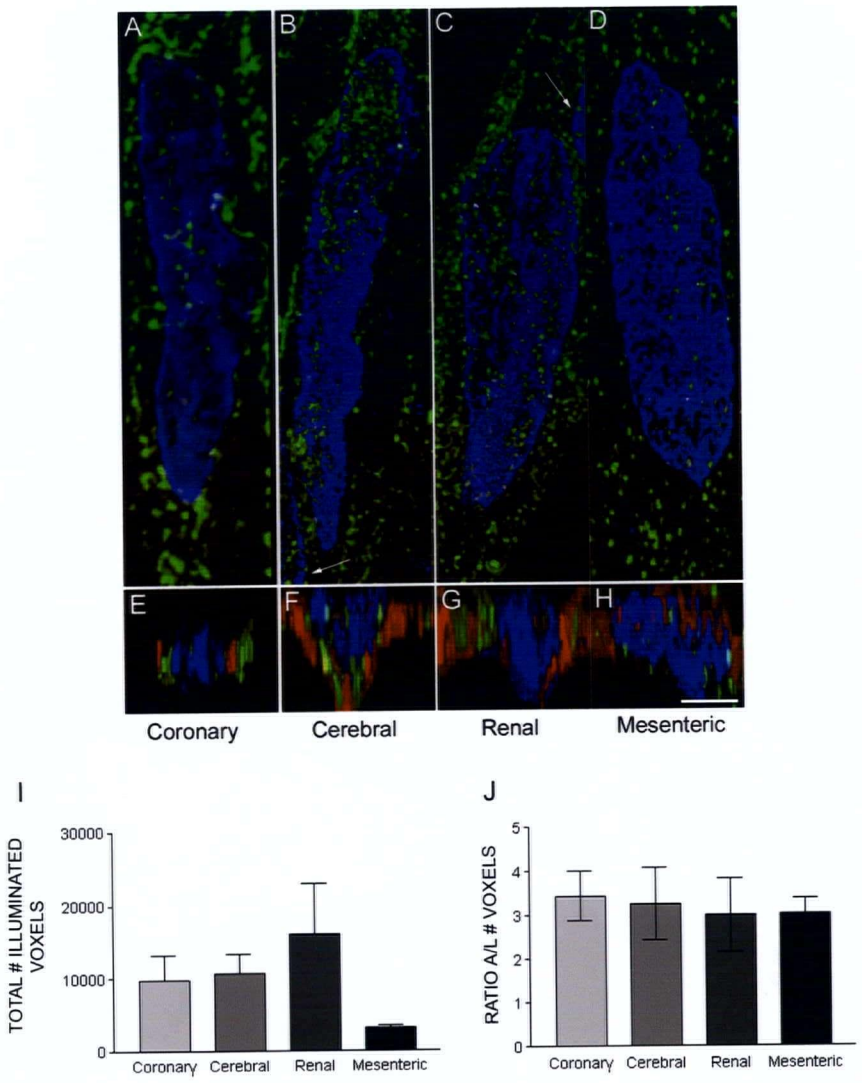

Figure 2.12 GLUT-4 subcellular distribution in ECs.
EC of coronary (A, E), cerebral (B, F), renal (C, G), and mesenteric (D, H) arteries labelled with antibodies specific for GLUT-4 (green), VE-cadherin (red; E-G) or caveolin (red; H) and nuclei with DAPI (blue). A-D) 3D reconstruction, view of the cells from the lumen. The white arrow indicates a small section of an adjacent cell. E-H) Half-micron thick cross-sections were obtained from (A-D), and then rotated 90° about the X-axis, luminal surface on top. White pixels indicate colocalization between GLUT-4 and DAPI (A-D) or between VE-cadherin or caveolin and GLUT-4 (E-H). Scale bar is 2 μm in each direction. I) Plot of the total number of illuminated voxel per cell (mean ± S.E.), each bar is the average of 5 cells from 2 rats for each vascular bed. J) Plot of the ratio of the number of abluminal to luminal voxels per cell (mean ± S.E.).

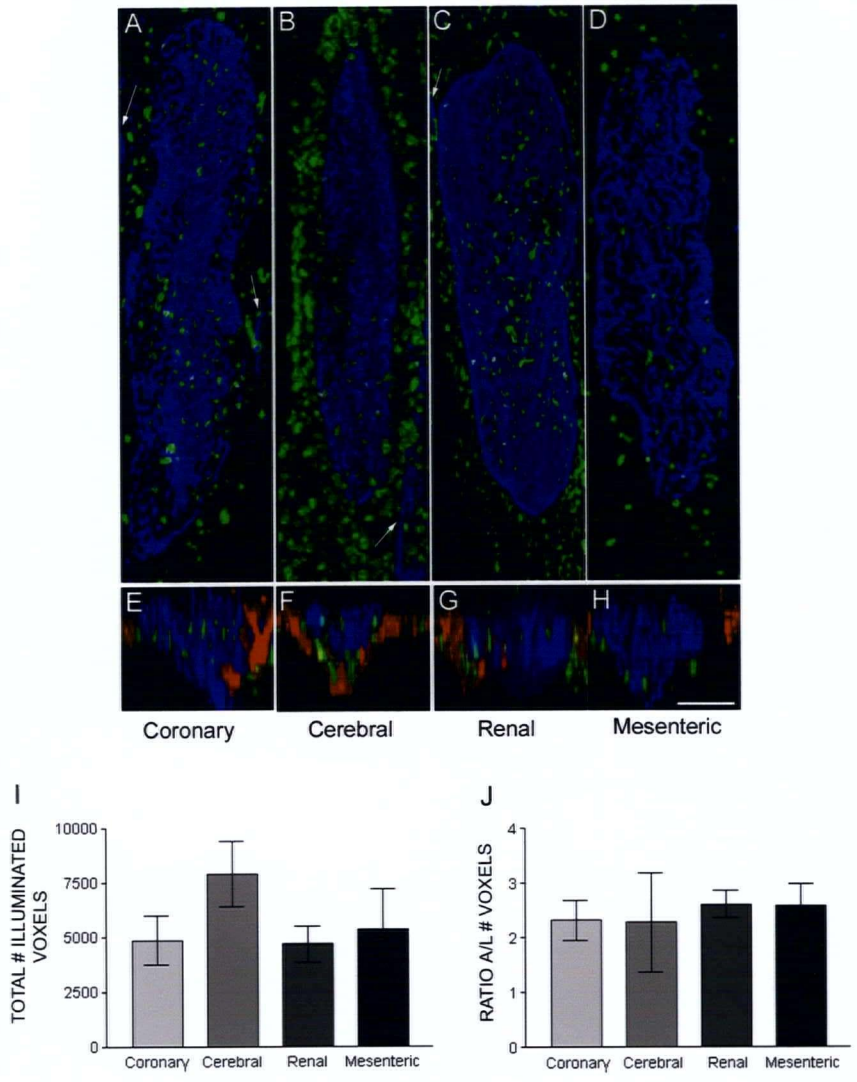

Figure 2.13 GLUT-5 subcellular distribution in ECs.

EC of coronary (A, E), cerebral (B, F), renal (C, G), and mesenteric (D, H) arteries labelled with antibodies specific for GLUT-5 (green), VE-cadherin (red) and nuclei with DAPI (blue). A-D) 3D reconstruction, view of the cells from the lumen. The white arrow indicates a small section of an adjacent cell. E-H) Half-micron thick cross-sections were obtained from (A-D), and then rotated 90° about the X-axis, luminal surface on top. White pixels indicate colocalization between GLUT-5 and DAPI (A-D) or between VE-cadherin and GLUT-5 (E-H). Scale bar is 2 μm in each direction. I) Plot of the total number of illuminated voxel per cell (mean ± S.E.), each bar is the average of 6 cells from 4 rats for each vascular bed. J) Plot of the ratio of the number of abluminal to luminal voxels per cell (mean ± S.E.).

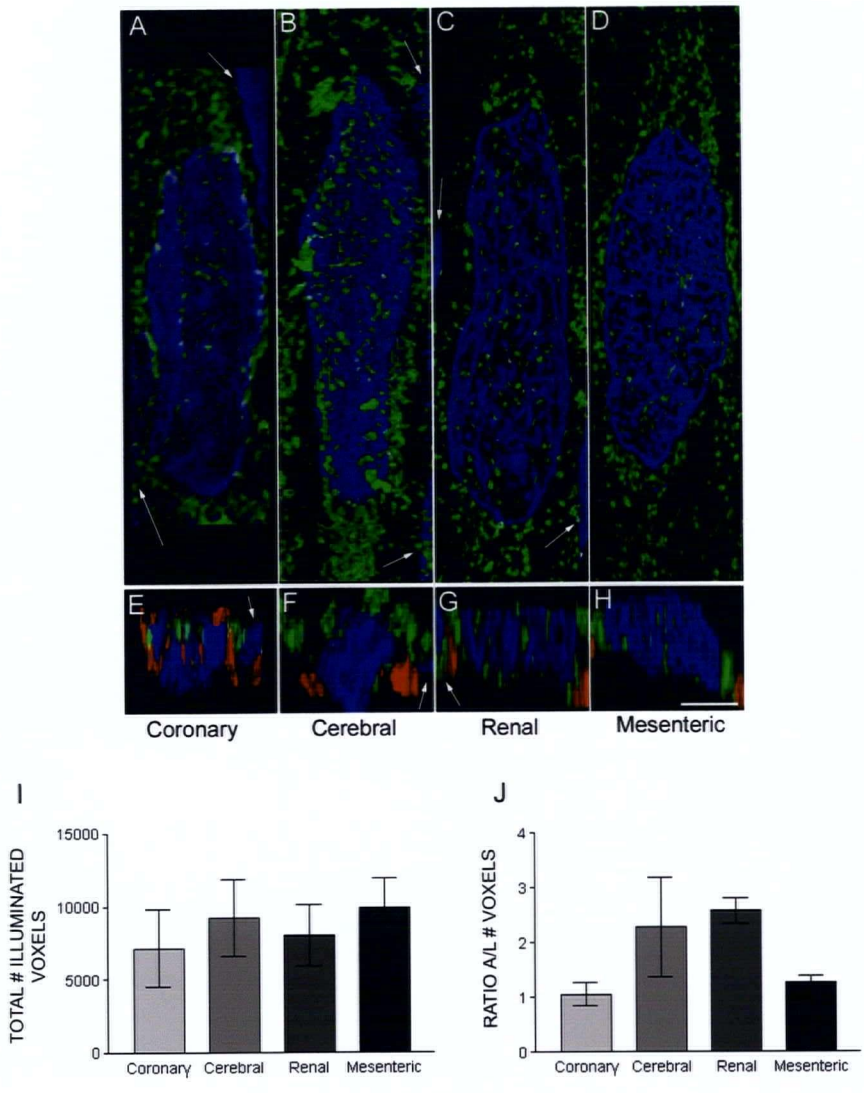

Figure 2.14 SGLT-1 subcellular distribution in ECs.

EC of coronary (A, E), cerebral (B, F), renal (C, G), and mesenteric (D, H) arteries labelled with antibodies specific for SGLT-1 (green), VE-cadherin (red) and nuclei with DAPI (blue). A-D) 3D reconstruction, view of the cells from the lumen. The white arrow indicates a small section of an adjacent cell. E-H) Half-micron thick cross-sections were obtained from (A-D), and then rotated 90° about the X-axis, luminal surface on top. White pixels indicate colocalization between SGLT-1 and DAPI (A-D) or between VE-cadherin and SGLT-1 (E-H). Scale bar is 2 μm in each direction. I) Plot of the total number of illuminated voxel per cell (mean ± S.E.), each bar is the average of 5 cells from 2 rats for each vascular bed. J) Plot of the ratio of the number of abluminal to luminal voxels per cell (mean ± S.E.).

The quantification of this distribution and a comparative analysis between the different vascular beds is presented. Figure 2.9 to Figure 2.14I show the total number of illuminated voxels for each artery expressed as the mean per cell, and its standard error. When the numbers of illuminated voxels for GLUT-1 were compared across the different vascular beds, no significant differences were found (Figure 2.9I). The numbers of illuminated voxels were also comparable between each artery for GLUT-2 (Figure 2.10I), GLUT-3 (Figure 2.11I), GLUT-4 (Figure 2.12I), GLUT-5 (Figure 2.13I), and SGLT-1 (Figure 2.14I).

We also determined the ratio of abluminal to luminal illuminated voxels for each transporter in all four arteries. The ratio for GLUT-1 in the coronary EC shown in Figure 2.9A and E was 10.6 and in a total of 7 coronary artery ECs examined the abluminal: luminal ratio was 8.9 ± 1.4 (mean ± S.E.), implying that the majority of GLUT-1 was on the abluminal side (Figure 2.9J). We found a similar subcellular distribution in cerebral (6.0 ± 0.8), renal (4.9 ± 1.0) and mesenteric (11.1 ± 2.4) arteries (Figure 2.9J). GLUT-2 was also mostly located on the abluminal side of the cells (Figure 2.10). We found comparable abluminal: luminal ratio amongst coronary (5.3 ± 0.7), cerebral (5.7 ± 1.1), renal (3.7 ± 1.0) and mesenteric (4.9 ± 1.6) arteries (Figure 2.10I). As for the other transporters, no significant differences were observed between vascular beds with the exception of GLUT-3, for which an ANOVA followed by Bonferroni's multiple comparison test indicated a significant higher ratio for the cerebral artery (4.8 ± 0.7) in comparison to both coronary (2.1 ± 0.3) and renal arteries (2.3 ± 0.3; $p<0.01$), but not to mesenteric artery (4.1 ± 0.5; Figure 2.11J). GLUT-4, GLUT-5 and SGLT-1 had a low ratio in all vascular beds examined, ranging from 3.4 ± 0.6 to 1.1 ± 0.2 (Figure 2.12 to Figure 2.14J).

The abluminal: luminal ratio was also compared between transporters for each vascular bed. In coronary artery, an analysis of variance of the mean abluminal: luminal ratios were significant ($p < 0.001$) and Bonferroni's multiple comparisons test indicated that the distributions fell into three different groups (Figure 2.15). SGLT-1 had an abluminal: luminal ratio that was not significantly different from 1, and was therefore symmetrically distributed. GLUT-3, 4 and 5 were more concentrated on the abluminal side with ratios that ranged from 2.1 to 3.5 and were not significantly different from each other. GLUT-1 had the most asymmetric distribution with a ratio of 8.9, which was significantly different from GLUT-3, 4, 5 and SGLT-1 ($p<0.001$), followed by GLUT-2 with a ratio of 5.4 significantly different from SGLT-1 ($p<0.05$). Although a similar trend was found in the other three vascular beds, only the mesenteric showed a GLUT-1 ratio significantly different from GLUT-2 ($p<0.05$), 3 ($p<0.05$), 4 ($p<0.01$), 5 ($p<0.01$), and SGLT-1 ($p<0.001$).

2.3.5 Effect of long-term hyperglycaemia

We looked at the effect of hyperglycaemia on the expression and subcellular distribution of the GLUTs and SGLT-1 in coronary arteries (Figure 2.16). Sustained hyperglycaemia (8 weeks) produced a reduction in the labelling for GLUT-1 (Figure 2.16A vs B), GLUT-3 (Figure 2.16I vs J), GLUT-4 (Figure 2.16M vs N) and slightly less for GLUT-5 (Figure 2.16Q vs R), but caused a dramatic increase in labelling for GLUT-2 (Figure 2.16E vs F). SGLT-1 labelling was not distinctively changed by hyperglycaemia (Figure 2.16U vs V). Quantification of the total number of voxels labelled for GLUT-1, 3, 4 and 5 revealed a significant reduction ranging from 77 to 95%, while the number of

voxels labelled for GLUT-2 was increased by 222% (Figure 2.17). SGLT-1 was also reduced by hyperglycaemia but to a lesser extent (39%). These changes did not significantly affect the abluminal: luminal distributions of any of the transporters (see Figure 2.16, GLUT-1 (C vs D), GLUT-2 (G vs H), GLUT-3 (K vs L), GLUT-5 (S vs T) and SGLT-1 (W vs X)) except GLUT-4 (Figure 2.16O vs P) where there was a significant shift towards the luminal side of the cell (Figure 2.15), in spite of a 77% reduction in the total number of illuminated voxels (Figure 2.17).

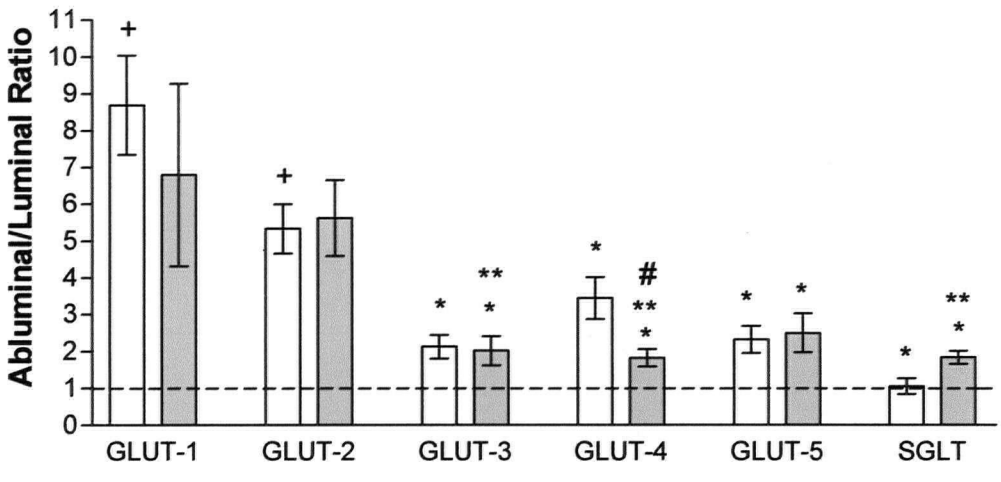

Figure 2.15 Effect of hyperglycaemia on the Abluminal: Luminal ratio.
Plot of the ratio of the number of abluminal to luminal voxels per cell (mean ± S.E.) for both control ☐ and diabetic animals ▭ (each bar is the average of 7 cells from 4 rats). *, **, + marks ratios that are significantly different from GLUT-1, GLUT-2 or SGLT-1, respectively. # indicates those transporters where the ratio is significantly different between the diabetic and the control group.

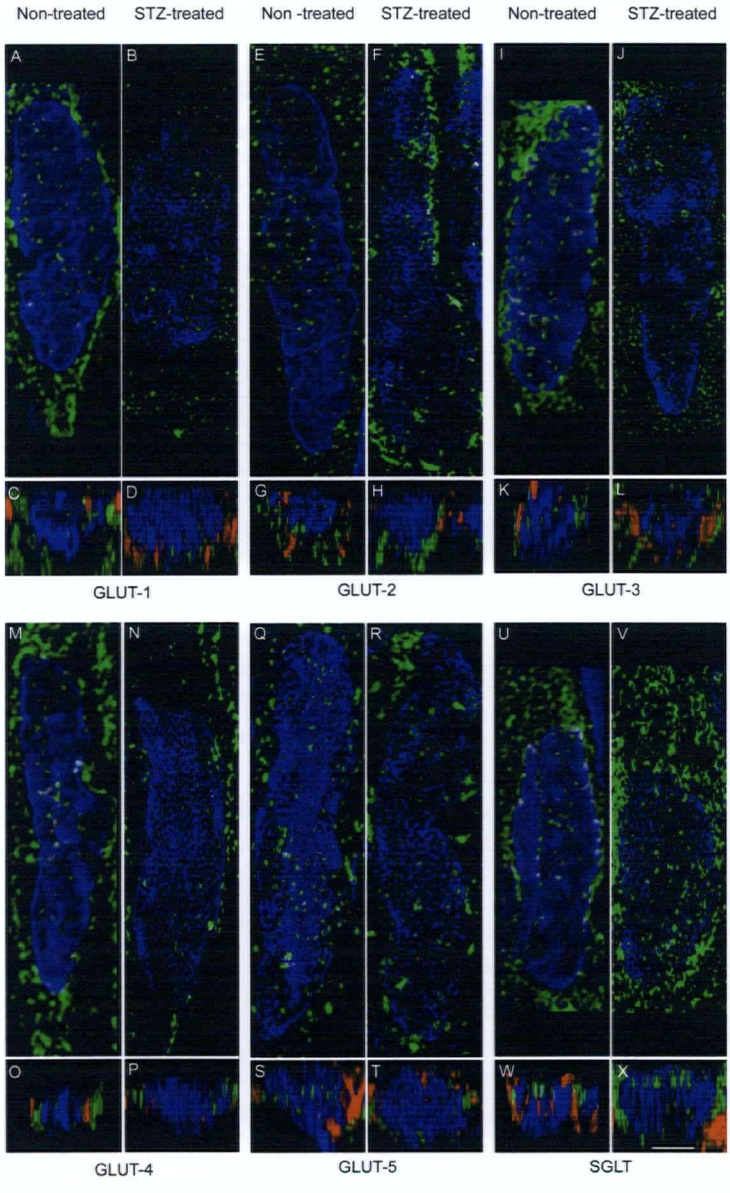

Figure 2.16 Effect of hyperglycaemia on transporters subcellular distribution.

Representative EC labelled with antibodies specific for a glucose transporter (green), VE-cadherin (red) (except GLUT-3 caveolin (red)) and nuclei with DAPI (blue). GLUT-1 (A to D), GLUT-2 (E to H), GLUT-3 (I to L), GLUT-4 (M to P), GLUT-5 (Q to T) and SGLT-1 (U to X). First and third rows: 3D reconstruction of an *en face* preparation, view of the cells from the lumen, each are 4 to 5 μm thick. Second and fourth rows: cross-sections, luminal side up, 0.5 μm thick. EC from Non-treated and STZ-treated rats alternate respectively from left to right. Scale bar is 2 μm.

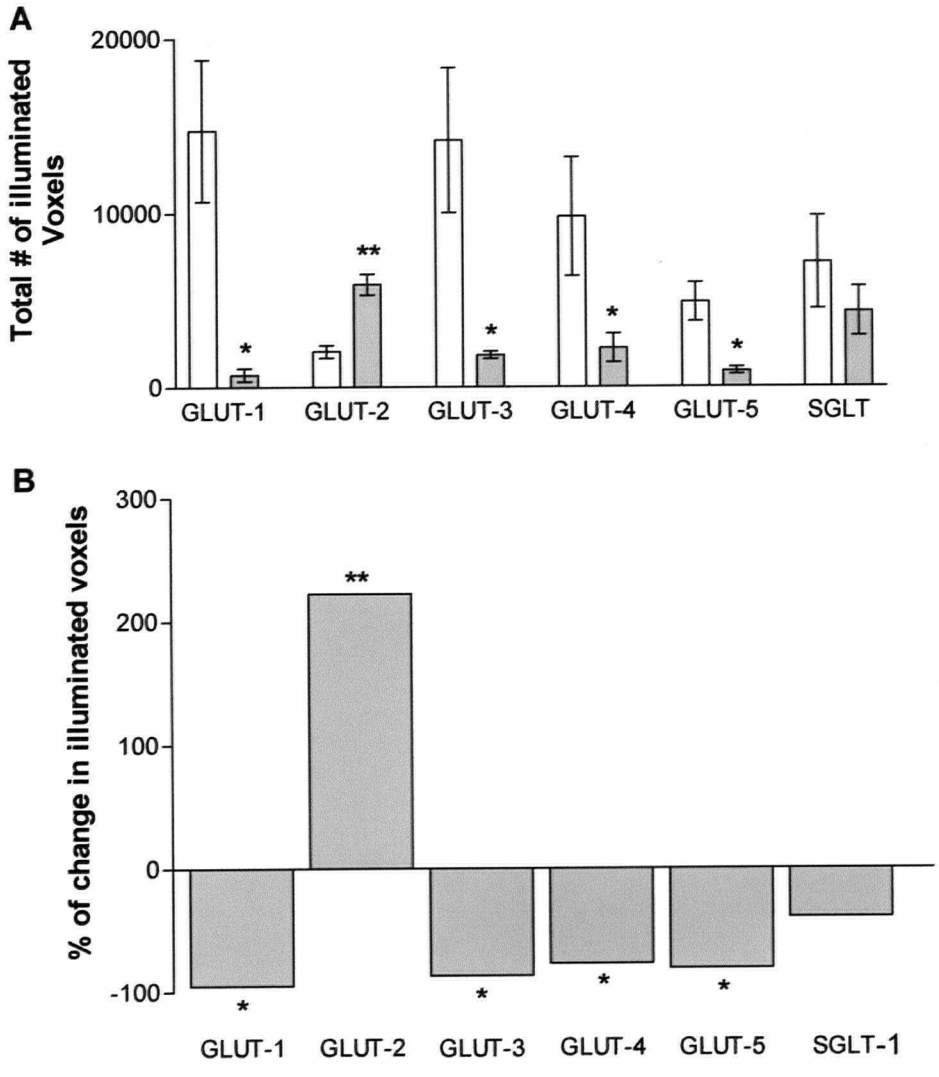

Figure 2.17 Effect of hyperglycaemia in the expression of the transporters.
A) Plot of the total number of illuminated voxels per cell (mean ± S.E.) for both control ☐ and diabetic animals ▭ . B) Plot of the percentage change in the number of illuminated voxels per cell in the diabetic compared to the control (from A). * ($p<0.05$) and ** ($p<0.0005$) indicates a significant change.

2.4 Discussion

Our principal findings are that the ECs of the coronary artery express GLUT-1 to 5 and SGLT-1, and that long-term hyperglycaemia induced by STZ

had a profound effect on their expression. We observed a downregulation of GLUT-1, 3, 4, and 5, and a three-fold increase of GLUT-2 in the ECs of STZ-diabetic rats. We examined an en face endothelial preparation because ECs structure is maintained by the surrounding environment and by interactions with neighbouring cells (Redmond *et al.*, 1995; Garlanda and Dejana, 1997). In particular, ECs, when cultured, have a tendency to lose the ability to express most of the GLUT and SGLT isoforms (McCall *et al.*, 1997; Mamchaoui *et al.*, 2002). By studying the endothelium of freshly dissected vessels, we preserved the cellular architecture of the ECs as close to the native state as possible. The endothelial markers allowed us to readily visualize the cells in the intact vessel, and the Ac-LDL uptake indicated that they remained viable throughout the dissection (Figure 2.2).

2.4.1 Immunostaining

We have interpreted an increase or decrease in the number of voxels labelled for a given transporter as increases or decreases in that transporter protein expression. We cannot draw any conclusions about the relative expression levels between the transporters since we do not know the affinity of either the primary or the secondary antibodies for their epitopes. The specificity of the antibodies used in these studies has been thoroughly tested. First, BLAST searches confirmed that the sequences of the epitopes recognized by the antibodies are unique to the proteins. Second, we obtained positive and negative controls for each antibody using immunohistochemistry in well-characterized cells and tissues. Third, Western blots produced single bands of the appropriate molecular weight for each of the GLUTs (Thorens *et al.*, 1988; James *et al.*, 1989;

Gould *et al.*, 1992; Mantych *et al.*, 1993b; Hirsch and Rosen, 1999). Fourth, control peptides for GLUT-3, 5 and SGLT-1 blocked the labelling. Together, these results indicate that the antibodies are specific for each glucose transporter isoform.

All of the GLUTs and SGLT-1 were distributed in discrete clusters. This organised distribution may reflect the capacity of the transporters to target specific subcellular sites and tether or anchor to cytoskeletal proteins, as has been observed for GLUT-1 (Bunn *et al.*, 1999). While most labelling surrounded the nucleus and the edge of the cells, a small amount seems to be located within the nucleus. A plane by plane analysis revealed that this labelling is located in deep folds of the nuclear envelope, typical for an EC's nucleus (Woolf, 1982), and constitutes perinuclear and not intranuclear labelling.

2.4.2 GLUT-1

In agreement with previous studies (Mann *et al.*, 2003), we found GLUT-1 in ECs. We also found that it is asymmetrically distributed, with a greater abundance on the abluminal side. A similar distribution of GLUT-1 has been previously reported in the BBB (Bolz *et al.*, 1996; Cornford *et al.*, 1998a; Dobrogowska and Vorbrodt, 1999), where GLUT-1 has long been considered the main glucose transporter (Pardridge *et al.*, 1990). GLUT-1's high affinity, intrinsic asymmetry (glucose extrusion from the cell can be 20 times faster than its uptake (Gould and Seatter, 1997; Kinne, 1997), and high abluminal density suggests its participation in the maintenance of a constant transport of glucose from the cytosol of ECs to the interstitial space in the vascular wall.

2.4.3 GLUT-2

To our knowledge, we are the first to report the presence of GLUT-2 in the ECs of a small artery. A basolateral distribution of GLUT-2 has been found in epithelial cells of kidney proximal tubules and small intestine (Takata, 1996; Thorens, 1996; Wallner *et al.*, 2001) where it enables the rapid extrusion of accumulated intracellular glucose, facilitating its transfer to the interstitium. If transcellular glucose transport occurs across the endothelium of coronary arteries, then the low-affinity/high-capacity of GLUT-2 and its high abluminal density would contribute to the transfer of glucose from the blood to the cells of the vascular wall. Thus, GLUT-1 may be responsible for glucose extrusion at basal concentrations, while GLUT-2 could potentially protect ECs from elevated intracellular glucose accumulation during brief periods of hyperglycaemia.

2.4.4 GLUT-3, 4, and 5

We also found that GLUT-3, 4 and 5 were present in these ECs. Other groups have previously reported the presence of both GLUT-3 (Mantych *et al.*, 1993b; Urabe *et al.*, 1996) and GLUT-5 (Mantych *et al.*, 1993b) in brain ECs. The presence of GLUT-4 has been previously found in ECs of the blood barrier (retinal and brain) (Frank and Pardridge, 1981; King *et al.*, 1983; McCall *et al.*, 1997) and in fat and muscle capillary ECs (Vilaro *et al.*, 1989), while it was absent from cultured cardiac (Thomas *et al.*, 1995), cultured aortic (McCall *et al.*, 1997), and human muscle capillary ECs (Friedman *et al.*, 1991). These contradictory findings may be explained in part by the heterogeneity found between ECs of different vascular beds and vessels of different calibres and by the fact that ECs, when cultured, have a tendency to lose the ability to express most of the GLUT

and SGLT isoforms (McCall *et al.*, 1997; Mamchaoui *et al.*, 2002) and the resulting reduced expression is likely to be interpreted as non significant.

2.4.5 SGLT-1

We found SGLT-1 in ECs of small contractile arteries. The presence of SGLT-1, also previously reported in bovine cortical artery ECs (Nishizaki *et al.*, 1995; Matsuoka *et al.*, 1998; Nishizaki and Matsuoka, 1998), raises the question of the role it plays in the cells of the vascular wall. As a permanent Na^+ gradient is maintained between the blood and the cytosol of the cell, one would expect a constant activation of SGLT in the ECs even during periods of low blood glucose level. Nishizaki et al. have shown that low glucose levels enhance the activity of SGLT in bovine cortical artery ECs (Nishizaki and Matsuoka, 1998). Thus, the activity of SGLT-1 may be of greater importance during stresses such as hypoglycaemia in ECs, in which case it's unique capacity to transport glucose against its concentration gradient may serve the cells of the vascular wall during prolonged periods of starvation.

2.4.6 Other transporters

In addition to the GLUT isoforms that we studied, there are another seven known isoforms (GLUT6 – 12) (Joost and Thorens, 2001), at least five other isoforms of SGLT (Wright, 2001) as well as the HMIT (Joost and Thorens, 2001). Antibodies to some of these transporters became available after this study was completed, and for this reason, we have not examined their role in the vascular EC.

2.4.7 Cell junction labelling

A surprising result was the preferential localization of all glucose transporter isoforms towards the edges of the cell, near the cell-to-cell junctions. This cell-to-cell junction labelling is mostly noticeable in the case of GLUT-1 (Figure 2.9A-D), but was also observed with the other isoforms (best examples in Figure 2.11C, Figure 2.12A&C, Figure 2.13B, Figure 2.14A&D). At these regions of the cells, the luminal and abluminal membranes are at their closest apposition. This, combined with the preferential distribution of the GLUTs on the abluminal side, suggests that there could be transcellular transport of glucose through ECs at their narrowest points. We cannot rule out the possibility that there is paracellular glucose transport, particularly given the discontinuous adherens junctions which are a characteristic of endothelia exposed to shear stress (Noria *et al.*, 1999), and given that glucose transport across the capillaries in the microvasculature is thought to be almost exclusively paracellular (Michel and Curry, 1999). Nevertheless, our results indicate that ECs possess the molecular architecture to promote rapid transcellular transport of glucose to the cells of the vascular wall, and with SGLT-1, GLUT-1 and GLUT-2 on the luminal side, to maintain transcellular transport across a wide range of glucose concentrations.

2.4.8 Similarity amongst vascular beds

We found a comparable expression for each GLUT isoform and SGLT-1 in all four vascular beds examined. The subcellular distribution of each isoform was also comparable between the different vascular beds with the exception of GLUT-3 in cerebral ECs found with greater abundance on the abluminal side than in other blood vessels. As each the arteries used in this study have a

comparable diameter, wall thickness and function, it is not surprising to find a similarity between the expression and subcellular distribution of glucose transporters in each of these arteries.

2.4.9 Effect of hyperglycaemia

Hyperglycaemia had profound effects on all of the GLUTs, significantly reducing the number of labelled voxels for all except GLUT-2, which was dramatically increased. The decrease in GLUT-1 staining is consistent with reports indicating that the expression of this transporter is downregulated in rat heart endothelium following STZ-induced diabetes (Hirsch and Rosen, 1999). There are no reports of the effects of prolonged hyperglycaemia on the expression of GLUT-3, 4 and 5 in the endothelium, but our results indicate that their expression is also reduced. In cultured bovine aortic endothelial cells (BAEC) exposed to hyperglycaemia for 48h, the expression of GLUT-1 and its Vmax are both reduced (Alpert *et al.*, 2002) a decrease which has been attributed to the enhanced production of 12-hydroxyeicosatetraenoic acid (12-HETE). There is no evidence to show whether the changes observed in the other GLUTs are due to the same mechanism. Nevertheless, it may represent an effective regulatory mechanism for the endothelium to protect itself from hyperglycaemia, were it not for GLUT-2. We observed a 165% increase in the number of voxels stained for GLUT-2 in STZ-treated rats (Figure 2.17). This is the first report concerning the endothelium, but our results are consistent with the dramatic increases in GLUT-2 expression seen in rat intestinal enterocytes (Corpe *et al.*, 1996) and kidney proximal tubule cells (Marks *et al.*, 2003) in response to STZ-induced diabetes. The presence of GLUT-2, and its increase in diabetes, would be

expected to have profound effects on the endothelial cell's ability to regulate their glucose uptake.

STZ-treatment is a well-established animal model of Type 1 diabetes. It may be argued that the observed changes in the GLUT isoforms are due to the effect of the STZ toxin, rather than to hyperglycaemia. Previous studies have shown that STZ toxicity is restricted to cells expressing GLUT-2 (Schnedl *et al.*, 1994), and that its effect, either no change or a decrease in the level of GLUT-2 protein expression (Wang and Gleichmann, 1998; Burkart *et al.*, 1999), is the opposite of that observed here. Although GLUT-2 may facilitate the transport of STZ in cells, it is not necessarily targeted by the toxin. Burkart et al. identified NAD^+ depletion caused by PARP activation, as the metabolic event leading to cell death. The study went on to demonstrate that knockout PARP-/- mice were completely resistant to the STZ toxin. The STZ-treated knockout mice were normoglycaemic, maintained a normal level of secreted insulin, and preserved their islet ultrastructure. In addition, the level of GLUT-2 protein expression found in the islets was unaffected by STZ (Burkart *et al.*, 1999). It is only following multiple doses of STZ (after 3 to 5 doses of 40 mg/kg/day), that Wang et al. observed a decrease in GLUT-2 protein levels in mice pancreatic beta-cells (Wang and Gleichmann, 1998), which preceded the development of hyperglycaemia and beta-cell destruction. In other tissues expressing GLUT-2 (liver, intestine and kidney proximal tubules), an increase in the protein level is observed following STZ-induced hyperglycaemia. This effect is reversed by insulin (Thulesen *et al.*, 1997), insulin-like growth factor (Asada *et al.*, 1998), or is abolished by overnight fasting (Marks *et al.*, 2003), indicating that the transporter upregulation is a direct effect of hyperglycaemia and/or hypoinsulinaemia.

Taken together, it is most likely that the increased level of GLUT-2 observed in our study is attributable to hyperglycaemia and/or hypoinsulinaemia rather than any direct effect of the STZ toxin.

2.4.10 Intracellular glucose accumulation

Our results seem to indicate that the ECs have a range of transporters that should protect them against accumulating intracellular glucose, as well as an adaptive response to hyperglycaemia, (a reduction in the expression of GLUT-1, 3, 4 and 5), that should reduce glucose uptake under these conditions. Why then do ECs have a high susceptibility to glucose toxicity? Despite appearances, we think that the subcellular organization of the GLUTs, and the inability to downregulate GLUT-2, may be unfavourable for the cell exposed to hyperglycaemia regardless of whether glucose transport through this endothelium is largely transcellular or paracellular. The high abluminal density of GLUT-2 may compromise the net extrusion rate of glucose on the abluminal side if the glucose concentration in the interstitial space remains elevated. This is likely to occur if the rate of glucose uptake by the SMCs is lower than the rate of extrusion by the EC, which is probable, given that SMCs are reported to downregulate glucose uptake far better than ECs (Howard, 1996b; Vinals *et al.*, 1999). The high abluminal density of GLUT-2 increases the possibility of glucose reuptake down its concentration gradient from the abluminal surface of ECs. The counter productive increase in GLUT-2 expression, if this represents the production of functional protein, would exacerbate this problem, and may explain why ECs are so susceptible to hyperglycaemic damage. If this hypothesis is correct, it follows that reducing the expression of GLUT-2 in the endothelial

cell may have beneficial effects. In support of this, recent clinical trials using an inhibitor of PKC-beta, which controls the transport of GLUT-2 to the membrane (Helliwell *et al.*, 2000), have demonstrated a significant improvement in endothelial function that might be explained, in part, by a reduction of GLUT-2 trafficking (Beckman *et al.*, 2002).

Our results suggest that vascular ECs are particularly susceptible to glucose toxicity due to their inability to decrease the expression of GLUT-2 during prolonged hyperglycaemia. Further studies will be required to determine the specific functional role of each transporter isoform.

Chapter 3
Measurements of glucose uptake in endothelial cells.

3.1 Introduction

3.1.1 Glucose as a principal source of energy

Carbohydrates are the body's principal source of energy. Some cells, like neurons and erythrocytes, depend almost exclusively on glucose and do not have the capacity to store it in the form of glycogen. It is therefore of great importance to maintain a basal level of plasma glucose to prevent hypoglycaemia, which could lead to nervous system dysfunction. Secondary functions of the carbohydrates include the formation of extracellular complexes with proteins and lipids of the plasma membrane (glycocalyx), and the participation of pentoses in the formation of nucleic acids. In adipose tissue, glucose is also essential to the formation of the glycerol molecule, an integral component of triglycerides, which are necessary for lipid storage. While carbohydrates constitute almost half of the energy from a North American diet, it is still possible to maintain health with a diet poor in carbohydrates since the body can provide most of its required energy through the oxidation of lipids and amino acids. 200g of carbohydrate per day is sufficient to maintain a basal plasma glucose level, below this, the body starts to catabolise stored lipids and proteins (Brosnan, 1999; Macdonald, 1999). Glucose is also the main source of energy for the cells of the vascular wall.

3.1.2 Glucose metabolism in EC

ECs actively metabolise glucose in order to fulfil their energy demands. With normoglycaemia, the catabolism of other substrates such as palmitate, lactate and certain amino acids (L-glutamine, L-alanine and L-arginine) is minimal and glucose constitutes the main source of energy (Krutzfeldt *et al.*, 1990). ECs sustain their energy requirements through glycolysis (Gerritsen and Burke, 1985; Krutzfeldt *et al.*, 1990). It is only during periods of hypoglycaemia that the Krebs cycle becomes the prominent pathway for glucose metabolism. Thus, ATP is primarily generated through the glycolytic pathway and ECs consume a low level of O_2. It is therefore not surprising that ECs adapt quite easily to hypoxic conditions and remain functional despite prolonged periods of substrate depletion (Mertens *et al.*, 1990; Culic *et al.*, 1999).

3.1.3 Regulation of glucose uptake in EC

Despite all the evidence linking glucose toxicity to an increased susceptibility to cardiovascular diseases in the diabetic population, very little is known about the regulation of glucose uptake in vascular ECs. Kaiser et al. were amongst the first to provide insights regarding the potential impact of a differential regulation of glucose transport between ECs and SMCs (Kaiser *et al.*, 1993). They reported that a 24 hour exposure to elevated glucose (22 mM) had negligible effects on the rate of 2-deoxyglucose (2DG) uptake (room temperature) in bovine aortic ECs, whereas the same treatment significantly decreased the Vmax of glucose transport in bovine SMCs (Kaiser *et al.*, 1993).

Other studies on the effect of an elevated ambient glucose concentration in cultures of bovine GM7373 (Giardino *et al.*, 1994), and mouse microvessel, ECs (Vinters *et al.*, 1985) have even reported an increased rate of glucose uptake in response to exposure to high glucose. Conversely, a study in human umbilical vein-derived ECs (HUVEC) has shown that a high glucose concentration decreased the rate of 2DG uptake at 37°C. However, this study also shows that the concentration-response curve for the inhibition of 2DG uptake by D-glucose was significantly shifted in HUVECs in comparison to other cell types; the concentration of D-glucose for half-maximal inhibition of the rate of 2DG uptake in HUVECs was 4 to 8 fold greater than that of glial cells (Walker *et al.*, 1988), myoblasts L6 (Walker *et al.*, 1989) and adipocytes 3T3-L1 (Tordjman *et al.*, 1990). Taken together, this suggests that glucose uptake in vascular ECs is regulated differently than in other cell types.

The inhibitory effect on the rate of glucose uptake in HUVEC exposed to elevated ambient glucose was also accompanied by a dramatic decrease in the ratio of phosphorylated 2DG to free 2DG. The decrease in the rate of glucose uptake was therefore attributed to the inhibition of glucose phosphorylation rather than to the decrease in transport (Vinals *et al.*, 1999). This indicates that glucose uptake in ECs is limited by its phosphorylation rate not its transport rate. This is in accordance with previous studies which showed that elevated glucose concentrations had neither an effect on the expression of GLUT-1 (Kaiser *et al.*, 1993; Giardino *et al.*, 1994; Vinals *et al.*, 1999) nor on the rate of uptake of 3-O-methylglucose (3OMG, a non-metabolizable glucose analog) (Takakura *et al.*, 1991; Kaiser *et al.*, 1993; Vinals *et al.*, 1999). Thus, when exposed to hyperglycaemia, ECs reduce glucose utilisation rather than glucose transport.

This may explain in part, the lack of inhibition of glucose uptake in ECs in the presence of elevated glucose concentrations at room temperature, where the rate of metabolism is slowed down (Kaiser *et al.*, 1993).

In contrast to elevated glucose, a low glucose concentration up-regulates glucose transport in ECs. Glucose starvation has been shown to increase the Vmax for 3OMG transport and GLUT-1 protein expression in bovine microvessel ECs (Takakura *et al.*, 1991). Similarly, the rate of 2DG uptake was also increased in primary cultures of brain and adrenal capillaries, and aortic ECs, deprived of glucose for periods of 48 hours (Gaposchkin and Garcia-Diaz, 1996). In accordance with these results, chronic hypoglycaemia but not hyperglycaemia, increases the transendothelial transport of glucose across the rodent BBB (Simpson *et al.*, 1999). Thus, in ECs, hypoglycaemia up-regulates glucose transport while hyperglycaemia inhibits glucose metabolism, with little effect on transport.

Like the presence of GLUT-4 in ECs (see Chapter 2) the effect of insulin on ECs remains controversial. On one hand, several studies have reported that the exposure to insulin produces no effect on the rate of glucose uptake in brain microvessel ECs (Drewes *et al.*, 1988; Takakura *et al.*, 1991), bovine retinal ECs (Betz *et al.*, 1983), cultured cardiac ECs (Thomas *et al.*, 1995), and HUVECs (Corkey *et al.*, 1981). On the other hand, others have observed an increased 2DG and/or 3OMG transport in response to insulin in ECs of mouse microvessels (Vinters *et al.*, 1985), rabbit coronary microvessels (Gerritsen and Burke, 1985), bovine retinal microvessels (Allen and Gerritsen, 1986), rat capillary (Kwok *et al.*, 1989), and human omental microvessels (Abe *et al.*, 1990).

The inconsistency in the observed effect of insulin on ECs may be due to the presence of different regulatory mechanisms amongst vascular beds of different calibres and functions. For instance, the effect of insulin on glucose uptake seems to be limited to the ECs of microvessels such as those from adipose tissue (Bar *et al.*, 1988) and the retina (King *et al.*, 1983) with no effect on ECs of larger vessels like the pulmonary artery and aorta (King *et al.*, 1983; Bar *et al.*, 1988). It is also possible that specific conditions need to be met in order to detect the effect of insulin on ECs of certain vascular beds. Thus, Gerritson at al. have demonstrated that glucose deprivation is required to enhance the effect of insulin on 2DG uptake in rabbit coronary microvessel ECs (Gerritsen *et al.*, 1988). Taken together, this may explain in part, the lack of insulin effect observed by studies performed in ECs of larger vessels and certain microvessels.

Estrogen (Shi *et al.*, 1997), VEGF (Sone *et al.*, 2000) and TNF-α (Pan *et al.*, 1995) are also known to increase glucose uptake in ECs through stimulation of GLUT-1 protein expression. IGF-1 has also been shown to stimulate glucose uptake in bovine retinal ECs (Bar *et al.*, 1989; DeBosch *et al.*, 2001; DeBosch *et al.*, 2002). The increase in glucose uptake in response to IGF-1 was shown to be dependent on the activation of phosphatidylinositol-3 kinase (PI3-kinase), PKC and mitogen-activated protein kinase (MAP-kinase) (DeBosch *et al.*, 2001; DeBosch *et al.*, 2002). PKC has also been implicated in the regulation of glucose transport in dog and human BBB (Drewes *et al.*, 1988). Although the authors have suggested that IGF-1 produces the increase in glucose transport through the translocation of GLUT-1 to the plasma membrane, other transporter isoforms are likely to be involved. PI3-kinase participates in the signalling pathway responsible for the enhanced glucose transport induced by insulin through

GLUT-4 translocation to the plasma membrane (Sakaue *et al.*, 1997). In addition, the activation of PI3-kinase and PKC have been shown to induce translocation of GLUT-2 to the plasma membrane of intestinal epithelial cells (Helliwell *et al.*, 2000; Helliwell *et al.*, 2003).

Despite the presence of GLUT-5 in human BBB (Mantych *et al.*, 1993b) and as shown by the present study in HCAECs and rat coronary, cerebral, mesenteric and renal ECs (see Chapter 2), the transport of fructose in ECs has yet to be demonstrated. The presence of GLUT-5 in the BBB remains particularly puzzling as fructose is not considered an energy substrate for the adult brain (Nualart *et al.*, 1999). Fructose could potentially be metabolised by the ECs themselves, but a clear demonstration of its uptake by the ECs, using a labelled fructose, needs to be performed.

The coupling of glucose and Na^+ transport by an SGLT-like transporter has been previously demonstrated in brain microvessels (Nishizaki *et al.*, 1995; Nishizaki and Matsuoka, 1998). More recently, SGLT-1 was identified at the luminal surface of the BBB (Elfeber *et al.*, 2004a), heart and skeletal muscle capillaries, and in cultured coronary ECs (Elfeber *et al.*, 2004b). Nishizaki et al. simultaneously recorded glucose-evoked Na^+ currents and monitored glucose uptake with radio labelled 2DG in cultured brain microvessel ECs. Glucose-evoked Na^+ current and 2DG uptake were enhanced by a 30-min pre-incubation in glucose free media and the addition of cytochalasin B, but inhibited by an increased concentration of glucose, or by phloridzin (an SGLT specific inhibitor), dinitrophenol (an inhibitor of energy metabolism), the removal of extracellular Na^+ (Nishizaki and Matsuoka, 1998). Elfeber et al. used a non-re-circulating

hindlimb perfusion method and measured glucose consumption by the skeletal muscles to demonstrate that phlorizin blunted the insulin-induced increase of glucose extraction from the perfusate (Elfeber *et al.*, 2004b). Because SGLT is not expressed in skeletal muscle, the inhibitory effect was attributed to a block of transcellular and/or paracellular transport at the capillary level. In addition, the same authors showed in ECs of BBB that SGLT expression is up-regulated after 1 day of ischemic occlusion followed by reperfusion (Elfeber *et al.*, 2004a). Taken together, these results show that SGLT actively co-transports glucose in ECs, and that low cytosolic glucose concentrations enhance its activity. Thus, SGLT may play an important role in the maintenance of an adequate supply of glucose to the ECs in periods of stress such as hypoglycaemia and ischemia.

The information available on the regulation of glucose uptake in ECs indicates that ECs are affected by the ambient glucose concentration. The rate of uptake in ECs is likely modulated by the plasma, cytosolic and interstitial glucose concentrations. The interstitial space contained in the vascular wall is also probably influenced by the SMC rate of glucose uptake. So what do we know about glucose metabolism and the regulation of glucose uptake in SMC?

3.1.4 Glucose metabolism in SMC

The glycolytic pathway is also the principal route of glucose metabolism and ATP generation in SMCs (Hardin and Pauley, 1995). The glycolytic and gluconeogenic pathways have been shown to be compartmentalised in SMCs. This means that intermediates from the glycolytic pathway do not diffuse uniformly in the cytosol and consequently do not become substrates for other

pathways (Lloyd and Hardin, 1999). This indicates the possibility of coupling between glucose transporters and the enzymes of each of the respective metabolic pathways. This coupling could facilitate the compartmentalisation process by localising pools of intracellular glucose. Such localised pools of glucose may in turn be responsible for the greater capacity of the SMCs to regulate their rate of glucose uptake.

While SMCs also store excess glucose, the glycogen content is rapidly depleted in the absence of extracellular glucose. Contracted SMCs derive about 10 % of their energy needs from glycogen, while glucose transported from the blood accounts for up to 50% of the total energy consumption (Allen and Hardin, 2000). At rest, glucose metabolism increases while the oxidation of fatty acids such as acetate and octanoate decreases (Barron *et al.*, 1998).

3.1.5 Regulation of glucose uptake in SMCs

The rate of glucose transport in SMCs is inversely proportional to the extracellular glucose concentration (Kaiser *et al.*, 1993; Fujiwara and Nakai, 1996; Howard, 1996b). Accordingly, Vmax for glucose uptake is decreased by high ambient glucose concentrations, with no changes in the transporter affinity (Kaiser *et al.*, 1993; Howard, 1996b). These changes in glucose transport activity have been correlated with a decrease in the amount of GLUT-1 in SMCs (Kaiser *et al.*, 1993; Quinn and McCumbee, 1998). Although the decrease in glucose transport in response to an elevated extracellular glucose concentration may have represented a mechanism of protection for the SMCs, it was demonstrated

that the intracellular glucose concentration remained abnormally elevated (Howard, 1996b).

Vascular SMCs from the rat aorta and posterior vena cava, as well as several cell lines, have been shown to be insulin-sensitive (Falholt *et al.*, 1985; Standley and Rose, 1994; Banz *et al.*, 1996), and to express GLUT-4 (Charron *et al.*, 1989; Banz *et al.*, 1996). Interestingly, a high glucose concentration has been shown to attenuate the effect of insulin in rat vascular SMCs, an effect attributed to a reduced activity of the glucose transporter system (Fujiwara and Nakai, 1996). Insulin-sensitivity and GLUT-4 expression have also been shown to be decreased in aortic SMCs of hypertensive rats (Atkins *et al.*, 2001). This indicates that the transport and metabolism of glucose in SMCs is likely to be affected by metabolic disorders such as diabetes and hypertension, which could have repercussions for the ECs.

Insulin enhancing drugs such as metformin and troglitazone have been shown to stimulate glucose uptake and GLUT-1 expression in human and bovine aortic SMCs (Sasson *et al.*, 1996; Kihara *et al.*, 1998). Amongst other modulators of glucose transport, angiotensin II (Low *et al.*, 1992; Quinn and McCumbee, 1998), IGF-1 (Standley and Rose, 1994), endothelial growth factor (EGF) (Low *et al.*, 1992), and platelet-derived growth factor (PDGF) (MacKenzie *et al.*, 2001) have been shown to stimulate glucose uptake in SMCs.

Thus, differences in glucose needs and transport regulation exist between ECs and SMCs. These differences may account for the increased susceptibility of the ECs to glucose toxicity.

3.1.6 Aims of the present study and hypothesis

The main goal of this study was to examine, in an intact vessel, the regulation of glucose transport in individual ECs. The initial step towards this goal was to determine the appropriate experimental conditions for recording fluorescent glucose uptake in live cells. This was done using cultured cells, a much simpler preparation than the intact vessel.

First, the presence and subcellular distribution of glucose transporters, not previously characterised in primary culture of human coronary artery ECs (HCAEC), was assessed through immunocytochemistry and fluorescence microscopy. It was hypothesised that the same glucose transporter isoforms previously identified in rat coronary artery ECs, GLUT-1, 2, 3, 4, 5 and SGLT-1, (see Chapter 2) would be detected in HCAECs.

Second, to elucidate the functional role of the glucose transporter isoforms identified in these ECs, the uptake of a fluorescent glucose analog was examined, in the presence of different compounds known to regulate glucose transport. This also enabled us to establish experimental conditions that would be applied to the intact vessel. It was hypothesised that well-known competitive inhibitors of glucose uptake such as D-glucose and cytochalasin B, would inhibit the accumulation of the fluorescent glucose analog in ECs. It was also hypothesised that insulin, because it stimulates the translocation of GLUT-4 to the plasma membrane, would increase the accumulation of the fluorescent glucose analog in ECs.

3.1.7 In vivo fluorescence microscopy

The pressure myograph technique presented in Chapter 1 was coupled to confocal microscopy. The arteriograph chamber allows the study of small blood vessels under both perfusion and superfusion. The bottom cover glass of the arteriograph chamber permits the imaging of the juxtaposed vessel wall. Changes of solutions and the addition of compound to the perfusate were performed with a small peristaltic pump used in an open system without disturbing the equilibrium of the vessel's basal tone. Such perfusion systems have been previously described and used into study the effect of intraluminal flow on myogenic tone (Falcone, 1995; Henrion *et al.*, 1997), and allows complete control over flow, pressure, temperature and oxygenation.

A confocal microscope has a narrow depth of field, which is needed to distinguish the fluorescence of the endothelial layer from that of the SMC layer. Although a wide field microscope coupled to deconvolution could potentially provide a better axial resolution (see chapter 2), the deconvolution algorithm was developed for punctate sources of light, and is not suitable for a uniform field of fluorescence, like that obtained with the fluorescent glucose analog in the vascular wall. A 20X objective suitable for both phase contrast and fluorescence was chosen, and its long working distance (160 μm) ensured that images could be obtained through the vessel wall (~ 30 μm). Phase contrast was used to determine the boundary of each cell in the field of view.

3.1.8 Fluorescent glucose analog

Deoxyglucose (2DG) uptake assays were developed by Sokoloff in 1977 (Sokoloff *et al.*, 1977). The difference between 2DG and D-glucose is at the C-2 position where the hydroxyl group of D-glucose has been replaced by a hydrogen atom. 2DG is transported into cells by glucose transporters and competes with D-glucose for the enzyme hexokinase, (phosphorylates glucose to produce glucose-6-phosphate). The missing hydroxyl group prevents the isomerization of 2DG into fructose-6-phosphate, which aborts further metabolism through the glycolytic pathway. The 2DG remains trapped in the cell, as it does not appear to be a substrate for the enzyme glucose-6-phosphatase. Previous studies have also demonstrated that the exit of radioactive 2DG before its phosphorylation is negligible, and it remains in the cytosol for a minimum of 30 min (Goodner *et al.*, 1980; Hom and Goodner, 1984; Vallerand *et al.*, 1987). Thus, when 2DG is labelled with a radioactive atom or with a fluorescent molecule, it becomes a useful tool for the imaging and quantification of glucose uptake in cells or tissues.

Two fluorescent glucose analogs, the 2- and 6-[N-(7-nitrobenz-2-oxa-1,3-diazol-4-yl)amino]-2-deoxyglucose (2-NBDG and 6-NBDG), are now available for measurements of glucose uptake in live individual cells. 6-NBDG was the first fluorescent hexose derivative to be synthesised to study the nature of the glucose transport system in erythrocytes (Speizer *et al.*, 1985). The compound was synthesised from 6-amino-6-deoxyglucose hydrochloride and 4-chloro-7-nitrobenz-2-oxa-1,3-diazol (NBD-Cl). When cells were exposed to 6-NBDG, thin layer chromatography (TLC) analyses of intracellular lysates identified a single

spot of fluorescence, indicating that the compound is not metabolised intracellularly (Speizer *et al.*, 1985; Shimada *et al.*, 1994). Modifications at neither the C-2 nor at the C-6 positions prevents transport across the plasma membrane, however, a modification at the C-6 position prevents the phosphorylation of the 2DG (Yoshioka *et al.*, 1996c). Consequently, both glucose analogs are taken up by the cell but only the 2-NBDG is trapped in the cell while the 6-NBDG can move freely in and out of the cell.

Yoshioka et al. have introduced the NBD molecule at the C-2 position in order to monitor further metabolic events. 2-NBDG was synthesised by reacting a molecule of D-glucosamine and NBD-Cl (Yoshioka *et al.*, 1996c). TLC analysis revealed 2 spots of fluorescence in the cytoplasmic fraction of Escherichia coli cells (E. coli) treated with the 2-NBDG compound. The first spot of fluorescence was comparable to the one found in the extracellular fraction. The second fluorescence spot found in the cytoplasmic faction was thought to be a phosphorylated derivative of the 2-NBDG (Yoshioka *et al.*, 1996c). The fate of the 2-NBDG was further examined in E. coli and it was confirmed that the 2-NBDG is rapidly converted into 2-NBDG-6-phosphate after is incorporation into cells. In E. coli, the 2-NBDG-6-phosphate was later decomposed into a non-fluorescent derivative (Yoshioka *et al.*, 1996b). Thus, it was concluded that the fluorescence intensity recorded from these cells may reflect a dynamic equilibrium between the incorporation and decomposition of 2-NBDG (Yoshioka *et al.*, 1996b). Additional observations showed that 2-NBDG is incorporated only in living cells, that it is not completely metabolised (remains fluorescent in the cytosol for a minimum of 10 min) and its accumulation does not cause a lethal effect in E. coli (Yoshioka *et al.*, 1996a; Yoshioka *et al.*, 1996c). 2-NBDG has also been used to

measure glucose uptake in a variety of mammalian cell types including isolated SMCs (Lloyd *et al.*, 1999), pancreatic β-cell (Yamada *et al.*, 2000), enterocytes (Roman *et al.*, 2001), cardiomyocytes (Ball *et al.*, 2002), neurons and astroglia cells (Itoh *et al.*, 2004).

The uptake of 2-NBDG and 6-NBDG has been shown to be inhibited by D-glucose and cytochalasin-B, suggesting that the uptake is mediated by glucose transporters (Speizer *et al.*, 1985; Lloyd *et al.*, 1999; Yamada *et al.*, 2000). D-glucose competes with both fluorescent glucose analogs for the binding site on the glucose transporter. L-glucose, its stereoisomer, is not transported in the cells and thus does not inhibit 2-NBDG uptake (Lloyd *et al.*, 1999). Cytochalasin B is a metabolite of the fungus Helminthosporum dermatoideum and a well-characterised inhibitor of the stereospecific transport of D-glucose in a variety of cell types (Gould and Seatter, 1997). Cytochalasin B has been shown to inhibit the efflux rather than the influx of D-glucose, which suggests an endofacial binding site for this molecule. Cytochalasin B inhibits all isoforms of the GLUTs with the exception of GLUT-5 which is insensitive to its effect (Burant and Bell, 1992; Burant *et al.*, 1992).

3.2 Methods

All chemicals were purchased from Sigma-Aldrich Ltd., unless otherwise stated. Animal handling was done in accordance with the guidelines of the Canadian Council on Animal Care and the Principles of laboratory animal care (National Institute of Health (NIH) publication no. 85-23, revised 1985).

3.2.1 Cell culture

Cryopreserved HCAECs (third passage) were obtained from a male donor; 29 years old, with no known diabetic or cardiovascular conditions (Cambrex Bio Science Walkersville, inc., Walkersville, MD). The cells were re-suspended in Endothelial Growth Medium-2 (EGM-2; Cambrex Bio Science Walkersville, inc.) containing supplements and growth factors (hydrocorticosterone, hEGF (epidermal growth factor, recombinant), FBS (foetal bovine serum), VEGF, hFGF-B (fibroblastic growth factor, recombinant), R3-IGF(insulin-like growth factor) -1, ascorbic acid, heparin and gentamicin/amphotericin-B) and seeded at a density of 5000 cells/cm^2 in a T-25 flask. HCAECs (4th and 5th passages) were plated on sterile Lab-Tek chambered coverglass (#1 borosilicate, 25 X 56 mm, Nalge Nunc international, Naperville, IL), coated with APES (3-aminopropyltriethoxysilane) for glucose uptake measurements, or on a coverslip (#1 borosilicate, 25 X 25 mm) in six-well multidishes for both immunocytochemistry and the preparation of whole cell lysate. The cells were cultured for 96 to 120 hrs, or until they reached 90% confluence at 37°C in a humidified incubator gassed with 5% CO_2-95% air.

3.2.2 Immunocytochemistry

HCAECs were fixed in 2% paraformaldehyde dissolved in PBS for 10 min. Fixation was quenched with a 10-min rinse in 100 mmol/l glycine (pH 7.4) and the cells were permeabilized with 0.06% saponin in PBS for 10 min at room temperature followed by 3 x 10-min rinses with PBS. Non-specific binding sites were blocked by incubating the fixed, permeabilized tissue in 10% donkey serum dissolved in PBS for one hour at room temperature. The cells were then

incubated for 4 hours with two antibodies raised in different species; one against a glucose transporter isoform (GLUT-1 to 5 or SGLT-1), and one against VE-cadherin. The same antibody concentrations used with the vessel preparation were applied to the monolayer of HCAECs. All antibodies were diluted in antibody buffer. The antibody sources, concentrations, epitope, and suppliers are listed in Table 2.2.

Excess antibody was removed by 3 x 10-min rinses in antibody wash solution. The tissue was then incubated for 2 hours with two donkey affinity-purified secondary antibodies that had been solid-phase adsorbed to minimize species cross-reactivity (Jackson ImmunoResearch Laboratories). The secondary antibodies were conjugated to either fluorescein isothiocyanate (FITC) or Texas Red and diluted in antibody buffer. Following incubation with the secondary antibodies, the tissue was rinsed 3 x 10 min in antibody wash solution. The cells' nuclei were then labelled with DAPI (0.3 μmol/l, Molecular Probes), for 5 min, followed by 3 x 10-min rinses in PBS. The labelled cells were mounted on a slide in DABCO mounting medium. Small sub-resolution beads were added to the DABCO; these fluoresce in all wavelengths and are used to align the image stacks. Two control experiments were conducted. In the first, the cells were labelled with a primary antibody and an inappropriately targeted secondary antibody. In the second, the primary antibody was omitted.

3.2.3 3D Image acquisition, deconvolution and analysis

As described in chapter 2, a series of two-dimensional fluorescent images was acquired through the depth of the cell with a standard Nikon Diaphot 200

inverted microscope equipped for epifluorescence (60X oil immersion objective, NA 1.4, 2X adaptor). The pixel size was 200 x 200 nm and the Z spacing was 250 nm. Images were recorded with a CCD camera. For each wavelength, a three-dimensional data set was acquired using narrow bandpass filters specific for Fluorescein, Texas Red, and DAPI. Images were background and dark current subtracted and corrected for photobleaching. A flat field was used to correct for non-uniform illumination and camera sensitivity across the field of view. Images were deconvolved using the algorithm developed by Carrington et al. (Carrington *et al.*, 1995) with an empirically determined PSF on an EPR client-server. After deconvolution, each image was thresholded. The threshold values were determined from control experiments where the cells were labelled with a primary antibody and an inappropriately targeted secondary antibody or where the primary antibody was omitted. The remaining fluorescence intensity acquired from these control experiments was used, as a threshold value, to apply to each image collected. The background was segmented from the image by assigning a zero value to all pixels with a grey level lower than the threshold. Deconvolved and thresholded images were aligned using the fiduciary markers. All images are 3D reconstruction of the indicated depth.

3.2.4 Measurements of 2-NBDG uptake in HCAECs

The experimental conditions for measuring 2-NBDG uptake were first determined in cultured cells. HCAECs were mounted on the stage of a Nikon inverted microscope Diaphot-TMD and superfused at a flow rate of 7.5 ml/hr with oxygenated Krebs buffer (pH maintained at 7.35 to 7.45 by continual oxygenation; room temperature). The microscope was attached to an MRC-600

laser confocal imaging system (Bio-Rad, Hercules, CA). The MRC-600, equipped with a mixed-gas (krypton-argon) laser, was used with a FITC filter block (BHS, excitation filter 488 nm DF10, 515 nm emission barrier) and neutral density (ND) filter #1 (transmits 10% of the incident light). Dual recordings of phase contrast and fluorescence were performed using a 20X objective (Fluor 20X, Ph3DL, N.A. 0.75). Phase contrast was used to determine the position and the boundary of each cell and glucose uptake was monitored using the fluorescently tagged glucose analog 2-NBDG (Yoshioka *et al.*, 1996a; Yoshioka *et al.*, 1996b; Yoshioka *et al.*, 1996c). The emitted fluorescence was collected in confocal mode (confocal aperture of 1.55 mm diameter, 4X zoom), with an estimated lateral resolution of 3.7 μm and an axial resolution of 9.3 μm with an image depth of 16.9 μm. The resolution and depth of field were determined with a fluorescent bead (Appendix 3). An image was acquired for a group of cells observed in the field of view. The fluorescence collected corresponded to the amount of 2-NBDG sequestered intracellularly. The average fluorescence intensity per cell was quantified over time.

3.2.5 Measurements of 2-NBDG uptake in ECs of intact vessels

Male Wistar rats (200-235 g; University of British Columbia Animal Care Centre, Vancouver, B.C.) were sacrificed with a peritoneal injection of pentobarbital (30 mg/kg). Segments of approximately 0.6 to 1.0 mm in length of septal coronary arteries were carefully dissected. The tissue was immersed in ice-cold oxygenated (95% O_2/ 5% CO_2) Krebs buffer solution during the dissection. The vessels were mounted on glass cannulae in an arteriograph chamber (Living System Instrumentation) providing both intraluminal flow and superfusion of

the adventitial tissue with oxygenated Krebs solution (pH of 7.35 to 7.45) at room temperature. The adventitial surface was continuously superfused at 20-25 ml/min with oxygenated Krebs buffer containing 5 mM D-glucose. Intraluminal flow of Krebs buffer solution was maintained at 5.5 ml/hr (a normal physiological rate) and constant pressure using a small peristaltic pump (model P720, tubing of 0.093" internal diameter; Instech Laboratories, Inc., Plymouth Meeting, PA). A windkessel (a "T" connector with a closed end containing trapped air) was placed in the output line of the pump in order to reduce to a minimum the frequency and amplitude of the pulses generated by the pump. The intraluminal pressure was monitored with a pressure transducer (PT/F, Flow-thru monolithic chip, Luer fittings; Living System Instrumentation) and kept constant at 20 mmHg. The chamber was mounted on the stage of the microscope. Phase contrast was used to locate the axial position of ECs in the vascular wall and to determine the position and the boundary of each cell. Glucose uptake was monitored using the fluorescently tagged glucose analog 2-NBDG. The lumen was perfused with 1mM 2-NBDG in Krebs solution for various times followed by a 10-min wash period (Krebs solution). Images of EC fluorescence were acquired after each 10-min wash. The fluorescence collected corresponded to the intracellular sequestered 2-NBDG. The average fluorescence intensity per cell was quantified over time.

3.2.6 Experimental protocols

The time course of 2-NBDG accumulation in HCAECs was examined. These experiments were performed to determine the conditions (time and concentration) from which to measure 2-NBDG in its initial rate of uptake, before

equilibrium is reached. HCAECs were superfused with a Krebs solution containing a total of 5 mM glucose; between 0.1 to 3 mM of 2-NBDG and the rest was of L-glucose. The rate of uptake was obtained from consecutive exposures to 2-NBDG, adapted from the protocols used by others (Lloyd *et al.*, 1999; Yamada *et al.*, 2000; Roman *et al.*, 2001). The cells were exposed to a superfusion of 2-NBDG for 5 min, then washed with a Krebs solution containing 5 mM D-glucose for a subsequent 5 min. Following this wash, an image of the cells was acquired. Thereafter, the cells were further superfused with 2-NBDG for another 5 min, washed for 5 min and an image was acquired. This represented an accumulation of intracellular 2-NBDG for a total of 10 min. The superfusion with 2-NBDG was then repeated twice more for consecutive 10 and 15 min periods, each followed by 5-min wash and image acquisition. Thus, the same cells were imaged at a total time of exposure to 2-NBDG of 5, 10, 20, and 35 min (Figure 3.1A). The same protocol was repeated with concentration of 0.1, 0.5 and 1 mM. A second protocol was used where the cells were superfused with 2-NBDG for 5 min, washed for 5 min and imaged. This was repeated 6 times so that the cells were imaged at a total time of exposure to 2-NBDG of 5, 10, 15, 20, 25, and 30 min (Figure 3.1B). This protocol was used with concentrations of 2 and 3 mM 2-NBDG. The comparison between the rate of uptake of 0.1 mM of 2-NBDG and 6-NBDG was obtained from consecutive superfusion of 2-NBDG of 5, 5, 10, 10, 15, and 15 min, each followed by a 5-min wash and image acquisition. Thus, the same cells were imaged for a total time of exposure to 2-NBDG of 5, 10, 20, 30, 45 and 60 min (Figure 3.1C). In each case, the image acquisition consisted of both phase contrast and fluorescence recordings.

The effect of D-glucose (4 and 9 mM), cytochalasin B (10 μM) and insulin (2.5 μU/ml; Humulin R, human biosynthetic H1-210; Eli Lilly Canada Inc., Toronto, ON) were tested on a 20-min exposure to a Krebs solution containing a total of 5 mM glucose; 1 mM 2-NBDG and 4mM L-glucose (9 mM L-glucose were compared with 9mM D-glucose). A 10 and 20-min pre-incubation with cytochalasin B and insulin respectively, in a Krebs solution containing 4 mM L-glucose, preceded the addition of 2-NBDG to the solution. The effect of insulin (2.5 μU/ml) was also tested in HCAECs on a 30-min exposure to a Krebs solution containing 1 mM 2-NBDG and 4 mM D-glucose preceded by a 20-min pre-incubation with insulin and 5 mM D-glucose.

In intact vessels, the lumen was perfused with a Krebs solution containing a total of 5 mM glucose; 1 mM 2-NBDG and 4 mM L-glucose. Each exposure to 2-NBDG was followed by a 10-min wash with a Krebs solution containing 5 mM D-glucose. Phase contrast and fluorescence images were acquired after each wash. To determine the rate of uptake of 2-NBDG, the vessels were perfused with 2-NBDG for consecutive 5, 5, 10, 10, 15, and 15 min, each followed by a wash and image acquisition. Thus, the same cells were imaged for a total time of exposure to 2-NBDG of 5, 10, 20, 30, 45 and 60 min (Figure 3.1D). For all other experiments, the vessels were exposed to 2-NBDG for a period of 20 min in which the effect of D-glucose (replaced by the same amount of L-glucose), cytochalasin B (10 μM) and insulin (2.5 μU/ml) were tested. After each 20 min of perfusion with 1 mM 2-NBDG, the vessels were perfused with the washing solution for 10 min and imaged. Pre-incubations of 10 min and 20 min with cytochalasin B and insulin, respectively, in a Krebs solution containing 4 mM L-glucose, were also performed prior to exposure to 2-NBDG.

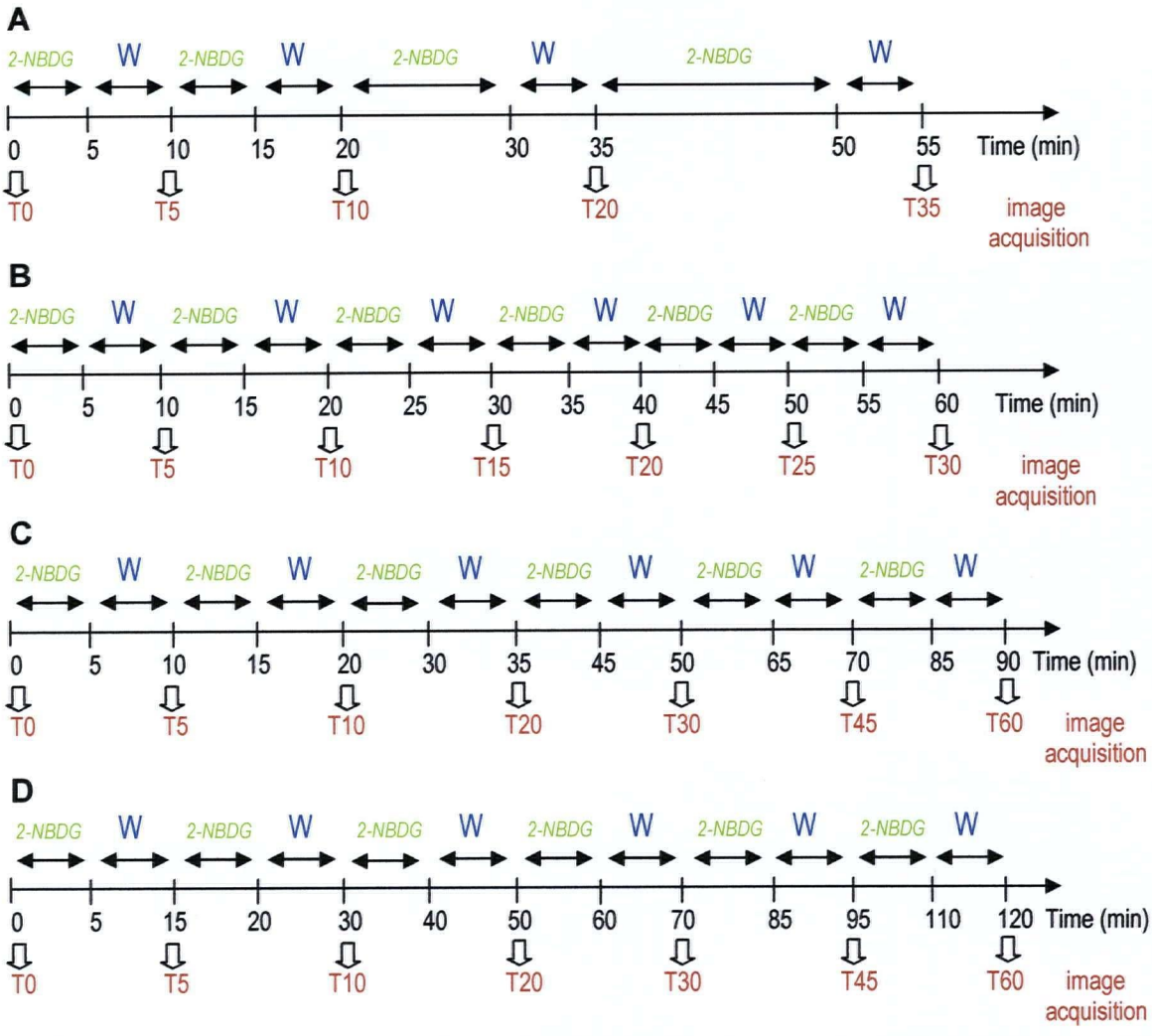

Figure 3.1 Time course of 2-NBDG uptake; experimental protocols.
A) Protocol used for concentration of 0.1, 0.5, and 1 mM 2-NBDG in HCAECs. B) Protocol used for concentration of 2 and 3 mM 2-NBDG in HCAECs. C) Protocol used for comparisons between 0.1 mM 2-NBDG and 6-NBDG. D) Protocol used for 1 mM 2-NBDG in vessel preparation. *2-NBDG*: period of incubation with 2-NBDG, W: period of wash, T0-T60: represents a time of total exposure to the fluorescent glucose analog at which an image was collected.

3.2.7 Fluorescence quantification and analysis

The data collected were analysed with Scion Image Beta 4.02 for Windows XP (2000 Scion Corporation, NIH, USA). Each cell boundary was determined

using phase contrast image. The freehand selection tool was used to define a region on the phase contrast image from which the average fluorescence per pixel (for each individual cell) was measured (Figure 3.2). The background fluorescence recorded prior to 2-NBDG incubation was subtracted from this value. The measured intensity per pixel from each cell analysed was averaged and compared between different conditions. The same analysis was performed with the data collected from the intact vessel. The data are presented as mean ± SE and are compared using ANOVA and t-test as required.

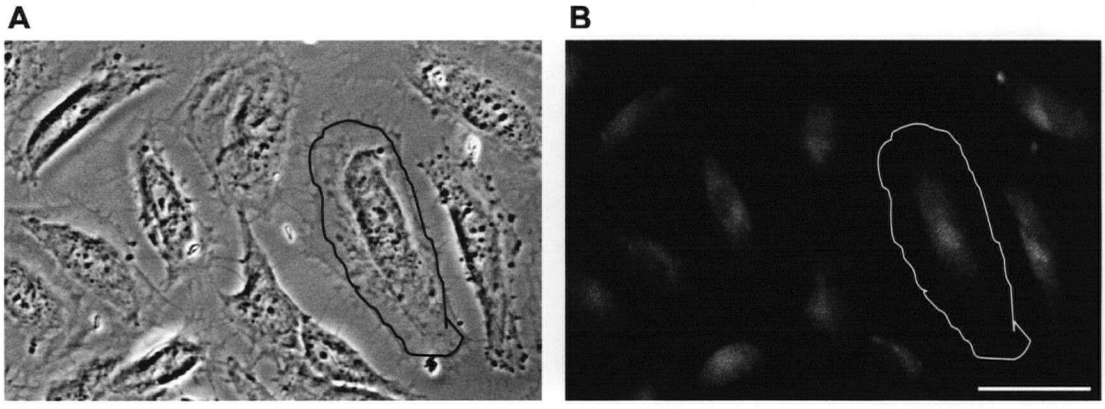

Figure 3.2 Dual Imaging of phase contrast and fluorescence in HCAECs.
Both phase contrast (A) and 2-NBDG fluorescence (B) images were acquired from HCAECs following 2-NBDG incubation (20 min) and a 5-min wash. An individual cell boundary was determined on the phase contrast image from which the average fluorescence intensity per pixel was measured (Scion Image; scale bar is 25 μm).

3.3 Results

3.3.1 EC identification in cultured HCAECs

As presented in Chapter 2, Western blots were performed on HCAECs. In the HCAEC lysate, VE-cadherin was present at the expected molecular weight of 130 KDa while no band was found for the SMC specific protein α-actin (Figure 2.3). HCAECs were also fixed and labelled with VE-cadherin and DAPI. VE-cadherin was found at the cell-to-cell junction of adjacent cells (Figure 3.3A & Figure 3.7A) but was absent where a cell was without a neighbour (Figure 3.4A) and discontinued in area that had not reached complete confluence (Figure 3.5A,Figure 3.8A, and Figure 3.9A). From a side view it could also be observed that VE-cadherin is in close proximity to the coverslip and that the bulk of the nuclei mass are above the VE-cadherin (Figure 3.3B). The morphology of the HCAECs was found to be different from that of ECs of the intact coronary artery. HCAECs were not elongated and their overall size was bigger than that of an EC from a native vessel (a typical rat native EC is ~3μm wide and ~12μm long in comparison to ~18μm wide by ~50μm long for a HCAEC).

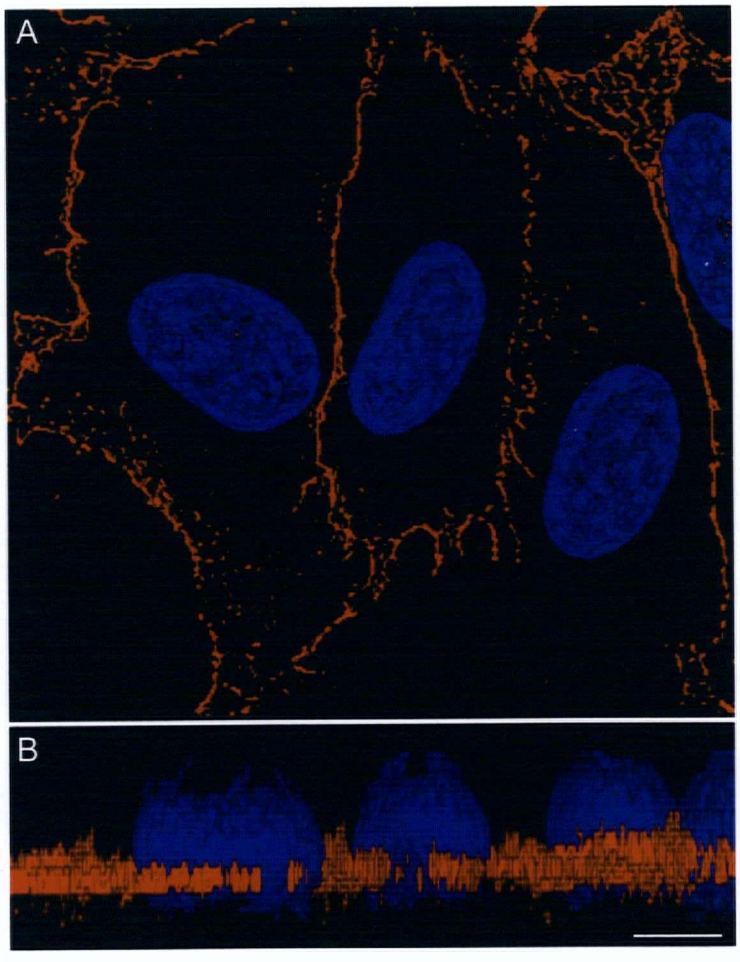

Figure 3.3 Identification of ECs in culture of HCAECs.
Deconvolved images of HCAECs. VE-cadherin (red) and nuclei (blue). A) *En face* view, the image is 6.5 μm deep. B) Side view obtained from the 3D image in A, rotated 90° about the X-axis. The image is 68 μm deep. Scale bar is 8 μm.

We have shown previously that each of the classical GLUTs and SGLT-1 were found in the HCAEC lysate, at the same M.W. as that found in the native endothelium lysate, with the exception of GLUT-2 for which a lower M.W. in HCAECs was found (Figure 2.4). We then assessed, through immunocytochemistry, the subcellular distribution of each of these glucose transporter isoforms. A representative cell is shown labelled with GLUT-1 (Figure 3.4), GLUT-2 (Figure 3.5), GLUT-3 (Figure 3.6), GLUT-4 (Figure 3.7),

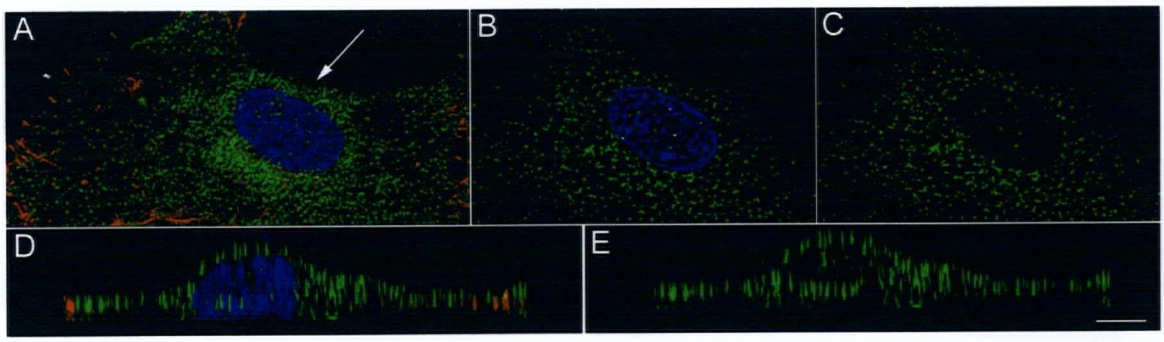

Figure 3.4 GLUT-1 in HCAEC

Deconvolved images of HCAEC labelled with antibodies specific for GLUT-1 (green), VE-cadherin (red) and nuclei with DAPI (blue). A) *En face* view of the full 3D reconstruction of the cell, 7.5 μm deep. The arrow points to an area without an adjacent cell and without VE-cadherin. B&C) Central planes (0.750 μm deep) obtained from A. B) GLUT-1 and DAPI labelling, C) only GLUT-1 labelling. D & E) Side view obtained from a 90° rotation about the X-axis of the image in A, 2 μm deep cross-sections; coverslip at the bottom of the images. D) GLUT-1, VE-cadherin and DAPI labelling, E) only GLUT-1 labelling. Scale bar is 8 μm.

GLUT-5 (Figure 3.8), and SGLT-1 (Figure 3.9). Each of the transporters was seen on the periphery of the cell, more likely on the plasma membrane. All of the transporters had a uniform distribution above and below the nucleus, with no indication of the asymmetric subcellular distribution found in the native endothelium. Also missing in the HCAECs is the distinctive tendency of the GLUTs and SGLT-1 to locate at the cell-to-cell junctions found previously in the native endothelium (Figure 3.4 to Figure 3.9A). A dense perinuclear labelling was found for most transporters with the exception of GLUT-4 and GLUT-5 (Figure 3.7B&C and Figure 3.8B&C). Figure 3.4B&C, Figure 3.5B&C, Figure 3.6B&C, and Figure 3.9B&C show, from a thin section taken from the middle of the cell, the labelling surrounding the nucleus, and the lack of labelling inside the nucleus of the same section. GLUT-4 was the only isoform with a high prevalence of labelling located in the nuclear area (Figure 3.7B & C). In the case of GLUT-1, 2, 3 and SGLT-1, labelling was observed in the cytosol (Figure 3.4D&E, Figure

3.5D&E, Figure 3.6D&E and Figure 3.9D & E). GLUT-4 and 5 were not found in the cytosol of HCAECs (Figure 3.7D&E and Figure 3.8D & E).

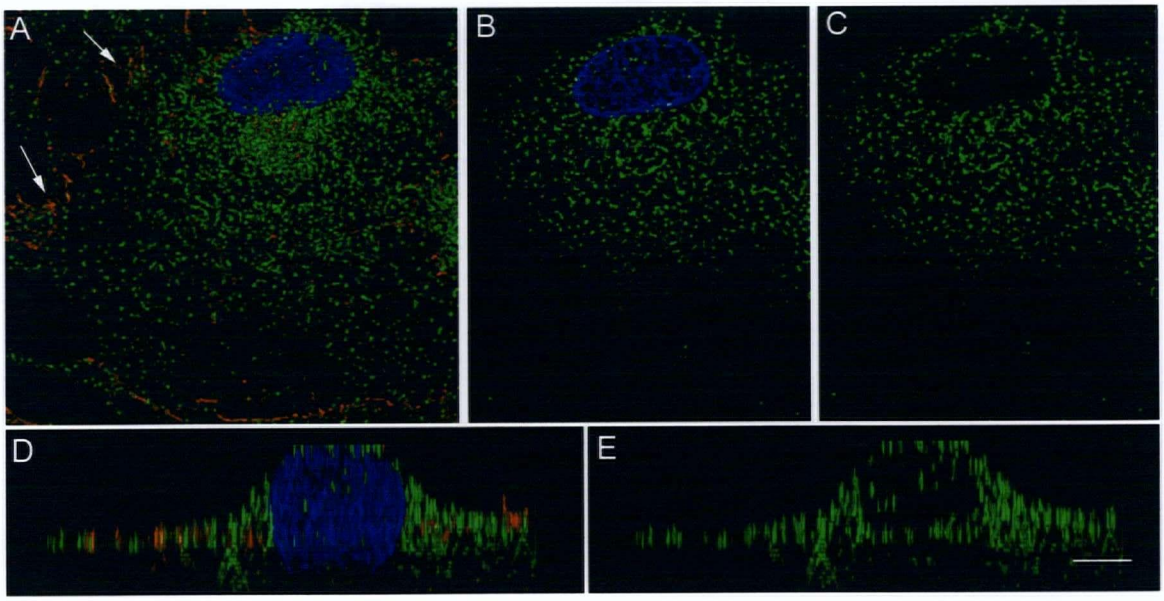

Figure 3.5 GLUT-2 in HCAEC

Deconvolved images of HCAEC labelled with antibodies specific for GLUT-2 (green), VE-cadherin (red) and nuclei with DAPI (blue). A) *En face* view of the full 3D reconstruction of the cell, 8 μm deep. The arrows point to discontinuous contacts between adjacent cells. B & C) Central planes (1 μm deep) obtained from A. B) GLUT-2 and DAPI labelling, C) only GLUT-2 labelling. D & E) Side view obtained from a 90° rotation about the X-axis of the image in A, 4 μm deep cross-sections, coverslip at the bottom of the images. D) GLUT-2, VE-cadherin and DAPI labelling, E) only GLUT-2 labelling. Scale bar is 8 μm.

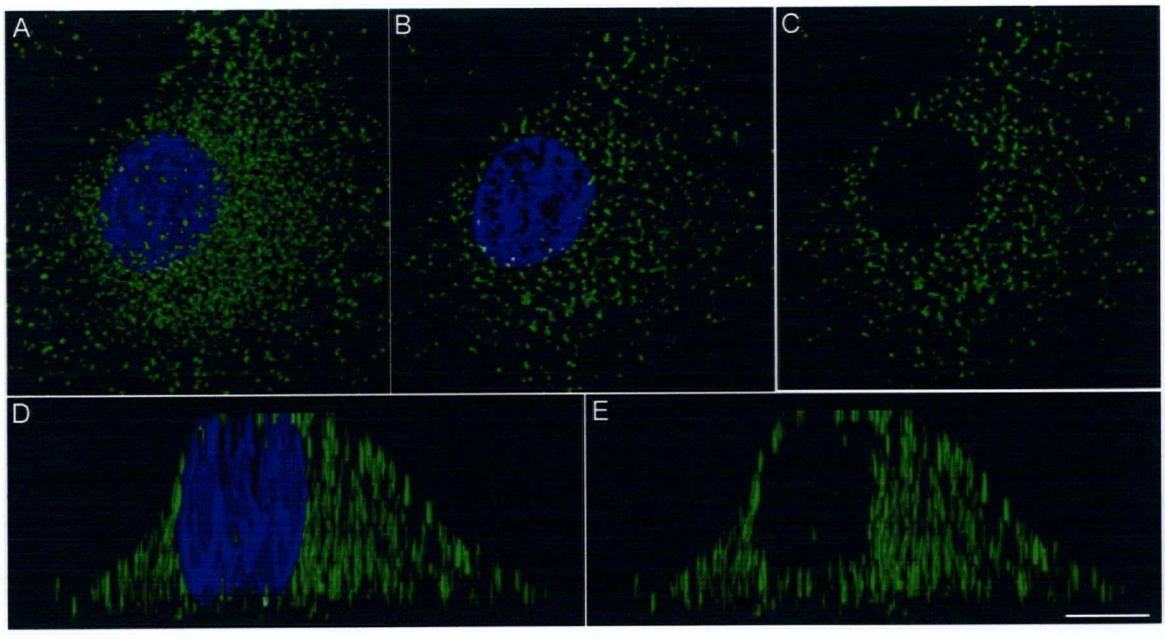

Figure 3.6 GLUT-3 in HCAEC

Deconvolved images of HCAEC labelled with antibodies specific for GLUT-3 (green), VE-cadherin (red) and nuclei with DAPI (blue). A) *En face* view of the full 3D reconstruction of the cell, 8.5 μm deep. B & C) Central planes (1 μm deep) obtained from A. B) GLUT-3 and DAPI labelling, C) only GLUT-3 labelling. D & E) Side view obtained from a 90° rotation about the X-axis of the image in A, 4 μm deep cross-sections, coverslip at the bottom of the images. D) GLUT-3, VE-cadherin and DAPI labelling, E) only GLUT-3 labelling. Scale bar is 8 μm.

Figure 3.10 shows secondary antibody labelling in HCAECs. The donkey anti-rabbit FITC (Figure 3.10A), anti-mouse FITC (Figure 3.10B), anti-goat FITC (Figure 3.10C) and anti-goat Texas red (Figure 3.10D) failed to label the HCAECs on their own. No immunostaining was observed when primary antibodies were applied in combination with a secondary antibody targeting an irrelevant species. Figure 3.11 shows HCAECs labelled with a single primary antibody and two secondary antibodies. The relevant secondary antibody produced labelling in HCAECs (Figure 3.11C&F for Texas Red and G, J, M, P, and S for FITC). The irrelevant secondary antibodies, in each case, did not produce any labelling in HCAECs (Figure 3.11A&D for FITC and I, L, O, R, and U for Texas Red). The

middle column in Figure 3.11B, E, H, K, N, Q, and T, shows, as a landmark, the nucleus of each cell labelled with DAPI.

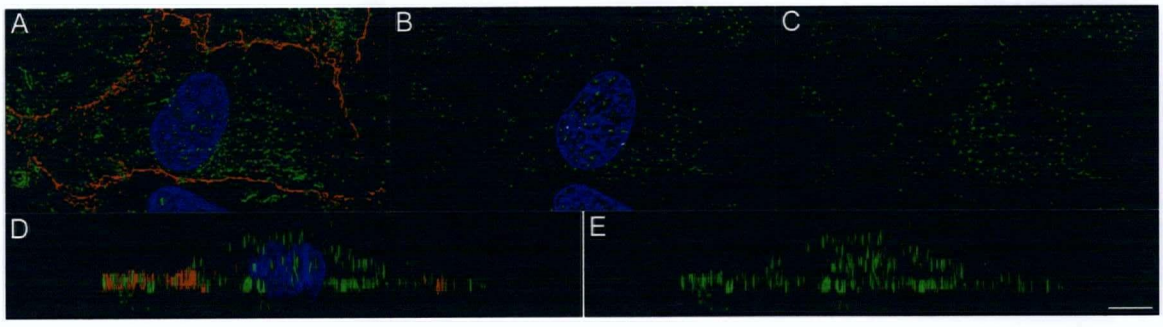

Figure 3.7 GLUT-4 in HCAEC

Deconvolved images of HCAEC labelled with antibodies specific for GLUT-4 (green), VE-cadherin (red) and nuclei with DAPI (blue). A) *En face* view of the full 3D reconstruction of the cell, 9 μm deep. B & C) Central planes (1.25 μm deep) obtained from A. B) GLUT-4 and DAPI labelling, C) only GLUT-4 labelling. D & E) Side view obtained from a 90° rotation about the X-axis of the image in A, 4 μm deep cross-sections, coverslip at the bottom of the images. D) GLUT-4, VE-cadherin and DAPI labelling, E) only GLUT-4 labelling. Scale bar is 8 μm.

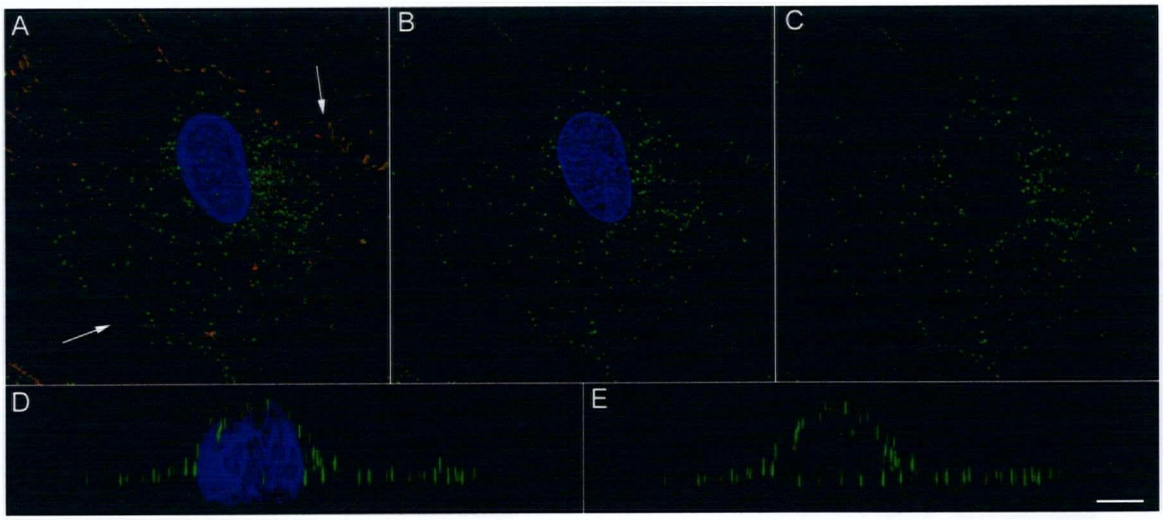

Figure 3.8 GLUT-5 in HCAEC

Deconvolved images of HCAEC labelled with antibodies specific for GLUT-5 (green), VE-cadherin (red) and nuclei with DAPI (blue). A) *En face* view of the full 3D reconstruction of the cell, 8.5 μm deep. The upper arrow points to discontinuous contacts between adjacent cells, the lower arrow points to an area without adjacent cell and without VE-cadherin. B & C) Central planes (1 μm thick) obtained from A. B) GLUT-5 and DAPI labelling, C) only GLUT-5 labelling. D & E) Side view obtained from a 90° rotation about the X-axis of the image in A, 4 μm deep cross-sections, coverslip at the bottom of the images. D) GLUT-5, VE-cadherin and DAPI labelling, E) only GLUT-5 labelling. Scale bar is 8 μm.

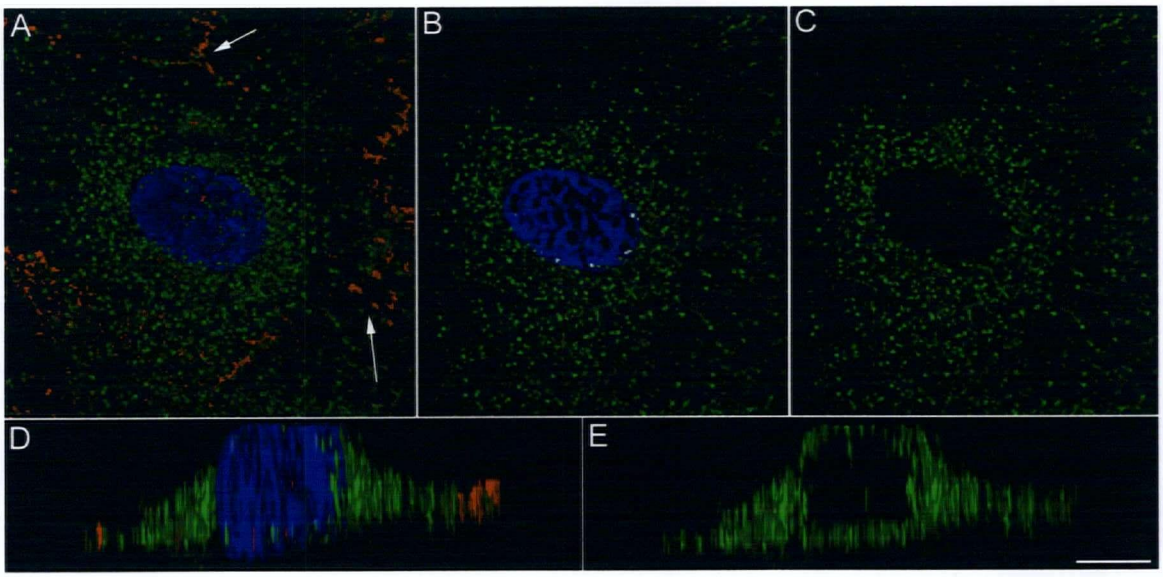

Figure 3.9 SGLT-1 in HCAEC

Deconvolved images of HCAEC labelled with antibodies specific for SGLT-1 (green), VE-cadherin (red) and nuclei with DAPI (blue). A) *En face* view of the full 3D reconstruction of the cell, 6.5 μm deep. The arrows point to discontinuous contacts between adjacent cells. B & C) Central planes (4.8 μm deep) obtained from A. B) SGLT-1 and DAPI labelling, C) only SGLT-1 labelling. D & E) Side view obtained from a 90° rotation about the X-axis of the image in A, 4 μm deep cross-sections, coverslip at the bottom of the images. D) SGLT-1, VE-cadherin and DAPI labelling, E) only SGLT-1 labelling. Scale bar is 8 μm.

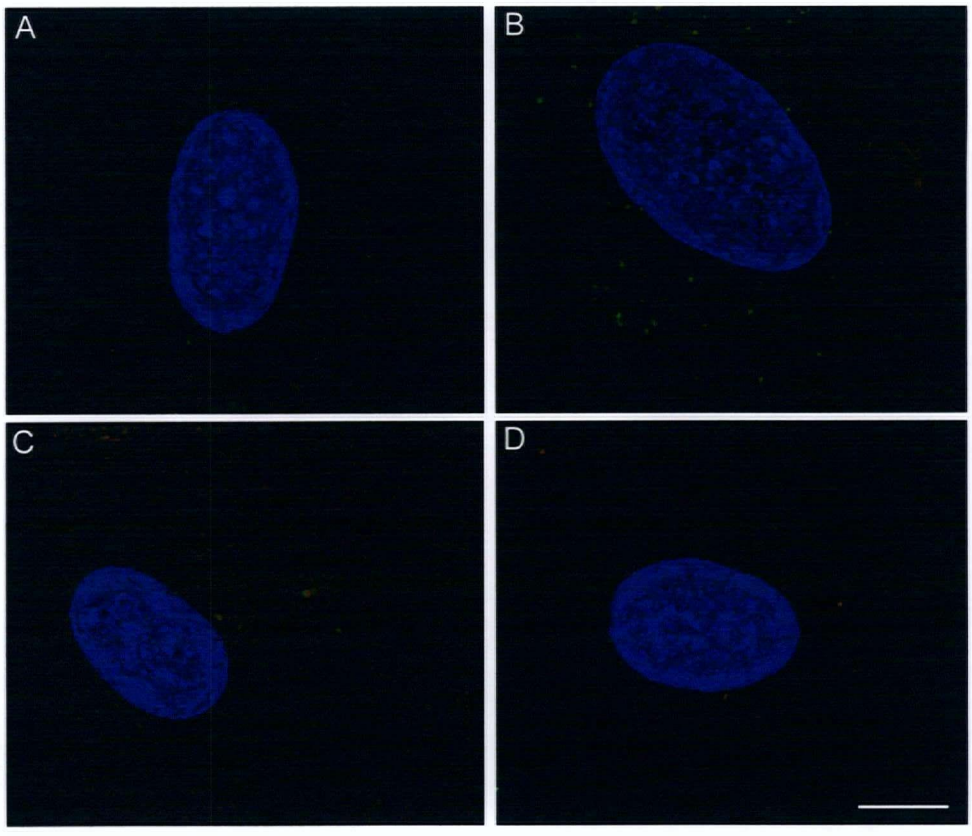

Figure 3.10 Secondary antibody controls in HCAECs.
Images are 3D reconstruction of HCAECs, *en face* view of the cells. HCAECs are labelled with DAPI (blue) and a single secondary antibody (FITC: green or Texas Red: red); A) donkey anti-rabbit FITC, B) donkey anti-mouse FITC, C) donkey anti-goat FITC and D) donkey anti-goat Texas Red. Images are 5.5 μm deep; scale bar is 8 μm.

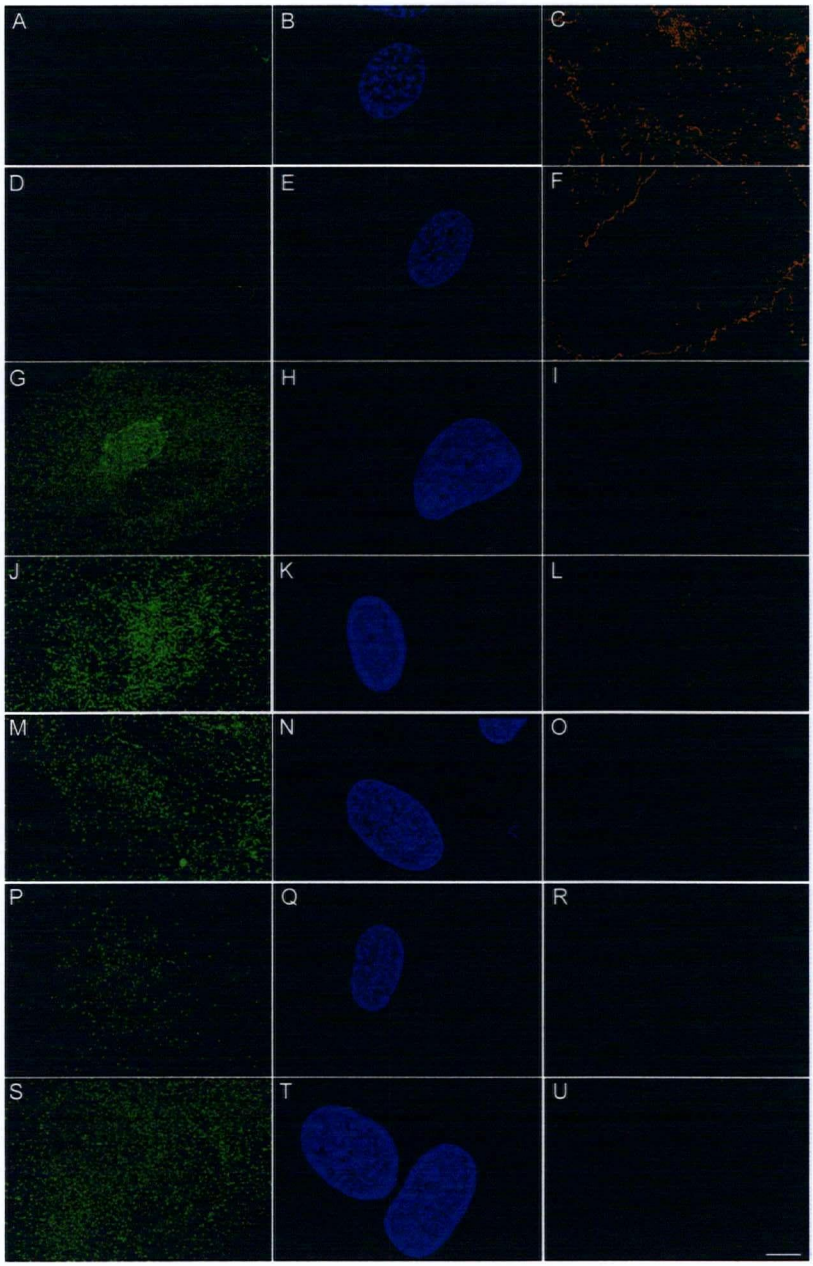

Figure 3.11 Secondary antibody cross-reactivity controls in HCAECs.
Images are 3D reconstruction of HCAECs, *en face* view of the cells. HCAECs are labelled with a single primary antibody: A-F) anti-VE-cadherin, G-I) rabbit anti-GLUT-1, J-L) rabbit anti-GLUT-2, M-O) mouse anti-GLUT-4, P-R) rabbit anti-GLUT-5, S-U) rabbit anti-SGLT, and dual secondary anti-body : A-C, G-L &P-U) donkey anti-rabbit FITC (green, 1st column) and donkey anti-goat Texas Red (red, 3rd column), D-F & M-O) donkey anti-mouse FITC (green, 1st column) and donkey anti-goat Texas Red (red, 3rd column). DAPI (blue) is shown in 2nd column. Images are 5.5 μm deep; scale bar is 8 μm.

3.3.2 2-NBDG uptake in HCAECs

The immunocytochemistry identified six different transporters in HCAECs. The next step was to test whether these transporters were functional. To proceed, a concentration and time point from the linear portion of the initial rate of uptake of 2-NBDG was determined. Then, we examined the regulation of 2-NBDG uptake in the presence of compounds known to enhance or inhibit specific GLUT and SGLT isoforms.

First, it was determined that the fluorescent images should be acquired following a 5-min wash, during which non-incorporated 2-NBDG was removed. The possibility of imaging the cytosol of HCAECs in the presence of extracellular 2-NBDG was rejected due to insufficient axial resolution. The image depth was ~17 μm while the thinnest cytosolic section of HCAECs was ~2 μm, therefore the image was dominated by extracellular fluorescence.

It is impossible to predict, a priori, how much 2-NBDG to use or for how long the cells should be incubated with the compound before recording. The initial series of experiments were therefore designed to determine these parameters. We tested concentrations of 2-NBDG ranging from 0.1 mM to 3 mM, adding enough L-glucose to bring the total glucose concentration to the normal physiological value of 5 mM. The uptake of 1 mM 2-NBDG was linear (r^2=0.99) over 30 min (Figure 3.12A), while at 0.1 mM the uptake was linear (r^2=0.996) over 60 min (Figure 3.12D). At higher concentrations of 2-NBDG (3 mM), the uptake remained linear over time (r^2=0.86) but increased in variability (Figure 3.12B). The plot of the rate of uptake of 2-NBDG at concentrations of 0.1, 0.5, 1, 2, and 3

mM 2-NBDG (Figure 3.12C) was better described by a single exponential (r^2=0.95) then a linear regression (r^2=0.93). Nevertheless, for concentrations below 1 mM, the rate of 2-NBDG uptake was more accurately linear (r^2= 0.98) to the concentration (see inset in Figure 3.12C). The rate of uptake of 2-NBDG and 6-NBDG were also compared in HCAECs to determine the effect of phosphorylation on the rate of uptake (Figure 3.12D). The rate of uptake of the 6-NBDG was 35% higher than the rate of uptake of the 2-NBDG. Significant differences in the average fluorescence intensity accumulated over time in HCAECs were found at 20 min of exposure to the 2-NBDG and 6-NBDG, and beyond. From these observations, it was decided that subsequent experiments would be performed at concentration of 1 mM 2-NBDG and for an incubation time of 20 min. This concentration (1 mM) was selected because of the greater precision of the linearity over time of the fluorescence recorded. The time point (20 min) was chosen because it was clearly on the linear portion of the curve and was not approaching saturation of the transporters and/or that of hexokinase.

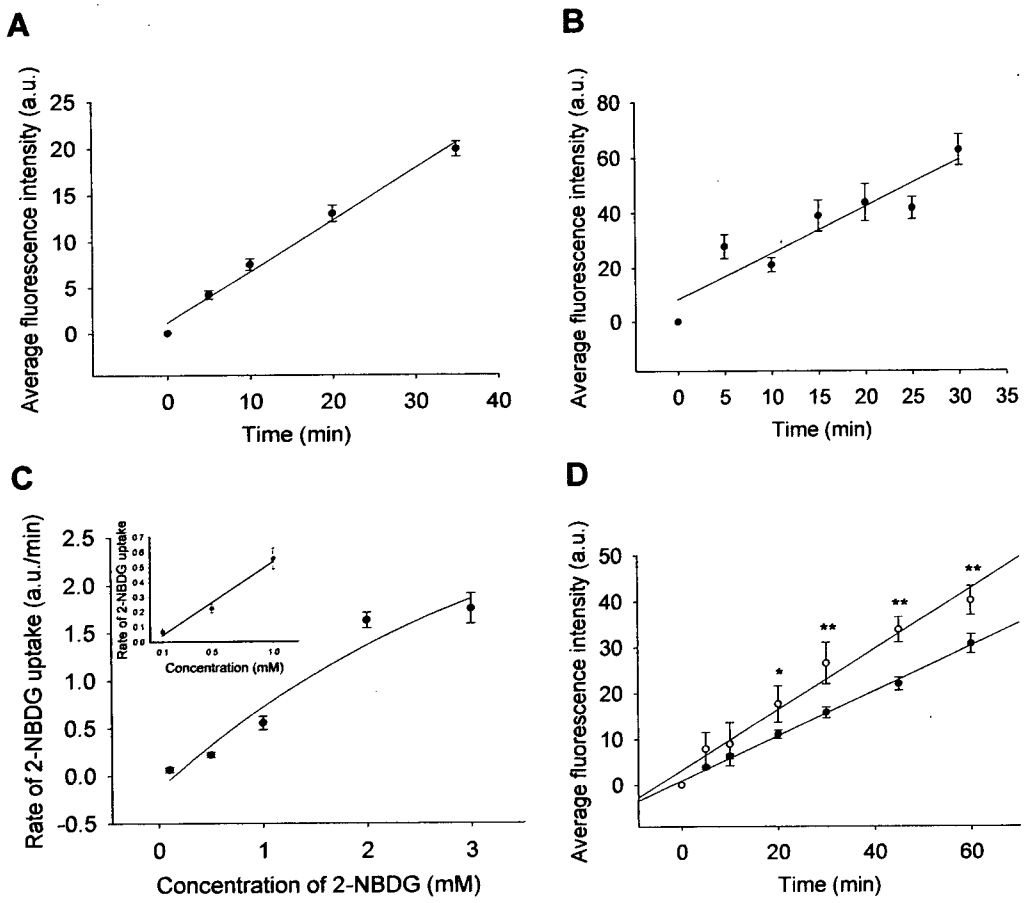

Figure 3.12 Rate of fluorescent glucose uptake in HCAECs
A) Plot of 1 mM 2-NBDG uptake over time (r^2=0.99), average of 12 cells from 3 different experiments B) Plot of 3 mM 2-NBDG uptake over time (r^2=0.86), average of 18 cells from 5 different experiments. C) Plot of the rate of uptake versus the concentration of 2-NBDG, single exponential (r^2=0.95), each rate is the average of 10 cells from 1 to 5 different experiments. The inset shows a linear relation between the rate of uptake of 2-NBDG and concentration below 1 mM (r^2= 0.98). D) Plot of 0.1 mM 2-NBDG (open circle) and 6-NBDG (closed circle) uptake over time (r^2=0.99 and 0.97 respectively), each plot is the average of 15 and 6 cells from 3 and 2 different experiments respectively.

To demonstrate that the uptake of 2-NBDG by HCAECs occurs through GLUTs and/or SGLT, we assessed the competitive inhibitory effect of D-glucose and cytochalasin B on the rate of uptake of 2-NBDG. Concentrations of 4 mM and 9 mM of D-glucose reduced significantly the accumulation of fluorescence

intensity in HCAECs by 55% ($p<0.05$) and 76% ($p<0.001$) respectively (Figure 3.13). These were compared to values obtained in solution where the same concentration of D-glucose was replaced by L-glucose.

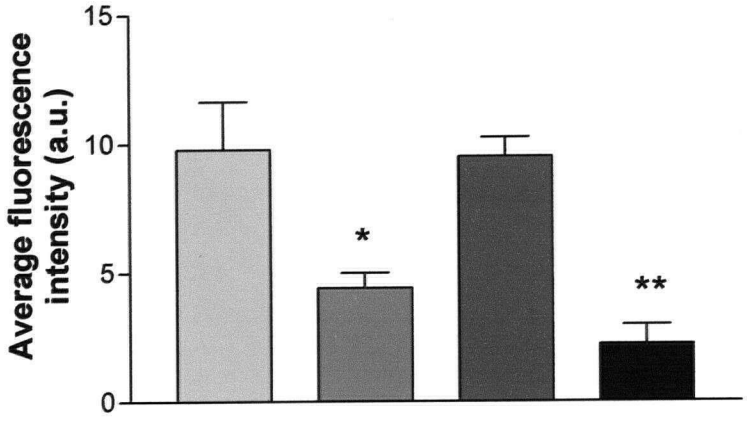

Figure 3.13 D-glucose inhibition of 2-NBDG uptake in HCAECs.
Effect of 4 mM and 9 mM L-glucose and 4 mM and 9 mM D-glucose on the rate of uptake of 1 mM 2-NBDG over a period of 20 min. Each bar is the average of 9 cells from 2 different experiments. Significant differences are indicated; * $p<0.05$ (4 mM) and ** $p<0.001$ (9 mM).

Cytochalasin B, a commonly used inhibitor of glucose transport by GLUTs, also inhibited the rate of 2-NBDG uptake in HCAECs. The fluorescence intensity accumulated in HCAECs over 15 min of exposure to 1 mM 2-NBDG was significantly reduced by 35% ($p<0.05$) in the presence of 10 μM cytochalasin B (Figure 3.14). These experiments were done at 15 min incubation with 2-NBDG rather than 20 min because of the effects of cytochalasin B on the cell cytoskeleton, changing their shape and the consequent fluorescence intensity, independently of the accumulation of 2-NBDG in the cell.

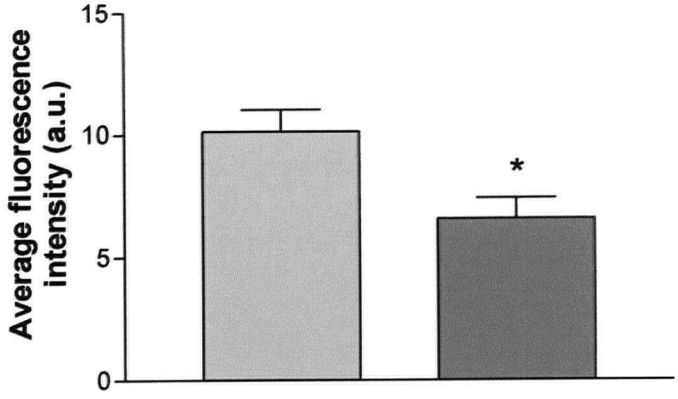

Figure 3.14 Effect of cytochalasin B on 2-NBDG uptake in HCAECs.
Uptake of 2-NBDG (1 mM) over 15 min, in the absence ☐ or presence ■ of 10 μM cytochalasin B. Each bar is the average of 8 and 7 cells respectively from 2 different experiments; (* $P<0.05$).

The effect of insulin on the rate of uptake of 2-NBDG was tested in HCAECs to determine the functionality of GLUT-4. A concentration of 2.5 μU/ml of insulin significantly increased, by 64% ($p<0.0001$), the accumulation of fluorescence intensity in HCAECs incubated for 20 min in a Krebs solution containing 4 mM L-glucose (Figure 3.15A). Although the same concentration of insulin only produced a 31% ($p<0.05$) increase in accumulated fluorescence intensity in HCAECs incubated for 30 min in a Krebs solution containing 4 mM D-glucose (Figure 3.15B). In addition, we observed no effect of insulin on the average fluorescence intensity accumulated in HCAECs exposed to a lower ratio of 2-NBDG and D-glucose (0.1 mM 2-NBDG in presence of 5 mM D-glucose, see Appendix 4).

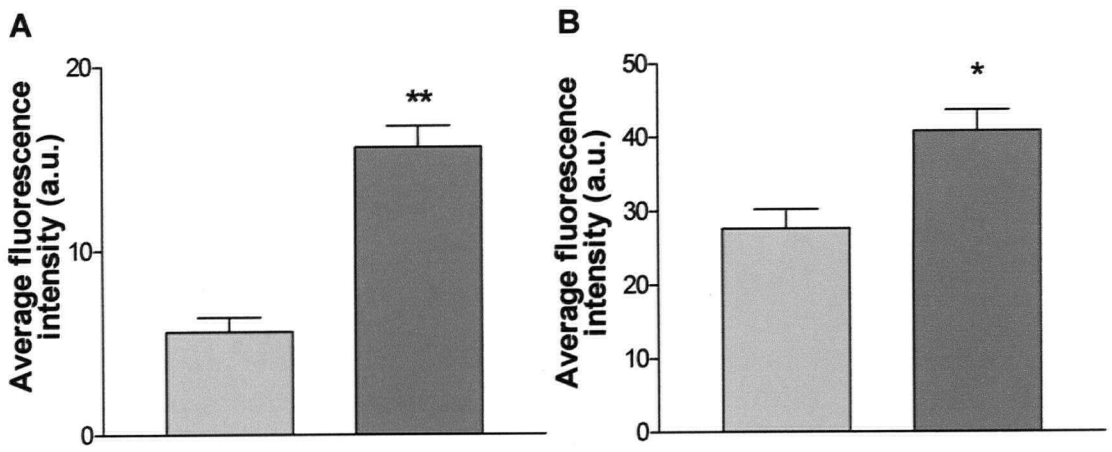

Figure 3.15 Effect of insulin on 2-NBDG uptake in HCAECs

Uptake of 1 mM 2-NBDG in the absence ☐ or presence ■ of 2.5 μU/ml of insulin. A) over 20 min in the presence of 4 mM L-glucose, each bar is the average of 18 and 33 cells from 2 different experiments respectively, (** $P < 0.0001$). B) over 30 min in the presence of 4 mM D-glucose, each bar is the average of 16 and 15 cells from 2 and 3 different experiments respectively; (* $P<0.05$).

3.3.3 2-NBDG uptake in native endothelium of intact coronary artery.

2-NBDG uptake was then measured in the endothelium of native coronary arteries. Figure 3.16 shows a schematic representation of a vessel from which phase contrast and confocal fluorescence images were acquired at different focal planes through the vessel wall. Phase contrast was used to image a small section of the vessel wall touching the coverslip of the arteriograph chamber (Figure 3.16B). Individual ECs were identified through phase contrast by their characteristic longitudinal fusiform shape oriented parallel to the blood flow (Figure 3.16C). Phase contrast was also used to locate the axial position of ECs and SMCs in the vascular wall (Figure 3.16 D to G left). The lumen of this vessel was perfused with 1 mM 2-NBDG for 40 min, followed by a 10-min wash with Krebs solution containing 5 mM D-glucose. The fluorescence emitted by trapped

intracellular 2-NBDG and the phase contrast images were acquired simultaneously. While no fluorescence could be detected from both the lumen (Figure 3.16D right) and the coverslip (Figure 3.16G right), a strong fluorescence at the periphery of each EC was observed (Figure 3.16E right). From the SMC layer, strong fluorescence in long strips, oriented perpendicularly to the blood flow were also observed (Figure 3.16F, right). As shown by the fluorescence acquired from the EC and SMC layers, 16 μm apart, it is possible to distinguish the fluorescence accumulated from one layer of cells to the other with the 20X objective, which has an axial resolution of 9.3 μm and an image depth of 16.9 μm.

From the above experiment, it was shown that emitted fluorescence could be measured in ECs, without interference from light emitted by the SMCs in the vascular wall of a coronary artery. Before proceeding with further experiments on the regulation of glucose uptake in the native endothelium we examined the rate of uptake of 2-NBDG in ECs of the vascular wall. The plot of the uptake of 1 mM of 2-NBDG over 60 min (Figure 3.17) was better described by a single exponential (r^2=0.98) then a linear regression (r^2=0.94). Nevertheless, for the first 20 min, the rate of uptake was more accurately linear over time (see inset from Figure 3.17, r^2=0.99). Time points beyond 20 min also revealed an increased in variability of the fluorescence intensity as shown by the error bars on Figure 3.17. The effects of D-glucose, cytochalasin B and insulin on 2-NBDG uptake were therefore tested on periods of 20 min of exposure to concentration of 1 mM of 2-NBDG. This time point is in the linear portion of the curve from which one can effectively approximate the tangent to the curve and sensitively measure variations in the initial rate of uptake.

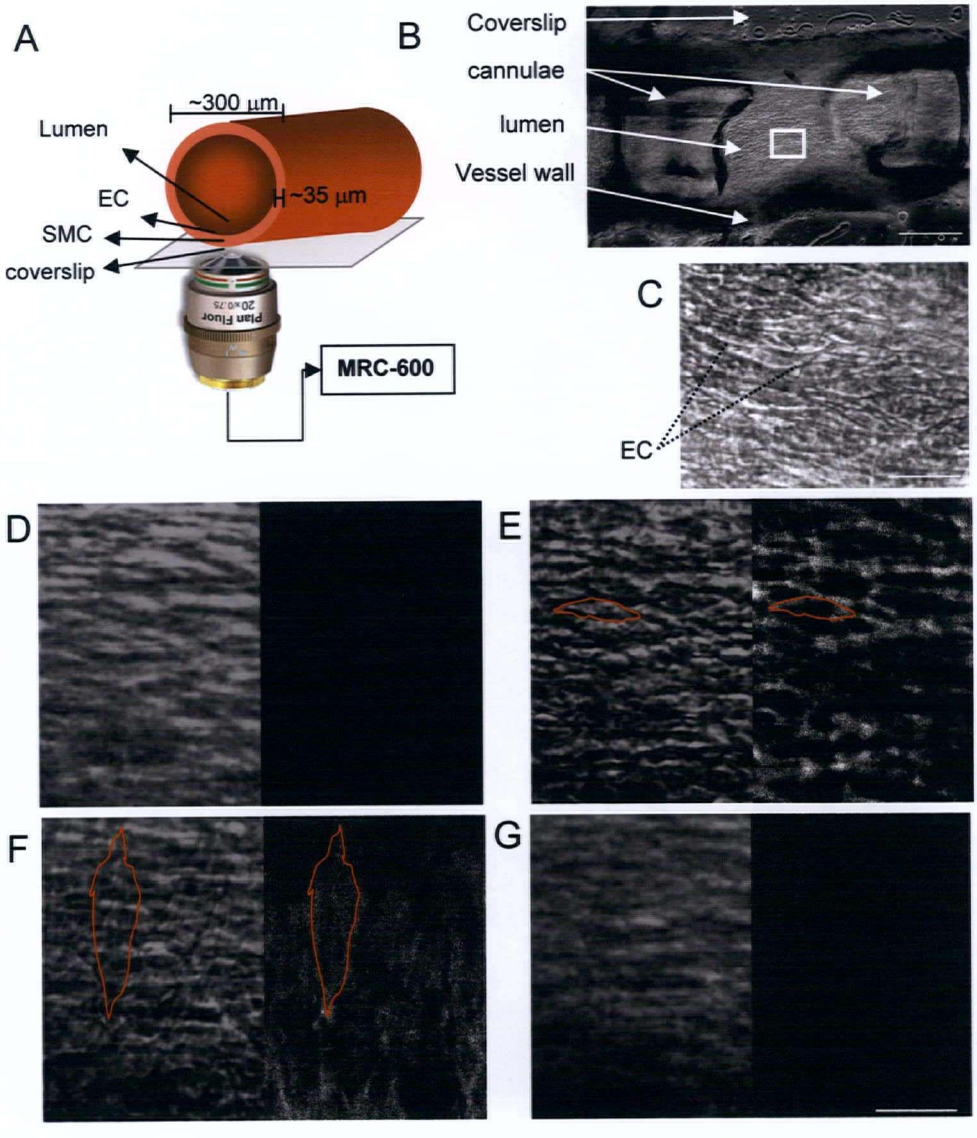

Figure 3.16 Phase contrast and fluorescence in whole vessel preparation.
Representative coronary artery mounted on glass cannulae in an arteriograph chamber. A) Schematic representation of the vessel in relation to the coverslip and the 20X objective. B) Phase contrast image of the vessel attached to the cannulae; scale bar is 100 µm. C) Higher magnification of the inset from B; scale bar is 25 µm. D to G) simultaneous recording of phase contrast (left) and fluorescence (right) after 40 min incubation with 1 mM 2-NBDG and 10-min wash; scale bar is 25 µm. D) lumen imaged at 52 µm above the cover slip. E) ECs imaged at 32 µm above the coverslip. F) SMCs imaged at 16 µm above the coverslip. G) Image at the coverslip. In red, EC (E) and SMC (F) boundaries.

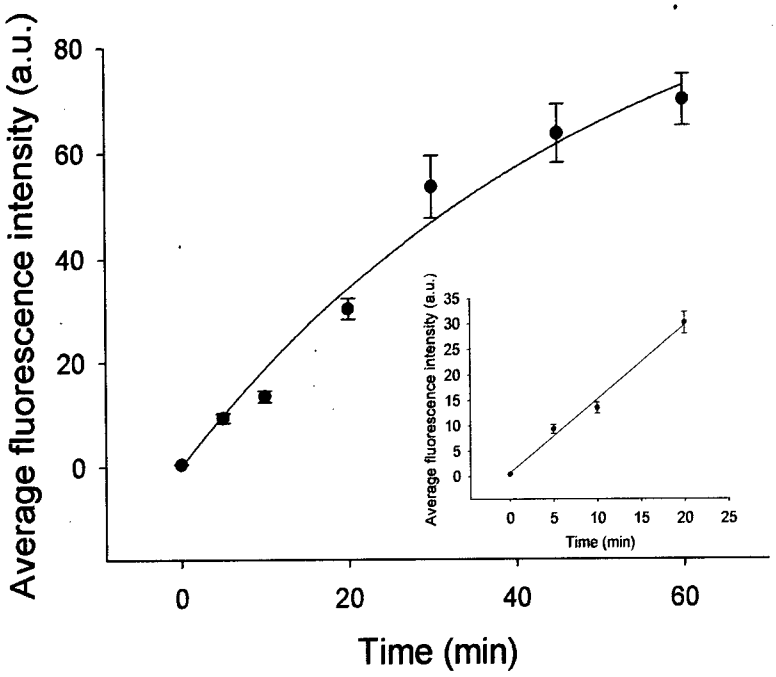

Figure 3.17 Rate of 2-NBDG uptake in ECs of intact coronary artery.
Representative rate of 2-NBDG uptake from a rat coronary artery. The vessel was perfused with a solution containing 1 mM 2-NBDG and 4 mM of L-glucose for cumulative periods of 5, 10 and 15 min, each followed by 10-min wash and image acquisition. The plot is the average of 5 cells, single exponential (r^2 = 0.98). The inset shows a linear uptake over time points below 20 min (r^2=0.99).

To demonstrate that the uptake of 2-NBDG occurred also through GLUTs and/or SGLTs transporter proteins in ECs of an intact arteries, we repeated the competitive inhibitory assay performed in HCAECs with D-glucose and cytochalasin B, this time in the cannulated vessel, expecting to find similar results. The average fluorescence intensity accumulated in the endothelium of intact coronary artery over 20 min was reduced significantly by 41% ($p<0.0001$) in vessels perfused with a solution containing 4 mM D-glucose in comparison to a vessel perfused with a solution containing L-glucose.

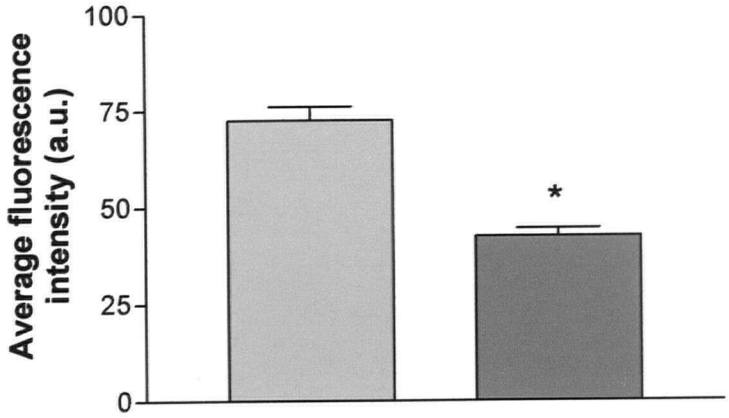

Figure 3.18 Effect of D-glucose on 2-NBDG uptake in native ECs.
Uptake of 1 mM 2-NBDG in ECs of intact coronary artery in presence of 4 mM L-glucose ▭ or D-glucose ▬. Each bar is the average of 37 and 24 cells respectively, from 3 different experiments; * $p<0.0001$.

Similarly, the addition of 10 μM of cytochalasin B reduced significantly by 27% ($p<0.0001$) the fluorescence intensity recorded in ECs of intact arteries, accumulated over 20 min of perfusion with a solution containing 1 mM of 2-NBDG and 4 mM of L-glucose (Figure 3.19).

Lastly, we tested the effect of insulin in the endothelium of intact coronary artery to determine the functionality of GLUT-4 previously identified in these cells. The addition of 2.5 μU/ml of insulin increased significantly by 23% ($p<0.05$) the fluorescence intensity of the ECs of intact arteries perfused with a solution of 1 mM 2-NBDG and 4 mM L-glucose for 20 min (Figure 3.20).

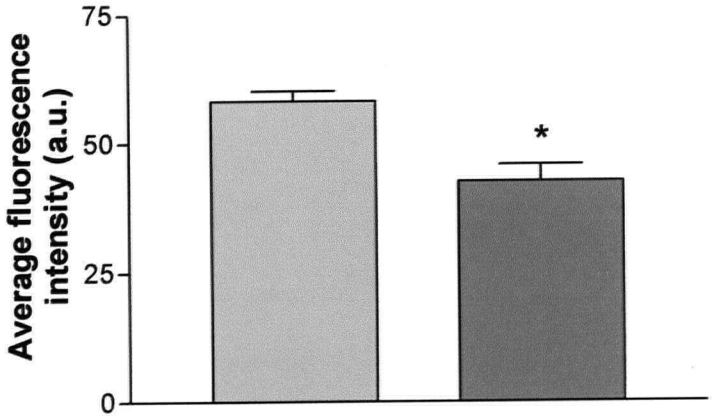

Figure 3.19 Effect of cytochalasin B on 2-NBDG uptake in native ECs.
Uptake of 1 mM 2-NBDG in a Krebs solution containing 4 mM L-glucose in ECs of intact coronary artery in the absence ▭ or in the presence of 10 μM cytochalasin B ▬. Each bar is the average of 31 and 20 cells respectively, from 3 different experiments; * $p<0.0001$.

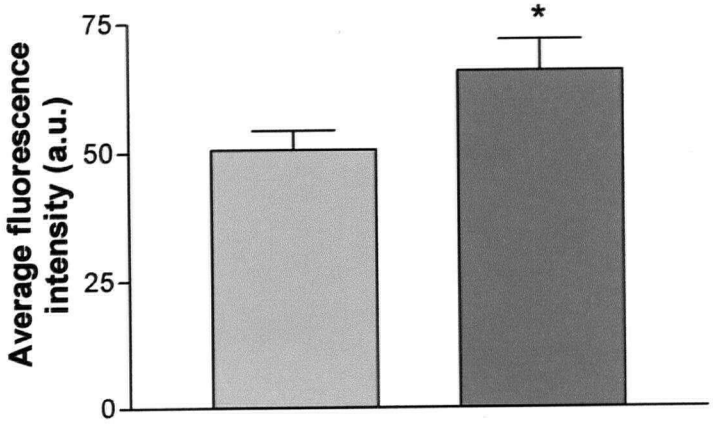

Figure 3.20 Effect of insulin on 2-NBDG uptake in native ECs.
Uptake of 1 mM 2-NBDG in a Krebs solution containing 4 mM L-glucose in ECs of intact coronary artery in the absence ▭ or in the presence of 2.5 μU/ml of insulin ▬. Each bar is the average of 18 and 19 cells respectively, from 2 different experiments; * $p<0.05$.

3.4 Discussion

This study examined the regulation of glucose transport in both cultured and native ECs. We describe for the first time the measurement of glucose uptake in individual cells of an intact microvessel. We first showed the presence and symmetrical distribution of GLUT-1, 2, 3, 4, 5, and SGLT-1 in HCAECs. Secondly, we used the fluorescent glucose analog 2-NBDG to quantify glucose uptake in ECs. While the different variables and technical difficulties were more easily identified in experimentation with cultured cells, measurements in individual cells of an intact vascular wall were also demonstrated. Results from experiments with HCAECs and an intact vessel indicate that coronary artery ECs are insulin-sensitive.

3.4.1 GLUTs and SGLT-1 identification in HCAECs

We used HCAECs at the 4th passage for immunocytochemistry. Previous studies have shown that ECs tend to reduce the expression of GLUT isoforms, other than GLUT-1, when cultured beyond the 4th passage (McCall *et al.*, 1997; Mamchaoui *et al.*, 2002). The HCAECs were fixed when they reached 80% confluence as this type of cell can become irreversibly contact-inhibited and detached from the coverslip if allowed to reach confluence. In this regard, VE-cadherin labelled only neighbouring cell-junctions (Figure 3.3). Most cells showed discontinuous attachments to their neighbours and therefore VE-cadherin labelling also appeared discontinuous (Figure 3.4A, Figure 3.5A, Figure 3.8A and Figure 3.9A). This is in agreement with previous reports that VE-cadherin is expressed only at the intercellular boundaries of confluent monolayers of ECs (Dejana and Plantier, 1996).

We have previously identified GLUT-1, 2, 3, 4, 5, and SGLT-1 in rat coronary artery ECs (see chapter 2). In the present study, we extend these results to the HCAECs. We used the same antibodies (Table 2.2) for which the specificity had been previously well characterised (see chapter 2). As expected, we found a symmetric distribution of each transporter isoform examined. As the ECs in culture tend to lose their characteristics, it is not surprising that the asymmetrical distributions, found previously in rat native coronary endothelium, was missing in HCAECs. It is possible that in a native environment, the blood flow on one side and the interaction of the SMCs on the other side produces an asymmetric distribution. Accordingly, laminar flow has been previously shown to induce polarity of secretion in cultured bovine aortic ECs (Grimm *et al.*, 1988). In addition, the lack of neighbouring cells with which to form tight junctions may represent a key missing element for the development of polarity. Thus, others have shown that a disturbance of the BBB tight junctions was associated with a reduced polarity of GLUT-1 distribution in a model of stroke-prone spontaneous hypertensive rat (Lippoldt *et al.*, 2000).

In rat coronary artery ECs we have found a distinct tendency of the transporters to localise at the cell-to-cell junctions. This subcellular organisation was not observed in HCAECs. Transporters did not concentrate at the boundary of either confluent or non-confluent cells, and this may also be linked to the loss of polarity of the HCAECs in culture.

Each transporter isoform was located all around the periphery of the ECs, presumably on the cell membrane and in the cytosol of the cell, potentially in vesicles, being recycled, or in the process of translocation to or from the plasma

membrane. In certain cases, such as shown with GLUT-2 (Figure 3.5D) and GLUT-4 (Figure 3.7D), the transporters were located in the nuclear area. As this labelling tends to coincide with deep holes in the nucleus, we consider these transporters to be located between the deep folds of the nuclear envelope and the plasmalemma (Fricker *et al.*, 1997). This morphology is typical for an EC's nucleus (Woolf, 1982).

3.4.2 2-NBDG uptake in HCAECs

In this study, concentrations of 2-NBDG ranging from 0.1 to 3 mM were tested in HCAECs. The uptake was linear for a minimum of 30 min, regardless of the 2-NBDG concentration. The rate of uptake also increased in a concentration dependent manner (Figure 3.12). This indicated that no saturation of 2-NBDG transport was reached during this time and within this range of concentrations.

The rate of uptake of the 6-NBDG was 35% higher than the rate of uptake of 2-NBDG. Significant differences in the accumulation of 2-NBDG and 6-NBDG occurred after 20 min of exposure to each of the fluorescent glucose analogs. As the 6-NBDG is not phosphorylated, it can be transported out of the cell. Conversely, 2-NBDG is phosphorylated by hexokinase, and is trapped in the cell. Therefore, a faster accumulation of 2-NBDG was expected.

One explanation for this discrepancy could be that phosphorylation, in HCAECs inhibits glucose uptake. This has been previously observed in ECs exposed to elevated glucose concentrations (Vinals *et al.*, 1999). It is also possible that the transporters have different affinities for 2-NBDG and 6-NBDG. Loaiza et

al. have measured the rate of uptake of both 2-NBDG and 6-NBDG in cultures of astrocytes in a near zero-trans entry condition (Loaiza *et al.*, 2003); meaning that the initial intracellular glucose concentration was minimal and therefore what was measured from this rate of uptake is the sugar binding affinity with negligible effects of the phosphorylation step (Gould and Seatter, 1997). The rate of uptake of 2-NBDG was shown to be about 60% slower than that of 6-NBDG in these astrocytes. In the present study, lower concentrations than that used in astrocytes, for both 2-NBDG and 6-NBDG were used (0.1mM vs 0.3 mM). Thus, the difference in the rate of uptake between 2-NBDG and 6-NBDG in HCAECs is more likely attributable to a difference in affinity for the binding site of the glucose transporters between the two glucose analogs than an inhibitory effect on the part of the hexokinase. One last possibility, as reported previously in E. Coli (Yoshioka *et al.*, 1996b), is that following its phosphorylation, 2-NBDG is further metabolised into a non-fluorescent compound. This transformation however was not reported in studies in mammalian cells (Lloyd *et al.*, 1999; Yamada *et al.*, 2000; Roman *et al.*, 2001). From these observations, a concentration of 1 mM 2-NBDG and a maximal time of incubation of 20 min, were selected for further experiments.

3.4.3 Inhibitory effect of D-glucose and cytochalasin B in HCAECs

The uptake of 2-NBDG was significantly inhibited by both D-glucose and cytochalasin B in HCAECs. This confirmed that the 2-NBDG uptake in ECs occurs through a system of glucose transporters in agreement with previous reports from other cell types (Yoshioka *et al.*, 1996a; Lloyd *et al.*, 1999; Yamada *et al.*, 2000). L-glucose, the stereoisomer of D-glucose is not transported in the cell

and was therefore used in control assays to maintain an equivalent osmotic pressure. Although no statistical differences were found between the 55% inhibition with 4 mM and 75% inhibition with 9 mM, the trend implied a concentration dependent inhibition by D-glucose on the uptake rate of 2-NBDG, as previously described by others (Yoshioka *et al.*, 1996a).

The inhibitory effect of cytochalasin B, although well documented in other glucose transport assays, was very difficult to demonstrate with a fluorescent glucose analog and confocal microscopy. Cytochalasin B depolymerises F actin and consequently changes the cell shape (Iglic *et al.*, 2001; Pedersen *et al.*, 2001). This cell shape change can increase or decrease the fluorescence intensity independently of the accumulated 2-NBDG. The period of incubation with Cytochalasin B was therefore reduced to 15 min. Cells whose shapes were significantly affected by cytochalasin B treatment even with this shorter period of incubation were not imaged and/or considered for analysis.

3.4.4 Effect of insulin in HCAECs

We observed a significant increase of 64% in 2-NBDG uptake in the presence of 2.5 μU/ml of insulin in HCAECs. These results reflect the functionality of GLUT-4 in HCAECs. Other studies have also reported insulin sensitivity of the vascular endothelium (Gerritsen and Burke, 1985; Vinters *et al.*, 1985; Allen and Gerritsen, 1986; Kwok *et al.*, 1989; Abe *et al.*, 1990) and the presence of GLUT-4 in ECs of various microvascular beds (Frank and Pardridge, 1981; King *et al.*, 1983; Vilaro *et al.*, 1989; McCall *et al.*, 1997), still, this is not generally accepted, and remains highly controversial.

Other studies have reported in other vascular beds, mostly of greater calibre but also in BBB, that ECs are not sensitive to insulin (Corkey *et al.*, 1981; Betz *et al.*, 1983; Drewes *et al.*, 1988; Takakura *et al.*, 1991; Thomas *et al.*, 1995). The present results may therefore not be extended to all vascular endothelia. On the other hand as we report insulin sensitivity in both human and rat coronary artery and since others have previously described similar responses in rabbit coronary artery ECs (Gerritsen and Burke, 1985; Gerritsen *et al.*, 1988), it is likely that ECs from coronary arteries of most other species are responsive to insulin and express GLUT-4.

In the present study, 2.5 μU/ml insulin produced a greater increase in 2-NBDG uptake in HCAECs pre-incubated and exposed to a Krebs solution containing L-glucose than in HCAECs pre-incubated and exposed to a Krebs solution containing D-glucose (Figure 3.15). This is in agreement with previous observations, by Gerritson at al., that glucose deprivation enhances the effect of insulin on 2DG uptake in coronary microvessel ECs (Gerritsen *et al.*, 1988). Although, this previous study found that glucose deprivation was necessary to obtain a significant effect of insulin, we found a lower but still significant effect of insulin in HCAECs pre-incubated in D-glucose. This discrepancy may be explained by the longer exposure to both insulin and 2-NBDG (30 min) in the present study compared to the previous one (6 min uptake of radiolabeled 2DG). Since coronary ECs accumulate unphosphorylated (between 30-60%) 2DG, it has been suggested that the limiting step for glucose uptake in ECs is not glucose transport but glucose phosphorylation (Betz *et al.*, 1983; Gerritsen *et al.*, 1988). This may potentially explain the increased sensitivity of insulin in ECs previously deprived of glucose. ECs pre-incubated with D-glucose, especially in

the presence of insulin, are likely to experience a lower phosphorylation rate for any subsequent transported labelled 2DG, due to saturation of hexokinase. The consequent increased in intracellular unphosphorylated labelled 2DG may increase its transport out of the cell or inhibit its entry. On the other hand, in cells deprived of glucose, the labelled 2DG is not facing competition for hexokinase, and a faster rate of phosphorylation increases its accumulation. Taken together, this may explain in part, the lack of insulin effect observed by other studies performed in ECs of larger vessels and certain microvessels.

3.4.5 2-NBDG uptake in native EC

The recording of 2-NBDG uptake in ECs of an intact, perfused, vessel was demonstrated in this study. As a distance of approximately 16 μm separates the ECs from the SMCs in the wall of a rat coronary artery, the respective intracellular fluorescence was easily distinguished and separated from one another with the 20X objective.

The subcellular localisation of 2-NBDG in an intact coronary artery was found most prominently at the periphery of the ECs. The cytosol of native ECs is mainly occupied by the nucleus, this may explain in part the peripheral accumulation of 2-NBDG. In addition, the subcellular accumulation of 2-NBDG co-localizes with the prevalent distribution of GLUT isoforms at the cell-to-cell junction of ECs (see Chapter 2). Such compartmentalised organisation may serve a purpose. ECs accumulate free (non-phosphorylated) 2DG even in the presence of physiological concentrations of glucose (Betz *et al.*, 1983; Gerritsen *et al.*, 1988), non-phosphorylated glucose can be transported out of the cells. Taken together,

the accumulation of 2-NBDG at the periphery of the cells where the cytosol is at its thinnest, with the high prevalence of glucose transporters in the same subcellular area and the possibility that this 2-NBDG is mostly free, suggests the involvement of transcellular transport of glucose from the blood to the interstitium of the vascular wall. Further experiments are needed to test this possibility, but the implications of such a process may explain to some extent the high susceptibility of ECs to glucose toxicity.

Then again, in the ECs of the intact vessel, the uptake of 1 mM 2-NBDG remained linear for a minimum of 20 min and began to level off after 30 min of exposure to the 2-NBDG, contrary to the linear uptake of 1 mM 2-NBDG observed in HCAECs. This may, on the one hand, represent a saturation of the transporters. On the other hand, looking back at the differences in the distribution of the GLUTs and SGLT observed between HCAECs and ECs of an intact coronary artery, this may be a reflection of transcellular transport of glucose. As suggested by the asymmetric distribution of the transporters, which are higher in numbers on the abluminal side in native ECs (see chapter 2), an accumulation of non-phosphorylated 2-NBDG in a narrow cytosolic space is likely to produce a driving force for its extrusion on the abluminal side of the ECs.

3.4.6 Inhibitory effect of D-glucose and cytochalasin B in native EC

The uptake of 2-NBDG was also significantly inhibited by both D-glucose and cytochalasin B in native ECs. This confirmed that the 2-NBDG uptake in ECs of an intact vascular wall also occurs through a system of glucose transporters in

agreement with previous observations in cultured HCAECs. In comparison to the effect produced in the HCAECs, cytochalasin B did not change noticeably the shape of the native ECs. The environment of the intact vessel could have made such change in EC's shape difficult to observe. It is also possible that the surrounding environment has compensated for this effect and provided scaffolding for the ECs deprived of an intact cytoskeleton.

3.4.7 Effect of insulin in native EC

An increase of 23% in 2-NBDG uptake was observed in the presence of 2.5 μU/ml of insulin in ECs of an intact vessel. These results confirm previous observations in HCAECs and reflect the functionality of GLUT-4 also identified in ECs of intact rat coronary artery (see Chapter 2).

3.4.8 Difference in responses between HCAECs and native ECs

The same response to D-glucose, cytochalasin B and insulin were observed in both HCAECs and native ECs, although in average, a 10% lower inhibitory response and a 40 % lower stimulating response were observed in native ECs. These lower responses in native ECs, may be related to a reduced sensitivity and/or increased signal to noise ratio of the system. This may be accounted for by the increased light diffraction from the other cell layers and components of the vascular wall. It may also be due to the further distance from the coverslip at which the ECs of the vascular wall were imaged in comparison to that of the HCAECs directly apposed to the coverslip. This lower effect may also be attributed to distinctions between culture and native cells and/or to differences between rat and human tissue.

On the other hand, the 40% lower uptake rate stimulated by insulin in native ECs compared to cultured HCAECs may be explained by an increased transcellular transport of glucose in presence of insulin. In accordance, we have found previously a higher distribution of GLUT-4 on the abluminal side of native ECs. As glucose is taken up from the blood on the luminal side, a translocation of GLUT-4 to the abluminal plasma membrane mediated by insulin would stimulate mainly transport of glucose out of the cell in the interstitial space between ECs and SMCs. This glucose could then be used to feed the SMCs of the vascular wall.

Interestingly, GLUT-4 was downregulated in native ECs submitted to chronic hyperglycaemia and hypoinsulinaemia (see Chapter 2). This down-regulation of GLUT-4 was also accompanied with a significant reduction in the ratio of abluminal to luminal GLUT-4. It is therefore possible that transcellular transport of glucose mediated by insulin is reduced in diabetes.

Since coronary vascular diseases are strongly associated with diabetes and ECs are highly susceptible to glucose toxicity, it is of great importance to consider the implications of insulin therapies on the accumulation of intracellular glucose in vascular ECs. Further studies in this regard will need to be pursued in order to determine the impact of insulin on the regulation of glucose uptake by the endothelium of diabetic patients, and determine if insulin treatment restores this potential transcellular transport of glucose or if it increases intracellular glucose uptake in native ECs.

Epilogue

The clear association between glucose toxicity in ECs and an increased prevalence of cardiovascular diseases in the diabetic population has motivated this research, the question of interest being: how and why glucose accumulates in EC. The difficulty of harvesting and culturing ECs without losing most of their morphological and behavioural characteristics has been a major obstacle in endothelial research. Therefore, the ultimate goal of the present study was to use an experimental design and protocol that preserved the native environment of the ECs and their close structural relationship with the SMCs.

Initial research, on the myogenic tone of small contractile arteries conducted in Dr. Laher's laboratory, has greatly influenced the approach and means employed to measure, in real time, glucose uptake in individual ECs of an intact vascular wall. In addition, the development of a fluorescent glucose analog provided a good tool for studying glucose uptake in individual cells in their native environment. The specific aims and hypothesis of this study were also formulated with regards to previous findings from immunohistochemistry work, which identified six different sugar transporter isoforms in ECs of intact coronary arteries.

While measurements of 2-NBDG uptake were successfully achieved in both cultured and native ECs, due to time constraints and the difficult nature of these experiments, several interesting questions and hypotheses have not yet been addressed or tested. In addition, unexpected limitations of this

experimental approach were encountered and often made it difficult to quantify measurements of glucose uptake in live cells. The following is a discussion of unexplored avenues and hypotheses that could potentially be tested with the experimental setting presented in chapter 3.

One of the aims for developing this methodology was to measure 2-NBDG uptake in ECs and SMCs in the same vessel, at the same time. In the first attempt, a continuous perfusion of 2-NBDG and an image acquisition every minute from four different focal planes representing the lumen, ECs, SMCs, and the coverslip, was done. No washing steps were included prior to the image acquisition for the entire period (30 min) of perfusion with 2-NBDG. The fluorescence recorded from the EC and SMC layers increased over time, reached a plateau phase and decreased at a similar rate during the subsequent washing period. To our astonishment, the addition of D-glucose or cytochalasin B increased the fluorescence intensity of each layer. These observations made us suspect that a non-negligible amount of 2-NBDG was possibly in the interstitial space, surrounding the cells or trapped between the EC and SMC layers. Following this observation, a more cautious and systematic approach was used. A washing step was included after each period of incubation with the 2-NBDG prior to the image acquisition and we focused on the EC layer as a priority. Nevertheless, these observations possibly constitute evidence for the transcellular transport of glucose in ECs of small contractile arteries. A first piece of evidence is the report, in a previous study, that non-phosphorylated cytosolic 2DG is present in ECs at a physiological glucose concentration (Betz *et al.*, 1983). This means that intracellular accumulated glucose can be transported out of the ECs. An additional piece of evidence comes from our studies showing asymmetric

distribution of the GLUTs and SGLT-1 in ECs of intact arteries and a concentration of the transporter at the edge of the cell-to-cell junction where the cell thickness is minimal. One way to examine this possibility would be to use simultaneously a fluorescent L-glucose analog (not-transported by the GLUTs and SGLTs) with the 2-NBDG to measure and compare how much glucose penetrates the vascular wall through paracellular transport and through transcellular transport. Talks with The Molecular Probes Co. about the possibility of synthesising such a compound were undertaken but had to be terminated, as the chemical required for the synthesis of a fluorescent analog of L-glucose, L-glucosamine, was unavailable at that time.

One of the most important findings of this work is that coronary ECs are insulin-sensitive. For a long time, this possibility was ignored due to conflicting reports in various cultured cell lines and preparations. We provided evidence for the presence of GLUT-4 in both ECs of intact rat coronary artery and in culture from human coronary artery. In addition, we showed that in both preparations, insulin stimulates the uptake of the fluorescent glucose analog 2-NBDG. Because of the importance of these results and the current controversial status of insulin sensitivity of the endothelium, additional experiments were initiated to further demonstrate that the increase in 2-NBDG observed following insulin stimulation was indeed a reflection of GLUT-4 translocation to the plasma membrane. Insulin increases glucose uptake through the translocation of GLUT-4 via a signalling pathway mediated by PI3-kinase, 3-phosphoinositide-dependent kinase-1 (PDK-1) and protein kinase B (PKB) (Khan and Pessin, 2002). Wortmannin, a PI3-kinase inhibitor, has been previously shown to inhibit both GLUT-4 translocation and glucose uptake (Yu *et al.*, 1999). Wortmannin was

therefore used to test the participation of GLUT-4 in the insulin response observed in ECs. Our results from these studies were inconclusive due to other unexpected effects of wortmannin on the cell shape. HCAECs changed shape; they shrank and retracted from each other, when incubated with wortmannin. This change increased the axial thickness of the cell and therefore produced an increase in fluorescence intensity unrelated to glucose uptake. PI3-kinase has been shown to play a significant role in the regulation of cell volume, an effect shown to be inhibited by both wortmannin and an independent IP_3-kinase inhibitor, LY294002 (Feranchak *et al.*, 1998). Thus, in this experimental setting, where a stable cell shape is required for accurate quantification of the fluorescence, a compound like wortmannin cannot be used. A good alternative to wortmannin may potentially be indinavir, an HIV protease inhibitor. Indinavir has been shown to directly and specifically inhibit GLUT-4 translocation without any effects on intracellular signalling (Murata *et al.*, 2000).

GLUT-2 was found to be expressed in both rat intact coronary artery endothelium and human coronary cultured ECs. Its functionality was tested in preliminary experiments with both an activator and an inhibitor of PKC, presented in Appendix 5. The inhibition of PKC, but not its activation, produced an effect on 2-NBDG uptake in the presence of 20 mM D-glucose. As Calpostin C inhibits all PKC isoforms, which could contribute to the inhibition of GLUT-4 translocation, it would therefore be preferable to use a specific inhibitor of the PKC_β isoform, shown previously to be specific to GLUT-2 translocation signalling (Helliwell *et al.*, 2003). In addition, other activators of PKC such as phorbol ester could be used at basal glucose concentrations (Drewes *et al.*, 1988).

Although GLUT-5 was identified in both rat and human coronary ECs, the functionality of this transporter was not assessed. At the time of the study, a fluorescent fructose analog was not available. The synthesis of such a compound would enable the observation and quantification of fructose uptake in individual ECs and SMCs of an intact vascular wall.

SGLT-1 was also identified in both rat and human ECs. Its functionality has been investigated at a basal glucose concentration with the specific inhibitor phloridzin in HCAECs (Appendix 5). No effects on the uptake of 2-NBDG were observed. As previously reported, SGLT activity is enhanced by hypoglycaemic and hypoxic conditions. It would therefore be worthwhile to test the effect of phloridzin under these conditions in ECs. In addition, changes in ambient Na^+ concentration may potentially activate SGLT-1 and should therefore be tested in coronary ECs.

Finally, important changes in the expression of the glucose transporters of the rat coronary artery ECs were observed with long-term diabetes. It would be of great interest to determine the impact of these changes induced by diabetes, on ECs glucose uptake. The synthesis of a fluorescent L-glucose analog could also permit, if used simultaneously with the 2-NBDG, testing the possibility of an interstitial accumulation of 2-NBDG glucose due to a slower rate of uptake from the SMCs and/or to the increased ECs transcellular and/or paracellular transport of 2-NBDG in hyperglycaemic conditions. The role of GLUT-2 upregulation in diabetes is also of particular interest and may potentially be addressed with the use of a PKC_β-specific inhibitor in diabetic animals. All of these avenues

represent potential future directions to be pursued with the measurements of glucose uptake in a live vessel preparation.

References

Abdel-Hamid, K. M. and Baimbridge, K. G.: The effects of artificial calcium buffers on calcium responses and glutamate-mediated excitotoxicity in cultured hippocampal neurons. Neuroscience, 81, (3): *673-87*, 1997.

Abe, M., Ono, J., Sato, Y., Okeda, T. and Takaki, R.: Effects of glucose and insulin on cultured human microvascular endothelial cells. Diabetes Res Clin Pract, 9, (3): *287-95*, 1990.

Abordo, E. A., Westwood, M. E. and Thornalley, P. J.: Synthesis and secretion of macrophage colony stimulating factor by mature human monocytes and human monocytic THP-1 cells induced by human serum albumin derivatives modified with methylglyoxal and glucose-derived advanced glycation endproducts. Immunol Lett, 53, (1): *7-13*, 1996.

Alemany, R., Kleuser, B., Ruwisch, L., Danneberg, K., Lass, H., Hashemi, R., Spiegel, S., Jakobs, K. H. and Meyer zu Heringdorf, D.: Depolarisation induces rapid and transient formation of intracellular sphingosine-1-phosphate. FEBS Lett, 509, (2): *239-44*, 2001.

Allen, B. G. and Walsh, M. P.: The biochemical basis of the regulation of smooth-muscle contraction. Trends Biochem Sci, 19, (9): *362-8*, 1994.

Allen, L. A. and Gerritsen, M. E.: Regulation of hexose transport in cultured bovine retinal microvessel endothelium by insulin. Exp Eye Res, 43, (4): *679-86*, 1986.

Allen, T. J. and Hardin, C. D.: Influence of glycogen storage on vascular smooth muscle metabolism. Am J Physiol Heart Circ Physiol, 278, (6): *H1993-2002*, 2000.

Alpert, E., Gruzman, A., Totary, H., Kaiser, N., Reich, R. and Sasson, S.: A natural protective mechanism against hyperglycaemia in vascular endothelial and smooth-muscle cells: role of glucose and 12-hydroxyeicosatetraenoic acid. Biochem J, 362, (Pt 2): *413-22*, 2002.

Andrea, J. E. and Walsh, M. P.: Protein kinase C of smooth muscle. Hypertension, 20, (5): *585-95*, 1992.

Anonymous: The relationship of glycemic exposure (HbA1c) to the risk of development and progression of retinopathy in the diabetes control and complications trial. Diabetes, 44, (8): *968-83*, 1995.

Anonymous: Intensive blood-glucose control with sulphonylureas or insulin compared with conventional treatment and risk of complications in patients with type 2 diabetes (UKPDS 33). UK Prospective Diabetes Study (UKPDS) Group [published erratum appears in Lancet 1999 Aug 14;354(9178):602] [see comments]. Lancet, 352, (9131): *837-53*, 1998.

Anonymous: Diabetes mellitus: a major risk factor for cardiovascular disease. A joint editorial statement by the American Diabetes Association; The National Heart, Lung, and Blood Institute; The Juvenile Diabetes Foundation International; The National Institute of Diabetes and Digestive and Kidney Diseases; and The American Heart Association. Circulation, 100, (10): *1132-3*, 1999.

Appleman, J. R. and Lienhard, G. E.: Kinetics of the purified glucose transporter. Direct measurement of the rates of interconversion of transporter conformers. Biochemistry, 28, (20): *8221-7*, 1989.

Araki, S., Ito, M., Kureishi, Y., Feng, J., Machida, H., Isaka, N., Amano, M., Kaibuchi, K., Hartshorne, D. J. and Nakano, T.: Arachidonic acid-induced Ca^{2+} sensitization of smooth muscle contraction through activation of Rho-kinase. Pflugers Arch, 441, (5): *596-603*, 2001.

Aronson, D. and Rayfield, E. J.: How hyperglycemia promotes atherosclerosis: molecular mechanisms. Cardiovasc Diabetol, 1, (1): *1.*, 2002.

Ar'Rajab, A. and Ahren, B.: Long-term diabetogenic effect of streptozotocin in rats. Pancreas, 8, (1): *50-7*, 1993.

Asada, T., Takakura, S., Ogawa, T., Iwai, M. and Kobayashi, M.: Overexpression of glucose transporter protein 5 in sciatic nerve of streptozotocin-induced diabetic rats. Neurosci Lett, 252, (2): *111-4*, 1998.

Atkins, K. B., Johns, D., Watts, S., Clinton Webb, R. and Brosius, F. C., 3rd: Decreased vascular glucose transporter expression and glucose uptake in DOCA-salt hypertension. J Hypertens, 19, (9): *1581-7*, 2001.

Badimon, L., Badimon, J. J., Penny, W., Webster, M. W., Chesebro, J. H. and Fuster, V.: Endothelium and atherosclerosis. J Hypertens, 10, (2): *S43-50*, 1992.

Bakker, E. N., Kerkhof, C. J. and Sipkema, P.: Signal transduction in spontaneous myogenic tone in isolated arterioles from rat skeletal muscle. Cardiovasc Res, 41, (1): *229-36.*, 1999.

Ball, S. W., Bailey, J. R., Stewart, J. M., Vogels, C. M. and Westcott, S. A.: A fluorescent compound for glucose uptake measurements in isolated rat cardiomyocytes. Can J Physiol Pharmacol, 80, (3): *205-9*, 2002.

Banting, F. G. and Best, C. H.: Pancreatic extracts. 1922. J Lab Clin Med, 115, (2): *254-72*, 1990.

Banz, W. J., Abel, M. A. and Zemel, M. B.: Insulin regulation of vascular smooth muscle glucose transport in insulin-sensitive and resistant rats. Horm Metab Res, 28, (6): *271-5*, 1996.

Bar, R. S., Booth, B. A., Boes, M. and Dake, B. L.: Insulin-like growth factor-binding proteins from vascular endothelial cells: purification, characterization, and intrinsic biological activities. Endocrinology, 125, (4): *1910-20*, 1989.

Bar, R. S., Siddle, K., Dolash, S., Boes, M. and Dake, B.: Actions of insulin and insulinlike growth factors I and II in cultured microvessel endothelial cells from bovine adipose tissue. Metabolism, 37, (8): *714-20*, 1988.

Barrett, M. P., Walmsley, A. R. and Gould, G. W.: Structure and function of facilitative sugar transporters. Curr Opin Cell Biol, 11, (4): *496-502.*, 1999.

Barrett-Connor, E. L., Cohn, B. A., Wingard, D. L. and Edelstein, S. L.: Why is diabetes mellitus a stronger risk factor for fatal ischemic heart disease in women than in men? The Rancho Bernardo Study. Jama, 265, (5): *627-31*, 1991.

Barron, J. T., Barany, M., Gu, L. and Parrillo, J. E.: Metabolic fate of glucose in vascular smooth muscle during contraction induced by norepinephrine. J Mol Cell Cardiol, 30, (3): *709-19*, 1998.

Bayliss, W. M.: On the local reactions of the arterial wall to changes in internal pressure. J Physiol, 28: *220-231*, 1902.

Beckman, J. A., Goldfine, A. B., Gordon, M. B., Garrett, L. A. and Creager, M. A.: Inhibition of protein kinase C-beta prevents impaired endothelium-dependent vasodilation caused by hyperglycemia in humans. Circ Res, 90, (1): *107-11*, 2002.

Bell, G. I., Burant, C. F., Takeda, J. and Gould, G. W.: Structure and function of mammalian facilitative sugar transporters. J Biol Chem, 268, (26): *19161-4*, 1993.

Betz, A. L., Bowman, P. D. and Goldstein, G. W.: Hexose transport in microvascular endothelial cells cultured from bovine retina. Exp Eye Res, 36, (2): *269-77*, 1983.

Blakemore, S. J., Aledo, J. C., James, J., Campbell, F. C., Lucocq, J. M. and Hundal, H. S.: The GLUT5 hexose transporter is also localized to the basolateral membrane of the human jejunum. Biochem J, 309, (Pt 1): *7-12.*, 1995.

Bolz, S., Farrell, C. L., Dietz, K. and Wolburg, H.: Subcellular distribution of glucose transporter (GLUT-1) during development of the blood-brain barrier in rats. Cell Tissue Res, 284, (3): *355-65*, 1996.

Bolz, S. S., Vogel, L., Sollinger, D., Derwand, R., Boer, C., Pitson, S. M., Spiegel, S. and Pohl, U.: Sphingosine kinase modulates microvascular tone and myogenic responses through activation of RhoA/Rho kinase. Circulation, 108, (3): *342-7*, 2003.

Brayden, J. E. and Nelson, M. T.: Regulation of arterial tone by activation of calcium-dependent potassium channels. Science, 256, (5056): *532-5*, 1992.

Brenner, R., Perez, G. J., Bonev, A. D., Eckman, D. M., Kosek, J. C., Wiler, S. W., Patterson, A. J., Nelson, M. T. and Aldrich, R. W.: Vasoregulation by the beta1 subunit of the calcium-activated potassium channel. Nature, 407, (6806): *870-6*, 2000.

Brolin, S. E. and Naeser, P.: Sorbitol in aortic endothelium of diabetic rats. Diabetes Res, 8, (2): *59-61*, 1988.

Brosnan, J. T.: Comments on metabolic needs for glucose and the role of gluconeogenesis. Eur J Clin Nutr, 53 Suppl 1: *S107-11*, 1999.

Brownlee, M.: Glycation products and the pathogenesis of diabetic complications. Diabetes Care, 15, (12): *1835-43*, 1992.

Brownlee, M.: Biochemistry and molecular cell biology of diabetic complications. Nature, 414, (6865): *813-20.*, 2001.

Brownlee, M., Cerami, A. and Vlassara, H.: Advanced glycosylation end products in tissue and the biochemical basis of diabetic complications. N Engl J Med, 318, (20): *1315-21*, 1988.

Brownlee, M., Vlassara, H. and Cerami, A.: Nonenzymatic glycosylation products on collagen covalently trap low-density lipoprotein. Diabetes, 34, (9): *938-41*, 1985.

Bunn, R. C., Jensen, M. A. and Reed, B. C.: Protein interactions with the glucose transporter binding protein GLUT1CBP that provide a link between GLUT1 and the cytoskeleton. Mol Biol Cell, 10, (4): *819-32*, 1999.

Burant, C. F. and Bell, G. I.: Mammalian facilitative glucose transporters: evidence for similar substrate recognition sites in functionally monomeric proteins. Biochemistry, 31, (42): *10414-20*, 1992.

Burant, C. F., Takeda, J., Brot-Laroche, E., Bell, G. I. and Davidson, N. O.: Fructose transporter in human spermatozoa and small intestine is GLUT5. J Biol Chem, 267, (21): *14523-6*, 1992.

Burchell, A.: A re-evaluation of GLUT 7 [letter]. Biochem J, 331, (Pt 3): *973*, 1998.

Burg, M. B. and Kador, P. F.: Sorbitol, osmoregulation, and the complications of diabetes. J Clin Invest, 81, (3): *635-40*, 1988.

Burkart, V., Wang, Z. Q., Radons, J., Heller, B., Herceg, Z., Stingl, L., Wagner, E. F. and Kolb, H.: Mice lacking the poly(ADP-ribose) polymerase gene are resistant to pancreatic beta-cell destruction and diabetes development induced by streptozocin. Nat Med, 5, (3): *314-9*, 1999.

Carayannopoulos, M. O., Chi, M. M., Cui, Y., Pingsterhaus, J. M., McKnight, R. A., Mueckler, M., Devaskar, S. U. and Moley, K. H.: GLUT8 is a glucose transporter responsible for insulin-stimulated glucose uptake in the blastocyst. Proc Natl Acad Sci U S A, 97, (13): *7313-8*, 2000.

Carrington, W. A., Forgarty, K. E. and Fay, F. S.: The handbook of biological confocal microscopy. New York, 1989.

Carrington, W. A., Lynch, R. M., Moore, E. D., Isenberg, G., Fogarty, K. E. and Fay, F. S.: Superresolution three-dimensional images of fluorescence in cells with minimal light exposure. Science, 268, (5216): *1483-7*, 1995.

Casteels, R., Kitamura, K., Kuriyama, H. and Suzuki, H.: Excitation-contraction coupling in the smooth muscle cells of the rabbit main pulmonary artery. J Physiol, 271, (1): *63-79*, 1977.

Cerami, A., Vlassara, H. and Brownlee, M.: Role of advanced glycosylation products in complications of diabetes. Diabetes Care, 11, (Suppl 1): *73-9*, 1988.

Charron, M. J., Brosius, F. C. d., Alper, S. L. and Lodish, H. F.: A glucose transport protein expressed predominately in insulin-responsive tissues. Proc Natl Acad Sci U S A, 86, (8): *2535-9*, 1989.

Chikumi, H., Vazquez-Prado, J., Servitja, J. M., Miyazaki, H. and Gutkind, J. S.: Potent activation of RhoA by Galpha q and Gq-coupled receptors. J Biol Chem, 277, (30): *27130-4*, 2002.

Cobbold, P. H. and Rink, T. J.: Fluorescence and bioluminescence measurement of cytoplasmic free calcium. Biochem J, 248, (2): *313-28*, 1987.

Concha, II, Velasquez, F. V., Martinez, J. M., Angulo, C., Droppelmann, A., Reyes, A. M., Slebe, J. C., Vera, J. C. and Golde, D. W.: Human erythrocytes express GLUT5 and transport fructose. Blood, 89, (11): *4190-5.*, 1997.

Corkey, R. F., Corkey, B. E. and Gimbrone, M. A., Jr.: Hexose transport in normal and SV40-transformed human endothelial cells in culture. J Cell Physiol, 106, (3): *425-34*, 1981.

Cornford, E. M., Hyman, S., Black, K. L., Cornford, M. E., Vinters, H. V. and Pardridge, W. M.: High expression of the Glut1 glucose transporter in human brain hemangioblastoma endothelium. J Neuropathol Exp Neurol, 54, (6): *842-51*, 1995.

Cornford, E. M., Hyman, S., Cornford, M. E., Damian, R. T. and Raleigh, M. J.: A single glucose transporter configuration in normal primate brain endothelium: comparison with resected human brain. J Neuropathol Exp Neurol, 57, (7): *699-713*, 1998a.

Cornford, E. M., Hyman, S., Cornford, M. E., Landaw, E. M. and Delgado-Escueta, A. V.: Interictal seizure resections show two configurations of endothelial Glut1 glucose transporter in the human blood-brain barrier. J Cereb Blood Flow Metab, 18, (1): *26-42*, 1998b.

Corpe, C. P., Basaleh, M. M., Affleck, J., Gould, G., Jess, T. J. and Kellett, G. L.: The regulation of GLUT5 and GLUT2 activity in the adaptation of intestinal brush-border fructose transport in diabetes. Pflugers Arch, 432, (2): *192-201*, 1996.

Cosentino, F. and Luscher, T. F.: Endothelial dysfunction in diabetes mellitus. J Cardiovasc Pharmacol, 32, (Suppl 3): *S54-61.*, 1998.

Crane, R. K.: Intestinal absorption of sugars. Physiol Rev, 40: *789-825*, 1960.

Culic, O., Decking, U. K. and Schrader, J.: Metabolic adaptation of endothelial cells to substrate deprivation. Am J Physiol Cell Physiol, 276, (5 Pt 1): *C1061-8*, 1999.

D'Angelo, G., Davis, M. J. and Meininger, G. A.: Calcium and mechanotransduction of the myogenic response. Am J Physiol Heart Circ Physiol, 273, (1 Pt 2): *H175-82.*, 1997a.

D'Angelo, G., Mogford, J. E., Davis, G. E., Davis, M. J. and Meininger, G. A.: Integrin-mediated reduction in vascular smooth muscle $[Ca^{2+}]_i$ induced by RGD-containing peptide. Am J Physiol Heart Circ Physiol, 272, (4 Pt 2): *H2065-70*, 1997b.

Davis, M. J.: Myogenic response gradient in an arteriolar network. Am J Physiol Heart Circ Physiol, 264, (6 Pt 2): *H2168-79*, 1993.

Davis, M. J., Donovitz, J. A. and Hood, J. D.: Stretch-activated single-channel and whole cell currents in vascular smooth muscle cells. Am J Physiol Heart Circ Physiol, 262, (4 Pt 1): *C1083-8*, 1992.

Davis, M. J. and Hill, M. A.: Signaling mechanisms underlying the vascular myogenic response. Physiol Rev, 79, (2): *387-423*, 1999.

Davis, M. J., Wu, X., Nurkiewicz, T. R., Kawasaki, J., Davis, G. E., Hill, M. A. and Meininger, G. A.: Integrins and mechanotransduction of the vascular myogenic response. Am J Physiol Heart Circ Physiol, 280, (4): *H1427-33*, 2001.

Dawson, P. A., Mychaleckyj, J. C., Fossey, S. C., Mihic, S. J., Craddock, A. L. and Bowden, D. W.: Sequence and functional analysis of GLUT10: a glucose transporter in the Type 2 diabetes-linked region of chromosome 20q12-13.1. Mol Genet Metab, 74, (1-2): *186-99*, 2001.

DeBosch, B. J., Baur, E., Deo, B. K., Hiraoka, M. and Kumagai, A. K.: Effects of insulin-like growth factor-1 on retinal endothelial cell glucose transport and proliferation. J Neurochem, 77, (4): *1157-67*, 2001.

DeBosch, B. J., Deo, B. K. and Kumagai, A. K.: Insulin-like growth factor-1 effects on bovine retinal endothelial cell glucose transport: role of MAP kinase. J Neurochem, 81, (4): *728-34*, 2002.

Degenhardt, T. P., Thorpe, S. R. and Baynes, J. W.: Chemical modification of proteins by methylglyoxal. Cell Mol Biol (Noisy-le-grand), 44, (7): *1139-45*, 1998.

Dejana, E. and Plantier, J.-L.: Molecular organization of endothelial cell to cell junctions.; in Vascular Endothelium: responses to injury. *167-171*. New York, 1996.

Dessy, C., Matsuda, N., Hulvershorn, J., Sougnez, C. L., Sellke, F. W. and Morgan, K. G.: Evidence for involvement of the PKC-alpha isoform in myogenic contractions of the coronary microcirculation. Am J Physiol Heart Circ Physiol, 279, (3): *H916-23*, 2000.

Diez-Sampedro, A., Eskandari, S., Wright, E. M. and Hirayama, B. A.: Na^+-to-sugar stoichiometry of SGLT3. Am J Physiol Renal Physiol, 280, (2): *F278-82*, 2001.

Dillon, P. F., Aksoy, M. O., Driska, S. P. and Murphy, R. A.: Myosin phosphorylation and the cross-bridge cycle in arterial smooth muscle. Science, 211, (4481): *495-7*, 1981.

Dobrogowska, D. H. and Vorbrodt, A. W.: Quantitative immunocytochemical study of blood-brain barrier glucose transporter (GLUT-1) in four regions of mouse brain. J Histochem Cytochem, 47, (8): *1021-30*, 1999.

Doege, H., Bocianski, A., Scheepers, A., Axer, H., Eckel, J., Joost, H. G. and Schurmann, A.: Characterization of human glucose transporter (GLUT) 11 (encoded by SLC2A11), a novel sugar-transport facilitator specifically expressed in heart and skeletal muscle. Biochem J, 359, (Pt 2): *443-9*, 2001.

Doi, T., Vlassara, H., Kirstein, M., Yamada, Y., Striker, G. E. and Striker, L. J.: Receptor-specific increase in extracellular matrix production in mouse mesangial cells by advanced glycosylation end products is mediated via platelet-derived growth factor. Proc Natl Acad Sci U S A, 89, (7): *2873-7*, 1992.

Doughty, J. M., Miller, A. L. and Langton, P. D.: Non-specificity of chloride channel blockers in rat cerebral arteries: block of the L-type calcium channel. J Physiol, 507 (Pt 2): *433-9*, 1998.

Drab, M., Verkade, P., Elger, M., Kasper, M., Lohn, M., Lauterbach, B., Menne, J., Lindschau, C., Mende, F., Luft, F. C., Schedl, A., Haller, H. and Kurzchalia, T. V.: Loss of caveolae, vascular dysfunction, and pulmonary defects in caveolin-1 gene-disrupted mice. Science, 293, (5539): *2449-52.*, 2001.

Drewes, L. R., Broderius, M. A. and Gerhart, D. Z.: Phorbol ester stimulates hexose uptake by brain microvessel endothelial cells. Brain Res Bull, 21, (5): *771-6*, 1988.

Droogmans, G., Raeymaekers, L. and Casteels, R.: Electro- and pharmacomechanical coupling in the smooth muscle cells of the rabbit ear artery. J Gen Physiol, 70, (2): *129-48*, 1977.

Du, X. L., Edelstein, D., Rossetti, L., Fantus, I. G., Goldberg, H., Ziyadeh, F., Wu, J. and Brownlee, M.: Hyperglycemia-induced mitochondrial superoxide overproduction activates the hexosamine pathway and induces plasminogen activator inhibitor-1 expression by increasing Sp1 glycosylation. Proc Natl Acad Sci U S A, 97, (22): *12222-6*, 2000.

Ebara, T., Conde, K., Kako, Y., Liu, Y., Xu, Y., Ramakrishnan, R., Goldberg, I. J. and Shachter, N. S.: Delayed catabolism of apoB-48 lipoproteins due to decreased heparan sulfate proteoglycan production in diabetic mice. J Clin Invest, 105, (12): *1807-18*, 2000.

Elfeber, K., Kohler, A., Lutzenburg, M., Osswald, C., Galla, H. J., Witte, O. W. and Koepsell, H.: Localization of the Na^+-D-glucose cotransporter SGLT1 in the blood-brain barrier. Histochem Cell Biol, 121, (3): *201-7*, 2004a.

Elfeber, K., Stumpel, F., Gorboulev, V., Mattig, S., Deussen, A., Kaissling, B. and Koepsell, H.: Na(+)-D-glucose cotransporter in muscle capillaries increases glucose permeability. Biochem Biophys Res Commun, 314, (2): *301-5*, 2004b.

Falcone, J. C.: Endothelial cell calcium and vascular control. Med Sci Sports Exerc, 27, (8): *1165-9*, 1995.

Falholt, K., Cutfield, R., Alejandro, R., Heding, L. and Mintz, D.: The effects of hyperinsulinemia on arterial wall and peripheral muscle metabolism in dogs. Metabolism, 34, (12): *1146-9*, 1985.

Farrell, C. L. and Pardridge, W. M.: Blood-brain barrier glucose transporter is asymmetrically distributed on brain capillary endothelial lumenal and ablumenal membranes: an electron microscopic immunogold study. Proc Natl Acad Sci U S A, 88, (13): *5779-83*, 1991.

Feranchak, A. P., Roman, R. M., Schwiebert, E. M. and Fitz, J. G.: Phosphatidylinositol 3-kinase contributes to cell volume regulation through effects on ATP release. J Biol Chem, 273, (24): *14906-11*, 1998.

Filo, R. S., Bohr, D. F. and Ruegg, J. C.: Gycerinated skeletal and smooth muscle: calcium and magnesium dependence. Science, 147: *1581-1583*, 1965.

Firth, J. A.: Endothelial barriers: from hypothetical pores to membrane proteins. J Anat, 200, (6): *541-8*, 2002.

Frank, H. J. and Pardridge, W. M.: A direct in vitro demonstration of insulin binding to isolated brain microvessels. Diabetes, 30, (9): *757-61*, 1981.

French, J. E.: Atherosclerosis in relation to the structure and function of the arterial intima, with special reference to the endothelium. Int Rev Exp Pathol, 5: *253-353*, 1966.

Fricker, M., Hollinshead, M., White, N. and Vaux, D.: Interphase nuclei of many mammalian cell types contain deep, dynamic, tubular membrane-bound invaginations of the nuclear envelope. J Cell Biol, 136, (3): *531-44*, 1997.

Friedman, J. E., Dudek, R. W., Whitehead, D. S., Downes, D. L., Frisell, W. R., Caro, J. F. and Dohm, G. L.: Immunolocalization of glucose transporter GLUT4 within human skeletal muscle. Diabetes, 40, (1): *150-4*, 1991.

Fu, X., Gong, M. C., Jia, T., Somlyo, A. V. and Somlyo, A. P.: The effects of the Rho-kinase inhibitor Y-27632 on arachidonic acid-, GTPgammaS-, and phorbol ester-induced Ca^{2+}-sensitization of smooth muscle. FEBS Lett, 440, (1-2): *183-7.*, 1998.

Fujiwara, R. and Nakai, T.: Effect of glucose, insulin, and insulin-like growth factor-I on glucose transport activity in cultured rat vascular smooth muscle cells. Atherosclerosis, 127, (1): *49-57*, 1996.

Fukata, Y., Amano, M. and Kaibuchi, K.: Rho-Rho-kinase pathway in smooth muscle contraction and cytoskeletal reorganization of non-muscle cells. Trends Pharmacol Sci, 22, (1): *32-9*, 2001.

Furchgott, R. F. and Zawadzki, J. V.: The obligatory role of endothelial cells in the relaxation of arterial smooth muscle by acetylcholine. Nature, 288, (5789): *373-6*, 1980.

Galbraith, C. G., Skalak, R. and Chien, S.: Shear stress induces spatial reorganization of the endothelial cell cytoskeleton. Cell Motility & the Cytoskeleton, 40, (4): *317-30*, 1998.

Gaposchkin, C. G. and Garcia-Diaz, J. F.: Modulation of cultured brain, adrenal, and aortic endothelial cell glucose transport. Biochim Biophys Acta, 1285, (2): *255-66*, 1996.

Garlanda, C. and Dejana, E.: Heterogeneity of endothelial cells. Specific markers. Arterioscler Thromb Vasc Biol, 17, (7): *1193-202*, 1997.

Geguchadze, R., Zhi, G., Lau, K. S., Isotani, E., Persechini, A., Kamm, K. E. and Stull, J. T.: Quantitative measurements of $Ca^{(2+)}$/calmodulin binding and activation of myosin light chain kinase in cells. FEBS Lett, 557, (1-3): *121-4*, 2004.

Gerritsen, M. E. and Burke, T. M.: Insulin binding and effects of insulin on glucose uptake and metabolism in cultured rabbit coronary microvessel endothelium. Proc Soc Exp Biol Med, 180, (1): *17-23*, 1985.

Gerritsen, M. E., Burke, T. M. and Allen, L. A.: Glucose starvation is required for insulin stimulation of glucose uptake and metabolism in cultured microvascular endothelial cells. Microvasc Res, 35, (2): *153-66*, 1988.

Ghitescu, L. and Robert, M.: Diversity in unity: the biochemical composition of the endothelial cell surface varies between the vascular beds. Microsc Res Tech, 57, (5): *381-9.*, 2002.

Giardino, I., Edelstein, D. and Brownlee, M.: Nonenzymatic glycosylation in vitro and in bovine endothelial cells alters basic fibroblast growth factor activity. A

model for intracellular glycosylation in diabetes [see comments]. J Clin Invest, 94, (1): *110-7*, 1994.

Gohla, A., Schultz, G. and Offermanns, S.: Role for G(12)/G(13) in agonist-induced vascular smooth muscle cell contraction. Circ Res, 87, (3): *221-7*, 2000.

Gokina, N. I. and Osol, G.: Temperature and protein kinase C modulate myofilament Ca2+ sensitivity in pressurized rat cerebral arteries. Am J Physiol Heart Circ Physiol, 274, (6 Pt 2): *H1920-7*, 1998.

Goldstein, J. L. and Brown, M. S.: Atherosclerosis: the low-density lipoprotein receptor hypothesis. Metabolism, 26, (11): *1257-75*, 1977.

Gong, M. C., Fujihara, H., Somlyo, A. V. and Somlyo, A. P.: Translocation of rhoA associated with Ca2+ sensitization of smooth muscle. J Biol Chem, 272, (16): *10704-9*, 1997.

Goodner, C. J., Hom, F. G. and Berrie, M. A.: Investigation of the effect of insulin upon regional brain glucose metabolism in the rat in vivo. Endocrinology, 107, (6): *1827-32*, 1980.

Gould, G. W., Brant, A. M., Kahn, B. B., Shepherd, P. R., McCoid, S. C. and Gibbs, E. M.: Expression of the brain-type glucose transporter is restricted to brain and neuronal cells in mice. Diabetologia, 35, (4): *304-9*, 1992.

Gould, G. W. and Seatter, M. J.: Introduction to the facilitative glucose transporter familly.; in Facilitative Glucose Transporter. *1-37*. New York, 1997.

Greene, D. A., Lattimer, S. A. and Sima, A. A.: Sorbitol, phosphoinositides, and sodium-potassium-ATPase in the pathogenesis of diabetic complications. N Engl J Med, 316, (10): *599-606*, 1987.

Grimm, J., Keller, R. and de Groot, P. G.: Laminar flow induces cell polarity and leads to rearrangement of proteoglycan metabolism in endothelial cells. Thromb Haemost, 60, (3): *437-41*, 1988.

Grundy, S. M., Benjamin, I. J., Burke, G. L., Chait, A., Eckel, R. H., Howard, B. V., Mitch, W., Smith, S. C., Jr. and Sowers, J. R.: Diabetes and cardiovascular disease: a statement for healthcare professionals from the American Heart Association. Circulation, 100, (10): *1134-46*, 1999.

Guo, Z., Su, W., Ma, Z., Smith, G. M. and Gong, M. C.: Ca2+-independent phospholipase A2 is required for agonist-induced Ca2+ sensitization of contraction in vascular smooth muscle. J Biol Chem, 278, (3): *1856-63*, 2003.

Guth, K. and Junge, J.: Low Ca^{2+} impedes cross-bridge detachment in chemically skinned Taenia coli. Nature, 300, (5894): *775-6.*, 1982.

Haffner, S. M., Mykkanen, L., Festa, A., Burke, J. P. and Stern, M. P.: Insulin-resistant prediabetic subjects have more atherogenic risk factors than insulin-sensitive prediabetic subjects: implications for preventing coronary heart disease during the prediabetic state. Circulation, 101, (9): *975-80*, 2000.

Haffner, S. M., Stern, M. P., Hazuda, H. P., Mitchell, B. D. and Patterson, J. K.: Cardiovascular risk factors in confirmed prediabetic individuals. Does the clock for coronary heart disease start ticking before the onset of clinical diabetes? [see comments]. Jama, 263, (21): *2893-8*, 1990.

Hajduch, E., Darakhshan, F. and Hundal, H. S.: Fructose uptake in rat adipocytes: GLUT5 expression and the effects of streptozotocin-induced diabetes. Diabetologia, 41, (7): *821-8*, 1998.

Hall, A.: Rho GTPases and the actin cytoskeleton. Science, 279, (5350): *509-14.*, 1998.

Haller, H.: Postprandial glucose and vascular disease. Diabet Med, 14 Suppl 3: *S50-6*, 1997.

Halpern, W., Osol, G. and Coy, G. S.: Mechanical behavior of pressurized in vitro prearteriolar vessels determined with a video system. Annals of Biomedical Engineering, 12, (5): *463-79*, 1984.

Hanefeld, M., Koehler, C., Henkel, E., Fuecker, K., Schaper, F. and Temelkova-Kurktschiev, T.: Post-challenge hyperglycaemia relates more strongly than fasting hyperglycaemia with carotid intima-media thickness: the RIAD Study. Risk Factors in Impaired Glucose Tolerance for Atherosclerosis and Diabetes. Diabet Med, 17, (12): *835-40*, 2000.

Hanefeld, M. and Temelkova-Kurktschiev, T.: Control of post-prandial hyperglycemia--an essential part of good diabetes treatment and prevention of cardiovascular complications. Nutr Metab Cardiovasc Dis, 12, (2): *98-107*, 2002.

Harder, D. R.: Pressure-dependent membrane depolarization in cat middle cerebral artery. Circ Res, 55, (2): *197-202*, 1984.

Harder, D. R., Gilbert, R. and Lombard, J. H.: Vascular muscle cell depolarization and activation in renal arteries on elevation of transmural pressure. Am J Physiol Renal Physiol, 253, (4 Pt 2): *F778-81*, 1987.

Harder, D. R., Smeda, J. and Lombard, J.: Enhanced myogenic depolarization in hypertensive cerebral arterial muscle. Circ Res, 57, (2): *319-22*, 1985.

Hardin, C. D. and Pauley, R. G.: Metabolism and energetics of vascular smooth muscle.; in Physiology and Pathophysiology of the Heart. *1069-1086*. 1995.

Harlan, J. M., Levine, J. D., Callahan, K. S., Schwartz, B. R. and Harker, L. A.: Glutathione redox cycle protects cultured endothelial cells against lysis by extracellularly generated hydrogen peroxide. J Clin Invest, 73, (3): *706-13*, 1984.

Hauguel-de Mouzon, S., Challier, J. C., Kacemi, A., Cauzac, M., Malek, A. and Girard, J.: The GLUT3 glucose transporter isoform is differentially expressed within human placental cell types. J Clin Endocrinol Metab, 82, (8): *2689-94*, 1997.

Hediger, M. A., Coady, M. J., Ikeda, T. S. and Wright, E. M.: Expression cloning and cDNA sequencing of the Na^+/glucose co-transporter. Nature, 330, (6146): *379-81*, 1987.

Helliwell, P. A., Richardson, M., Affleck, J. and Kellett, G. L.: Stimulation of fructose transport across the intestinal brush-border membrane by PMA is mediated by GLUT2 and dynamically regulated by protein kinase C. Biochem J, 350 Pt 1: *149-54*, 2000.

Helliwell, P. A., Rumsby, M. G. and Kellett, G. L.: Intestinal sugar absorption is regulated by phosphorylation and turnover of protein kinase C betaII mediated by phosphatidylinositol 3-kinase- and mammalian target of rapamycin-dependent pathways. J Biol Chem, 278, (31): *28644-50*, 2003.

Hemmila, J. M. and Drewes, L. R.: Glucose transporter (GLUT1) expression by canine brain microvessel endothelial cells in culture: an immunocytochemical study. Adv Exp Med Biol, 331: *13-8*, 1993.

Henrion, D., Dechaux, E., Dowell, F. J., Maclour, J., Samuel, J. L., Levy, B. I. and Michel, J. B.: Alteration of flow-induced dilatation in mesenteric resistance

arteries of L-NAME treated rats and its partial association with induction of cyclo-oxygenase-2. Br J Pharmacol, 121, (1): *83-90*, 1997.

Henrion, D. and Laher, I.: Effects of staurosporine and calphostin C, two structurally unrelated inhibitors of protein kinase C, on vascular tone. Can J Physiol Pharmacol, 71, (7): *521-4.*, 1993.

Herr, R. R., Eble, T. E., Bergy, M. E. and Jahnke, H. K.: Isolation and characterization of streptozotocin. Antibiot Annu, 7: *236-40*, 1959.

Hill, M. A., Falcone, J. C. and Meininger, G. A.: Evidence for protein kinase C involvement in arteriolar myogenic reactivity. Am J Physiol Heart Circ Physiol, 259, (5 Pt 2): *H1586-94.*, 1990.

Hill, T. L.: Sliding filament model of muscular contraction. V. Isometric force and interfilament spacing. J Theor Biol, 29, (3): *395-410.*, 1970.

Hirata, K., Kuroda, R., Sakoda, T., Katayama, M., Inoue, N., Suematsu, M., Kawashima, S. and Yokoyama, M.: Inhibition of endothelial nitric oxide synthase activity by protein kinase C. Hypertension, 25, (2): *180-5*, 1995.

Hirsch, B. and Rosen, P.: Diabetes mellitus induces long lasting changes in the glucose transporter of rat heart endothelial cells. Horm Metab Res, 31, (12): *645-52*, 1999.

Hogan, M., Cerami, A. and Bucala, R.: Advanced glycosylation endproducts block the antiproliferative effect of nitric oxide. Role in the vascular and renal complications of diabetes mellitus. J Clin Invest, 90, (3): *1110-5*, 1992.

Hom, F. G. and Goodner, C. J.: Insulin dose-response characteristics among individual muscle and adipose tissues measured in the rat in vivo with 3[H]2-deoxyglucose. Diabetes, 33, (2): *153-9*, 1984.

Horowitz, A., Clement-Chomienne, O., Walsh, M. P. and Morgan, K. G.: Epsilon-isoenzyme of protein kinase C induces a Ca(2+)-independent contraction in vascular smooth muscle. Am J Physiol Cell Physiol, 271, (2 Pt 1): *C589-94*, 1996a.

Horowitz, A., Menice, C. B., Laporte, R. and Morgan, K. G.: Mechanisms of smooth muscle contraction. Physiol Rev, 76, (4): *967-1003*, 1996b.

Howard, B. V.: Macrovascular Complications of Diabetes Mellitus; in Diabetes Mellitus. *792-797*. Philadelphia, 1996a.

Howard, R. L.: Down-regulation of glucose transport by elevated extracellular glucose concentrations in cultured rat aortic smooth muscle cells does not normalize intracellular glucose concentrations. J Lab Clin Med, 127, (5): *504-15*, 1996b.

Huijberts, M. S., Wolffenbuttel, B. H., Boudier, H. A., Crijns, F. R., Kruseman, A. C., Poitevin, P. and Levy, B. I.: Aminoguanidine treatment increases elasticity and decreases fluid filtration of large arteries from diabetic rats. J Clin Invest, 92, (3): *1407-11*, 1993.

Hunt, J. V., Smith, C. C. and Wolff, S. P.: Autoxidative glycosylation and possible involvement of peroxides and free radicals in LDL modification by glucose. Diabetes, 39, (11): *1420-4*, 1990.

Iglic, A., Veranic, P., Batista, U. and Kralj-Iglic, V.: Theoretical analysis of shape transformation of V-79 cells after treatment with cytochalasin B. J Biomech, 34, (6): *765-72*, 2001.

Iizuka, K., Yoshii, A., Samizo, K., Tsukagoshi, H., Ishizuka, T., Dobashi, K., Nakazawa, T. and Mori, M.: A major role for the rho-associated coiled coil forming protein kinase in G-protein-mediated Ca^{2+} sensitization through inhibition of myosin phosphatase in rabbit trachea. Br J Pharmacol, 128, (4): *925-33*, 1999.

Ikebe, M., Inagaki, M., Kanamaru, K. and Hidaka, H.: Phosphorylation of smooth muscle myosin light chain kinase by Ca^{2+}-activated, phospholipid-dependent protein kinase. J Biol Chem, 260, (8): *4547-50*, 1985.

Imig, J. D., Zou, A. P., Stec, D. E., Harder, D. R., Falck, J. R. and Roman, R. J.: Formation and actions of 20-hydroxyeicosatetraenoic acid in rat renal arterioles. Am J Physiol Regul Integr Comp Physiol, 270, (1 Pt 2): *R217-27*, 1996.

Inoguchi, T., Xia, P., Kunisaki, M., Higashi, S., Feener, E. P. and King, G. L.: Insulin's effect on protein kinase C and diacylglycerol induced by diabetes and glucose in vascular tissues. Am J Physiol Endocrinol Metab, 267, (3 Pt 1): *E369-79*, 1994.

Inoue, M., Kishimoto, A., Takai, Y. and Nishizuka, Y.: Studies on a cyclic nucleotide-independent protein kinase and its proenzyme in mammalian tissues. II. Proenzyme and its activation by calcium-dependent protease from rat brain. J Biol Chem, 252, (21): *7610-6.*, 1977.

Ishii, H., Koya, D. and King, G. L.: Protein kinase C activation and its role in the development of vascular complications in diabetes mellitus. J Mol Med, 76, (1): *21-31*, 1998.

Itoh, Y., Abe, T., Takaoka, R. and Tanahashi, N.: Fluorometric determination of glucose utilization in neurons in vitro and in vivo. J Cereb Blood Flow Metab, 24, (9): *993-1003*, 2004.

Jacobs, J., Sena, M. and Fox, N.: The cost of hospitalization for the late complications of diabetes in the United States. Diabet Med, 8 Spec No: *S23-9*, 1991.

James, D. E., Strube, M. and Mueckler, M.: Molecular cloning and characterization of an insulin-regulatable glucose transporter. Nature, 338, (6210): *83-7*, 1989.

Johnson, P. C.: The myogenic response in the microcirculation and its interaction with other control systems. J Hypertens Suppl, 7, (4): *S33-9; discussion S40*, 1989.

Joost, H. G., Bell, G. I., Best, J. D., Birnbaum, M. J., Charron, M. J., Chen, Y. T., Doege, H., James, D. E., Lodish, H. F., Moley, K. H., Moley, J. F., Mueckler, M., Rogers, S., Schurmann, A., Seino, S. and Thorens, B.: Nomenclature of the GLUT/SLC2A family of sugar/polyol transport facilitators. Am J Physiol Endocrinol Metab, 282, (4): *E974-6*, 2002.

Joost, H. G. and Thorens, B.: The extended GLUT-family of sugar/polyol transport facilitators: nomenclature, sequence characteristics, and potential function of its novel members (review). Mol Membr Biol, 18, (4): *247-56*, 2001.

Junod, A., Lambert, A. E., Stauffacher, W. and Renold, A. E.: Diabetogenic action of streptozotocin: relationship of dose to metabolic response. J Clin Invest, 48, (11): *2129-39*, 1969.

Kaiser, N., Sasson, S., Feener, E. P., Boukobza-Vardi, N., Higashi, S., Moller, D. E., Davidheiser, S., Przybylski, R. J. and King, G. L.: Differential regulation of glucose transport and transporters by glucose in vascular endothelial and smooth muscle cells. Diabetes, 42, (1): *80-9*, 1993.

Kandabashi, T., Shimokawa, H., Miyata, K., Kunihiro, I., Kawano, Y., Fukata, Y., Higo, T., Egashira, K., Takahashi, S., Kaibuchi, K. and Takeshita, A.: Inhibition of myosin phosphatase by upregulated rho-kinase plays a key role for coronary

artery spasm in a porcine model with interleukin-1beta. Circulation, 101, (11): *1319-23.*, 2000.

Karandikar, M. and Cobb, M. H.: Scaffolding and protein interactions in MAP kinase modules. Cell Calcium, 26, (5): *219-26*, 1999.

Kasahara, M. and Hinkle, P. C.: Reconstitution and purification of the D-glucose transporter from human erythrocytes. J Biol Chem, 252, (20): *7384-90*, 1977.

Kashiwagi, A., Asahina, T., Ikebuchi, M., Tanaka, Y., Takagi, Y., Nishio, Y., Kikkawa, R. and Shigeta, Y.: Abnormal glutathione metabolism and increased cytotoxicity caused by H_2O_2 in human umbilical vein endothelial cells cultured in high glucose medium. Diabetologia, 37, (3): *264-9*, 1994.

Katsuyama, H. and Morgan, K. G.: Mechanisms of Ca(2+)-independent contraction in single permeabilized ferret aorta cells. Circ Res, 72, (3): *651-7.*, 1993.

Kauser, K., Clark, J. E., Masters, B. S., Ortiz de Montellano, P. R., Ma, Y. H., Harder, D. R. and Roman, R. J.: Inhibitors of cytochrome P-450 attenuate the myogenic response of dog renal arcuate arteries. Circ Res, 68, (4): *1154-63*, 1991.

Kawano, Y., Yoshimi, H., Matsuoka, H., Takishita, S. and Omae, T.: Calcium supplementation in patients with essential hypertension: assessment by office, home and ambulatory blood pressure. J Hypertens, 16, (11): *1693-9.*, 1998.

Kawasaki, H., Nakayama, S. and Kretsinger, R. H.: Classification and evolution of EF-hand proteins. Biometals, 11, (4): *277-95.*, 1998.

Kayano, T., Burant, C. F., Fukumoto, H., Gould, G. W., Fan, Y. S., Eddy, R. L., Byers, M. G., Shows, T. B., Seino, S. and Bell, G. I.: Human facilitative glucose transporters. Isolation, functional characterization, and gene localization of cDNAs encoding an isoform (GLUT5) expressed in small intestine, kidney, muscle, and adipose tissue and an unusual glucose transporter pseudogene-like sequence (GLUT6). J Biol Chem, 265, (22): *13276-82*, 1990.

Keogh, R. J., Dunlop, M. E. and Larkins, R. G.: Effect of inhibition of aldose reductase on glucose flux, diacylglycerol formation, protein kinase C, and phospholipase A2 activation. Metabolism, 46, (1): *41-7*, 1997.

Kernohan, A. F., Perry, C. G. and Small, M.: Clinical impact of the new criteria for the diagnosis of diabetes mellitus. Clin Chem Lab Med, 41, (9): *1239-45*, 2003.

Khan, A. H. and Pessin, J. E.: Insulin regulation of glucose uptake: a complex interplay of intracellular signalling pathways. Diabetologia, 45, (11): *1475-83*, 2002.

Kihara, S., Ouchi, N., Funahashi, T., Shinohara, E., Tamura, R., Yamashita, S. and Matsuzawa, Y.: Troglitazone enhances glucose uptake and inhibits mitogen-activated protein kinase in human aortic smooth muscle cells. Atherosclerosis, 136, (1): *163-8*, 1998.

King, G. L., Buzney, S. M., Kahn, C. R., Hetu, N., Buchwald, S., Macdonald, S. G. and Rand, L. I.: Differential responsiveness to insulin of endothelial and support cells from micro- and macrovessels. J Clin Invest, 71, (4): *974-9*, 1983.

King, G. L., Kunisaki, M., Nishio, Y., Inoguchi, T., Shiba, T. and Xia, P.: Biochemical and molecular mechanisms in the development of diabetic vascular complications. Diabetes, 45, (Suppl 3): *S105-8*, 1996.

King, H., Aubert, R. E. and Herman, W. H.: Global burden of diabetes, 1995-2025: prevalence, numerical estimates, and projections. Diabetes Care, 21, (9): *1414-31*, 1998.

Kinne, R. K.: Endothelial and epithelial cells: general principles of selective vectorial transport. Int J Microcirc Clin Exp, 17, (5): *223-30.*, 1997.

Kirber, M. T., Walsh, J. V., Jr. and Singer, J. J.: Stretch-activated ion channels in smooth muscle: a mechanism for the initiation of stretch-induced contraction. Pflugers Arch, 412, (4): *339-45*, 1988.

Kitazawa, T., Eto, M., Woodsome, T. P. and Brautigan, D. L.: Agonists trigger G protein-mediated activation of the CPI-17 inhibitor phosphoprotein of myosin light chain phosphatase to enhance vascular smooth muscle contractility. J Biol Chem, 275, (14): *9897-900*, 2000.

Kitazawa, T., Masuo, M. and Somlyo, A. P.: G protein-mediated inhibition of myosin light-chain phosphatase in vascular smooth muscle. Proc Natl Acad Sci U S A, 88, (20): *9307-10*, 1991.

Kitazawa, T., Takizawa, N., Ikebe, M. and Eto, M.: Reconstitution of protein kinase C-induced contractile Ca^{2+} sensitization in triton X-100-demembranated rabbit arterial smooth muscle. J Physiol, 520, (Pt 1): *139-52.*, 1999.

Knot, H. J. and Nelson, M. T.: Regulation of membrane potential and diameter by voltage-dependent K^+ channels in rabbit myogenic cerebral arteries. Am J Physiol Heart Circ Physiol, 269, (1 Pt 2): *H348-55*, 1995.

Knot, H. J. and Nelson, M. T.: Regulation of arterial diameter and wall $[Ca^{2+}]$ in cerebral arteries of rat by membrane potential and intravascular pressure. J Physiol, 508, (Pt 1): *199-209.*, 1998.

Kolm-Litty, V., Sauer, U., Nerlich, A., Lehmann, R. and Schleicher, E. D.: High glucose-induced transforming growth factor beta1 production is mediated by the hexosamine pathway in porcine glomerular mesangial cells. J Clin Invest, 101, (1): *160-9*, 1998.

Kong, C. T., Yet, S. F. and Lever, J. E.: Cloning and expression of a mammalian Na^+/amino acid cotransporter with sequence similarity to Na^+/glucose cotransporters. J Biol Chem, 268, (3): *1509-12*, 1993.

Koskinen, P., Manttari, M., Manninen, V., Huttunen, J. K., Heinonen, O. P. and Frick, M. H.: Coronary heart disease incidence in NIDDM patients in the Helsinki Heart Study. Diabetes Care, 15, (7): *820-5*, 1992.

Koyama, M., Ito, M., Feng, J., Seko, T., Shiraki, K., Takaşe, K., Hartshorne, D. J. and Nakano, T.: Phosphorylation of CPI-17, an inhibitory phosphoprotein of smooth muscle myosin phosphatase, by Rho-kinase. FEBS Lett, 475, (3): *197-200.*, 2000.

Krebs, C., Fernandes, H. B., Sheldon, C., Raymond, L. A. and Baimbridge, K. G.: Functional NMDA receptor subtype 2B is expressed in astrocytes after ischemia in vivo and anoxia in vitro. J Neurosci, 23, (8): *3364-72*, 2003.

Kretsinger, R. H.: Calmodulin and myosin light chain kinase: how helices are bent. Science, 258, (5079): *50-1.*, 1992.

Krutzfeldt, A., Spahr, R., Mertens, S., Siegmund, B. and Piper, H. M.: Metabolism of exogenous substrates by coronary endothelial cells in culture. J Mol Cell Cardiol, 22, (12): *1393-404*, 1990.

Kuo, L., Chilian, W. M. and Davis, M. J.: Coronary arteriolar myogenic response is independent of endothelium. Circ Res, 66, (3): *860-6*, 1990.

Kureishi, Y., Kobayashi, S., Amano, M., Kimura, K., Kanaide, H., Nakano, T., Kaibuchi, K. and Ito, M.: Rho-associated kinase directly induces smooth muscle contraction through myosin light chain phosphorylation. J Biol Chem, 272, (19): *12257-60*, 1997.

Kwok, C. F., Goldstein, B. J., Muller-Wieland, D., Lee, T. S., Kahn, C. R. and King, G. L.: Identification of persistent defects in insulin receptor structure and function capillary endothelial cells from diabetic rats. J Clin Invest, 83, (1): *127-36*, 1989.

Lagaud, G., Gaudreault, N., Moore, E. D., Van Breemen, C. and Laher, I.: Pressure-dependent myogenic constriction of cerebral arteries occurs independently of voltage-dependent activation. Am J Physiol Heart Circ Physiol, 283, (6): *H2187-95.*, 2002.

Lagaud, G. J., Skarsgard, P. L., Laher, I. and van Breemen, C.: Heterogeneity of endothelium-dependent vasodilation in pressurized cerebral and small mesenteric resistance arteries of the rat. J Pharmacol Exp Ther, 290, (2): *832-9*, 1999.

Laher, I. and Bevan, J. A.: Staurosporine, a protein kinase C inhibitor, attenuates Ca2+-dependent stretch-induced vascular tone. Biochem Biophys Res Commun, 158, (1): *58-62.*, 1989.

Lange, A., Gebremedhin, D., Narayanan, J. and Harder, D.: 20-Hydroxyeicosatetraenoic acid-induced vasoconstriction and inhibition of potassium current in cerebral vascular smooth muscle is dependent on activation of protein kinase C. J Biol Chem, 272, (43): *27345-52*, 1997.

Laporte, R., Haeberle, J. R. and Laher, I.: Phorbol ester-induced potentiation of myogenic tone is not associated with increases in Ca^{2+} influx, myoplasmic free Ca^{2+} concentration, or 20-kDa myosin light chain phosphorylation. J Mol Cell Cardiol, 26, (3): *297-302.*, 1994.

Leach, L., Clark, P., Lampugnani, M. G., Arroyo, A. G., Dejana, E. and Firth, J. A.: Immunoelectron characterisation of the inter-endothelial junctions of human term placenta. J Cell Sci, 104 (Pt 4): *1073-81*, 1993.

Lee, I. K., Kim, H. S. and Bae, J. H.: Endothelial dysfunction: its relationship with acute hyperglycaemia and hyperlipidemia. Int J Clin Pract Suppl, (129): *59-64.*, 2002.

Lee, T. S., Saltsman, K. A., Ohashi, H. and King, G. L.: Activation of protein kinase C by elevation of glucose concentration: proposal for a mechanism in the development of diabetic vascular complications [published erratum appears in Proc Natl Acad Sci U S A 1991 Nov 1;88(21):9907] [see comments]. Proc Natl Acad Sci U S A, 86, (13): *5141-5*, 1989.

Leino, R. L., Gerhart, D. Z., van Bueren, A. M., McCall, A. L. and Drewes, L. R.: Ultrastructural localization of GLUT 1 and GLUT 3 glucose transporters in rat brain. J Neurosci Res, 49, (5): *617-26*, 1997.

Leite, R. and Webb, R. C.: Microtubule disruption potentiates phenylephrine-induced vasoconstriction in rat mesenteric arterial bed. Eur J Pharmacol, 351, (1): *R1-3*, 1998.

Libby, P. and Plutzky, J.: Diabetic macrovascular disease: the glucose paradox? Circulation, 106, (22): *2760-3*, 2002.

Lin, S. J., Hong, C. Y., Chang, M. S., Chiang, B. N. and Chien, S.: Increased aortic endothelial death and enhanced transendothelial macromolecular transport in streptozotocin-diabetic rats. Diabetologia, 36, (10): *926-30*, 1993.

Lippoldt, A., Kniesel, U., Liebner, S., Kalbacher, H., Kirsch, T., Wolburg, H. and Haller, H.: Structural alterations of tight junctions are associated with loss of polarity in stroke-prone spontaneously hypertensive rat blood-brain barrier endothelial cells. Brain Res, 885, (2): *251-61*, 2000.

Lloyd, P. G. and Hardin, C. D.: Role of microtubules in the regulation of metabolism in isolated cerebral microvessels. Am J Physiol Cell Physiol, 277, (6 Pt 1): *C1250-62*, 1999.

Lloyd, P. G., Hardin, C. D. and Sturek, M.: Examining glucose transport in single vascular smooth muscle cells with a fluorescent glucose analog. Physiol Res, 48, (6): *401-10*, 1999.

Loaiza, A., Porras, O. H. and Barros, L. F.: Glutamate triggers rapid glucose transport stimulation in astrocytes as evidenced by real-time confocal microscopy. J Neurosci, 23, (19): *7337-42*, 2003.

Loirand, G., Cario-Toumaniantz, C., Chardin, P. and Pacaud, P.: The Rho-related protein Rnd1 inhibits Ca^{2+} sensitization of rat smooth muscle. J Physiol, 516, (Pt 3): *825-34*, 1999.

Low, B. C., Ross, I. K. and Grigor, M. R.: Angiotensin II stimulates glucose transport activity in cultured vascular smooth muscle cells. J Biol Chem, 267, (29): *20740-5*, 1992.

Lu, M., Kuroki, M., Amano, S., Tolentino, M., Keough, K., Kim, I., Bucala, R. and Adamis, A. P.: Advanced glycation end products increase retinal vascular endothelial growth factor expression. J Clin Invest, 101, (6): *1219-24*, 1998.

Lusis, A. J.: Atherosclerosis. Nature, 407, (6801): *233-41*, 2000.

Lutz, A. J. and Pardridge, W. M.: Insulin therapy normalizes GLUT1 glucose transporter mRNA but not immunoreactive transporter protein in streptozocin-diabetic rats. Metabolism, 42, (8): *939-44*, 1993.

Ma, Y. H., Gebremedhin, D., Schwartzman, M. L., Falck, J. R., Clark, J. E., Masters, B. S., Harder, D. R. and Roman, R. J.: 20-Hydroxyeicosatetraenoic acid is an endogenous vasoconstrictor of canine renal arcuate arteries. Circ Res, 72, (1): *126-36*, 1993.

Macdonald, I. A.: Carbohydrate as a nutrient in adults: range of acceptable intakes. Eur J Clin Nutr, 53 Suppl 1: *S101-6*, 1999.

MacDonald, J. A., Borman, M. A., Muranyi, A., Somlyo, A. V., Hartshorne, D. J. and Haystead, T. A.: Identification of the endogenous smooth muscle myosin phosphatase-associated kinase. Proc Natl Acad Sci U S A, 98, (5): *2419-24.*, 2001.

Mackenzie, B., Loo, D. D., Panayotova-Heiermann, M. and Wright, E. M.: Biophysical characteristics of the pig kidney Na^+/glucose cotransporter SGLT2 reveal a common mechanism for SGLT1 and SGLT2. J Biol Chem, 271, (51): *32678-83*, 1996.

Mackenzie, B., Panayotova-Heiermann, M., Loo, D. D., Lever, J. E. and Wright, E. M.: SAAT1 is a low affinity Na^+/glucose cotransporter and not an amino acid transporter. A reinterpretation. J Biol Chem, 269, (36): *22488-91*, 1994.

MacKenzie, C. J., Wakefield, J. M., Cairns, F., Dominiczak, A. F. and Gould, G. W.: Regulation of glucose transport in aortic smooth muscle cells by cAMP and cGMP. Biochem J, 353, (Pt 3): *513-9*, 2001.

Maesaki, R., Ihara, K., Shimizu, T., Kuroda, S., Kaibuchi, K. and Hakoshima, T.: The structural basis of Rho effector recognition revealed by the crystal structure of human RhoA complexed with the effector domain of PKN/PRK1. Mol Cell, 4, (5): *793-803.*, 1999.

Maher, F., Simpson, I. A. and Vannucci, S. J.: Alterations in brain glucose transporter proteins, GLUT1 and GLUT3, in streptozotocin diabetic rats. Adv Exp Med Biol, 331: *9-12*, 1993.

Mamchaoui, K., Makhloufi, Y. and Saumon, G.: Glucose transporter gene expression in freshly isolated and cultured rat pneumocytes. Acta Physiol Scand, 175, (1): *19-24.*, 2002.

Mandarino, L. J., Finlayson, J. and Hassell, J. R.: High glucose downregulates glucose transport activity in retinal capillary pericytes but not endothelial cells. Invest Ophthalmol Vis Sci, 35, (3): *964-72*, 1994.

Mann, G. E., Yudilevich, D. L. and Sobrevia, L.: Regulation of amino acid and glucose transporters in endothelial and smooth muscle cells. Physiol Rev, 83, (1): *183-252.*, 2003.

Manson, J. E., Colditz, G. A., Stampfer, M. J., Willett, W. C., Krolewski, A. S., Rosner, B., Arky, R. A., Speizer, F. E. and Hennekens, C. H.: A prospective study of maturity-onset diabetes mellitus and risk of coronary heart disease and stroke in women. Arch Intern Med, 151, (6): *1141-7*, 1991.

Mantych, G. J., Hageman, G. S. and Devaskar, S. U.: Characterization of glucose transporter isoforms in the adult and developing human eye. Endocrinology, 133, (2): *600-7*, 1993a.

Mantych, G. J., James, D. E. and Devaskar, S. U.: Jejunal/kidney glucose transporter isoform (Glut-5) is expressed in the human blood-brain barrier. Endocrinology, 132, (1): *35-40*, 1993b.

Marks, J., Carvou, N. J., Debnam, E. S., Srai, S. K. and Unwin, R. J.: Diabetes increases facilitative glucose uptake and GLUT2 expression at the rat proximal tubule brush border membrane. J Physiol, 553, (Pt 1): *137-45*, 2003.

Martinez-Lemus, L. A., Wu, X., Wilson, E., Hill, M. A., Davis, G. E., Davis, M. J. and Meininger, G. A.: Integrins as unique receptors for vascular control. J Vasc Res, 40, (3): *211-33*, 2003.

Masumoto, N., Nakayama, K., Oyabe, A., Uchino, M., Ishii, K., Obara, K. and Tanabe, Y.: Specific attenuation of the pressure-induced contraction of rat cerebral artery by herbimycin A. Eur J Pharmacol, 330, (1): *55-63*, 1997.

Matrougui, K., Tanko, L. B., Loufrani, L., Gorny, D., Levy, B. I., Tedgui, A. and Henrion, D.: Involvement of Rho-kinase and the actin filament network in angiotensin II-induced contraction and extracellular signal-regulated kinase activity in intact rat mesenteric resistance arteries. Arterioscler Thromb Vasc Biol, 21, (8): *1288-93*, 2001.

Matsuoka, T., Nishizaki, T. and Kisby, G. E.: Na^+-dependent and phlorizin-inhibitable transport of glucose and cycasin in brain endothelial cells. J Neurochem, 70, (2): *772-7*, 1998.

Mavrikakis, M. E., Sfikakis, P. P., Kontoyannis, D., Horti, M., Kittas, C., Koutras, D. A. and Raptis, S. A.: Macrovascular disease of coronaries and cerebral arteries in streptozotocin-induced diabetic rats. A controlled, comparative study. Exp Clin Endocrinol Diabetes, 106, (1): *35-40*, 1998.

McCall, A. L., van Bueren, A. M., Huang, L., Stenbit, A., Celnik, E. and Charron, M. J.: Forebrain endothelium expresses GLUT4, the insulin-responsive glucose transporter. Brain Research, 744, (2): *318-26*, 1997.

McCarron, J. G., Crichton, C. A., Langton, P. D., MacKenzie, A. and Smith, G. L.: Myogenic contraction by modulation of voltage-dependent calcium currents in isolated rat cerebral arteries. J Physiol, 498 (Pt 2): *371-9*, 1997.

McCarron, J. G., Osol, G. and Halpern, W.: Myogenic responses are independent of the endothelium in rat pressurized posterior cerebral arteries. Blood Vessels, 26, (5): *315-9*, 1989.

McPhillips, J. B., Barrett-Connor, E. and Wingard, D. L.: Cardiovascular disease risk factors prior to the diagnosis of impaired glucose tolerance and non-insulin-dependent diabetes mellitus in a community of older adults. Am J Epidemiol, 131, (3): *443-53*, 1990.

Medalie, J. H., Papier, C. M., Goldbourt, U. and Herman, J. B.: Major factors in the development of diabetes mellitus in 10,000 men. Arch Intern Med, 135, (6): *811-7*, 1975.

Meininger, G. A., Zawieja, D. C., Falcone, J. C., Hill, M. A. and Davey, J. P.: Calcium measurement in isolated arterioles during myogenic and agonist stimulation. Am J Physiol Heart Circ Physiol, 261, (3 Pt 2): *H950-9*, 1991.

Mendelsohn, M. E.: Mechanisms of estrogen action in the cardiovascular system. J Steroid Biochem Mol Biol, 74, (5): *337-43*, 2000.

Mendelsohn, M. E. and Karas, R. H.: The protective effects of estrogen on the cardiovascular system. N Engl J Med, 340, (23): *1801-11*, 1999.

Mertens, S., Noll, T., Spahr, R., Krutzfeldt, A. and Piper, H. M.: Energetic response of coronary endothelial cells to hypoxia. Am J Physiol Heart Circ Physiol, 258, (3 Pt 2): *H689-94*, 1990.

Michel, C. C. and Curry, F. E.: Microvascular permeability. Physiol Rev, 79, (3): *703-61*, 1999.

Miller, F. J., Jr., Dellsperger, K. C. and Gutterman, D. D.: Myogenic constriction of human coronary arterioles. Am J Physiol Heart Circ Physiol, 273, (1 Pt 2): *H257-64*, 1997.

Mita, M., Yanagihara, H., Hishinuma, S., Saito, M. and Walsh, M. P.: Membrane depolarization-induced contraction of rat caudal arterial smooth muscle involves Rho-associated kinase. Biochem J, 364, (Pt 2): *431-40*, 2002.

Miyazaki, K., Yano, T., Schmidt, D. J., Tokui, T., Shibata, M., Lifshitz, L. M., Kimura, S., Tuft, R. A. and Ikebe, M.: Rho-dependent agonist-induced spatio-temporal change in myosin phosphorylation in smooth muscle cells. J Biol Chem, 277, (1): *725-34*, 2002.

Mogford, J. E., Davis, G. E. and Meininger, G. A.: RGDN peptide interaction with endothelial alpha5beta1 integrin causes sustained endothelin-dependent vasoconstriction of rat skeletal muscle arterioles. J Clin Invest, 100, (6): *1647-53*, 1997.

Mogford, J. E., Davis, G. E., Platts, S. H. and Meininger, G. A.: Vascular smooth muscle alpha v beta 3 integrin mediates arteriolar vasodilation in response to RGD peptides. Circ Res, 79, (4): *821-6*, 1996.

Mompeo, B., Popov, D., Sima, A., Constantinescu, E. and Şimionescu, M.: Diabetes-induced structural changes of venous and arterial endothelium and smooth muscle cells. J Submicrosc Cytol Pathol, 30, (4): *475-84*, 1998.

Moore, E. D., Becker, P. L., Fogarty, K. E., Williams, D. A. and Fay, F. S.: Ca^{2+} imaging in single living cells: theoretical and practical issues. Cell Calcium, 11, (2-3): *157-79*, 1990.

Moore, E. D., Etter, E. F., Philipson, K. D., Carrington, W. A., Fogarty, K. E., Lifshitz, L. M. and Fay, F. S.: Coupling of the Na^+/Ca^{2+} exchanger, Na^+/K^+ pump and sarcoplasmic reticulum in smooth muscle. Nature, 365, (6447): *657-60.*, 1993.

Morgan, J. P. and Morgan, K. G.: Vascular smooth muscle: the first recorded Ca^{2+} transients. Pflugers Arch, 395, (1): *75-7*, 1982.

Morgan, K. G. and Gangopadhyay, S. S.: Invited review: cross-bridge regulation by thin filament-associated proteins. J Appl Physiol, 91, (2): *953-62.*, 2001.

Morgan, K. G., Khalil, R. A., Suematsu, E. and Katsuyama, H.: Calcium-dependent and calcium-independent pathways of signal transduction in smooth muscle. Jpn J Pharmacol, 58, (Suppl 2): *47P-53P.*, 1992.

Mueckler, M.: Facilitative glucose transporters. Eur J Biochem, 219, (3): *713-25*, 1994.

Mueckler, M., Caruso, C., Baldwin, S. A., Panico, M., Blench, I., Morris, H. R., Allard, W. J., Lienhard, G. E. and Lodish, H. F.: Sequence and structure of a human glucose transporter. Science, 229, (4717): *941-5*, 1985.

Murata, H., Hruz, P. W. and Mueckler, M.: The mechanism of insulin resistance caused by HIV protease inhibitor therapy. J Biol Chem, 275, (27): *20251-4*, 2000.

Murphy, R. A.: Contractile system function in mammalian smooth muscle. Blood Vessels, 13, (1-2): *1-23.*, 1976.

Murthy, K. S., Zhou, H., Grider, J. R., Brautigan, D. L., Eto, M. and Makhlouf, G. M.: Differential signalling by muscarinic receptors in smooth muscle: m2-mediated inactivation of myosin light chain kinase via Gi3, Cdc42/Rac1 and p21-

activated kinase 1 pathway, and m3-mediated MLC20 (20 kDa regulatory light chain of myosin II) phosphorylation via Rho-associated kinase/myosin phosphatase targeting subunit 1 and protein kinase C/CPI-17 pathway. Biochem J, 374, (Pt 1): *145-55*, 2003.

Narayanan, J., Imig, M., Roman, R. J. and Harder, D. R.: Pressurization of isolated renal arteries increases inositol trisphosphate and diacylglycerol. Am J Physiol Heart Circ Physiol, 266, (5 Pt 2): *H1840-5*, 1994.

Nelson, M. T., Cheng, H., Rubart, M., Santana, L. F., Bonev, A. D., Knot, H. J. and Lederer, W. J.: Relaxation of arterial smooth muscle by calcium sparks. Science, 270, (5236): *633-7*, 1995.

Nelson, M. T., Conway, M. A., Knot, H. J. and Brayden, J. E.: Chloride channel blockers inhibit myogenic tone in rat cerebral arteries. J Physiol, 502, (Pt 2): *259-64*, 1997.

Netland, P. A., Zetter, B. R., Via, D. P. and Voyta, J. C.: In situ labelling of vascular endothelium with fluorescent acetylated low density lipoprotein. Histochem J, 17, (12): *1309-20*, 1985.

Nishikawa, M., Hidaka, H. and Adelstein, R. S.: Phosphorylation of smooth muscle heavy meromyosin by calcium-activated, phospholipid-dependent protein kinase. The effect on actin-activated MgATPase activity. J Biol Chem, 258, (23): *14069-72*, 1983.

Nishikawa, M., Shirakawa, S. and Adelstein, R. S.: Phosphorylation of smooth muscle myosin light chain kinase by protein kinase C. Comparative study of the phosphorylated sites. J Biol Chem, 260, (15): *8978-83.*, 1985.

Nishioka, T., Oda, Y., Seino, Y., Yamamoto, T., Inagaki, N., Yano, H., Imura, H., Shigemoto, R. and Kikuchi, H.: Distribution of the glucose transporters in human brain tumors. Cancer Res, 52, (14): *3972-9*, 1992.

Nishizaki, T., Kammesheidt, A., Sumikawa, K., Asada, T. and Okada, Y.: A sodium- and energy-dependent glucose transporter with similarities to SGLT1-2 is expressed in bovine cortical vessels. Neurosci Res, 22, (1): *13-22.*, 1995.

Nishizaki, T. and Matsuoka, T.: Low glucose enhances Na^+/glucose transport in bovine brain artery endothelial cells. Stroke, 29, (4): *844-9*, 1998.

Noria, S., Cowan, D. B., Gotlieb, A. I. and Langille, B. L.: Transient and steady-state effects of shear stress on endothelial cell adherens junctions. Circ Res, 85, (6): *504-14*, 1999.

Nualart, F., Godoy, A. and Reinicke, K.: Expression of the hexose transporters GLUT1 and GLUT2 during the early development of the human brain. Brain Research, 824, (1): *97-104*, 1999.

Ohara, Y., Sayegh, H. S., Yamin, J. J. and Harrison, D. G.: Regulation of endothelial constitutive nitric oxide synthase by protein kinase C. Hypertension, 25, (3): *415-20*, 1995.

Olson, A. L. and Pessin, J. E.: Structure, function, and regulation of the mammalian facilitative glucose transporter gene family. Annu Rev Nutr, 16: *235-56*, 1996.

Osol, G., Laher, I. and Cipolla, M.: Protein kinase C modulates basal myogenic tone in resistance arteries from the cerebral circulation. Circ Res, 68, (2): *359-67.*, 1991.

Osol, G., Laher, I. and Kelley, M.: Myogenic tone is coupled to phospholipase C and G protein activation in small cerebral arteries. Am J Physiol Heart Circ Physiol, 265, (1 Pt 2): *H415-20.*, 1993.

Pan, M., Wasa, M. and Souba, W. W.: Tumor necrosis factor stimulates system XAG- transport activity in human endothelium. J Surg Res, 58, (6): *659-64*, 1995.

Pardridge, W. M., Boado, R. J. and Farrell, C. R.: Brain-type glucose transporter (GLUT-1) is selectively localized to the blood-brain barrier. Studies with quantitative western blotting and in situ hybridization. J Biol Chem, 265, (29): *18035-40*, 1990.

Patterson, A. J., Henrie-Olson, J. and Brenner, R.: Vasoregulation at the molecular level: a role for the beta1 subunit of the calcium-activated potassium (BK) channel. Trends Cardiovasc Med, 12, (2): *78-82.*, 2002.

Paul, R. J., Bowman, P. S. and Kolodney, M. S.: Effects of microtubule disruption on force, velocity, stiffness and [Ca(2+)](i) in porcine coronary arteries. Am J Physiol Heart Circ Physiol, 279, (5): *H2493-501*, 2000.

Pedersen, S. F., Hoffmann, E. K. and Mills, J. W.: The cytoskeleton and cell volume regulation. Comp Biochem Physiol A Mol Integr Physiol, 130, (3): *385-99*, 2001.

Pekala, P., Marlow, M., Heuvelman, D. and Connolly, D.: Regulation of hexose transport in aortic endothelial cells by vascular permeability factor and tumor necrosis factor-alpha, but not by insulin. J Biol Chem, 265, (30): *18051-4*, 1990.

Perler, B. A. and Becker, G. J.: Vascular intervention, A clinical Approch. New York, 1998.

Persechini, A. and Kretsinger, R. H.: Toward a model of the calmodulin-myosin light-chain kinase complex: implications for calmodulin function. J Cardiovasc Pharmacol, 12, (Suppl 5): *S1-12.*, 1988.

Phay, J. E., Hussain, H. B. and Moley, J. F.: Cloning and expression analysis of a novel member of the facilitative glucose transporter family, SLC2A9 (GLUT9). Genomics, 66, (2): *217-20*, 2000.

Pierschbacher, M. D. and Ruoslahti, E.: Influence of stereochemistry of the sequence Arg-Gly-Asp-Xaa on binding specificity in cell adhesion. J Biol Chem, 262, (36): *17294-8*, 1987.

Pontremoli, S., Melloni, E., Sparatore, B., Michetti, M., Salamino, F. and Horecker, B. L.: Isozymes of protein kinase C in human neutrophils and their modification by two endogenous proteinases. J Biol Chem, 265, (2): *706-12.*, 1990.

Portilla, D., Dai, G., Peters, J. M., Gonzalez, F. J., Crew, M. D. and Proia, A. D.: Etomoxir-induced PPARalpha-modulated enzymes protect during acute renal failure. Am J Physiol Renal Physiol, 278, (4): *F667-75*, 2000.

Pouliot, J. F. and Beliveau, R.: Palmitoylation of the glucose transporter in blood-brain barrier capillaries. Biochim Biophys Acta, 1234, (2): *191-6*, 1995.

Quinn, L. A. and McCumbee, W. D.: Regulation of glucose transport by angiotensin II and glucose in cultured vascular smooth muscle cells. J Cell Physiol, 177, (1): *94-102*, 1998.

Randriamboavonjy, V., Busse, R. and Fleming, I.: 20-HETE-induced contraction of small coronary arteries depends on the activation of Rho-kinase. Hypertension, 41, (3 Pt 2): *801-6*, 2003.

Reagan, L. P., Magarinos, A. M., Lucas, L. R., van Bueren, A., McCall, A. L. and McEwen, B. S.: Regulation of GLUT-3 glucose transporter in the hippocampus of diabetic rats subjected to stress. Am J Physiol Endocrinol Metab, 276, (5 Pt 1): *E879-86*, 1999.

Redmond, E. M., Cahill, P. A. and Sitzmann, J. V.: Perfused transcapillary smooth muscle and endothelial cell co-culture-- a novel in vitro model. In Vitro Cell Dev Biol Anim, 31, (8): *601-9.*, 1995.

Rerup, C. C.: Drugs producing diabetes through damage of the insulin secreting cells. Pharmacol Rev, 22, (4): *485-518*, 1970.

Rogers, S., Macheda, M. L., Docherty, S. E., Carty, M. D., Henderson, M. A., Soeller, W. C., Gibbs, E. M., James, D. E. and Best, J. D.: Identification of a novel glucose transporter-like protein-GLUT-12. Am J Physiol Endocrinol Metab, 282, (3): *E733-8*, 2002.

Roman, Y., Alfonso, A., Louzao, M. C., Vieytes, M. R. and Botana, L. M.: Confocal microscopy study of the different patterns of 2-NBDG uptake in rabbit enterocytes in the apical and basal zone. Pflugers Arch, 443, (2): *234-9*, 2001.

Rosen, G. M. and Freeman, B. A.: Detection of superoxide generated by endothelial cells. Proc Natl Acad Sci U S A, 81, (23): *7269-73*, 1984.

Ross, R. and Glomset, J. A.: The pathogenesis of atherosclerosis (second of two parts). N Engl J Med, 295, (8): *420-5*, 1976.

Sajan, M. P., Bandyopadhyay, G., Kanoh, Y., Standaert, M. L., Quon, M. J., Reed, B. C., Dikic, I. and Farese, R. V.: Sorbitol activates atypical protein kinase C and GLUT4 glucose transporter translocation/glucose transport through proline-rich tyrosine kinase-2, the extracellular signal-regulated kinase pathway and phospholipase D. Biochem J, 362, (Pt 3): *665-74*, 2002.

Sakaue, H., Ogawa, W., Takata, M., Kuroda, S., Kotani, K., Matsumoto, M., Sakaue, M., Nishio, S., Ueno, H. and Kasuga, M.: Phosphoinositide 3-kinase is required for insulin-induced but not for growth hormone- or hyperosmolarity-induced glucose uptake in 3T3-L1 adipocytes. Mol Endocrinol, 11, (10): *1552-62*, 1997.

Sakurada, S., Takuwa, N., Sugimoto, N., Wang, Y., Seto, M., Sasaki, Y. and Takuwa, Y.: Ca2+-dependent activation of Rho and Rho kinase in membrane

depolarization-induced and receptor stimulation-induced vascular smooth muscle contraction. Circ Res, 93, (6): *548-56*, 2003.

Sanders, K. M.: Invited review: mechanisms of calcium handling in smooth muscles. J Appl Physiol, 91, (3): *1438-49.*, 2001.

Sank, A., Wei, D., Reid, J., Ertl, D., Nimni, M., Weaver, F., Yellin, A. and Tuan, T. L.: Human endothelial cells are defective in diabetic vascular disease. J Surg Res, 57, (6): *647-53*, 1994.

Sasson, S., Gorowits, N., Joost, H. G., King, G. L., Cerasi, E. and Kaiser, N.: Regulation by metformin of the hexose transport system in vascular endothelial and smooth muscle cells. Br J Pharmacol, 117, (6): *1318-24*, 1996.

Sato, Y., Ito, T., Udaka, N., Kanisawa, M., Noguchi, Y., Cushman, S. W. and Satoh, S.: Immunohistochemical localization of facilitated-diffusion glucose transporters in rat pancreatic islets. Tissue Cell, 28, (6): *637-43.*, 1996.

Schmidt, A. M., Hori, O., Chen, J. X., Li, J. F., Crandall, J., Zhang, J., Cao, R., Yan, S. D., Brett, J. and Stern, D.: Advanced glycation endproducts interacting with their endothelial receptor induce expression of vascular cell adhesion molecule-1 (VCAM-1) in cultured human endothelial cells and in mice. A potential mechanism for the accelerated vasculopathy of diabetes. J Clin Invest, 96, (3): *1395-403*, 1995.

Schnedl, W. J., Ferber, S., Johnson, J. H. and Newgard, C. B.: STZ transport and cytotoxicity. Specific enhancement in GLUT2-expressing cells. Diabetes, 43, (11): *1326-33*, 1994.

Schror, K.: Blood vessel wall interactions in diabetes. Diabetes, 46, (Suppl 2): *S115-8*, 1997.

Schubert, R., Kalentchuk, V. U. and Krien, U.: Rho kinase inhibition partly weakens myogenic reactivity in rat small arteries by changing calcium sensitivity. Am J Physiol Heart Circ Physiol, 283, (6): *H2288-95.*, 2002.

Schubert, R. and Mulvany, M. J.: The myogenic response: established facts and attractive hypotheses. Clinical Science, 96, (4): *313-26*, 1999.

Setoguchi, M., Ohya, Y., Abe, I. and Fujishima, M.: Stretch-activated whole-cell currents in smooth muscle cells from mesenteric resistance artery of guinea-pig. J Physiol, 501 (Pt 2): *343-53*, 1997.

Sheetz, M. J. and King, G. L.: Molecular understanding of hyperglycemia's adverse effects for diabetic complications. Jama, 288, (20): *2579-88.*, 2002.

Shi, J., Zhang, Y. Q. and Simpkins, J. W.: Effects of 17beta-estradiol on glucose transporter 1 expression and endothelial cell survival following focal ischemia in the rats. Exp Brain Res, 117, (2): *200-6*, 1997.

Shimada, M., Kawamoto, S., Hirose, Y., Nakanishi, M., Watanabe, H. and Watanabe, M.: Regional differences in glucose transport in the mouse hippocampus. Histochem J, 26, (3): *207-12*, 1994.

Shimizu, T., Ihara, K., Maesaki, R., Kuroda, S., Kaibuchi, K. and Hakoshima, T.: An open conformation of switch I revealed by the crystal structure of a Mg^{2+}-free form of RHOA complexed with GDP. Implications for the GDP/GTP exchange mechanism. J Biol Chem, 275, (24): *18311-7.*, 2000.

Shin, H. M., Je, H. D., Gallant, C., Tao, T. C., Hartshorne, D. J., Ito, M. and Morgan, K. G.: Differential association and localization of myosin phosphatase subunits during agonist-induced signal transduction in smooth muscle. Circ Res, 90, (5): *546-53*, 2002.

Shirao, S., Kashiwagi, S., Sato, M., Miwa, S., Nakao, F., Kurokawa, T., Todoroki-Ikeda, N., Mogami, K., Mizukami, Y., Kuriyama, S., Haze, K., Suzuki, M. and Kobayashi, S.: Sphingosylphosphorylcholine is a novel messenger for Rho-kinase-mediated Ca^{2+} sensitization in the bovine cerebral artery: unimportant role for protein kinase C. Circ Res, 91, (2): *112-9*, 2002.

Simmons, D. A. and Winegrad, A. I.: Mechanism of glucose-induced (Na^+, K^+)-ATPase inhibition in aortic wall of rabbits. Diabetologia, 32, (7): *402-8*, 1989.

Simpson, I. A., Appel, N. M., Hokari, M., Oki, J., Holman, G. D., Maher, F., Koehler-Stec, E. M., Vannucci, S. J. and Smith, Q. R.: Blood-brain barrier glucose transporter: effects of hypo- and hyperglycemia revisited. J Neurochem, 72, (1): *238-47*, 1999.

Skarsgard, P., van Breemen, C. and Laher, I.: Estrogen regulates myogenic tone in pressurized cerebral arteries by enhanced basal release of nitric oxide. Am J Physiol, 273, (5 Pt 2): *H2248-56*, 1997.

Smith, P. G., Garcia, R. and Kogerman, L.: Strain reorganizes focal adhesions and cytoskeleton in cultured airway smooth muscle cells. Exp Cell Res, 232, (1): *127-36*, 1997.

Sokoloff, L., Reivich, M., Kennedy, C., Des Rosiers, M. H., Patlak, C. S., Pettigrew, K. D., Sakurada, O. and Shinohara, M.: The [^{14}C]deoxyglucose method for the measurement of local cerebral glucose utilization: theory, procedure, and normal values in the conscious and anesthetized albino rat. J Neurochem, 28, (5): *897-916*, 1977.

Solaro, R. J.: Myosin light chain phosphatase: a Cinderella of cellular signaling. Circ Res, 87, (3): *173-5*, 2000.

Somlyo, A. P. and Somlyo, A. V.: Ultrastructural aspects of activation and contraction of vascular smooth muscle. Fed Proc, 35, (6): *1288-93.*, 1976.

Somlyo, A. P. and Somlyo, A. V.: Signal transduction and regulation in smooth muscle. Nature, 372, (6503): *231-6*, 1994.

Somlyo, A. P. and Somlyo, A. V.: Signal transduction by G-proteins, rho-kinase and protein phosphatase to smooth muscle and non-muscle myosin II. J Physiol, 522, (Pt 2): *177-85*, 2000.

Somlyo, A. P. and Somlyo, A. V.: Ca^{2+} sensitivity of smooth muscle and nonmuscle myosin II: modulated by G proteins, kinases, and myosin phosphatase. Physiol Rev, 83, (4): *1325-58*, 2003.

Sone, H., Deo, B. K. and Kumagai, A. K.: Enhancement of glucose transport by vascular endothelial growth factor in retinal endothelial cells. Invest Ophthalmol Vis Sci, 41, (7): *1876-84*, 2000.

Speizer, L., Haugland, R. and Kutchai, H.: Asymmetric transport of a fluorescent glucose analogue by human erythrocytes. Biochim Biophys Acta, 815, (1): *75-84*, 1985.

Standley, P. R. and Rose, K. A.: Insulin and insulin-like growth factor-1 modulation of glucose transport in arterial smooth muscle cells: implication of GLUT-4 in the vasculature. Am J Hypertens, 7, (4 Pt 1): *357-62*, 1994.

Sward, K., Dreja, K., Susnjar, M., Hellstrand, P., Hartshorne, D. J. and Walsh, M. P.: Inhibition of Rho-associated kinase blocks agonist-induced Ca^{2+} sensitization of myosin phosphorylation and force in guinea-pig ileum. J Physiol, 522, (Pt 1): *33-49*, 2000.

Taggart, M. J., Leavis, P., Feron, O. and Morgan, K. G.: Inhibition of PKCalpha and rhoA translocation in differentiated smooth muscle by a caveolin scaffolding domain peptide. Exp Cell Res, 258, (1): *72-81*, 2000.

Takagi, H., King, G. L. and Aiello, L. P.: Hypoxia upregulates glucose transport activity through an adenosine-mediated increase of GLUT1 expression in retinal capillary endothelial cells. Diabetes, 47, (9): *1480-8*, 1998.

Takai, Y., Kishimoto, A., Inoue, M. and Nishizuka, Y.: Studies on a cyclic nucleotide-independent protein kinase and its proenzyme in mammalian tissues. I. Purification and characterization of an active enzyme from bovine cerebellum. J Biol Chem, 252, (21): *7603-9.*, 1977.

Takakura, Y., Kuentzel, S. L., Raub, T. J., Davies, A., Baldwin, S. A. and Borchardt, R. T.: Hexose uptake in primary cultures of bovine brain microvessel endothelial cells. I. Basic characteristics and effects of D-glucose and insulin. Biochim Biophys Acta, 1070, (1): *1-10*, 1991.

Takata, K.: Glucose transporters in the transepithelial transport of glucose. J Electron Microsc (Tokyo), 45, (4): *275-84.*, 1996.

Tapley, P. M. and Murray, A. W.: Modulation of Ca^{2+}-activated, phospholipid-dependent protein kinase in platelets treated with a tumor-promoting phorbol ester. Biochem Biophys Res Commun, 122, (1): *158-64*, 1984.

Taylor, P. D., Oon, B. B., Thomas, C. R. and Poston, L.: Prevention by insulin treatment of endothelial dysfunction but not enhanced noradrenaline-induced contractility in mesenteric resistance arteries from streptozotocin-induced diabetic rats. Br J Pharmacol, 111, (1): *35-41*, 1994.

Temelkova-Kurktschiev, T., Henkel, E., Schaper, F., Koehler, C., Siegert, G. and Hanefeld, M.: Prevalence and atherosclerosis risk in different types of non-

diabetic hyperglycemia. Is mild hyperglycemia an underestimated evil? Exp Clin Endocrinol Diabetes, 108, (2): *93-9*, 2000.

Tesfamariam, B. and Cohen, R. A.: Free radicals mediate endothelial cell dysfunction caused by elevated glucose. Am J Physiol Heart Circ Physiol, 263, (2 Pt 2): *H321-6*, 1992.

Thomas, J., Linssen, M., van der Vusse, G. J., Hirsch, B., Rosen, P., Kammermeier, H. and Fischer, Y.: Acute stimulation of glucose transport by histamine in cardiac microvascular endothelial cells. Biochim Biophys Acta, 1268, (1): *88-96*, 1995.

Thorens, B.: Glucose transporters in the regulation of intestinal, renal, and liver glucose fluxes. Am J Physiol Gastrointest Liver Physiol, 270, (4 Pt 1): *G541-53.*, 1996.

Thorens, B., Sarkar, H. K., Kaback, H. R. and Lodish, H. F.: Cloning and functional expression in bacteria of a novel glucose transporter present in liver, intestine, kidney, and beta-pancreatic islet cells. Cell, 55, (2): *281-90*, 1988.

Thornalley, P. J.: The glyoxalase system: new developments towards functional characterization of a metabolic pathway fundamental to biological life. Biochem J, 269, (1): *1-11*, 1990.

Throckmorton, D. C., Packer, C. S. and Brophy, C. M.: Protein kinase C activation during Ca^{2+}-independent vascular smooth muscle contraction. J Surg Res, 78, (1): *48-53*, 1998.

Thulesen, J., Orskov, C., Holst, J. J. and Poulsen, S. S.: Short-term insulin treatment prevents the diabetogenic action of streptozotocin in rats. Endocrinology, 138, (1): *62-8*, 1997.

Todoroki-Ikeda, N., Mizukami, Y., Mogami, K., Kusuda, T., Yamamoto, K., Miyake, T., Sato, M., Suzuki, S., Yamagata, H., Hokazono, Y. and Kobayashi, S.: Sphingosylphosphorylcholine induces Ca(2+)-sensitization of vascular smooth muscle contraction: possible involvement of rho-kinase. FEBS Lett, 482, (1-2): *85-90*, 2000.

Tomlinson, D. R.: Mitogen-activated protein kinases as glucose transducers for diabetic complications. Diabetologia, 42, (11): *1271-81*, 1999.

Tomlinson, K. C., Gardiner, S. M., Hebden, R. A. and Bennett, T.: Functional consequences of streptozotocin-induced diabetes mellitus, with particular reference to the cardiovascular system. Pharmacol Rev, 44, (1): *103-50*, 1992.

Tordjman, K. M., Leingang, K. A. and Mueckler, M.: Differential regulation of the HepG2 and adipocyte/muscle glucose transporters in 3T3L1 adipocytes. Effect of chronic glucose deprivation. Biochem J, 271, (1): *201-7*, 1990.

Trepakova, E. S., Csutora, P., Hunton, D. L., Marchase, R. B., Cohen, R. A. and Bolotina, V. M.: Calcium influx factor directly activates store-operated cation channels in vascular smooth muscle cells. J Biol Chem, 275, (34): *26158-63*, 2000.

Trepakova, E. S., Gericke, M., Hirakawa, Y., Weisbrod, R. M., Cohen, R. A. and Bolotina, V. M.: Properties of a native cation channel activated by Ca^{2+} store depletion in vascular smooth muscle cells. J Biol Chem, 276, (11): *7782-90*, 2001.

Tsien, R. Y.: Fluorescence measurement and photochemical manipulation of cytosolic free calcium. Trends Neurosci, 11, (10): *419-24*, 1988.

Uchida, E. and Bohr, D. F.: Myogenic tone in isolated perfused resistance vessels from rats. Am J Physiol---Legacy Content, 216, (6): *1343-50*, 1969.

Uchigata, Y., Yamamoto, H., Kawamura, A. and Okamoto, H.: Protection by superoxide dismutase, catalase, and poly(ADP-ribose) synthetase inhibitors against alloxan- and streptozotocin-induced islet DNA strand breaks and against the inhibition of proinsulin synthesis. J Biol Chem, 257, (11): *6084-8*, 1982.

Uehata, M., Ishizaki, T., Satoh, H., Ono, T., Kawahara, T., Morishita, T., Tamakawa, H., Yamagami, K., Inui, J., Maekawa, M. and Narumiya, S.: Calcium sensitization of smooth muscle mediated by a Rho-associated protein kinase in hypertension. Nature, 389, (6654): *990-4*, 1997.

Umemoto, S., Bengur, A. R. and Sellers, J. R.: Effect of multiple phosphorylations of smooth muscle and cytoplasmic myosins on movement in an in vitro motility assay. J Biol Chem, 264, (3): *1431-6.*, 1989.

Urabe, T., Hattori, N., Nagamatsu, S., Sawa, H. and Mizuno, Y.: Expression of glucose transporters in rat brain following transient focal ischemic injury. J Neurochem, 67, (1): *265-71*, 1996.

Vallerand, A. L., Perusse, F. and Bukowiecki, L. J.: Cold exposure potentiates the effect of insulin on in vivo glucose uptake. Am J Physiol Endocrinol Metab, 253, (2 Pt 1): *E179-86*, 1987.

Van Aelst, L. and D'Souza-Schorey, C.: Rho GTPases and signaling networks. Genes Dev, 11, (18): *2295-322.*, 1997.

van Breemen, C., Chen, Q. and Laher, I.: Superficial buffer barrier function of smooth muscle sarcoplasmic reticulum. Trends Pharmacol Sci, 16, (3): *98-105*, 1995.

Van den Enden, M. K., Nyengaard, J. R., Ostrow, E., Burgan, J. H. and Williamson, J. R.: Elevated glucose levels increase retinal glycolysis and sorbitol pathway metabolism. Implications for diabetic retinopathy. Invest Ophthalmol Vis Sci, 36, (8): *1675-85*, 1995.

Van Lierop, J. E., Wilson, D. P., Davis, J. P., Tikunova, S., Sutherland, C., Walsh, M. P. and Johnson, J. D.: Activation of smooth muscle myosin light chain kinase by calmodulin. Role of LYS(30) and GLY(40). J Biol Chem, 277, (8): *6550-8.*, 2002.

VanBavel, E., van der Meulen, E. T. and Spaan, J. A.: Role of Rho-associated protein kinase in tone and calcium sensitivity of cannulated rat mesenteric small arteries. Exp Physiol, 86, (5): *585-92.*, 2001.

VanBavel, E., Wesselman, J. P. and Spaan, J. A.: Myogenic activation and calcium sensitivity of cannulated rat mesenteric small arteries. Circ Res, 82, (2): *210-20*, 1998.

Vannucci, S. J., Koehler-Stec, E. M., Li, K., Reynolds, T. H., Clark, R. and Simpson, I. A.: GLUT4 glucose transporter expression in rodent brain: effect of diabetes. Brain Research, 797, (1): *1-11*, 1998.

Vannucci, S. J., Maher, F. and Simpson, I. A.: Glucose utilization and glucose transporter proteins GLUT-1 and GLUT-3 in brains of diabetic (db/db) mice. Am J Physiol Endocrinol Metab, 272, (2 Pt 1): *E267-74*, 1997.

Varbiro, S., Nadasy, G. L., Monos, E., Vajo, Z., Acs, N., Miklos, Z., Tokes, A. M. and Szekacs, B.: Effect of ovariectomy and hormone replacement therapy on small artery biomechanics in angiotensin-induced hypertension in rats. J Hypertens, 18, (11): *1587-95*, 2000.

Vilaro, S., Palacin, M., Pilch, P. F., Testar, X. and Zorzano, A.: Expression of an insulin-regulatable glucose carrier in muscle and fat endothelial cells. Nature, 342, (6251): *798-800*, 1989.

Vinals, F., Gross, A., Testar, X., Palacin, M., Rosen, P. and Zorzano, A.: High glucose concentrations inhibit glucose phosphorylation, but not glucose transport, in human endothelial cells. Biochim Biophys Acta, 1450, (2): *119-29.*, 1999.

Vinters, H. V., Beck, D. W., Bready, J. V., Maxwell, K., Berliner, J. A., Hart, M. N. and Cancilla, P. A.: Uptake of glucose analogues into cultured cerebral microvessel endothelium. J Neuropathol Exp Neurol, 44, (5): *445-58*, 1985.

Waddell, I. D., Zomerschoe, A. G., Voice, M. W. and Burchell, A.: Cloning and expression of a hepatic microsomal glucose transport protein. Comparison with liver plasma-membrane glucose-transport protein GLUT 2. Biochem J, 286, (Pt 1): *173-7*, 1992.

Waitkus-Edwards, K. R., Martinez-Lemus, L. A., Wu, X., Trzeciakowski, J. P., Davis, M. J., Davis, G. E. and Meininger, G. A.: alpha(4)beta(1) Integrin activation of L-type calcium channels in vascular smooth muscle causes arteriole vasoconstriction. Circ Res, 90, (4): *473-80*, 2002.

Walker, P. S., Donovan, J. A., Van Ness, B. G., Fellows, R. E. and Pessin, J. E.: Glucose-dependent regulation of glucose transport activity, protein, and mRNA in primary cultures of rat brain glial cells. J Biol Chem, 263, (30): *15594-601*, 1988.

Walker, P. S., Ramlal, T., Donovan, J. A., Doering, T. P., Sandra, A., Klip, A. and Pessin, J. E.: Insulin and glucose-dependent regulation of the glucose transport system in the rat L6 skeletal muscle cell line. J Biol Chem, 264, (11): *6587-95*, 1989.

Wallner, E. I., Wada, J., Tramonti, G., Lin, S. and Kanwar, Y. S.: Status of glucose transporters in the mammalian kidney and renal development. Ren Fail, 23, (3-4): *301-10.*, 2001.

Walmsley, A. R., Barrett, M. P., Bringaud, F. and Gould, G. W.: Sugar transporters from bacteria, parasites and mammals: structure-activity relationships. Trends Biochem Sci, 23, (12): *476-81*, 1998.

Walsh, M. P., Kargacin, G. J., Kendrick-Jones, J. and Lincoln, T. M.: Intracellular mechanisms involved in the regulation of vascular smooth muscle tone. Can J Physiol Pharmacol, 73, (5): *565-73.*, 1995.

Wang, Z. and Gleichmann, H.: GLUT2 in pancreatic islets: crucial target molecule in diabetes induced with multiple low doses of streptozotocin in mice. Diabetes, 47, (1): *50-6*, 1998.

Watanabe, J., Karibe, A., Horiguchi, S., Keitoku, M., Satoh, S., Takishima, T. and Shirato, K.: Modification of myogenic intrinsic tone and $[Ca^{2+}]_i$ of rat isolated arterioles by ryanodine and cyclopiazonic acid. Circ Res, 73, (3): *465-72*, 1993.

Webb, B. L., Hirst, S. J. and Giembycz, M. A.: Protein kinase C isoenzymes: a review of their structure, regulation and role in regulating airways smooth muscle tone and mitogenesis. Br J Pharmacol, 130, (7): *1433-52*, 2000.

Weber, L. P., Seto, M., Sasaki, Y., Sward, K. and Walsh, M. P.: The involvement of protein kinase C in myosin phosphorylation and force development in rat tail arterial smooth muscle. Biochem J, 352, (Pt 2): *573-82*, 2000.

Weber, L. P., Van Lierop, J. E. and Walsh, M. P.: Ca^{2+}-independent phosphorylation of myosin in rat caudal artery and chicken gizzard myofilaments. J Physiol, 516, (Pt 3): *805-24.*, 1999.

Wells-Knecht, K. J., Zyzak, D. V., Litchfield, J. E., Thorpe, S. R. and Baynes, J. W.: Mechanism of autoxidative glycosylation: identification of glyoxal and arabinose as intermediates in the autoxidative modification of proteins by glucose. Biochemistry, 34, (11): *3702-9*, 1995.

Welsh, D. G., Morielli, A. D., Nelson, M. T. and Brayden, J. E.: Transient receptor potential channels regulate myogenic tone of resistance arteries. Circ Res, 90, (3): *248-50*, 2002.

Welsh, D. G., Nelson, M. T., Eckman, D. M. and Brayden, J. E.: Swelling-activated cation channels mediate depolarization of rat cerebrovascular smooth muscle by hyposmolarity and intravascular pressure. J Physiol, 527 Pt 1: *139-48*, 2000.

Wesselman, J. P., Schubert, R., VanBavel, E. D., Nilsson, H. and Mulvany, M. J.: KCa-channel blockade prevents sustained pressure-induced depolarization in rat mesenteric small arteries. Am J Physiol Heart Circ Physiol, 272, (5 Pt 2): *H2241-9*, 1997.

Williams, S. B., Goldfine, A. B., Timimi, F. K., Ting, H. H., Roddy, M. A., Simonson, D. C. and Creager, M. A.: Acute hyperglycemia attenuates endothelium-dependent vasodilation in humans in vivo. Circulation, 97, (17): *1695-701*, 1998.

Wilson, D. P., Sutherland, C. and Walsh, M. P.: Ca^{2+} activation of smooth muscle contraction: evidence for the involvement of calmodulin that is bound to the triton insoluble fraction even in the absence of Ca^{2+}. J Biol Chem, 277, (3): *2186-92.*, 2002.

Wingard, C. J., Nowocin, J. M. and Murphy, R. A.: Cross-bridge regulation by Ca(2+)-dependent phosphorylation in amphibian smooth muscle. Am J Physiol Regul Integr Comp Physiol, 281, (6): *R1769-77.*, 2001.

Wolffenbuttel, B. H. and van Haeften, T. W.: Prevention of complications in non-insulin-dependent diabetes mellitus (NIDDM). Drugs, 50, (2): *263-88*, 1995.

Wood, I. S. and Trayhurn, P.: Glucose transporters (GLUT and SGLT): expanded families of sugar transport proteins. Br J Nutr, 89, (1): *3-9*, 2003.

Woolf, N.: Pathology of atherosclerosis. London, 1982.

Wright, E. M.: Renal Na(+)-glucose cotransporters. Am J Physiol Renal Physiol, 280, (1): *F10-8*, 2001.

Wright, E. M., Loo, D. D., Panayotova-Heiermann, M., Hirayama, B. A., Turk, E., Eskandari, S. and Lam, J. T.: Structure and function of the Na^+/glucose cotransporter. Acta Physiol Scand Suppl, 643: *257-64*, 1998.

Wu, X. and Davis, M. J.: Characterization of stretch-activated cation current in coronary smooth muscle cells. Am J Physiol Heart Circ Physiol, 280, (4): *H1751-61*, 2001.

Xie, L., Clunn, G. F., Lymn, J. S. and Hughes, A. D.: Role of intracellular calcium ([Ca2+]i) and tyrosine phosphorylation in adhesion of cultured vascular smooth muscle cells to fibrinogen. Cardiovasc Res, 39, (2): *475-84*, 1998.

Yamada, K., Nakata, M., Horimoto, N., Saito, M., Matsuoka, H. and Inagaki, N.: Measurement of glucose uptake and intracellular calcium concentration in single, living pancreatic beta-cells. J Biol Chem, 275, (29): *22278-83*, 2000.

Yamagishi, S., Fujimori, H., Yonekura, H., Yamamoto, Y. and Yamamoto, H.: Advanced glycation endproducts inhibit prostacyclin production and induce plasminogen activator inhibitor-1 in human microvascular endothelial cells. Diabetologia, 41, (12): *1435-41*, 1998.

Yamamoto, H., Uchigata, Y. and Okamoto, H.: Streptozotocin and alloxan induce DNA strand breaks and poly(ADP-ribose) synthetase in pancreatic islets. Nature, 294, (5838): *284-6*, 1981.

Yamasaki, Y., Kawamori, R., Matsushima, H., Nishizawa, H., Kodama, M., Kubota, M., Kajimoto, Y. and Kamada, T.: Asymptomatic hyperglycaemia is associated with increased intimal plus medial thickness of the carotid artery. Diabetologia, 38, (5): *585-91*, 1995.

Yeon, D. S., Kim, J. S., Ahn, D. S., Kwon, S. C., Kang, B. S., Morgan, K. G. and Lee, Y. H.: Role of protein kinase C- or RhoA-induced Ca(2+) sensitization in stretch-induced myogenic tone. Cardiovasc Res, 53, (2): *431-8.*, 2002.

Yoshioka, K., Oh, K. B., Saito, M., Nemoto, Y. and Matsuoka, H.: Evaluation of 2-[N-(7-nitrobenz-2-oxa-1,3-diazol-4-yl)amino]-2-deoxy-D-glucose, a new fluorescent derivative of glucose, for viability assessment of yeast Candida albicans. Appl Microbiol Biotechnol, 46, (4): *400-4*, 1996a.

Yoshioka, K., Saito, M., Oh, K. B., Nemoto, Y., Matsuoka, H., Natsume, M. and Abe, H.: Intracellular fate of 2-NBDG, a fluorescent probe for glucose uptake activity, in Escherichia coli cells. Biosci Biotechnol Biochem, 60, (11): *1899-901*, 1996b.

Yoshioka, K., Takahashi, H., Homma, T., Saito, M., Oh, K. B., Nemoto, Y. and Matsuoka, H.: A novel fluorescent derivative of glucose applicable to the assessment of glucose uptake activity of Escherichia coli. Biochim Biophys Acta, 1289, (1): *5-9*, 1996c.

Yu, B., Poirier, L. A. and Nagy, L. E.: Mobilization of GLUT-4 from intracellular vesicles by insulin and K(+) depolarization in cultured H9c2 myotubes. Am J Physiol Heart Circ Physiol, 277, (2 Pt 1): *E259-67*, 1999.

Zhang, B., Zhang, Y., Wang, Z. and Zheng, Y.: The role of Mg^{2+} cofactor in the guanine nucleotide exchange and GTP hydrolysis reactions of Rho family GTP-binding proteins. J Biol Chem, 275, (33): *25299-307.*, 2000.

Zou, H., Ratz, P. H. and Hill, M. A.: Role of myosin phosphorylation and $[Ca^{2+}]_i$ in myogenic reactivity and arteriolar tone. Am J Physiol Heart Circ Physiol, 269, (5 Pt 2): *H1590-6*, 1995.

Appendix 1

Calphostin C and Y-27632 non-interaction with Fura-2

The possibility of an interaction between Fura-2 and both Calphostin C and Y-27632 were tested on a Cary Eclipse fluorescence spectrometer (Varian Canada Inc., Mississauga, ON). Fura-2 pentapotassium salt (0.1%) wad added to samples of PSS with and without 1.6 mM $CaCl_2$. Calphostin C and Y-27632 were added to sample of PSS with both Ca^{2+} and Fura-2. Each sample was placed in a fluorescence cuvette in the multicell holder of the Cary Eclipse fluorescence spectrophotometer. The temperature of the solution inside the cuvette was set to 37 °C. Using the scan application, each solution was repeatedly excited at 340 and 380 nm. The scan speed was set to 600 nm/min for best signal to noise ratio. The emission scans were recorded for Fura-2 between 450 and 600nm of wavelength with a PMT (800 volts). For each sample, four replicas were averaged. The ratio of the corrected spectra from the 340 and 380 excitations were calculated for each sample and compared. The 340/380 ratio spectra of Fura-2 obtained in presence of Ca^{2+} is not affected by neither calphostin C nor Y-27632 (Figure A1). These data demonstrated that Calphostin C and Y-27632 do not interact with Fura-2. Moreover, when compared at the wavelength of 510 nm (the emission collected during physiological experiment with the photomultiplier detection system from Photon Technology International and using Felix quantitative ratio fluorescence software), the 340/380 ratio of the 0 Ca^{2+} solution was significantly lower than all other solution containing 1.6mM Ca^{2+} ($p<0.001$). We found no significant difference in the 340/380 ratio between solution without and with Y-27632 (1 μM) or calphostin C (1 μM) (Figure A2).

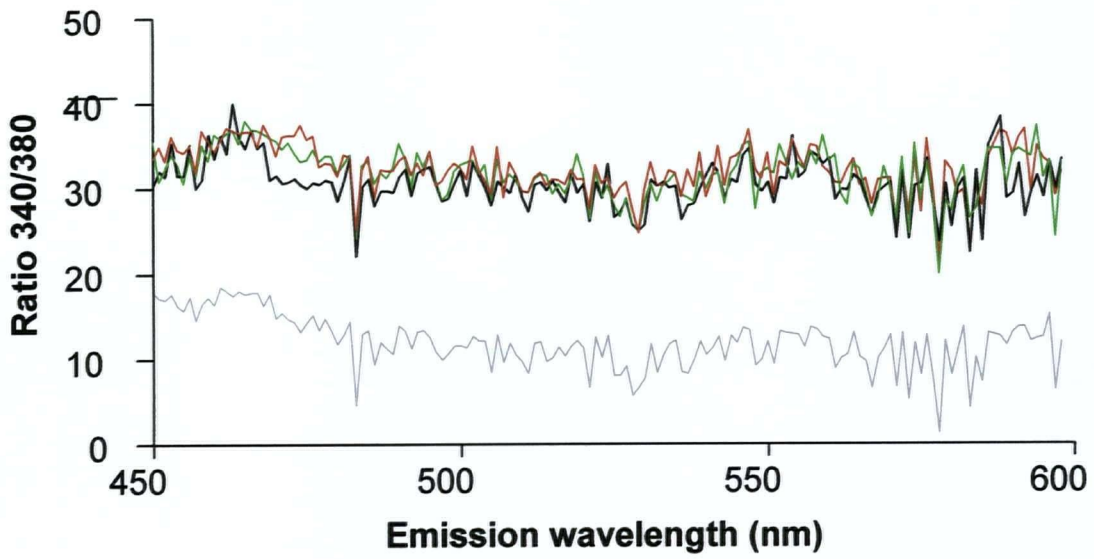

Figure A1 Spectrum of the 340/380 ratio

Solution with 0 Ca^{2+} ——, 1.6mM Ca^{2+} ——, 1.6mM Ca^{2+} and 1 μM Y-27632 ——, and 1.6mM Ca^{2+} and 1 μM calphostin C ——.

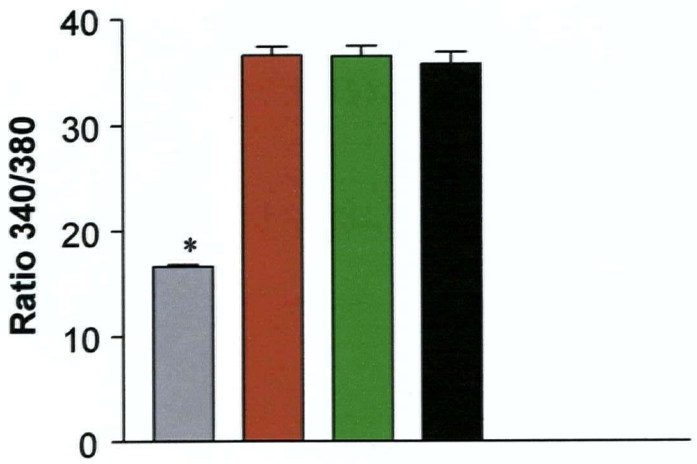

Figure A2 Histogram of the 340/380 ratio.

Recorded at a wavelength emission of 510 nm. 0 Ca^{2+} ▭, 1.6mM Ca^{2+} ▭, 1.6 mM Ca^{2+} and 1 μM Y-27632 ▭, 1.6 mM Ca^{2+} and 1 μM calphostin C ▭. * marks ratios significantly different from others ($p<0.001$; ANOVA followed by Bonferroni test).

Appendix 2
Western blots negative controls

Control experiments were performed concomitantly with the data shown in Figure 2.4. In these control experiments, the same amount of protein (30 μg to 45 μg) from rat septal coronary artery (vessel), human coronary artery ECs (HCAECs), epididymal adipose tissue (Fat), heart, jejunum (GUT) and brain cortex was loaded and resolved on SDS-PAGE and transferred to nitrocellulose membrane. All incubations with the membranes were performed at 37 ºC with gentle agitation. Non-specific binding sites were blocked with 10% non-fat dry milk in Tris-buffered saline Tween (TBS-T; 50 mmol/l Tris, 0.09% NaCl, and 0.01% Tween; pH 7.6). The membranes were then incubated in 5% non-fat dry milk in TBS-T without the primary antibody, rinsed with TBS-T and further incubated with the appropriate horseradish peroxidase conjugated secondary antibodies (1:20000), also diluted in 5% non-fat dry milk in TBS-T (Figure A3).

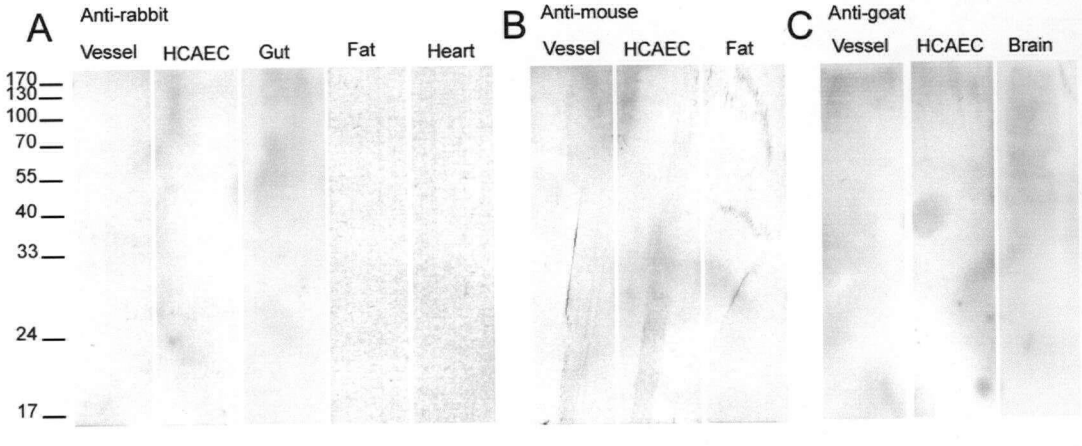

Figure A3 Secondary antibody negative controls

A) anti-rabbit, B) anti-mouse, and C) anti-goat.

Appendix 3
FWHM and image depth measurements

The lateral and axial resolution of the Fluor 20X, N.A. 0.75 were measured using a Tetraspeck sphere; 200 nm diameter. A Z-stack of 2D images of the bead were acquired using the same system settings as those used for both the HCAECs and the intact vessel (confocal aperture of 1.55 mm in diameter, pixel size of 156 nm and Z step of 500 nm (satisfied Nyquist criteria), ND filter #1, BHS filter (488 nm excitation wavelength), and mode of acquisition (gain 10, black level 4.8)). The fluorescence intensity was plotted as a function of distance from the brightest pixel in both the X and Y (Figure A4) and Z (Figure A5) directions. An estimate of the full width half max (FWHM) of 3.7 μm and 9.3 μm for the lateral and axial dimensions respectively was calculated from the Gaussian curve (r^2 of 0.90 and 0.88 respectively). The image depth, corresponding to the axial depth from which light will be collected, calculated from the same Gaussian curve was estimated to be 16.9 μm.

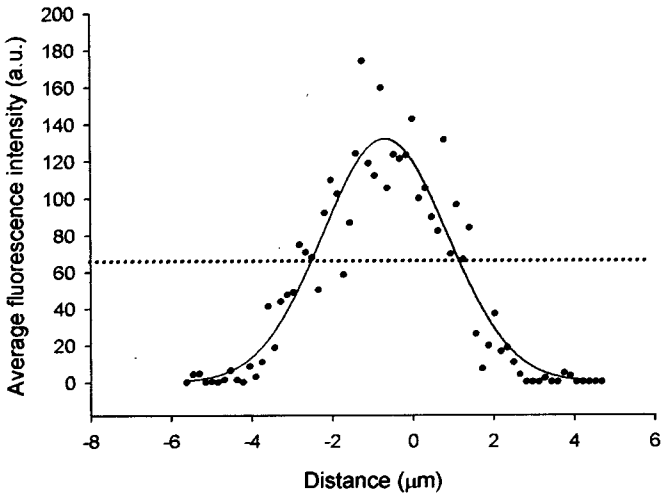

Figure A4 Lateral fluorescence intensity distribution.

Plot of the fluorescence intensity as a function of the lateral distance from the brightest pixel. The solid line represents the Gaussian fit. The dashed line indicates the position of X-Y coordinates at half of the maximal intensity.

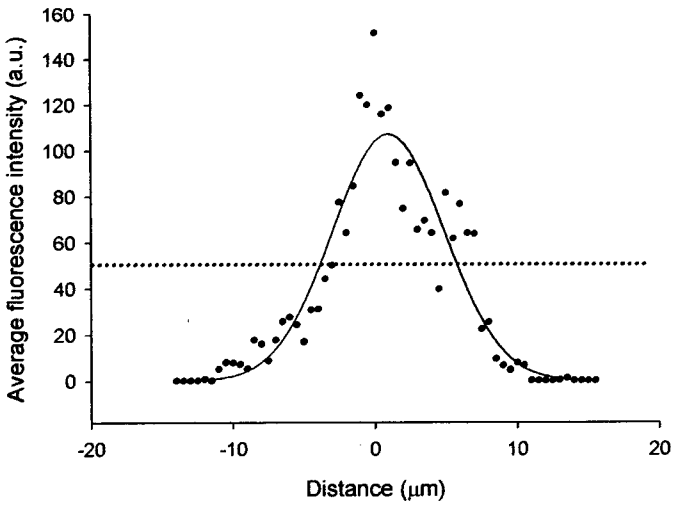

Figure A5 Axial fluorescence intensity distribution.

Plot of the fluorescence intensity as a function of the axial distance from the brightest pixel. The solid line represents the Gaussian fit. The dashed line indicates the position of Z coordinates at half of the maximal intensity.

Appendix 4

D-glucose blunts insulin effects in HCAECs

The effect of 2.5 μU/ml of insulin were investigated, on a 20-min exposure to a Krebs solution containing 0.1 mM 2-NBDG and 5 mM D-glucose. A 20-min pre-incubation with 5 mM D-glucose and 2.5 μU/ml of insulin preceded the addition of 2-NBDG to the solution. Insulin had no effect on the rate of accumulation of 2-NBDG in HCAECs in these conditions (Figure A6).

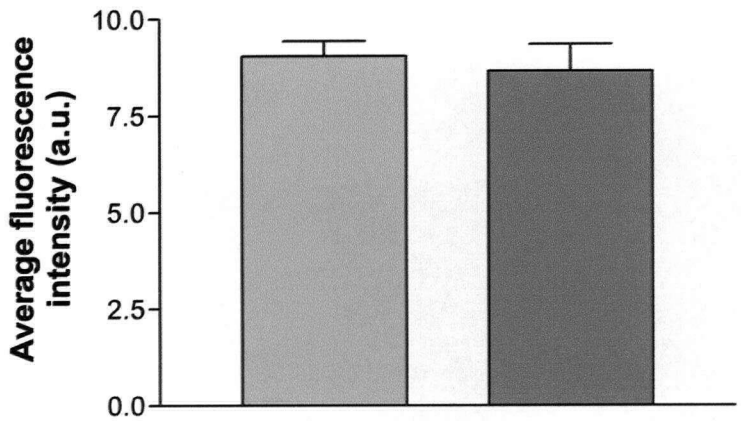

Figure A6 Effect of D-glucose on insulin stimulation in HCAECs.

Uptake of 0.1 mM 2-NBDG over 20 min, in the absence or presence of 2.5 μU/ml of insulin, in a Krebs solution containing 5 mM D-glucose. Each bar is the average of 14 and 17 cells from 3 different experiments respectively.

Appendix 5
Modulation of PKC and SGLT

We also performed a preliminary investigation on the effect of indolactan (1 μM), calphostin C (1 μM; Biomol Research Laboratories, Inc.), and phloridzin (phloretin 2′-β-D-glucoside; 50 μM), known to activate, and inhibit GLUT-2 and SGLT respectively, on a 20-min exposure to a Krebs solution containing a total of 5 mM (for phloridzin) or 20 mM (for indolactam and calphostin C) D-glucose and 0.1 mM of 2-NBDG. For each experiment, a 10-min pre-incubation with the respective compound preceded the addition of 2-NBDG to the solution.

First, the regulation of glucose uptake by PKC (involved in the translocation of GLUT-2 to the plasma membrane) was assessed in the presence of 20 mM of D-glucose in HCAECs. PKC activation with 1 μM indolactan had no significant effect on the average fluorescence intensity recorded after a 20 min exposure to 0.1 mM 2-NBDG. On the other hand, the inhibition of PKC with 1 μM calphostin C reduced significantly by 37% ($p<0.05$) the accumulation of fluorescence intensity in HCAECs (Figure A7).

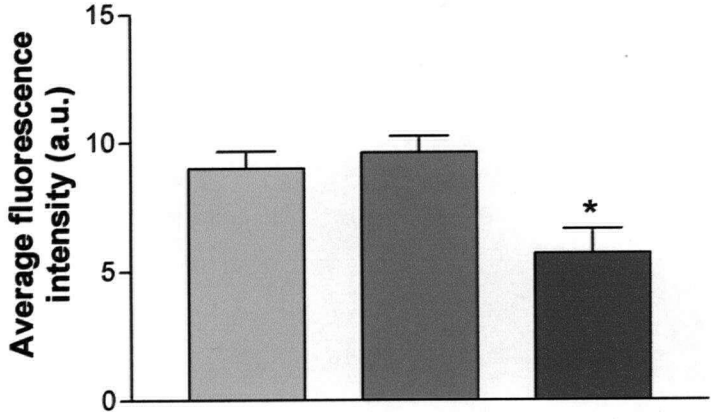

Figure A7 Regulation by PKC of the 2-NBDG uptake in HCAECs.

Uptake of 0.1 mM 2-NBDG over 20 min, in a solution of 20 mM D-glucose, in the absence ▭ or in the presence of 1 μM Indolactam ▭ or 1 μM Calphostin C ▭. Each bar is the average of 10, 16 and 9 cells respectively, from 3 different experiments. Significant differences between control and indolactant are indicated as follow; * $p<0.05$.

Secondly, phloridzin, a specific inhibitor of SGLT, was tested in order to determine the functionality of the Na^+-dependent co-transporter in HCAECs. Phloridzin produced no significant inhibition on the average accumulation of fluorescence intensity in HCAECs exposed to 0.1 mM 2-NBDG, at a basal concentration of 5 mM of D-glucose, for 20 min (Figure A8).

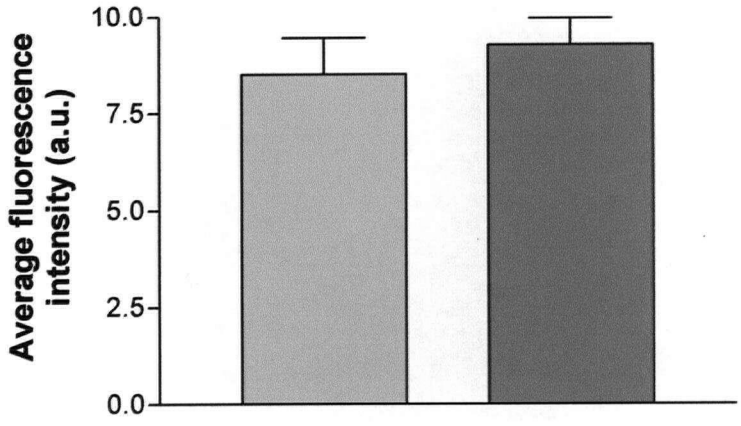

Figure A8 Effect of Phloridzin on 2-NBDG uptake in HCAECs.

Uptake of 0.1 mM 2-NBDG in presence of 5 mM D-glucose for a period of 20 min, in the absence ▭ or in the presence of 50 μM Phloridzin ▬ . Each bar is the average of 20 and 21 cells respectively, from 4 different experiments.

The regulation of glucose transport by PKC has been previously reported in ECs. Phorbol ester, IGF-1 and VEGF have been shown to mediate through PKC, glucose uptake increases in brain microvessel and retinal ECs (Drewes *et al.*, 1988; Sone *et al.*, 2000; DeBosch *et al.*, 2001). The effect of phorbol ester was reported to be greatest in primary or first passage cells and to be diminished or lost completely in older culture (beyond the 4th passage) (Drewes *et al.*, 1988). IGF-1 was shown to induce glucose uptake in the absence of an increase in GLUT-1 transcript or protein level (DeBosch *et al.*, 2001). However, the increased in glucose uptake following VEGF stimulation also associated with no change in total GLUT-1 protein content was shown to be accompanied with a 75% translocation of GLUT-1 from the cytosol to the plasma membrane (Sone *et al.*, 2000). Both studies performed in retinal ECs have identified PKC_{β} as the isoform responsible for the regulation of glucose uptake in response to IGF-1 and VEGF stimulations. Interestingly, the traffic of GLUT-2 from the cytosol to the brush-

border of epithelial cells has also been shown to be mediated by PKC_{β} (Helliwell *et al.*, 2000). In contrast, in signalling pathways modulated by insulin and sorbitol, the activation of atypical PKC isoforms were associated with GLUT-4 translocation from the cytosol to the plasma membrane of adipocytes and myocytes (Sajan *et al.*, 2002). As each of these transporter isoforms were identified in HCAECs and previously in rat coronary artery ECs, we therefore cannot rule out the possibility that the inhibitory effect on 2-NBDG uptake, produced by calphostin C, is the result of the blockade of the translocation of GLUT-1, GLUT-2, GLUT-4 or a combination of them to the plasma membrane.

In this study, experiments performed with calphostin C and indolactam were done in presence of 20 mM of D-glucose. GLUT-2 unlike other transporter isoforms has a low affinity for glucose and a high Km value, making it the most efficient transporter in presence of high glucose concentration. As indolactam, the PKC activator, did not increase any further 2-NBDG uptake in HCAECs, it is possible that GLUT-2, had already been translocated to the plasma membrane, through PKC activation, in response to the elevated glucose concentration. In agreement with this concept, calphostin C, the PKC inhibitor, reduced significantly the uptake of 2-NBDG in presence of 20 mM D-glucose.

Phloridzin, the SGLT specific inhibitor, was used in presence of much lower concentration of D-glucose (5 mM) in HCAECs. Although, we and others have previously identified SGLT-1 in ECs (Nishizaki and Matsuoka, 1998; Elfeber *et al.*, 2004a; Elfeber *et al.*, 2004b), 50 μM of phloridzin produced no significant effect on the uptake of 2-NBDG in HCAECs. A previous confocal microscopy study has shown an inhibition of 2-NBDG by phloridzin as low as 35% in rabbit

enterocytes (Roman *et al.*, 2001). Since SGLT-1 is likely to play a more important role in enterocytes than in vascular ECs, the inhibitory effect of phloridzin on 2-NBDG in ECs was expected to be very low. As shown by Nishizaki et al., the activity of SGLT is greatly enhanced by low cytosolic glucose concentrations in brain microvessel ECs (Nishizaki and Matsuoka, 1998). Since SGLT is more likely to participate in glucose uptake in ECs in periods of stress such as hypoglycaemia and ischemia, such conditions may need to be reproduced in ECs in order to determine the functionality of SGLT-1.